ABSTRACT

Title of Document:	CHARACTHERIZATION OF DELAYED ETTRINGITE FORMATION IN MARYLAND BRIDGES
	Micah Shalom Ceary, Ph.D., 2007
Directed By:	Professor, Amde M. Amde, Civil and Environmental Engineering

The research investigated the significance of Delayed Ettringite Formation (DEF) presences in the Maryland Bridge Inventory. The objective of the research included investigating possible presence of DEF, correlations between the presence of DEF in cast-in-place concrete and moist map cracking, and correlations between presence of DEF in cast-in-place concrete and air entrainment agents (AEA). The research required coring a target population, so that scanning electron microscope (SEM) with energy dispersive analysis x-ray (EDAX) could be utilized to identify DEF in the concrete. Combination of visual identification, SEM and elemental identification with EDAX are used to verify the presence of DEF in the concrete samples.

The research was conducted in two phases with the first suggesting a possible link between moist map cracking and DEF. The research identified numerous ettringite morphologies in bridge concrete. Characterization of the ettringite

morphologies suggested that lamellar ettringite could be linked to DEF-related damage. From this work, a second phase was developed to establish a link between degree of moist map cracking and DEF. Furthermore, other research showed that ettringite grew well in a solution of AEA. The second phase research developed a population to test both hypothesis and attempted to show positive or negative correlations between these two theories and DEF presence.

Phase 2 research shows no correlation between concrete mixes with AEA and DEF. Therefore, the conclusion is that AEA does not have any measurable adverse effects regarding DEF. Whereas, the research shows a strong correlation between widespread moist map cracking and significant DEF quantities, but that a DEF presence is not necessarily indicative of DEF-related damages. Once a threshold is exceeded, DEF-related damages are observed and are found throughout the affected concrete. These results are independent of alkali-silica reaction (ASR), since ASR was not found in any of the Phase 2 samples selected.

Overall, both phases of research shows that Maryland bridge concrete contains ettringite, but that not all ettringite formations appear to lead to damage of the concrete. Moist map cracking, a suggested DEF-related damage, appears to be correlated with lamellar ettringite formations and high quantities of DEF with in the concrete.

CHARACTHERIZATION OF DELAYED ETTRINGITE FORMATION IN MARYLAND BRIDGES

By

Micah Shalom Ceary

Dissertation submitted to the Faculty of the Graduate School of the
University of Maryland, College Park, in partial fulfillment
of the requirements for the degree of
Doctorate of Philosophy
2007

Advisory Committee:
Professor Amde M. Amde, Chair
Professor M. Sherif Aggour
Professor Chung C. Fu
Professor Donald W. Vannoy
Professor Sung W. Lee

Dedication

This research and dissertation is dedicated to my loving and supporting family. A special thanks to my tolerant wife who put up with the long hours and preoccupied mind.

Acknowledgements

The research reported herein was sponsored by the Maryland State Highway Administration (MDSHA). Sincere thanks are due to Mr. Earle S. Freedman, Deputy Chief Engineer of Bridge Development, MDSHA; Mr. Peter Stephanos, Director of Materials and Technology, MDSHA; and Mr. Jeffrey H. Smith and Allison Hardt, Research Division, MDSHA, for their guidance and support. The author is very grateful to Mr. Paul Finnerty, Office of Materials and Technology, Precast/Prestressed Concrete Division, MDSHA, for his extensive technical advice and support throughout the project and for coordinating and administrating support from the State of Maryland. The author is also very grateful to Ms. Barbara Adkins and Mr. Rodney C. Wynn, for their advice and support throughout the project. The project also acknowledges Mr. Joseph Miller, Office of Bridge Inspection & Remedial, Engineering Division, MDSHA, for assisting with the development of the sample population using the MDSHA databases. The author also appreciates the support provided by Ms. Vicki Stewart, MDSHA.

The project is very grateful to Dr. W. Clayton Ormsby, Research Chemist, Salut, Inc., for the help and expertise provided on the Scanning Electron Microscope work.

Table of Contents

List of Tables

Page

List of Figures

Page

Page

Page

Page

Page

Chapter 1
Introduction and Overview

1.1 Statement of the Problem

With the cost of materials and labor increasing, premature deterioration of concrete has gained world wide recognition and interest. In particular, the transportation systems are significant since constructing and maintaining these structures are very expensive. One form of premature deterioration is due to expansion resulting from delayed ettringite formation (DEF) in hardened concrete, which appears on the surface of the affected concrete as moist map cracking. DEF is associated with microcracking of the concrete paste, and results in loss of strength of the concrete matrix.

DEF has been found to be a worldwide problem which affects both precast and cast-in-place concrete structures. Cases have been including:

- Precast Concrete
    - Railroad sleepers (ties)
    - Slab panels
    - Prestressed beams

- Cast-in-place concrete
    - Dam structures
    - Concrete pavement
    - Highway bridges
    - Marine structures
    - Substation slabs

From this list, it is apparent that research should be conducted into understanding the role of DEF in the deterioration progress and methods of mitigating future damage of DEF in new or existing concrete structures.

This research was conducted in two phases. Phase 1 research will investigate the geographic extent within the Maryland Bridge Inventory, Maryland State Highway Administration owned bridges. The research will focus on documenting cases of DEF in bridges which show signs of distress. Livingston and Amde proposed a link between moist map cracking and DEF in concrete (2000). The population will investigate bridges with moist map cracking. The goal is to observe trends in the presences of DEF and the geographic extent of the prevalence of DEF throughout the State of Maryland.

The results of phase 1 showed DEF throughout the state. Also, the results revealed several different ettringite morphologies and apparent differences in the prevalence of ettringite in bridges with greater damage. Phase 2 was initiated to investigate the differences in morphology and apparent quantities. Several possible differences were investigated including the degree of moist map cracking and the

usage of air entrainment agent in order to establish a link with DEF in the concrete. If a link can be established, mitigation or prevention methods can be developed.

Phase 2 consisted of field studies and laboratory testing. The laboratory work involved testing methods of treating existing concrete. The test is modeled after previous work conducted at the University of Maryland (Amde et al 2006, 2005a, 2005b, 2005c, 2005d, 2005e, 2004, 2003a, 2003b) and (Livingston et al. 2006, 2002, 2001a, 2001b). The test was modified to include mitigation treatments after the concrete has developed ettringite. The goal of the test is reduce the expansion of the concrete.

1.2 Background

Delayed ettringite formation is a form of Internal Sulfate Attack (ISA), which is believe to be cause of most expansion and decrease of durability in concrete. Sulfate attacks use chemical and physical processes to change the chemical and microstructure of the cement past, which causes changes in the mechanical properties of the concrete resulting in deterioration.

Shimada et al. (2005) has preformed an extensive literature review of DEF-related expansion. They indicate that ettringite forms in the cement paste and causes expansion of the paste prior to being visible using the scanning electron microscope (SEM). This is supported by the research showing neat mortar suffering from DEF-related expansion. They further indicate that large crystal ettringite formed by a through-solution mechanism and dispersed in cracks, air voids, aggregate-paste interfaces, or bulk solution lead to little or no expansion. This type of ettringite in

open spaces is the result of "Ostwald ripening" which promotes dissolution of the fine ettringite crystal into the pore solution. The ettringite then recrystallizes in large formations in open areas.

A review of literature shows numerous publications of DEF in concrete. In 1965, Kennerly investigated deterioration of cold joints of the Roxburgh Dam, Otago, New Zealand. He found DEF in the deteriorated areas and showed that formation of ettringite was due to variations of calcium hydroxide (CH) concentrations. Ettringite was found in areas with high CH concentration, due to the solubility of ettringite which is inversely proportionate to the CH concentration in the solution.

Pettifer and Nixon found several incidence of ettringite in the pores, voids, and around the aggregates (1980). The affected concrete included concrete bases in the English Midlands and substations in Western England and South Wales. There research, although, found the co-existence of DEF with gel from alkali-aggregate reaction (AAR) (Pettifer and Nixon, 1980). AAR is another form of internal sulfate attack (ISA). The co-existence of DEF and AAR has since resulted in confusion as to which ISA causes the damage. In the same year, Pettifer and Nixon also found ettringite in the Pirow Street Bridge in Cape Town, South Africa just four (4) years after placement (1980).

In the 1980's, several marine structures also were found containing DEF. Volkwein and Springenschmid located needle-like ettringite crystals in the splash zone of concrete bridge decks (1981). They theorized that the chloride-contaminated bridge encouraged the development of ettringite utilizing sulfate originating in the concrete. El-Sayed observed deterioration of three (3) reinforced concrete marine

structures in Egypt (1987). Ettringite was found in existing cracks, leading El-Sayed to attribute the damage to DEF.

Even though DEF had been observed for over 20 years, most researches did not consider this a major problem. This changed in the late 1980's when the DEF problem gained widespread attention (Thomas 2001). In Germany, ettringite was found in the pores and cracks of precast concrete railway sleepers (ties) that had been cured at high temperatures (75-80°C) (Heinz 1987 and Tepponen 1987). The same problem was also observed in the United States. Like in Germany, the East Coast of the United States had early deterioration of precast concrete railway ties. Marusin revealed DEF crystals in the cracks of the concrete paste (1995). These results lead to significant changes in the methods of heat curing. Follow-up research was conducted and new regulations were throughout most of the world. Due to the widespread attention given to the case in Germany, the problem of DEF was commonly only associated with precast heat cured concrete, even though DEF had been discovered and documented in cast-in-place structures for over 20 years.

In the 1990's, Lawrence et al. examined numerous structures throughout Texas and found DEF related deterioration in both precast and cast-in-place concrete. He studied fifteen prestressed and reinforced concrete structures cast between 1963 and 1969 and observed expansive cracking after 15 to 20 year of service (1990). Later at the request of Texas Department of Transportation (TxDOT), Lawrence et al. looked into the premature deterioration of fifty-six (56) precast / prestressed concrete box beams (1999). The beams, which were to be installed for a highway bridges, had deteriorated in the fabricator storage yard. The research team suggested the primary

mechanism for distress was due to ettringite formations found in the concrete. Lawrence et al. (1999) documents Texas Department of Transportation's (TxDOT) experience with DEF and premature concrete deterioration. They indicate in numerous cases that DEF caused microcracking leading to premature deterioration. Their results came from scanning electron microscope (SEM) analysis of corings. The case of interest is four cast-in-place high mast lighting pole foundations constructed in 1989. The foundations exhibited extensive map cracking throughout, and TxDOT attributed the damage solely to DEF. The damage was so extensive that the foundations were considered structurally deficient and an emergency contract was executed to remove the high mast lighting poles. In addition to the high mast lighting pole foundations, a parking garage, constructed in 1986 and 1987, show cracking in the cast-in-place concrete foundation piers after just eight years of service. Both cases were attributed to DEF, by Lawrence et al. (1999).

In the 1990's, Gress (1997) in Iowa and Stark and Bollman (1997) in Germany reported cases of DEF in concrete pavement. In both cases the concrete pavement was showing signs of premature deterioration with cracking after less than 15 years of service.

In 2000, Brewer Stadium at Appalachian State University, Boone, North Carolina was found with 375 of 860 precast units that exhibited severe cracking and spalling. Ettringite was found in the cracks, voids, and around aggregates in the concrete paste (Ozol, 2000). The defects were significant enough that total reconstruction of the stadium was the economical solution.

In 2006, Divet, Pavoine, and Clement documented cases of ettringite in cast-in-place bridge concrete in France. Their results were very similar to cases of ettringite found in Maryland bridge concrete, by Amde et al. (2004).

1.3 Objectives and Scope of Work

The research will be conducted in two phases. The first phase primary objective was to increase the database on DEF occurrences through a systematic survey of representative Maryland bridges. Another objective was to evaluate two nondestructive test (NDT) methods that could provide indirect evidence of DEF damage. The ultrasonic Impact-Echo method evaluated the extent of cracking and deterioration of the concrete. Potassium autoradiography measured the level of potassium, which is believed to be important in the formation of ettringite. In addition to NDT, a limited number of cores were analyzed by scanning electron microscope (SEM) with energy dispersive analysis x-ray (EDAX). The findings of this research are presented in Ceary (2003).

The current research involved a comprehensive Scanning Electron Microscope study of concrete taken for selected bridges. From the information gathered, a second phase of the research was conducted.

Phase 2 was initiated following the results of Phase 1 field survey, which showed DEF in Maryland bridges. During Phase 1 research, Delayed Ettringite Formation (DEF) was identified in bridges throughout the State of Maryland (Amde et al. 2004b). The goal of Phase 1 research involved documenting the existence of DEF, so a "sick" patient population was utilized. The underlying theory stated that DEF

was prevalent in bridges with moist map cracking on the concrete surface. A total of 8 bridges with moist map cracking and 2 bridges without moist map crack were selected as the 8 "sick" bridges and 2 control bridges. The investigation found DEF in all bridges, but the quantity and morphology varied widely. Phase 1 work left several questions unanswered including:

1. The role of DEF in causing map cracking.
2. The significance of DEF morphology.
3. The prevalence of DEF in bridges without moist map cracking.

The purpose of Phase 2 research was to focus on unanswered questions 2 and 3, with the intent of the study to develop correlations between DEF morphology and moist map cracking. In order to accomplish meaningful correlations, wider selection criteria were used versus the Phase 1 population. Half the population was selected with moist map cracking and the other half without moist map cracking. The bridges with moist map cracking also had more variation in degree of moist map cracking than Phase 1 population in order to understand variations in DEF relative to extent of surface damage.

In addition, the population will consider the role of air entrainment agent (AEA) on the prevalence of DEF in bridges that used AEA versus bridges constructed before AEA was required. Additional literature research indicated that ettringite grows well in AEA (Cody et al 2001). According to the Office of Materials and Technology for the Maryland State Highway Administration, AEA was introduced into the concrete mix in 1980 or 1981 depending on the letting of the construction contract. In order to insure that AEA was used or not used the concrete tested, no

bridges were selected from 1980 or 1981. Half the population was selected with construction dates before 1980 and the other half with construction dates after 1981.

1. Develop a population to investigate the affects of air entrainment agent (AEA) and degree of moist map cracking. This population will contain half of the bridges with and half without the item under investigation to develop a better understanding of the role of AEA or moist map cracking.
2. Analyze the cores obtained using Scanning Electron Microscope (SEM) and Energy Dispersive Analysis X-ray (EDAX).
3. Analyze the cores obtained for alkali-silica reaction (ASR) using the UV-light test.
4. Develop trends or correlation between the geographic location, AEA, or moist map cracking and DEF.

Beyond field testing, Phase 2 also will investigate mitigation treatment for existing concrete affected with DEF. Mitigation test program will be developed including mitigation products, testing program, concrete mix, curing conditions, and storage conditions.

1.4 Outline of the Report

Chapter 2 discussed cement chemistry and focuses on the mechanisms and causes of DEF.

Chapter 3 describes the statistical sampling methodology, along with the structure of the Maryland Bridge Inventory, including the current bridge management databases and documents existing bridge inspection practices. The chapter discusses the development and presents the selected population for both phase 1 and 2 research.

Chapter 4 presents the results of the phase 1 coring program. The chapter details the methods and the equipment used to analyze the cores. The chapter concludes with a summary of findings.

Chapter 5 presents the results of the phase 2 coring program. The chapter details the results by coring location for uses in identifying trends with an affected bridge. The chapter concludes with a summary of findings.

Chapter 6 presents analysis of both phases of coring. The chapter discusses methods of correlating DEF to AEA or moist map cracking in phase 2 population. Then the trends were tested against the phase 1 population to verify. Finally, the findings are summarized.

Chapter 7 presents the laboratory program development for testing mitigation treatments for existing concrete. A literature review was conducted into identifying treatments for testing. The testing regimen is outlined, and results are discussed.

Chapter 8 provides the conclusions from the research, discusses remaining questions, and suggests future work arising out of the study.

Chapter 2
Cement Chemistry and Delayed Ettringite Formation

2.1 Introduction

Portland cement concrete is a widely used construction material because of its pourability, giving the user flexibility to shape as desired while providing high strength. Premature deterioration can significantly reduce the service life of concrete, and delayed ettringite formation (DEF) is one of the many forms of premature deterioration. Day, based on a comprehensive study of available literature, describes DEF as an expansion mechanism which is associated with extensive distributed cracking, commonly called map cracking, and reduced service life (1992). Structures with DEF may add life cycle cost to the bridge maintenance system by requiring unplanned repairs or replacements.

2.2 Cement Chemistry

Cement hydration is simply the reaction of water with various components of cement. Two theories attempt to explain the hardening of concrete. The Le Chatelier Theory states that the cement compounds go into solution first, then reconstitute in an interlocking maze. The Colloidal Theory states that cohesion is the result of direct solid state reaction which produces a gelatinous mass. Hydration does not typically

occur for all cement compounds, with some remaining unhydrated for years. This report assumes the reader has a working knowledge of cement components and hydration process. For an in-depth discussion of cement hydration, see (Taylor 1990). Cement chemist's notation will be used.

Table 2.1: Cement Chemists' Notation

Notation	Compound
C	CaO
S	SiO_2
$\hat{S}$	SO_3
A	Al_2O_3
H	H_2O

Of particular interest to this study is the hydration of aluminates, which is fundamental to the proper setting of concrete. Due to the rapid hydration of the aluminates (C_3A), the cement paste would immediately harden not allowing the formation of the concrete matrix. The addition of gypsum retards the rapid hydration of C_3A. The retardation occurs because ettringite ($C_6A\hat{S}_3H_{32}$) forms a coating around the C_3A particle (Collepardi et al. 1978). As ettringite grows, the cement remains plastic, and once the gap between cement particles is bridged, the setting process occurs. Depending on the cement composition, the ettringite can endure, but it typically reacts further (Taylor 1990). The formation of ettringite during the setting process in called Primary Ettringite Formation. Primary Ettringite Formation does not cause damage to the concrete.

2.3 Delayed Ettringite Formation

After the concrete has hardened, ettringite can form and expand in a process called Delayed Ettringite Formation (DEF, also called Secondary or Late Ettringite Formation). (Day 1992, Taylor 1993, Heinz and Ludwig 1987) have documented DEF and the deleterious effects on hardened concrete. Early studies focused on precast concrete members, which had high temperature heat treatments. Batic et al. (2000) indicate that DEF can occur at ambient temperature. Field studies of cast-in-place concrete have shown DEF in deteriorated concrete (Kennerly 1965; Pettifer and Nixon 1980; Volkwein and Springenschid 1981; El-Sayed 1987; Heinz 1987; Tepponen 1987; Larive and Louran 1992; Lawrence et al. 1990; Marusin 1995; Gress 1987; Stark and Bollman 1997, Lawrence 1999; Schlorholtz 2000; Ozol 2000; Amde et al. 2004; and Divet, Pavoine, and Clement 2006). Still it is difficult to directly correlate the potential for expansion with the deterioration occurring in the field, since the mechanism of DEF has not been established. Lawrence et al. (1999) documents Texas Department of Transportation's (TxDOT) experience with DEF and premature concrete deterioration. They indicate in numerous cases that DEF caused microcracking leading to premature deterioration. Their results came from scanning electron microscope (SEM) analysis of corings. The case of interest is four cast-in-place high mast lighting pole foundations constructed in 1989. The foundations exhibited extensive map cracking throughout, and TxDOT attributed the damage solely to DEF. The damage was so extensive that the foundations were considered structurally deficient and an emergency contract was executed to remove the high mast lighting poles. Amde et al (2004) and Divet, Pavoine, and Clement (2006) show

cases of DEF in highway bridges with associated map cracking. Both research teams believe the ettringite has lead to the concrete deterioration. Gress (1997), Stark and Bollman (1997), and Cody et al. (2004) have demonstrated that concrete highway pavement can also exhibit DEF and premature deterioration of the roadway surface.

2.1.1 Mechanism of DEF Expansion

The mechanism of DEF expansion is a highly debated issue. Ettringite Crystal Growth Theory and Uniform Paste Expansion Theory are the two predominant theories. Heinz and Ludwig (1987), Lawrence et al. (1990) suggest the Ettringite Crystal Growth Theory, which attributes the expansion to pressure exerted by the growing ettringite crystals in the microcracks between the cement paste and the aggregate. Scrivener and Taylor (1993), Johanson et al. (1993) proposed the Uniform Paste Expansion Theory, which suggest that the concrete expands and then the ettringite forms in the newly created gaps. Yang et al. (1999) found no evidence to support the Uniform Paste Theory concluding that the ettringite present in the mortar produced the expansion. Lawrence (1994) further observed that the ettringite forms only partially around aggregates. The absence of ettringite in cracks around the entire aggregate tends to question the Uniform Paste Expansion Theory, since the theory accepts a uniform expansion and therefore a uniform distribution of ettringite. Unlike Lawrence and Yang et al., Shimada et al. (2005), in a recent literature review, indicates that the paste expansion theory explains the homogenous volume change observed in laboratory specimen. They also note that DEF was observed in neat paste specimen, which have no aggregates as required by the crystal growth theory. Both

theories lack conclusive evidence because DEF expansion leaves behind only the effect. Day (1993) suggests that both mechanisms are possible and depending on the environmental condition one may be more prevalent.

2.1.2 Potassium and DEF

Recent studies suggest that the potassium content of the concrete may be a significant factor in the damage process. (Gress 1997) indicated that there was a significant correlation between potassium content and degree of damage in field studies of concrete pavement. (Ramadan 2000) in laboratory studies also suggests that significant correlation is present between potassium content and degree of damage. (Livingston and Amde 2000) propose the following chemical reactions cause the formation of ettringite in which monosulfate ($C_4A\hat{S}H_{12}$) reacts to become ettringite ($C_6A\hat{S}_3H_{32}$).

$$C_4A\hat{S}H_{12} + 2Ca^{2+} + 2SO_4^{2-} + 20H_2O \rightarrow C_6A\hat{S}_3H_{32}$$

Potassium is commonly found in Portland cement as potassium sulfate and usually comes from illitic clay, which is used as a raw material in the production of Portland cement. Once water is added to the cement, the potassium sulfate reacts and calcium sulfate precipitates yielding the required ingredients for the reaction shown above.

$$K_2SO_4 + Ca^{2+} + 2OH^- \rightarrow 2K^+ + 2OH^- + CaSO_4$$

The potassium over time reacts with the atmosphere to produce potassium carbonate.

$$2K^+ + CO_3^{2-} \rightarrow K_2CO_3$$

Since potassium carbonate has a very low critical relative humidity for deliquescence (RH=43%), the surface cracks associated with DEF damage commonly exhibit a wet or moist zone along the cracks.

2.1.3 Alkali-Silica Reaction (ASR)

Premature deterioration of concrete due to alkali-silica reaction has been found throughout the world, and ASR is associated with map cracking on the surface of concrete members. Some members affected by ASR exhibit DEF as well, which leads to confusion as to the exact expansion mechanism that caused the damage.

Alkali oxides from cement and silica from aggregates are the key ingredients in the formation of ASR. Reactive aggregates include: chalcedony, certain forms of stained quartz, cherts, flints, and opals according to Mehta (1986). In the presences of water, the alkali hydroxides go into solution and then react with reactive silica, which produces calcium and alkali silicate gel. Taylor suggests the formation of the gel itself does not cause damage, absorption of water by the gel causes expansion and cracking once the tensile stress of the concrete is exceeded (1990).

Chapter 3

Field Studies: Maryland Bridge Inventory

3.1 Introduction

Characterization of bridge condition has traditionally involved an exhaustive approach. That is, all bridges in a specific inventory are periodically inspected and a standard set of data items are recorded. This approach is exemplified by the National Bridge Inventory and PONTIS. Recently several studies have used a statistical sampling approach, in which only a limited number of bridges are actually inspected, and the results are extrapolated to the entire population. Typically, this approach is used because the type of data being collected involves going beyond visual inspection to test methods that are time-consuming, expensive and may require destructive sampling. Consequently, the costs of an exhaustive survey of a given state's population of bridges, which can number on the order of thousands, would be prohibitively large. However, sampling introduces its own set of issues which must be considered. These include the statistical methodology, the appropriate sample size, the method of selecting the sample and level of confidence.

Field testing for ettringite involved Maryland State Highway Administration (MDSHA) bridge inventory, which includes all bridges on state routes, US routes, and most interstate bridges. MDSHA is divided into seven districts, (see Figure 3.1).

The MDSHA bridge inventory contains reinforced concrete, prestressed concrete, and steel bridges. The breakdown by type is given below, (see Table 3.1).

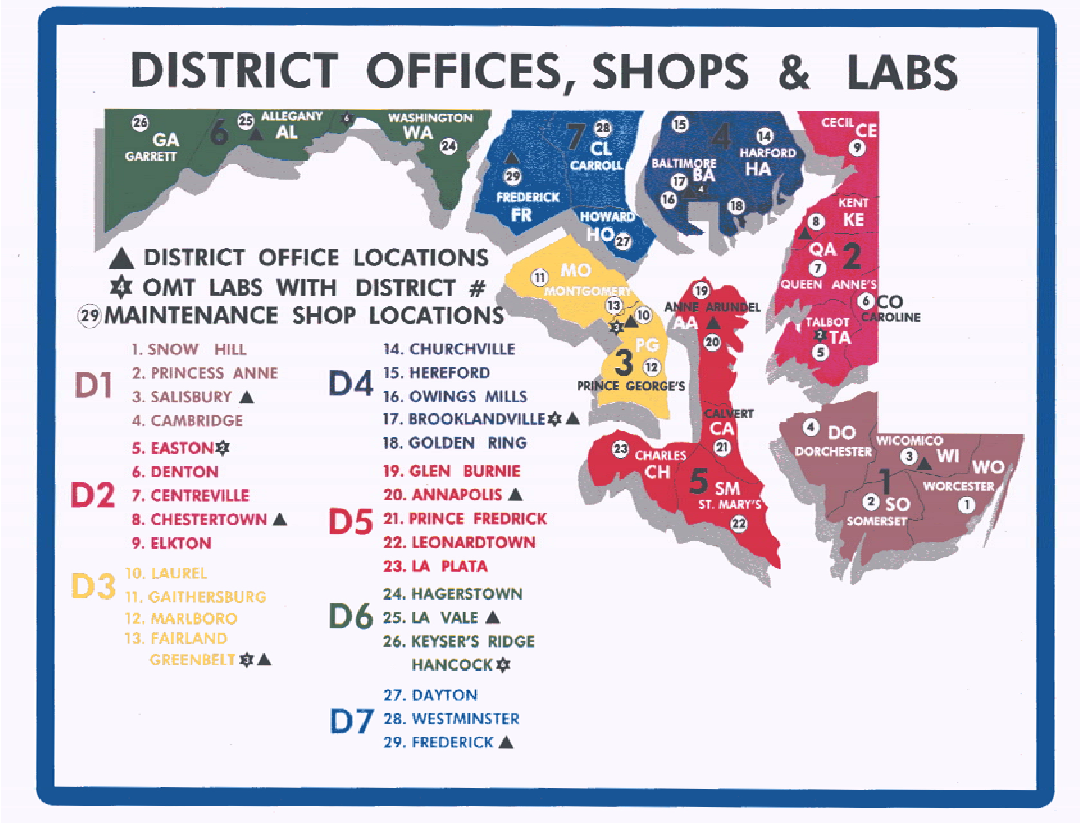

Figure 3.1: MDSHA District Map (Maryland State Highway Administration)

Table 3.1: Breakdown by Structure Type

Structure Type	District 1	District 2	District 3	District 4	District 5	District 6	District 7	State Total
Concrete	40	87	129	106	91	125	126	**704**
Concrete Continuous	7	11	3	5	3	6	18	**53**
Steel	45	74	204	231	136	136	175	**1001**
Steel Continuous	25	27	123	125	100	121	119	**640**
Prestressed (Pretensioned) Concrete	16	8	5	7	13	3	4	**56**
Prestressed (Pretensioned) Concrete Continuous	2	2	2	0	0	2	1	**9**
Prestressed (Post-tensioned) Concrete	0	0	0	0	0	0	0	**0**
Prestressed (Post-tensioned) Concrete Continuous	0	0	0	0	0	0	0	**0**
						Total		**2463**

3.2 Bridge Management Systems

American Association of State Highway and Transportation Officials (AASHTO) developed the "Manual for Condition Evaluation of Bridges" and encourages the use of Bridge Management Systems (BMS). AASHTO writes, "Bridge Management Systems may be used as a tool in allocating limited resources to the inspection, maintenance, rehabilitation and replacement of bridges" (American Association of State Highway and Transportation Officials 2000). MDSHA currently maintains two databases: PONTIS and Structural Inventory and Appraisal (SI&A). SI&A contains all information pertaining to the structure, such as age, materials, type, length, height, detour length, etc, and includes a general evaluation of the major components, such as the deck, superstructure, substructure, channel, etc. (Maryland State Highway Administration Office of Bridge Development 1993). PONTIS concentrates on evaluating the elements and quantifies the condition level of various elements (Maryland State Highway Administration Office of Bridge Development 1996). See Figure 3.2 for a sample PONTIS form. The example is a bridge that has

1078 feet precast concrete interior girders in good condition, so the form is coded as 1078 condition state 1 (CS1). The MDSHA PONTIS book gives the description for the condition state, which in this case is good condition with no repairs required. Along with the quantifiable condition evaluation, the bridge inspector gives explanation of the defects. The comments given in this example are that the beams are in good condition and a minor comment about a small spall. Unprotected slopes, another item from the example form, indicate that both unprotected slopes are condition state 3 (CS3), which in this case is in poor condition needing various repairs. The comments given by the inspectors try to clarify the type of work which should be preformed. All of the field inspectors' data goes into the database, and MDSHA utilizes Microsoft Access © to manage the bridge system by developing queries based on priority of needs. This allows MDSHA to match needs with limited funds in an efficient manner.

CECIL COUNTY BRIDGE INSPECTION REPORT

BRIDGE NUMBER: CE000300 INSPECTION DATE: 10/8/2001

(58) DECK:	7	**(59) SUPERSTRUCTURE:**	7	**(60) SUBSTRUCTURE:**	7
(61) CHANNEL:	5	**(62) CULVERT:**	N		

ELEMENT		TQ	CS 1	CS 2	CS 3	CS 4	CS 5
026	**Concrete Deck, Protected with Coated Bars (EA)**	1	1				
	Deck has random hairline longitudinal cracks including several full-length hairline cracks. The traffic paint markings have been totally worn away.						
104	**Prestressed Concrete Closed Web/Box Girders (LF)**	1078	1078				
	Good Condition. Minor spalls on upstream fascia beam, 3" diameter x ½"D and 1 ½" x 3" x ¼"D. Open drainge/port holes in bottom of beams.						
210	**Reinforced Concrete Pier Wall (LF)**	33	33				
	Good Condition. Scour is occurring around the pier. The footing is exposed by 12"- 18" in depth. No undermining is noted, but along the west side of the pier the streambed has lowered by as much as 22". No protection is provided for the pier footing.						
215	**Reinforced Concrete Abutment (LF)**	62	62				
	The abutment concrete caps are in good condition.						
217	**Other Material Abutment (LF)**	62		62			
	Good Condition. West abutment has missing mortar.						
253	**Other Material Wingwalls (LF)**	91		91			
	Wing walls have mortar missing in joints. The preformed joint between the northeast wing wall and the east abutment has failed. The southwest wing wall has a 4" x 12" x 2"D spall along cold joint exposing the third guardrail post anchor bolt. The northwest wing wall has a 4" x 4" x 3"D spall in the concrete cap along the bottom edge of cap. Above northeast wing wall, the outside of the parapet at the third guardrail post has a spall 12" x 4" x 2 ½"D with an exposed post anchor bolt. This spall continues on top of the wall 5" x 4".						
261	**Unprotected Slope (dirt) (EA)**	2			2		
	On the north east side of the bridge the bank has heavily eroded between the bridge and the point that Basin Run meets Octoraro Creek. Approximately 5' of erosion has occurred since the last inspection. Riprap bank protection is thin upstream from the bridge on the east side. Under the bridge the riprap is partially buried under sand.						

Figure 3.2: Sample PONTIS Form (Tuhin Basu & Associates 2002)

3.3 Bridge Selection for Field Sampling – Phase 1

In developing a population of bridges, several statistical models and methods were investigated. The purpose of the research involves investigating the existence of ettringite in concrete elements of MDSHA bridges, and because the objective only required investigating and not quantifying the existence of ettringite, a reduced population with a high probability was investigated. From this "sick patient" population, a spatial distribution was chosen to be representative of the distribution of MDSHA bridges.

In order to reduce the total population to the "sick" population, the PONTIS database was used by querying for concrete element with descriptions containing the phrase "map crack". From the query, a possible bridge element list was started with the basic bridge information, type of element with map cracking, and inspector's comments about that element. In order to have all information available in the project bridge list, the data from the SI&A database was added to provide the bridge demographics that are not included in the PONTIS database. Once the SI&A data is added, the project bridge list could be used to determine the breakdown by type and location throughout the state.

Of the 2463 bridges owned by the MDSHA, 905 bridges have at least one element with map cracks as noted by bridge inspectors in the PONTIS database. But map cracking alone was found to be too general as a description, since map cracking is often associated with several possible causes including: overstress, improper stripping of formwork, ASR, and DEF. Additional refinement of the list was needed to increase the probability of incidence in the selected bridges.

Livingston and Amde suggest that bridges with DEF often appear as map cracking with moisture surrounding the cracks, so bridges were selected from the project database based on the inspectors' verbiage matching this description (2000). To further reduce the "sick" population to the test population, test bridges were selected at random from the "sick" population within a given MDSHA district, which allowed the test population to match the spatial distribution of the overall MDSHA spatial distribution. Two bridges were also selected that did not exhibit map cracking, and provide control samples for the project. See Table 3.2 for spatial breakdown and Table 3.3 for test bridge list including the control bridges.

Table 3.2: Spatial Distribution of MDSHA Bridges

Structure Type	District 1	District 2	District 3	District 4	District 5	District 6	District 7	**State Total**
Concrete	40	87	129	106	91	125	126	**704**
Concrete Continuous	7	11	3	5	3	6	18	**53**
Steel	45	74	204	231	136	136	175	**1001**
Steel Continuous	25	27	123	125	100	121	119	**640**
Prestressed (Pretensioned) Concrete	16	8	5	7	13	3	4	**56**
Prestressed (Pretensioned) Concrete Continuous	2	2	2	0	0	2	1	**9**
Prestressed (Post-tensioned) Concrete	0	0	0	0	0	0	0	**0**
Prestressed (Post-tensioned) Concrete Continuous	0	0	0	0	0	0	0	**0**
	135	209	466	474	343	393	443	**2463**
	5.48%	8.49%	18.92%	19.24%	13.93%	15.96%	17.99%	**100.00%**

A testing population of 14 bridges and 2 control bridges was selected. See Table 3.4 for breakdown by district. This population was developed for non-destructive testing (NDT) methods research that was published under Pilot NDT Field Survey of Maryland Bridges for Delayed Ettringite Formation Damage (Ceary, 2003). Following the NDT research, scanning electron microscopy analysis was performed

on cores taken from 9 of the 16 bridges in the population. The detailed results are presented herein.

Table 3.3: Bridge Selection for Field Study – Phase 1

Testing #	Bridge #	Location	District
1	2203201	US 13 NB over MD 346	1
2	0500800	MD 404 over Watts Creek	2
3	1511300	Greentree Rd over I-495	3
4	1600400	US 1 over Paint Branch	3
5	1620003	MD198 over I-95	3
6	0311100	CSX over I-695	4
7	0314200	Old Court Rd Over I-695	4
8	0333402	I-795 over Franklin Blvd	4
9	0208303	MD 100 EB over MD 174	5
10	0800201	MD 5 NB over Zekiah Swamp	5
11	1102100	US 219 over Deep Creek Lake	6
12	2115004	I-70 WB over MD 632	6
13	0605800	Ladiesburg Rd. over Little Pipe Creek	7
14	1311000	MD 32 EB over US 1	7
C1	0333702	I-795 over Cockeys Mill Rd	3
C2	1301302	US 29 over Middle Patauxent River	7

Table 3.4: Distribution of Bridge Selection by District – Phase 1

District	Percentage of State's Bridge Population	Bridges Selected per District	Percentage of Test Population	Percentage of District Bridges Tested
1	5.48%	1	6.25%	0.74%
2	8.49%	1	6.25%	0.48%
3	18.92%	3	18.75%	0.64%
4	19.24%	4*	25.00%	0.84%
5	13.93%	2	12.50%	0.58%
6	15.96%	2	12.50%	0.51%
7	17.99%	3*	18.75%	0.68%
Total	100.00%	16	100.00%	0.65%

* Including Control Bridges

3.4 General Description of Selected Bridges – Phase 1

A brief description of each bridge tested is provided for reference. The element selected for testing is shown and the location is given in detail.

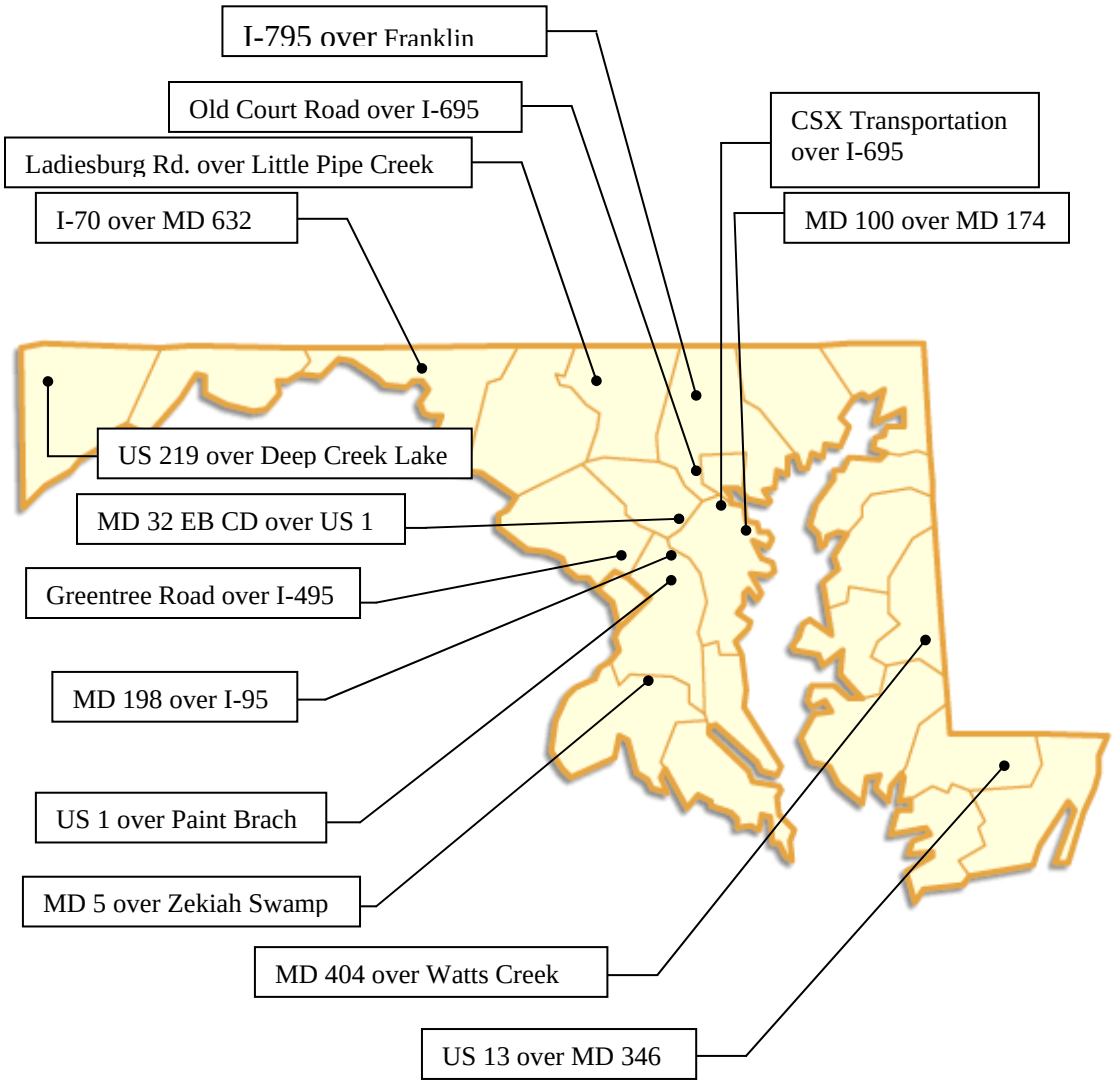

Figure 3.3: Bridge Locations

3.4.1 Bridge 2203201 (US 13 Northbound {NB} over MD 346)

Bridge 2203201 is a three span structure built in 1972, with 32 foot end spans supported by cast-in-place concrete girders and 76 foot center span carried by steel beams. Testing was preformed on the center concrete girder of the south end span, see Figure 3.4. The concrete girders exhibited minor map cracking (hairline cracks), see Figure 3.5 for a close-up of the side of the girder.

Figure 3.4: Test Location (2203201 – US 13 NB over MD 346)

Figure 3.5: Close-Up of Test Location (2203201 – US 13 NB over MD 346)

3.4.2 Bridge 0500800 (MD 404 over Watts Creek)

Bridge 0500800 is a four span structure originally built in 1949 and reworked in 1986, with four – 49 foot spans supported by steel beams, see Figure 3.6. Map cracking was not observed on this structure, and no testing was preformed.

Figure 3.6: General Elevation (0500800 – MD 404 over Watts Creek)

3.4.3 Bridge 1511300 (Greentree Rd over I-495)

Greentree Road bridge over I-495 (Capital Beltway) is a four span steel beam structure built in 1962 with 40 foot northern end span, 2 – 74 foot center spans, and a 48 foot southern end span. The roadway width for Greentree Road is 30 feet with sidewalks on both sides, and testing was conducted on the inside face of the west parapet wall on the span over I-495 Outer Loop. The parapet and sidewalk show heavy rusting possibly due to previous fencing and exhibit minor to severe map cracking throughout with occasional locations of efflorescence, see Figures 3.7 and 3.8 for the general test location and Figure 3.9 for a close-up.

Figure 3.7: General Test Location (1511300 - Greentree Rd over I-495)

Figure 3.8: Test Location (1511300 - Greentree Rd over I-495)

(a) Test Location – Clean **(d) Test Location - Dirty**

Figure 3.9: Greentree Rd over I-495 (1511300)

Two locations were identified for testing, a “clean” location which is a baseline reference location with as little map cracking as possible and a “dirty” location which exhibits heavy map cracking. This step is preformed for all bridges were possible. Some bridges exhibited a more uniform distribution of cracking which made the clean location must harder to select. Bridge 1511300 exhibited drastic difference between the clean and dirty locations.

3.4.4 Bridge 1600400 (US 1 over Paint Branch)

Bridge 1600400 is a two span steel girder structure built in 1980 with a roadway width of 68 feet not including sidewalks along both sides, and 2 -80 foot spans; see Figure 3.10 for general testing location and Figure 3.11 for bridge elevation. The test was preformed on the northwest wingwall, which exhibited moist map cracking throughout the wingwall see Figure 3.12.

Figure 3.10: General Test Location (1600400 - US 1 over Paint Branch)

Figure 3.11: Bridge Elevation (1600400 - US 1 over Paint Branch)

Figure 3.12: Test Location (1600400 - US 1 over Paint Branch)

3.4.5 Bridge 1620003 (MD 198 over I-95)

Bridge 1620003 is a four span steel girder structure over I-95 built in 1971 and has a roadway width of 52 feet, with a 57 foot northern end span, a 137 foot northern center span, a 157 foot southern center span, and a 105 foot southern end, see Figure 3.13. The test was preformed on the exterior side of the southwest parapet wall above the southwest wingwall, see Figure 3.14. The parapet and wingwall exhibited moist map cracking at random locations throughout the wingwall and parapet. A thorough visual inspection of the exterior side of the south parapet wall for map cracking was not possible due to the heavy traffic volume on I-95.

Figure 3.13: Bridge Elevation (1620003 – MD 198 over I-95)

Figure 3.14: Test Location (1620003 – MD 198 over I-95)

3.4.6 Bridge 0311100 (CSX Transportation over I-695)

CSX Transportation bridge over I-695 (Baltimore Beltway) is a two span steel girder structure built in 1957 with 2 - 75 foot spans and a roadway width for CSX Transportation of 57 feet and 4 inches, see Figure 3.15. Testing was conducted on the northwest wingwall. The wingwall exhibits minor to severe map cracking throughout with occasional locations of efflorescence, see Figure 3.16.

Figure 3.15: Bridge Elevation (0311100 - CSX Transportation over I-695)

Figure 3.16: Test Location (0311100 - CSX Transportation over I-695)

3.4.7 Bridge 0314200 (Old Court Rd over I-695)

Old Court Road bridge over I-695 (Baltimore Beltway) is a two span steel girder structure built in 1983, with a 137 foot eastern span, a 161 foot western span, and a roadway width for Old Court Road of 50 feet wide not including sidewalks on both sides, see Figure 3.17. Testing was conduced on the outside face of the north parapet wall over the northwest wingwall. The parapet wall exhibits minor map cracking in scattered locations, see Figures 3.18 and 3.19.

Figure 3.17: Bridge Elevation (0314200 - Old Court Rd over I-695)

Figure 3.18: Test Location (0314200 - Old Court Rd over I-695)

(a) Test Location - Clean **(d) Test Location - Dirty**

Figure 3.19: Old Court Rd over I-695 (0314200)

3.4.8 Bridge 0333402 (I-795 over Franklin Blvd.)

Bridge 0333402 is a two span steel girder structure built in 1985, with a 73 foot northern span, a 90 foot southern span, and a roadway width for I-795 of 50 feet wide, see Figure 3.20. Testing was conducted on the south side of the median pier. The pier exhibits minor map cracking in scattered locations and has been epoxy coated, see Figure 3.21.

Figure 3.20: Test Location (0333402 - I-795 over Franklin Blvd.)

Figure 3.21: I-795 over Franklin Blvd. (0333402)

3.4.9 Bridge 0208303 (MD 100 Eastbound {EB} over MD 174)

Bridge 0208303 is a four span steel beam structure built in 1985, with 33 feet end spans, 44 feet center spans, and a roadway width for MD 100 of 30 feet wide. Testing was conducted on the west abutment. The abutment exhibits minor map cracking in scattered locations and has been partially epoxy coated, see Figures 3.22 and 3.23.

Figure 3.22: Test Location (0208303 - MD 100 EB over MD 174)

Figure 3.23: MD 100 EB over MD 174 (0208303)

3.4.10 Bridge 0800201 (MD 5 NB over Zekiah Swamp)

Bridge 0800201 is a two span steel beam structure built in 1966, with 2 - 35 feet center spans, and a roadway width for MD 5 of 40 feet wide, see Figure 3.24. Testing was conducted on the inside face of the east parapet wall. The parapet wall exhibits minor map cracking in scattered locations around and on the curb, see Figures 3.25.

Figure 3.24: Bridge Elevation (0800201 - MD 5 NB over Zekiah Swamp)

Figure 3.25: Typical Map Cracking (0800201 - MD 5 NB over Zekiah Swamp)

3.4.11 Bridge 1102100 (US 219 over Deep Creek Lake)

US 219 over Deep Creek Lake is a three span steel girder structure built in 1987, with 210 feet end spans, 260 foot center span, and a roadway width for US 219 of 40 feet wide, see Figure 3.26. Testing was conducted on the northwest wingwall. The wingwall exhibits minor map cracking throughout, see Figure 3.27.

Figure 3.26: Bridge Elevation (1102100 - US 219 over Deep Creek Lake)

Figure 3.27: Test Location (1102100 - US 219 over Deep Creek Lake)

3.4.12 Bridge 2111504 (I-70 Westbound {WB} over MD 632)

I-70 westbound bridge over MD 632 is a four span steel beam structure built in 1966 with a 38 foot eastern end span, 2 – 47 foot center spans, a 41 foot western end span, and a roadway width for I-70 WB of 40 feet. Testing was conducted on the eastern pier. The dirty location was on the southern column, and the clean location was on the center column. The southern column exhibits minor map cracking throughout, see Figure 3.28.

Figure 3.28: Test Location (2111504 - I-70 WB over MD 632)

3.4.13 Bridge 0605800 (Ladiesburg Rd. over Little Pipe Creek)

Bridge 0605800 is a three span concrete girder structure built in 1965, with 3 - 35 feet spans and a roadway width for Ladiesburg Road of 24 feet wide, see Figure 3.29. Testing was conducted on the south abutment. The abutment exhibits minor map cracking in scattered locations, see Figure 3.30.

Figure 3.29: Bridge Elev. (0605800 – Ladiesburg Road over Little Pipe Creek)

Figure 3.30: Test Location (0605800 – Ladiesburg Road over Little Pipe Creek)

3.4.14 Bridge 1311000 (MD 32 EB over US 1)

MD 32 EB bridge over US 1 is a two span steel girder structure built in 1983, with a 111 foot eastern span, a 107 foot western span, and a roadway width for MD 32 EB of 43 feet, see Figure 3.31. Testing was conducted on the southeast wingwall, which exhibited minor map cracking throughout, see Figure 3.32.

Figure 3.31: General Test Location (1311000 - MD 32 EB over US 1)

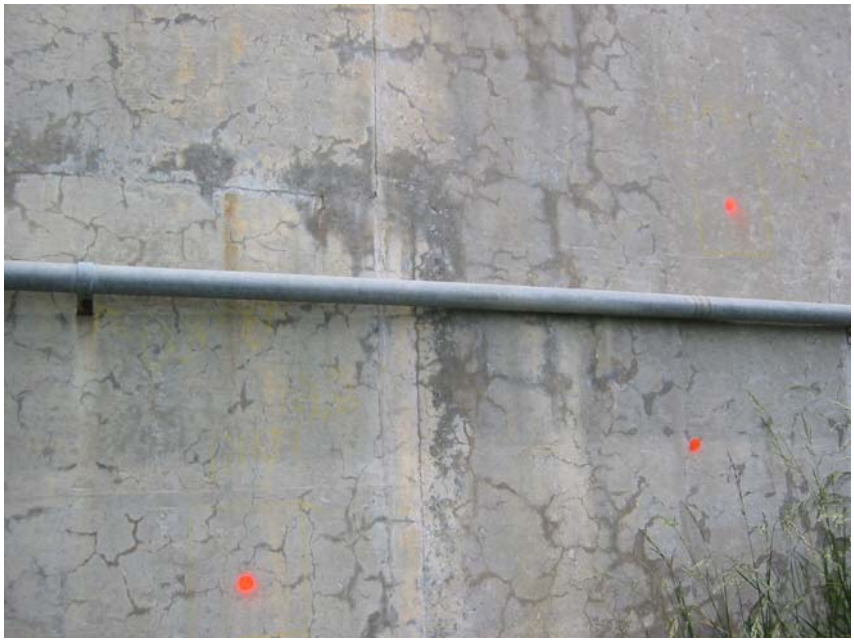

Figure 3.32: Test Location (1311000 - MD 32 EB over US 1)

3.4.15 Control Bridge 0333702 (I-795 bridge over Cockeys Mill Road)

I-795 bridge over Cockeys Mill Road is a three span steel girder structure built in 1985, with 38 foot end spans, a 66 foot center span, and a roadway width for I-795 of 50 feet, see Figure 3.33.

Figure 3.33: Test Location (0333702 – I-795 over Cockeys Mill Road)

3.4.16 Control Bridge 1301302 (US 29 Southbound {SB} over Middle Patuxent River)

US 29 bridge over Middle Patuxent River is a three span steel beam structure built in 1970, with 45 foot end spans, a 50 foot center span, and a roadway width for US 29 of 52 feet, see Figure 3.34.

Figure 3.34: Test Location (1301302 – US 29 SB over Middle Patuxent River)

3.5 Bridge Selection for Field Sampling – Phase 2

Phase II was initiated following the results of Phase I field survey, which showed DEF in Maryland bridges. During Phase 1 research, Delayed Ettringite Formation (DEF) was identified in bridges throughout the State of Maryland (Ceary et al. 2004). The goal of Phase 1 research involved documenting the existence of DEF, so a "sick" patient population was utilized. The underlying theory stated that DEF was prevalent in bridges with moist map cracking on the concrete surface. A total of 8 bridges with moist map cracking and 2 bridges without moist map crack were selected as the 8 "sick" bridges and 2 control bridges. The investigation found DEF in all bridges, but the quantity and morphology varied widely. Phase 1 work left several questions unanswered including:

1. The role of DEF in causing map cracking.
2. The significance of DEF morphology.
3. The prevalence of DEF in bridges without moist map cracking.

The purpose of Phase 2 research was to focus on unanswered questions 2 and 3, with the intent of the study to develop correlations between DEF morphology and moist map cracking. In order to accomplish meaningful correlations, wider selection criteria were used versus the Phase 1 population. The population was selected to investigate two independent variables. Half the population was selected with moist map cracking and the other half without moist map cracking. The bridges with moist map cracking also had more variation in degree of moist map cracking than Phase 1 population in order to understand variations in DEF relative to extent of surface damage.

In addition, the population will consider the role of air entrainment agent (AEA) on the prevalence of DEF in bridges that used AEA versus bridges constructed before AEA was required. Additional literature research indicated that ettringite grows well in AEA (Cody et al 2001). According to the Office of Materials and Technology for the Maryland State Highway Administration, AEA was introduced into the concrete mix in 1980 or 1981 depending on the letting of the construction contract. In order to insure that AEA was used or not used the concrete tested, no bridges were selected from 1980 or 1981. Half the population was selected with construction dates before 1980 and the other half with construction dates after 1981.

The two population selection criteria are independent; therefore one large population can be developed with both selection criteria in mind. The resulting population will have four subsets including:

1. Bridges without moist map cracking built before 1980.
2. Bridges without moist map cracking built after 1981.
3. Bridges with moist map cracking built before 1980.
4. Bridges with moist map cracking built after 1981.

The minimum statistically significant sample size is 3 bridges, which will result in a total population of 12 bridges. Bridges were selected from Maryland Bridge Inventory data that includes physical data like type, size, location, and date of construction and defect data like map cracking. Candidate bridges were selected on a random basis from the Greater Baltimore-Washington area (excluding Eastern Shore, Western Maryland, and Southern Maryland to limit driving distances). From this list,

target bridges were selected based on ease of access. The target bridges were than visited to verify if the bridge inventory data was accurate. Several bridges were rejected because moist map cracking was identified on the concrete surface that had not been indicated in the bridge inventory database. If the bridge was rejected due to the sub-subpopulation being filled, near by bridges were investigated which meet needed criteria. See Table 3.5 for the list of bridges in the total population and Table 3.6 for the population breakdown.

Table 3.5: Bridge Selection for Field Study – Phase 2

Bridge #	Route	Over	County	Year Built
0208304	MD 100 WB	MD 174	Anne Arundel	1963
0217202	MD 10 SB	MD 177	Anne Arundel	1988
0219000	Queenstown Rd	MD 100	Anne Arundel	1996
0311100	CSX	I-695	Baltimore	1957
0333900	MD 140 SB	I-795 Ramps 'I' & 'G'	Baltimore	1985
1005000	MD 77	Hunting Creek	Frederick	1970
1005600	MD 77	Double Pipe Creek	Frederick	1989
1011100	US 15 SB	Fishing Creek	Frederick	1961
1308603	MD 175 EB	US 29	Howard	1974
1315004	MD 100 WB	Dorsey Station Road	Howard	1996
1315700	MD 32	River Rd, Patapsco River	Howard	2003
1612300	I-95 X SB	I-495 OL	Prince Georges	1967

Table 3.6: Population Breakdown – Phase 2

	Bridges with Moist Map Cracking	Bridges without Moist Map Cracking
Pre 1980	0208304 0311100 1308603	1005000 1011100 1612300
Post 1980	0333900 1315004 1315700	0217202 0219000 1005600

3.5.1 Bridge 0208304 (MD 100 WB over MD 174)

Bridge 0208304 is a four span structure built in 1963, with 33 foot end spans and 44 foot interior spans supported by steel beams. The superstructure rests on cast-in-place concrete abutments and piers. Cores were taken from the west abutment under the north exterior beam; see Figure 3.35 for the general coring location and Figure 3.36 for the coring locations.

Figure 3.35: General Location (0208304 – MD 100 WB over MD 174)

Figure 3.36: Test Location (0208304 – MD 100 WB over MD 174)

3.5.2 Bridge 0217202 (MD 10 SB over MD 177)

Bridge 0217202 is a four span structure built in 1988, with 51 and 66 foot end spans and 82 foot interior spans supported by steel beams. The superstructure rests on cast-in-place concrete abutments and piers. Cores were taken from the outside face of the south parapet near the southwest wingwall; see Figure 3.37 for the general coring location and Figure 3.38 for the coring locations.

Figure 3.37: General Location (0217202 – MD 10 SB over MD 177)

Figure 3.38: Test Location (0217202 – MD 10 SB over MD 177)

3.5.3 Bridge 0219000 (Queenstown Road over MD 100)

Bridge 0219000 is a two span structure built in 1996, with 150 and 155 foot spans supported by steel girders. The superstructure rests on cast-in-place concrete abutments and pier. Cores were taken from the northeast wingwall; see Figure 3.39 for the general coring location and Figure 3.40 for the coring locations.

Figure 3.39: General Location (0219000 – Queenstown Road over MD 100)

Figure 3.40: Test Location (0219000 – Queenstown Road over MD 100)

3.5.4 Bridge 0311100 (CSX Transportation over I-695)

Bridge 0311100 is a two span structure built in 1957, with 75 foot spans supported by steel girders. The superstructure rests on cast-in-place concrete abutments and pier. Cores were taken from the northwest wingwall; see Figure 3.41 for the general coring location and Figure 3.42 for the coring locations.

Figure 3.41: General Location (0311000 – CSX Transportation over I-695)

Figure 3.42: Test Location (0311000 – CSX Transportation over I-695)

3.5.5 Bridge 0333900 (MD 140 SB over I-795 Ramps 'I' & 'G')

Bridge 0333900 is a two span structure built in 1985, with 132 foot spans supported by steel girders. The superstructure rests on cast-in-place concrete abutments and piers. Cores were taken from the northeast wingwall; see Figure 3.43 for the general coring location and Figure 3.44 for the coring locations.

Figure 3.43: Gen. Location (0333900 – MD 140 SB over I-795 Ramps 'I' & 'G')

Figure 3.44: Test Location (0333900 – MD 140 SB over I-795 Ramps 'I' & 'G')

3.5.6 Bridge 1005000 (MD 77 over Hunting Creek)

Bridge 1005000 is a three cell culvert structure built in 1970, with 10 foot by 7 foot cell openings. The culvert has cast-in-place concrete headwalls and wingwalls. Cores were taken from the southeast wingwall; see Figure 3.45 for the general coring location and Figure 3.46 for the coring locations.

Figure 3.45: General Location (1005000 – MD 77 over Hunting Creek)

Figure 3.46: Test Location (1005000 – MD 77 over Hunting Creek)

3.5.7 Bridge 1005600 (MD 77 over Double Pipe Creek)

Bridge 1005600 is a three span structure built in 1989, with 70 and 69 foot end spans and 71 foot interior span supported by steel girders. The superstructure rests on cast-in-place concrete abutments and piers. Cores were taken from the outside face of the south parapet over the southeast wingwall; see Figure 3.47 for the general coring location and Figure 3.48 for the coring locations.

Figure 3.47: General Location (1005600 – MD 77 over Double Pipe Creek)

Figure 3.48: Test Location (1005600 – MD 77 over Double Pipe Creek)

3.5.8 Bridge 1011100 (US 15 SB over Fishing Creek)

Bridge 1011100 is a three span structure built in 1961, with 21 foot end spans and 22 foot interior span supported by concrete slab. The superstructure rests on cast-in-place concrete abutments and piers. Cores were taken from the northwest wingwall; see Figure 3.49 for the general coring location and Figure 3.50 for the coring locations.

Figure 3.49: General Location (1011100 – US 15 SB over Fishing Creek)

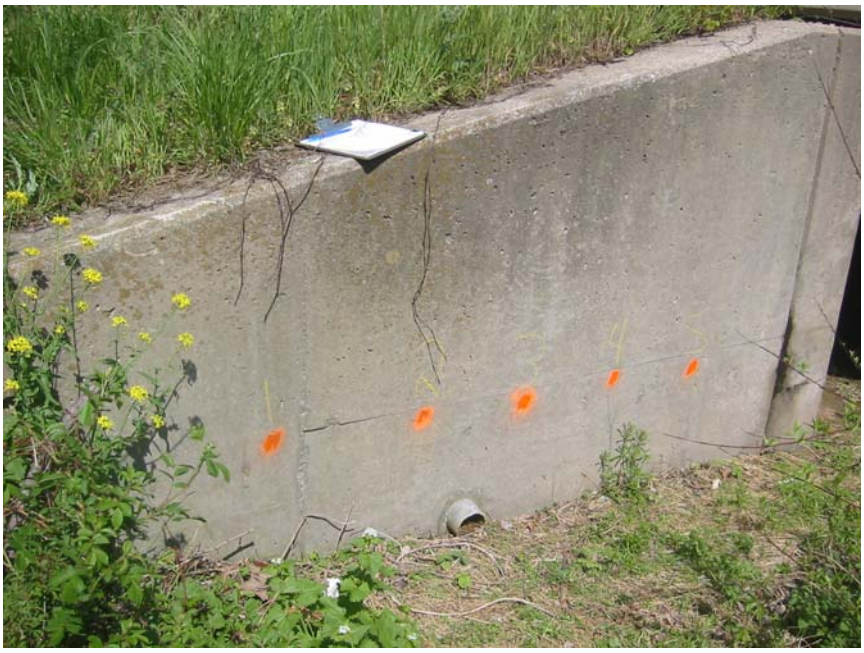

Figure 3.50: Test Location (1011100 – US 15 SB over Fishing Creek)

3.5.9 Bridge 1308603 (MD 175 EB over US 29)

Bridge 1308603 is a four span structure built in 1974, with 31 and 41 foot end spans and 96 foot interior spans supported by steel beams. The superstructure rests on cast-in-place concrete abutments and piers. Cores were taken from the outside face of the north parapet above the northeast wingwall; see Figure 3.51 for the general coring location and Figure 3.52 for the coring locations.

Figure 3.51: General Location (1308603 – MD 175 EB over US 29)

Figure 3.52: Test Location (1308603 – MD 175 EB over US 29)

3.5.10 Bridge 1315004 (MD 100 WB over Dorsey Station Road)

Bridge 1315004 is a single span structure built in 1996, with 85 foot span supported by steel girders. The superstructure rests on cast-in-place concrete abutments. Cores were taken from the northwest wingwall; see Figure 3.53 for the general coring location and Figure 3.54 for the coring locations.

Figure 3.53: Gen. Location (1315004 – MD 100 WB over Dorsey Station Road)

Figure 3.54: Test Location (1315004 – MD 100 WB over Dorsey Station Road)

3.5.11 Bridge 1315700 (MD 32 over River Road and Patapsco River)

Bridge 1315700 is a four span structure built in 2003, supported by concrete precast / prestessed girders. The superstructure rests on cast-in-place concrete abutments and piers. Cores were taken from the northeast wingwall; see Figure 3.55 for the general coring location and Figure 3.56 for the coring locations.

Figure 3.55: General Location

(1315700 – MD 32 over River Road and Patapsco River)

Figure 3.56: Test Location

(1315700 – MD 32 over River Road and Patapsco River)

3.5.12 Bridge 1612300 (I-95 X SB over I-495 OL)

Bridge 1612300 is a three span structure built in 1967, with 31 and 38 foot end spans and 89 foot interior span supported by steel beams. The superstructure rests on cast-in-place concrete abutments and piers. Cores were taken from the inside face of the east parapet above the northeast wingwall; see Figure 3.57 for the general coring location and Figure 3.58 for the coring locations.

Figure 3.57: General Location (1612300 – I-95 X SB over I-495 OL)

Figure 3.58: Test Location (1612300 – I-95 X SB over I-495 OL)

3.6 Summary

Testing methods and Phase 1 results are discussed in Chapter 4. Chapter 5 presents the findings from Phase 2 testing and analysis. From the work preformed in Phases 1 and 2, trends and correlations were attempted, and Chapter 6 presents the various methods used to develop the trends and correlations.

Chapter 4

Phase 1 Field Survey – Scanning Electron Microscopy Analysis

4.1 Introduction

The scanning electron microscopy (SEM) was utilized on this project to examine samples of concrete taken from bridges throughout Maryland State Bridge Inventory. The SEM provides images of the cement paste for microcracking and alkali-silica reaction (ASR) gel, the voids for crystal formations contained inside, and aggregate pullouts for cracking along the aggregate / paste interface and crystal formations. The intent of the core sampling was to develop a better understanding of concrete deterioration that exhibits map cracking on the surface of a concrete element.

4.2 Scanning Electron Microscopy

Ten bridges were cored during the project in order to verify the presence of ettringite. Ettringite is identified visually using the scanning electron microscope (SEM) and elemental analysis of the crystals can be preformed using energy

dispersive analysis x-ray (EDAX). The SEM using a voltage of 20 kilovolt (kV) directs a stream of electrons at a concrete sample, which interacts with the surface of the sample. See Figure 4.1 (a) for an example micrograph; the micrograph gives the accelerated voltage (20.0 kV), the magnification power (595x), and a scale. Two significant signals are produced, secondary electrons (SE) and x-rays. The SE are used to "see" the sample, and the SEM interprets the signal to produce a visual image for the operator. X-rays are used to identify the elements present in the region of interest, because EDAX works on the principle of discrete energy level for the various elements, and each element can only emit x-rays (photons) with specific energy levels. EDAX detects the emitted x-rays and the associated energy, and from a database, it associates the various x-rays with the corresponding element that produced the x-ray, which allows positive identification of the presence of ettringite in the samples. See Figure 4.1 (b) for an example EDAX output. The EDAX output shows a chart with the number of counts per energy level, the relative number of count is shown in the peak heights and the x-ray energy level is shown on the x-axis. The elements are identified above their count peak, with calcium having two peaks the first large and the second much smaller in size. Below the chart is a table with elemental analysis, which shows the percentage of the counts (At %) from each element. From the ZAF database the program calculates the percentage by weight (Wt %) for each element. The value used for the calculation are provided in the table, (K-ratio, Z, A, and F). The SEM can produce images of objects less than 100 nm in size, and for this project, the objects of interest were in the order of 1μm to 100μm.

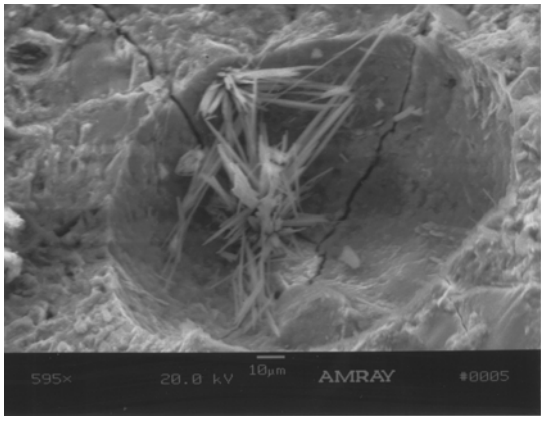

(a) Ettringite Crystals in Void – SEM

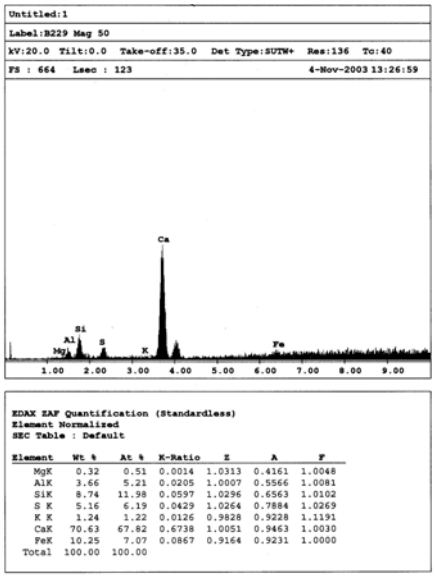

(b) Analysis of Ettringite Crystals in Void – EDAX

Figure 4.1: Sample Images from SEM and EDAX

4.3 Sample Preparation and Examination Methodology

A total of 29 cores, 2 inches in diameter and 3 inches deep, were taken from ten bridges throughout the state, see Figure 4.2. In order to analyze the concrete, smaller samples of concrete are needed. Each core is broken into small pieces with a five pound sledge hammer, and a sample is selected which has a relatively flat side to allow mounting.

(a) Two Inches Diameter by Three Inches Deep Core

(b) Fractured Core

Figure 4.2: Sample Preparation – 1

Once the sample is selected, the sample is dried. During the drying process, a cork and carbon stud is readied and the sample is logged. Carbon stud, adhesive, and coating are used since the X-ray energy level associated with carbon is not close to the elements of interest in concrete, ettringite, and ASR gel. After the sample is dried, the sample gets mounted onto the carbon stud with the carbon adhesive. The cork acts as a holder to keep the sample upright, as shown in Figure 4.3. The assembly is dried until the carbon adhesive is completely set. The final step is to coat the sample surface with carbon which provides a clear visual image of the surface and avoids electron charge buildup on the sample. The sample and stud are placed into a vacuum chamber, in which the pressure is lowered to 0.100 torr (1 torr = 1 millimeter of mercury or 133.32 pascal). At this pressure, the carbon coating is applied.

(a) Samples Drying **(b) Corks and Carbon Stubs**

(c) Samples Mounted with Carbon **(d) Carbon Coating Machine**

Figure 4.3: Sample Preparation – 2

After the coating, the sample is ready for the SEM. The sample assembly is placed into the SEM with the top surface at an approximately 30 degree angle to produce the maximum possible signal for the EDAX analysis process.

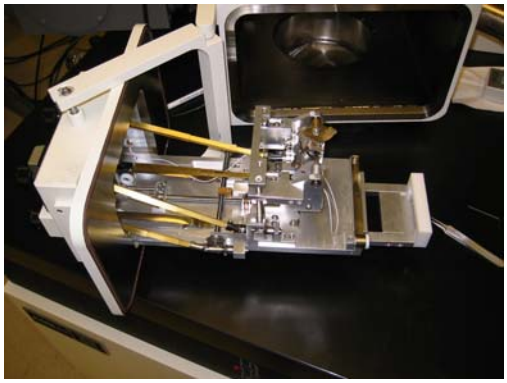

(a) Samples Mounted

(b) Scanning Electron Microscope

(c) Viewing an Image

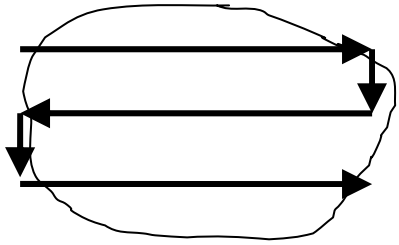

(d) Search Pattern

Figure 4.4: Sample Examination

The sample is searched in an across-down-across-down pattern for possible locations of DEF and ASR gel, see Figure 4.4. The intension of the search pattern is to document the prevalence of both forms of deterioration.

4.4 Literature Review: SEM Results for Ettringite and ASR gel

Many researchers have studied Delayed Ettringite Formations (DEF) and ASR attacks on hardened concrete. Despite the numerous investigations, DEF is still not well understood, and disagreements arise about the formation mechanism(s), whether different types of morphology exist, and the role, if any, DEF plays in the deterioration process.

Stark and Bollmann suggest the long ettringite crystals in the voids are hexagonal prismatic, see Figure 4.5.

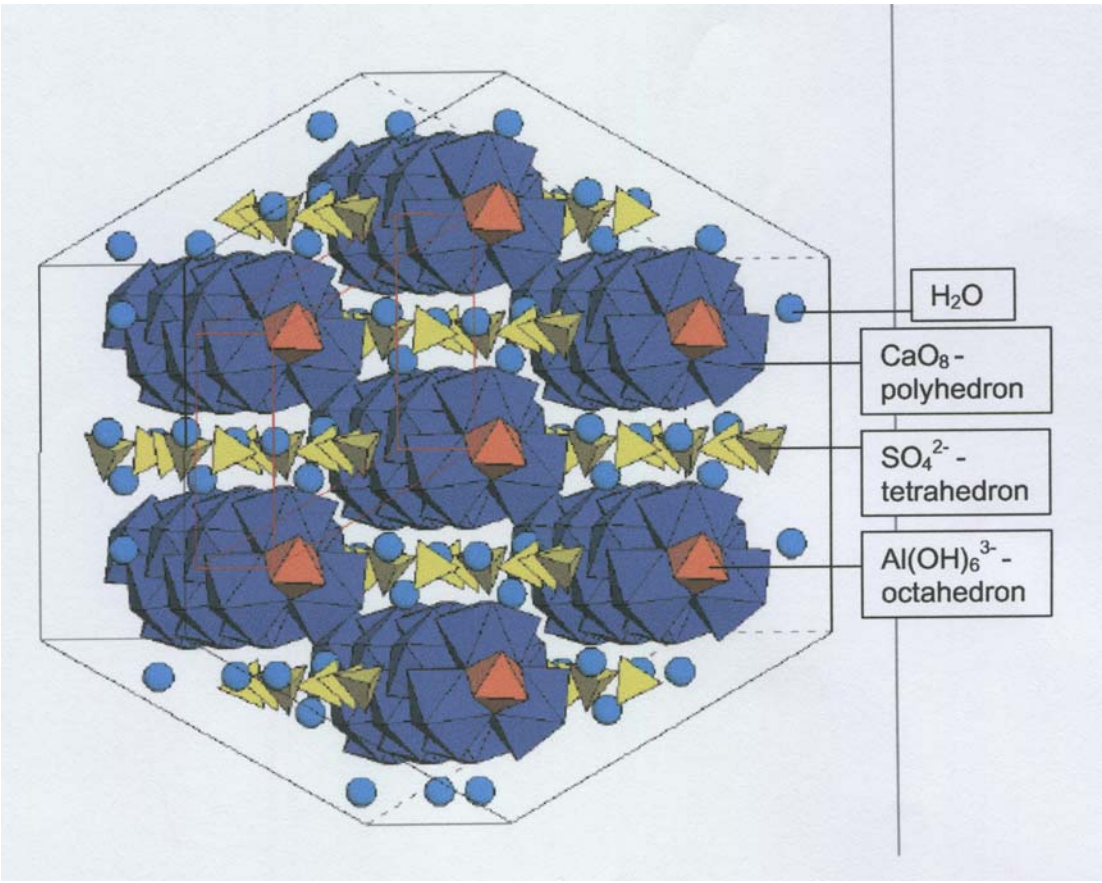

Figure 4.5: Proposed Crystal Formation (Stark and Bollmann)

Using an Environmental Scanning Electron Microscopy (ESEM), Stark and Bollmann, in a study of cast-in-place concrete, found long ettringite crystals exhibiting a hexagonal prismatic morphology, see Figures 4.6 (a) and (b). They also used SEM when analyzing samples for ettringite formations, see Figures 4.6 (c) and (d).

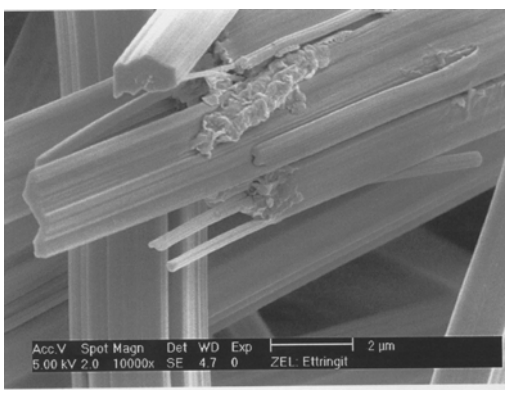

(a) Hexagonal Prismatic Ettringite

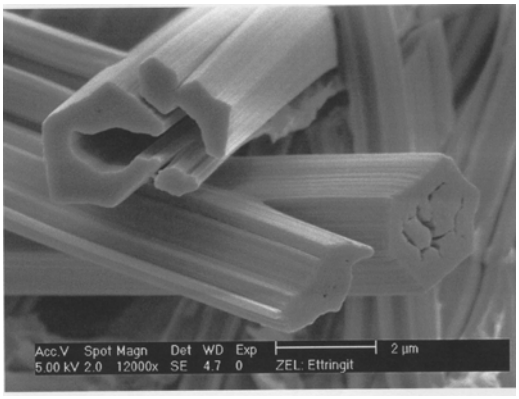

(b) Hexagonal Prismatic Ettringite

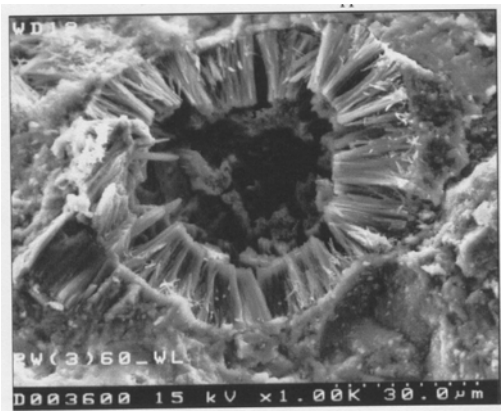

(c) Void with Ettringite Formations

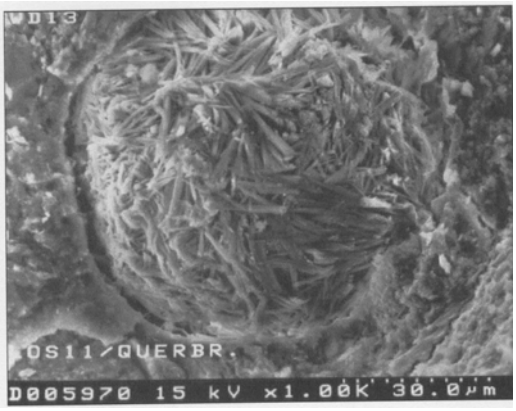

(d) Void with Ettringite Formations

Figure 4.6: Prismatic Ettringite Close-up and in Voids (Stark and Bollmann)

Despite finding ettringite in hardened concrete, Stark and Bollmann were unable to establish or deny that DEF was the cause of the deterioration in the concrete sampled. They believe that in samples were ettringite formations fill a portion of the void, the concrete is less likely to allow water transportation and the ettringite formations leave

less room for expansion. As a result, the concrete is more susceptible to freeze-thaw damage. Other researcher suggest that ASR or early strains in the curing process can crack the concrete paste causing microcrack in which ettringite forms near the crack tip and causes propagation of the crack. (Diamond, Ong, and Bonen 1994, Diamond, Zheng, and Olek 2002).

Many other theories exist to explain different ettringite formations and possible failure mechanisms. In this study, several forms of ettringite were found in the cores taken and discussions are included in the results section. The hexagonal prismatic long crystal is the most commonly observed form.

Since presence of ASR is possible in the cores, a separate test was preformed on a large sample taken from each core. AASHTO T299-93 defines the procedure for identifying ASR in the field (AASHTO Innovative Highway Technologies 1998). Since all of the tests were conducted in a lab, several simplication were made, but the basic procedure was still followed. The procedure requires fresh concrete surface to test, and a large fragment was selected after the cores were fractured. The sample is then washed with clean water and a solution of dilute uranyl acetate is applied. After the sample has dried from at least 3 minutes, the sample can be placed under a short wave ultra-violet (UV) light (~250 nm). Once viewed under the UV light, ASR will appear yellow-green and tends to be found in cracks or around aggregates, see Figure 4.7 for test procedure.

(a) Applying Uranyl Acetate **(b) Placing Sample Under UV Light**

Figure 4.7: Ultra-Violet Light ASR Test

4.5 Results

4.5.1 Bridge 1600400 (US 1 over Paint Branch)

Three cores were taken from the northwest wingwall; see Figure 4.8 for locations.

Figure 4.8: Coring Locations (1600400 – US 1 over Paint Branch)

All 3 cores exhibit ettringite formations throughout the samples. Most voids contain ettringite formations. See Figures 4.9 and 4.10. Energy Dispersive Analysis X-ray (EDAX) verifies the elemental composition of the crystal formations by showing the distinct aluminum, sulfur, and calcium pattern. The ettringite formations appear to be hexagonal prismatic morphology in voids and tightly-packed ettringite formation in cracks and on the fractured surface. The three cores do not vary considerably in the type of ettringite formations or in the prevalence of ettringite formations in the samples.

The UV light ASR test confirms the presence of ASR gel in the wingwall.

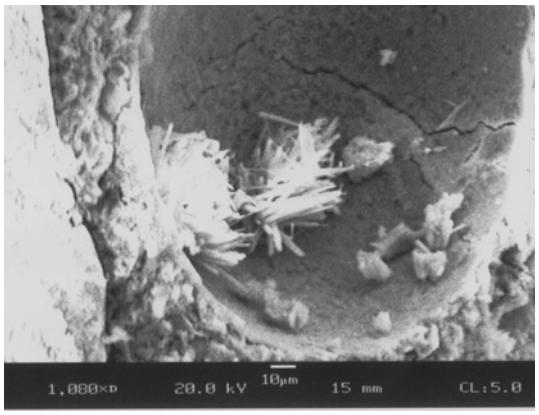

(a) Ettringite in Void with Microcracking in the Background

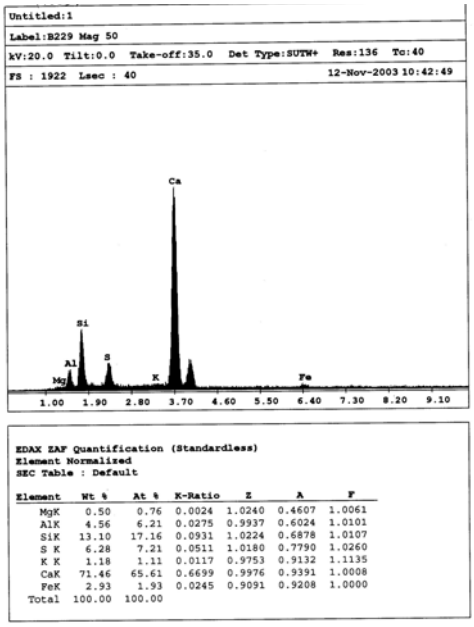

(b) Analysis of Crystals in (a)

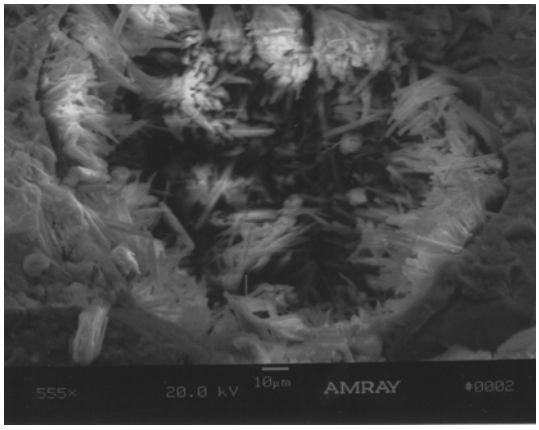

(c) Ettringite in Void

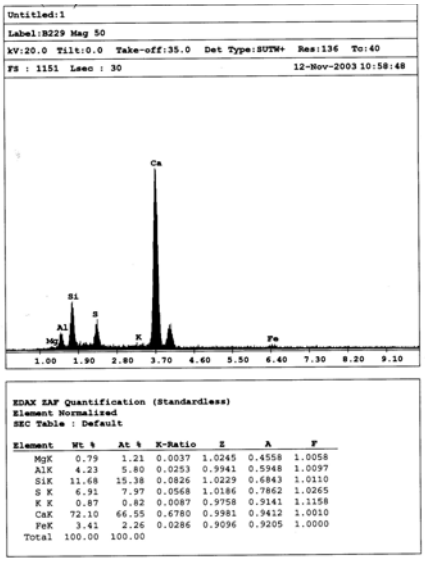

(d) Analysis of Whole Picture (c)

Figure 4.9: US 1 over Paint Branch (1600400)

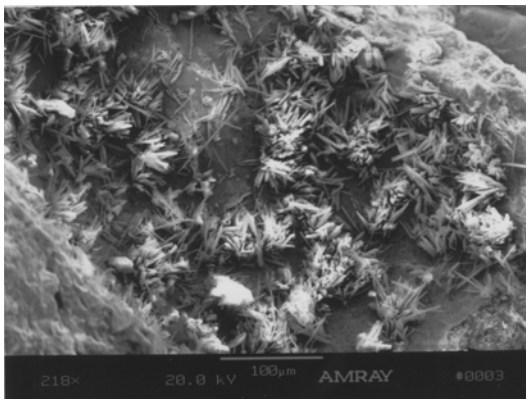

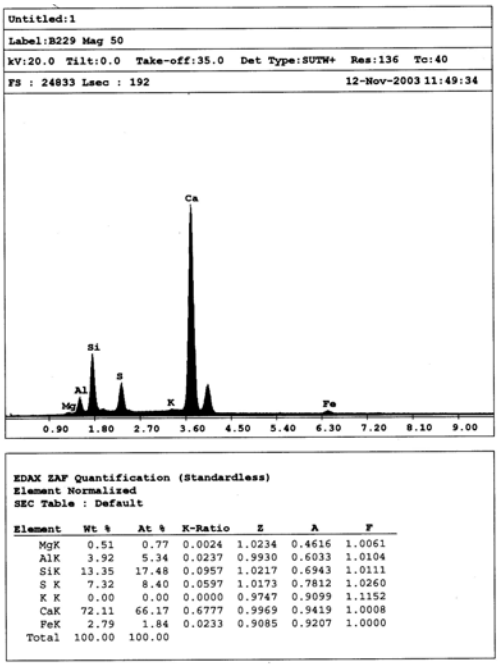

(a) Ettringite in Void **(b) Analysis of Whole Picture (a)**

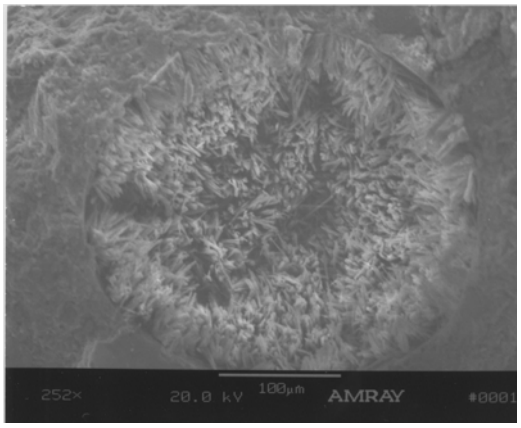

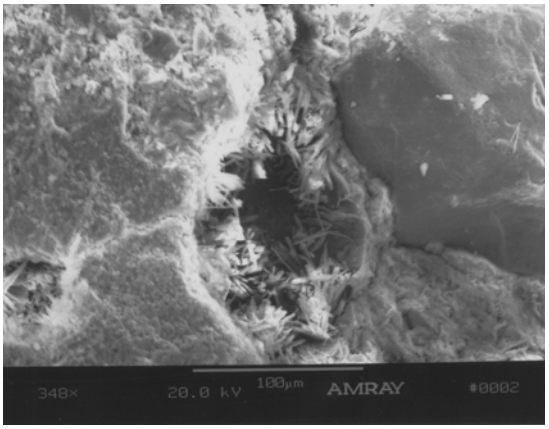

(c) Ettringite in Void

(d) Ettringite in Voids and Along Aggregate

Figure 4.10: US 1 over Paint Branch (1600400)

4.5.2 Bridge 1620003 (MD 198 over I-95)

Three cores were taken from the southwest wingwall; see Figure 4.11 for locations.

Figure 4.11: Coring Locations (1620003 – MD198 over I-95)

All three cores exhibit ettringite formations throughout the samples, and two different types of ettringite formations were observed in these cores. In Figure 4.12, the ettringite formations appear to be hexagonal prismatic in morphology. In Figures 4.13 and 4.14, the ettringite formations appear to be shorter in length and much closer together, and the morphology will be identified as tightly-packed ettringite or tightly-packed DEF throughout this report. These formations were observed in cracks, on the surface of the sample, and filling voids. In both cases, EDAX verifies the elemental composition of the crystal formations by showing the distinct aluminum, sulfur, and calcium pattern. In Figure 4.14, EDAX analysis shows the ettringite is in a crack

between a sand particle and the cement paste. The three cores do not vary considerably in the type of ettringite formations or in the prevalence of ettringite formations in the samples.

The UV light ASR test confirms the presence of ASR gel in the wingwall. Two of the three cores appeared to contain ASR gel as observed with the SEM, see Figure 4.15. In both cases, EDAX verifies the elemental composition of the gel by showing the distinct silicon and potassium pattern. For ASR gel, the silicon peak is very high when compared to the potassium peak.

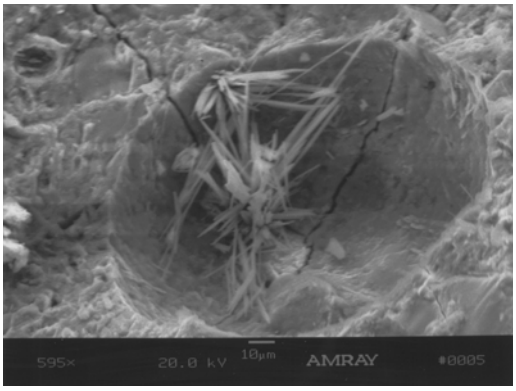

(a) Ettringite in Void with Microcracking in the Background

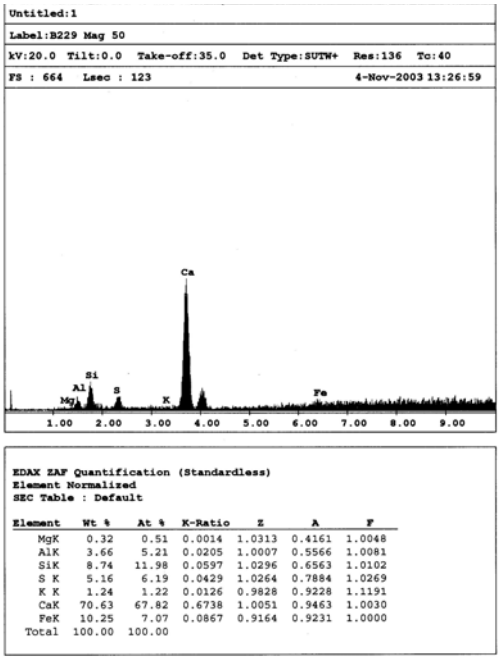

(b) Analysis of Crystals in (a)

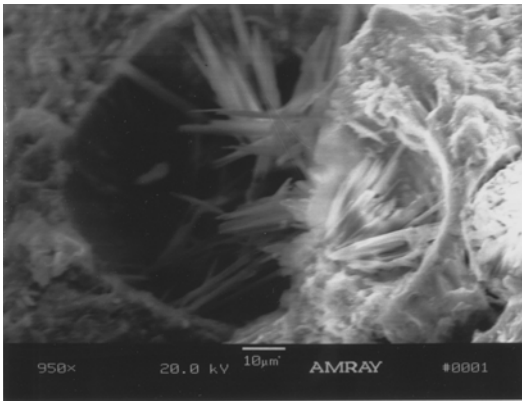

(c) Ettringite in Void

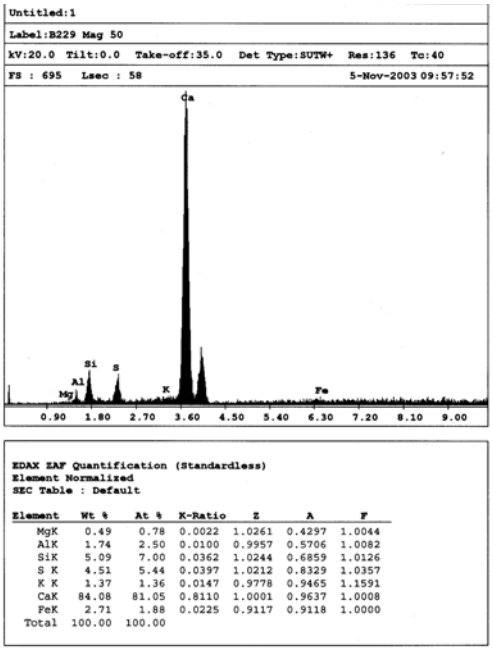

(d) Analysis of Crystals in (c)

Figure 4.12: MD198 over I-95 (1620003)

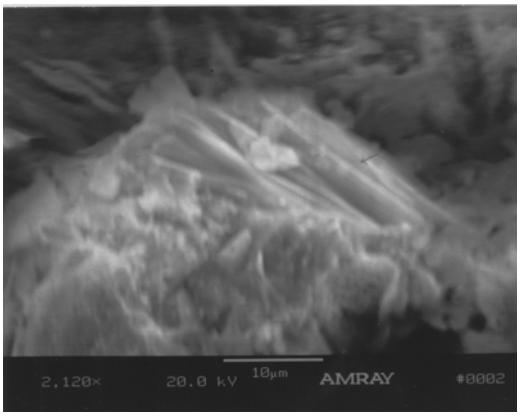

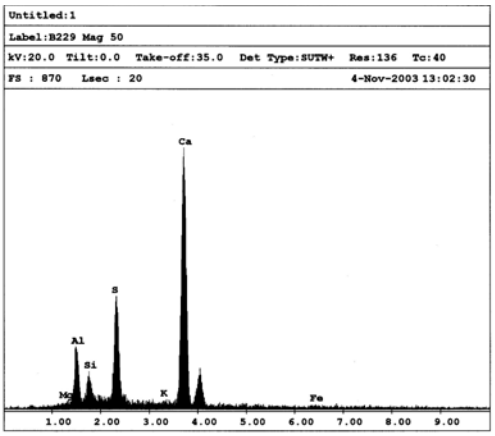

EDAX ZAF Quantification (Standardless)
Element Normalized
SEC Table : Default

Element	Wt %	At %	K-Ratio	Z	A	F
MgK	0.39	0.58	0.0019	1.0237	0.4826	1.0068
AlK	9.76	13.06	0.0612	0.9933	0.6257	1.0091
SiK	4.64	5.97	0.0318	1.0220	0.6605	1.0135
S K	18.49	20.81	0.1571	1.0170	0.8173	1.0222
K K	1.02	0.94	0.0095	0.9747	0.8804	1.0872
CaK	63.77	57.41	0.5814	0.9970	0.9140	1.0005
FeK	1.92	1.24	0.0161	0.9084	0.9240	1.0000
Total	100.00	100.00				

(a) Ettringite on Surface of the Sample

(b) Analysis of Whole Picture (a)

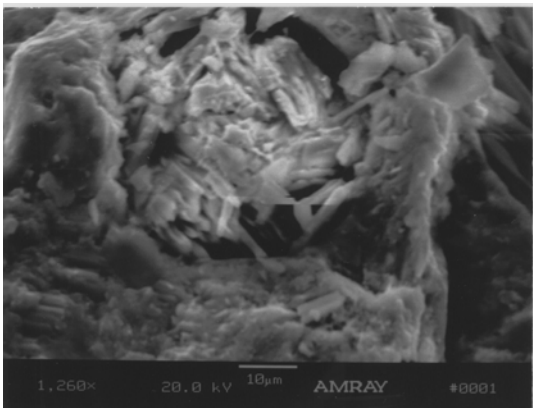

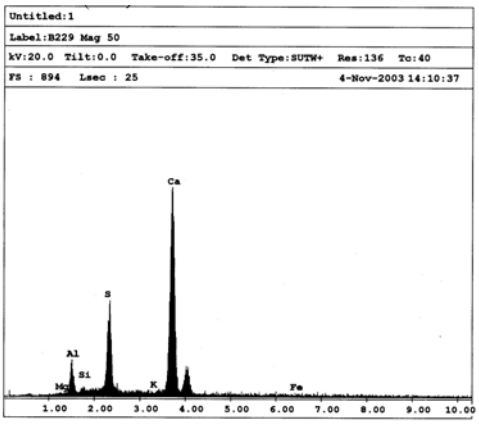

EDAX ZAF Quantification (Standardless)
Element Normalized
SEC Table : Default

Element	Wt %	At %	K-Ratio	Z	A	F
MgK	0.24	0.36	0.0011	1.0239	0.4660	1.0059
AlK	6.63	9.08	0.0406	0.9936	0.6106	1.0089
SiK	1.39	1.83	0.0097	1.0223	0.6763	1.0154
S K	19.70	22.72	0.1752	1.0178	0.8518	1.0259
K K	0.52	0.49	0.0049	0.9752	0.8903	1.1002
CaK	69.82	64.40	0.6437	0.9975	0.9239	1.0005
FeK	1.72	1.14	0.0144	0.9090	0.9194	1.0000
Total	100.00	100.00				

(c) Ettringite Filling Void

(d) Analysis of Ettringite Filling Void (c)

Figure 4.13: MD198 over I-95 (1620003)

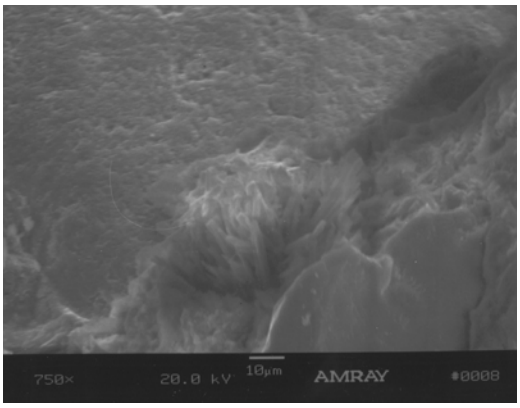

(a) Ettringite Filling Crack Between Sand Grain and Cement Paste

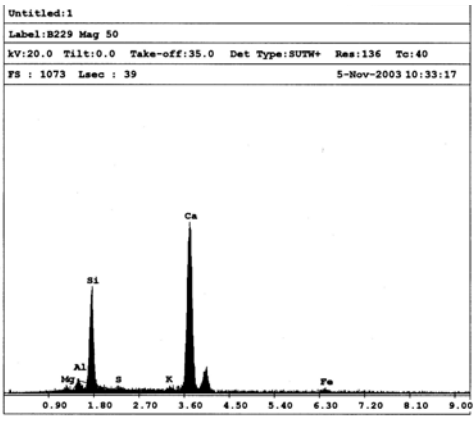

EDAX ZAF Quantification (Standardless)
Element Normalized
SEC Table : Default

Element	Wt %	At %	K-Ratio	Z	A	F
MgK	1.18	1.78	0.0056	1.0232	0.4597	1.0064
AlK	0.00	0.00	0.0000	0.9929	0.5950	1.0127
SiK	22.71	29.58	0.1693	1.0215	0.7232	1.0090
S K	0.88	1.00	0.0067	1.0171	0.7391	1.0244
K K	1.65	1.55	0.0164	0.9745	0.9157	1.1109
CaK	69.36	63.33	0.6500	0.9967	0.9390	1.0012
FeK	4.22	2.77	0.0354	0.9083	0.9232	1.0000
Total	100.00	100.00				

(b) Analysis of Cement Paste – Top Left of Photo (a)

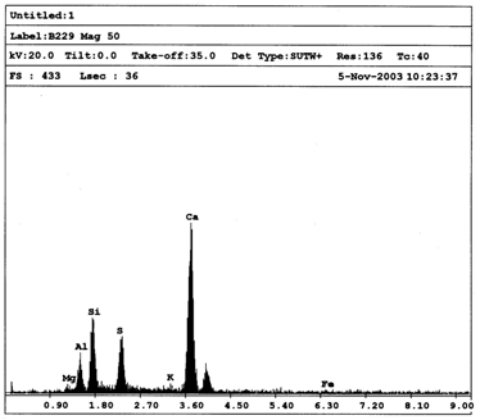

EDAX ZAF Quantification (Standardless)
Element Normalized
SEC Table : Default

Element	Wt %	At %	K-Ratio	Z	A	F
MgK	1.17	1.69	0.0061	1.0209	0.5051	1.0078
AlK	7.29	9.47	0.0468	0.9906	0.6398	1.0117
SiK	16.57	20.68	0.1182	1.0193	0.6922	1.0108
S K	13.44	14.69	0.1052	1.0136	0.7581	1.0190
K K	1.45	1.30	0.0132	0.9717	0.8736	1.0774
CaK	58.58	51.23	0.5283	0.9940	0.9069	1.0004
FeK	1.50	0.94	0.0126	0.9055	0.9285	1.0000
Total	100.00	100.00				

(c) Analysis of Ettringite Crystals – Middle of Photo (a)

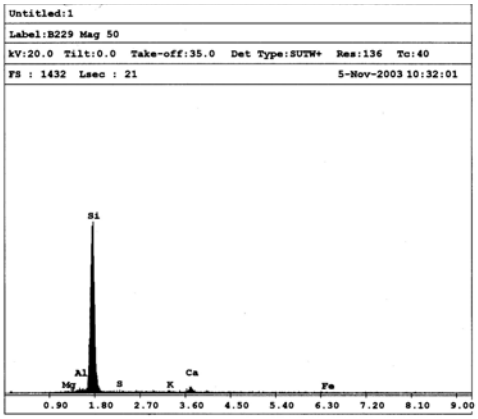

EDAX ZAF Quantification (Standardless)
Element Normalized
SEC Table : Default

Element	Wt %	At %	K-Ratio	Z	A	F
MgK	0.85	1.01	0.0068	1.0049	0.7713	1.0306
AlK	1.63	1.74	0.0147	0.9753	0.8722	1.0582
SiK	88.48	90.79	0.8234	1.0036	0.9264	1.0010
S K	1.11	1.00	0.0055	0.9929	0.4959	1.0015
K K	1.33	0.98	0.0097	0.9543	0.7634	1.0051
CaK	5.30	3.81	0.0424	0.9765	0.8195	1.0004
FeK	1.30	0.67	0.0112	0.8881	0.9721	1.0000
Total	100.00	100.00				

(d) Analysis of Sand Grain – Bottom Right of Photo (a)

Figure 4.14: MD198 over I-95 (1620003)

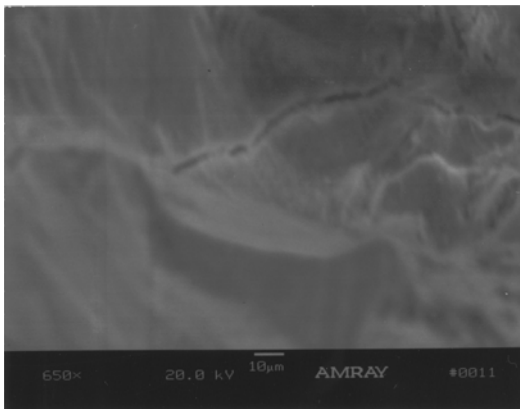

(a) ASR Gel

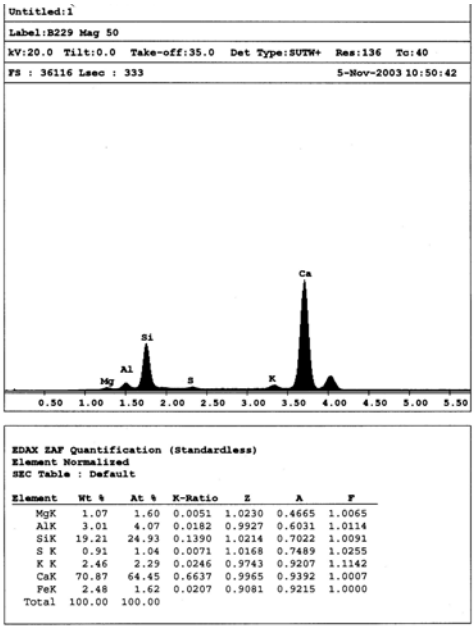

(b) Analysis of Whole Picture (a)

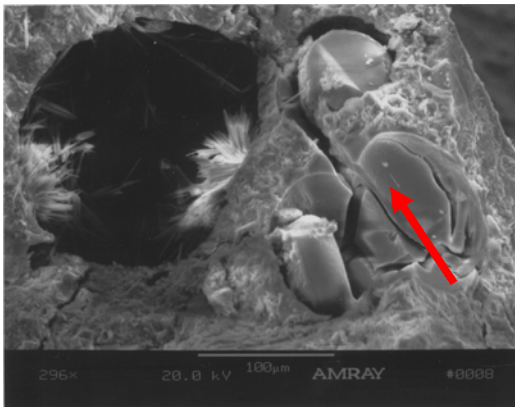

(c) Ettringite in Void (Left) and ASR Gel (Right)

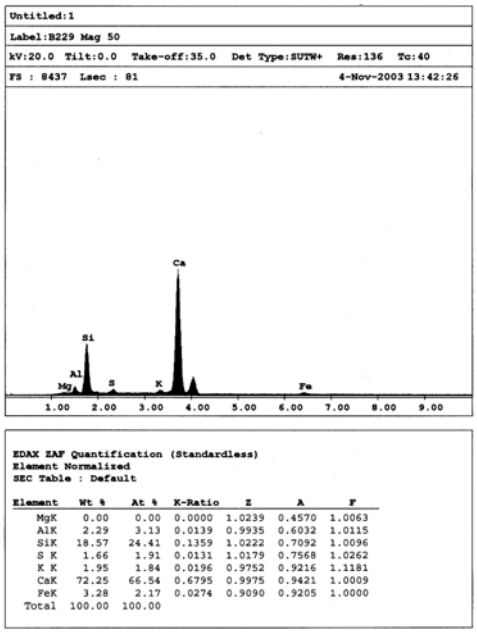

(d) Analysis of ASR gel (c)

Figure 4.15: MD 198 over I-95 (1620003)

4.5.3 Bridge 1511300 (Greentree Rd over I-495)

Three cores were taken from the inside face of the west parapet; see Figures 4.16 and 4.17 for locations.

Figure 4.16: Coring Locations (1511300 – Greentree Rd over I-495)

All three cores exhibit ettringite formations throughout the samples, and two different types of ettringite formations were observed in these cores. In Figure 4.18, the ettringite formations appear to be hexagonal prismatic in morphology, with tightly-packed ettringite formations in Figures 4.19 and 4.20. The tightly-packed ettringite formations were observed in cracks, on the surface of the sample, covering an aggregate, and filling voids. The right core, in the location of greatest distress as observed from the surface, exhibited significantly more tightly-packed DEF than any other core in this study. See Figure 4.17 for close-up of the right core location. The

cracks around the coring location are of measurable width using typical bridge inspection equipment. In both types of ettringite formations, EDAX verifies the elemental composition of the crystal formations by showing the distinct aluminum, sulfur, and calcium pattern. The three cores vary considerably in the type of ettringite formations with the tightly-packed ettringite being observed in the right and center cores and hexagonal prismatic ettringite formations being observed in the center and left cores. The prevalence of ettringite formations in the samples also varied and decreased from right to left with the location exhibiting more damage on the surface having more ettringite formations and the location with the least damage on the surface having less ettringite formations.

The UV light ASR test confirms the presence of ASR gel in the parapet. One possible location of ASR gel, as observed with the SEM, is shown in Figure 4.21.

Figure 4.17: Right Coring Location (1511300 – Greentree Rd over I-495)

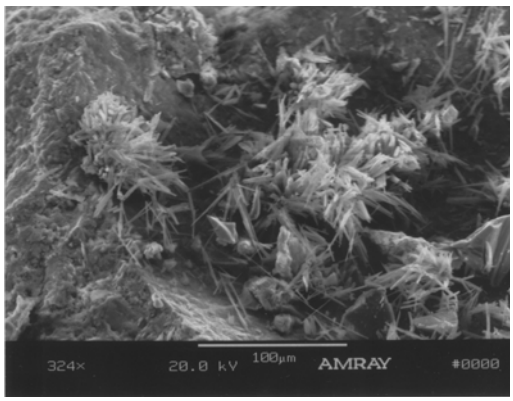

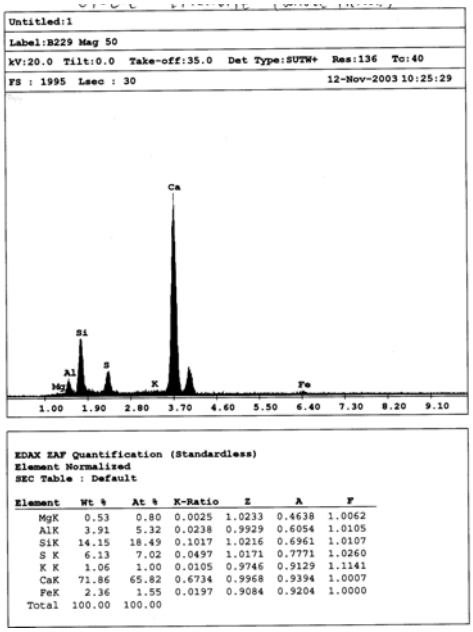

(a) Ettringite in Void **(b) Analysis of Whole Picture (a)**

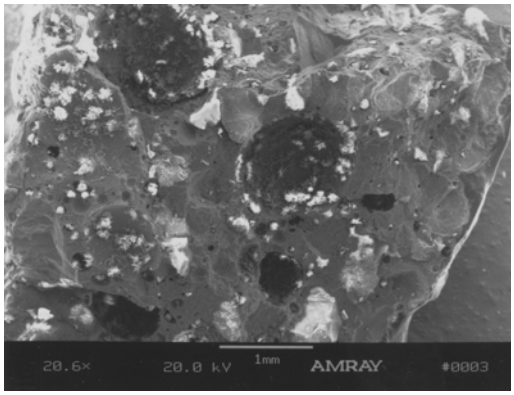

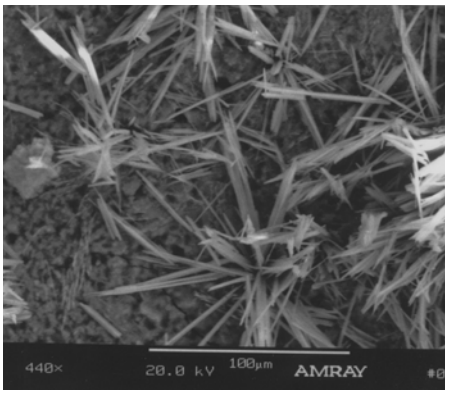

(c) Ettringite in Voids and on the Sample Surface (Low Magnification) **(d) Crystals in a Void from Picture (c)**

Figure 4.18: Greentree Rd over I-495 (1511300)

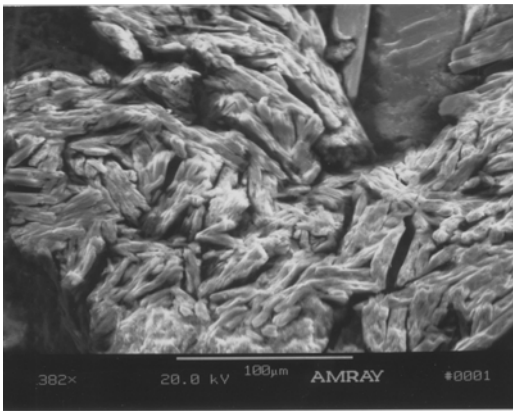

(a) Tightly-Packed Ettringite on Surface of the Sample

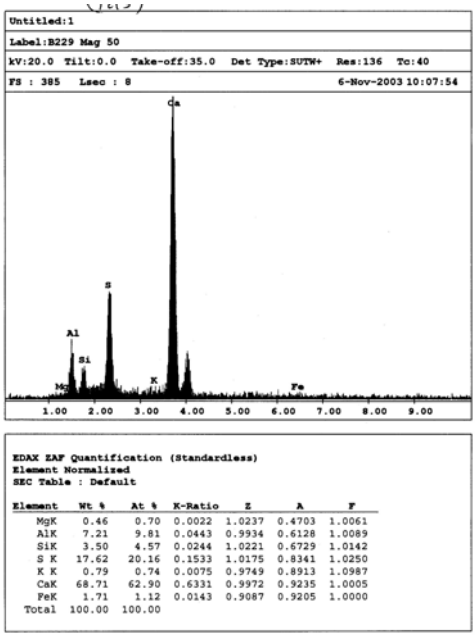

(b) Ettringite Mass in Picture (a)

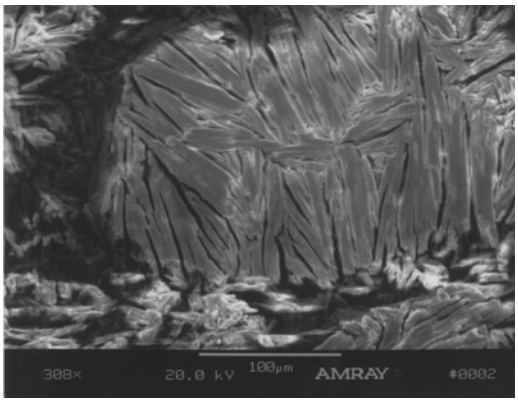

(c) Ettringite Filling Void

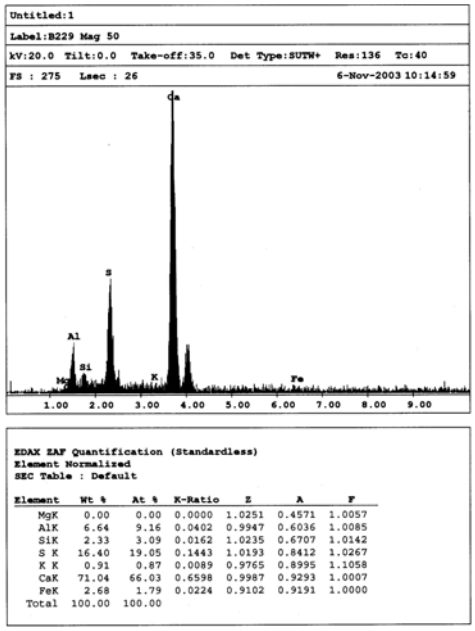

(d) Analysis of Ettringite Filling Void (c)

Figure 4.19: Greentree Rd over I-495 (1511300)

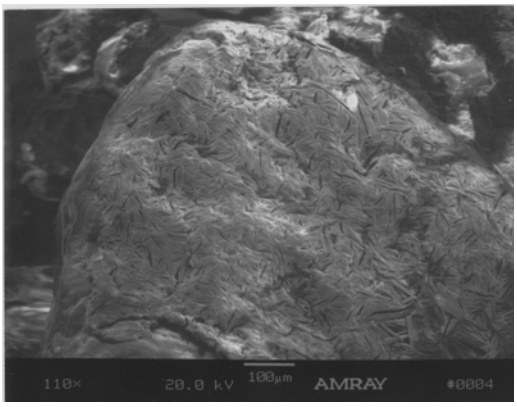

(a) Tightly-Packed Ettringite on Surface of the Aggregate

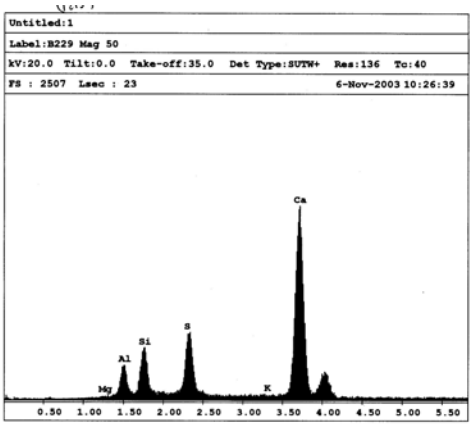

EDAX ZAF Quantification (Standardless)
Element Normalized
SEC Table : Default

Element	Wt %	At %	K-Ratio	Z	A	F
MgK	0.41	0.60	0.0021	1.0209	0.4970	1.0073
AlK	7.35	9.70	0.0471	0.9907	0.6401	1.0109
SiK	11.05	14.00	0.0789	1.0193	0.6923	1.0127
S K	16.37	18.17	0.1346	1.0140	0.7941	1.0215
K K	0.77	0.70	0.0071	0.9719	0.8786	1.0865
CaK	63.75	56.63	0.5792	0.9942	0.9137	1.0001
FeK	0.30	0.19	0.0025	0.9057	0.9241	1.0000
Total	100.00	100.00				

(b) Analysis of Whole Picture (a)

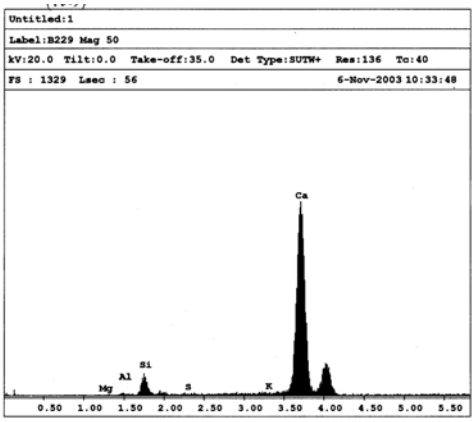

EDAX ZAF Quantification (Standardless)
Element Normalized
SEC Table : Default

Element	Wt %	At %	K-Ratio	Z	A	F
MgK	0.32	0.51	0.0014	1.0270	0.4184	1.0041
AlK	0.78	1.13	0.0044	0.9966	0.5601	1.0081
SiK	5.94	8.29	0.0422	1.0253	0.6850	1.0121
S K	0.26	0.31	0.0022	1.0224	0.8267	1.0394
K K	0.77	0.77	0.0086	0.9789	0.9625	1.1890
CaK	88.56	86.61	0.8687	1.0011	0.9789	1.0010
FeK	3.39	2.38	0.0282	0.9127	0.9099	1.0000
Total	100.00	100.00				

(c) Analysis of Aggregate Underneath Ettringite in Picture (a)

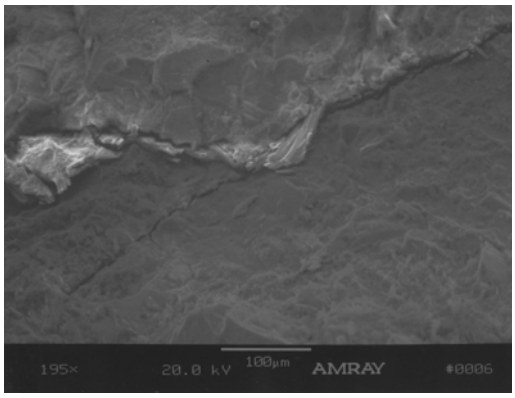

(d) Ettringite in Crack

Figure 4.20: Greentree Rd over I-495 (1511300)

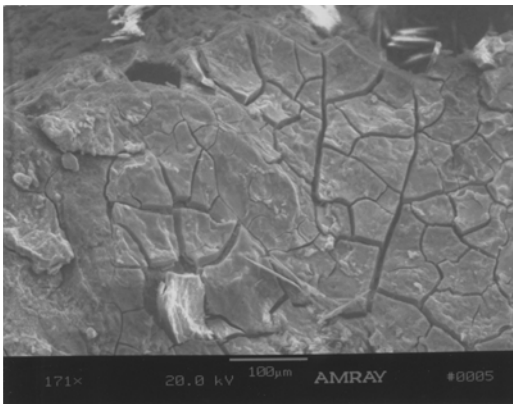

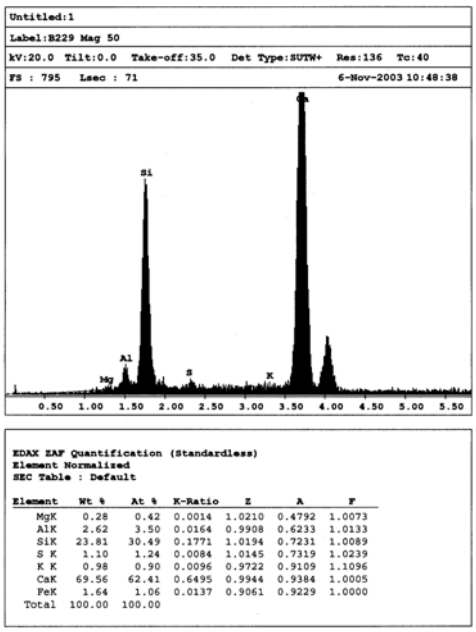

EDAX ZAF Quantification (Standardless)
Element Normalized
SEC Table : Default

Element	Wt %	At %	K-Ratio	Z	A	F
MgK	0.28	0.42	0.0014	1.0210	0.4792	1.0073
AlK	2.62	3.50	0.0164	0.9908	0.6233	1.0133
SiK	23.81	30.49	0.1771	1.0194	0.7231	1.0089
S K	1.10	1.24	0.0084	1.0145	0.7319	1.0239
K K	0.98	0.90	0.0096	0.9722	0.9109	1.1096
CaK	69.56	62.41	0.6495	0.9944	0.9384	1.0005
FeK	1.64	1.06	0.0137	0.9061	0.9229	1.0000
Total	100.00	100.00				

(a) Possible ASR Gel **(b) Analysis of Possible ASR Gel**

Figure 4.21: Greentree Rd over I-495 (1511300)

4.5.4 Bridge 0314200 (Old Court Rd Over I-695)

Three cores were taken from the parapet above the northwest wingwall; see Figure 4.22 for locations.

Figure 4.22: Coring Locations (0314200 – Old Court Rd over I-695)

All three cores exhibit ettringite formations throughout the samples, and two different types of ettringite formations were observed in these cores. In Figure 4.23, the ettringite formations appear to be hexagonal prismatic in morphology, but in Figures 4.24 (a) and (b), the ettringite formations appear to have needle-like crystal morphology and are smaller than typically observed. The ettringite formations have developed in holes in the cement paste and on the fractured surface. In both types of ettringite formations, EDAX verifies the elemental composition of the crystal formations by showing the distinct aluminum, sulfur, and calcium pattern. The right

and center cores were taken from the damaged section and exhibit DEF in the cracks. The left core exhibits DEF in voids only.

No locations of ASR gel were observed with the SEM in the samples from this bridge. The UV light ASR test agrees and does not show the presence of ASR gel in the parapet.

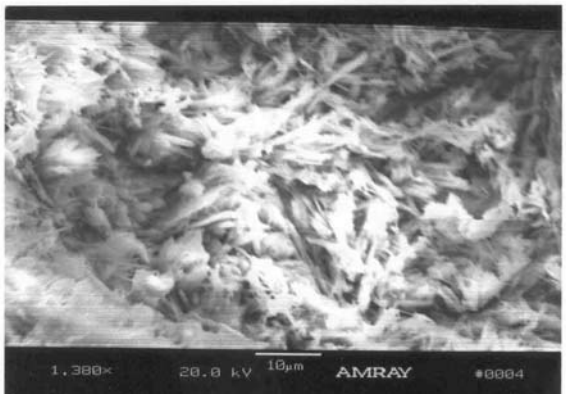

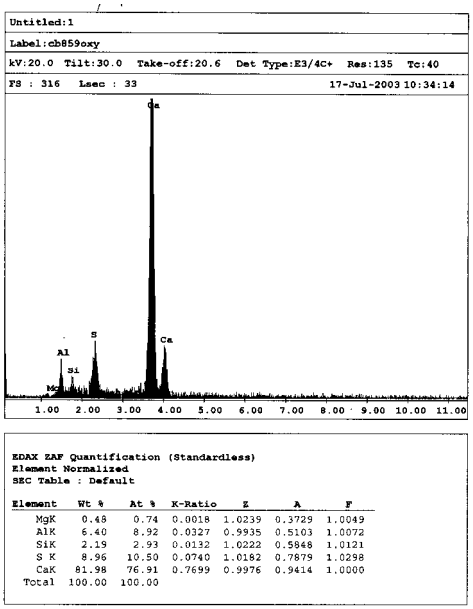

EDAX ZAF Quantification (Standardless)
Element Normalized
SEC Table : Default

Element	Wt %	At %	K-Ratio	Z	A	F
MgK	0.48	0.74	0.0018	1.0239	0.3729	1.0049
AlK	6.40	8.92	0.0327	0.9935	0.5103	1.0072
SiK	2.19	2.93	0.0132	1.0222	0.5848	1.0121
S K	8.96	10.50	0.0740	1.0182	0.7879	1.0298
CaK	81.98	76.91	0.7699	0.9976	0.9414	1.0000
Total	100.00	100.00				

(a) Ettringite on the Surface **(b) Analysis of Whole Picture (a)**

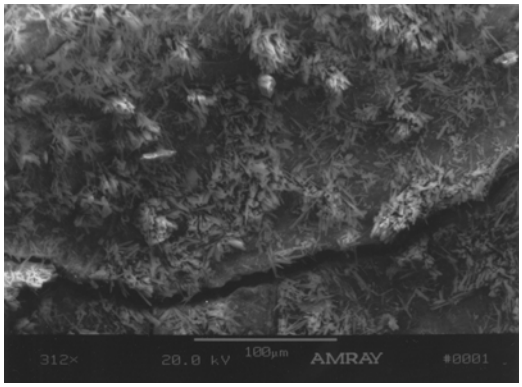

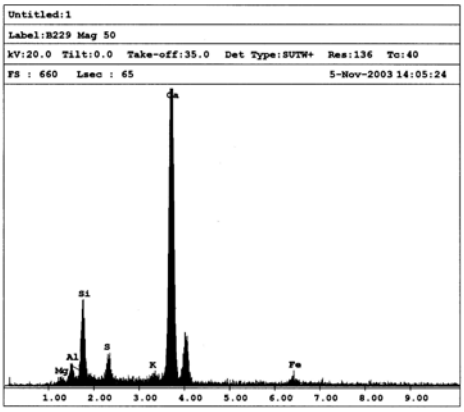

EDAX ZAF Quantification (Standardless)
Element Normalized
SEC Table : Default

Element	Wt %	At %	K-Ratio	Z	A	F
MgK	1.25	1.95	0.0056	1.0260	0.4334	1.0046
AlK	0.47	0.67	0.0027	0.9956	0.5679	1.0091
SiK	9.64	13.10	0.0694	1.0243	0.6945	1.0115
S K	4.12	4.90	0.0350	1.0208	0.8068	1.0314
K K	1.62	1.58	0.0169	0.9776	0.9359	1.1396
CaK	78.68	74.91	0.7518	0.9999	0.9545	1.0012
FeK	4.22	2.88	0.0352	0.9115	0.9159	1.0000
Total	100.00	100.00				

(c) Ettringite on the Surface of an Aggregate (Top) and Cement Paste (Below)

(d) Analysis of Whole Picture (c)

Figure 4.23: Old Court Rd over I-695 (0314200)

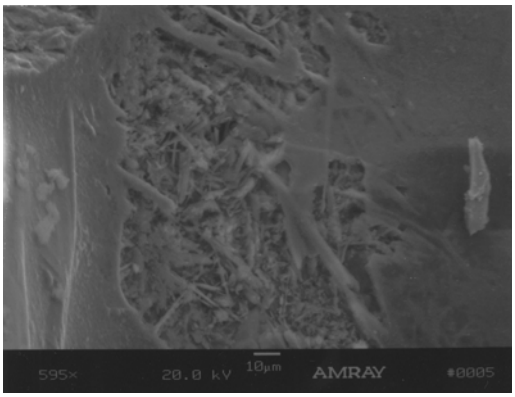

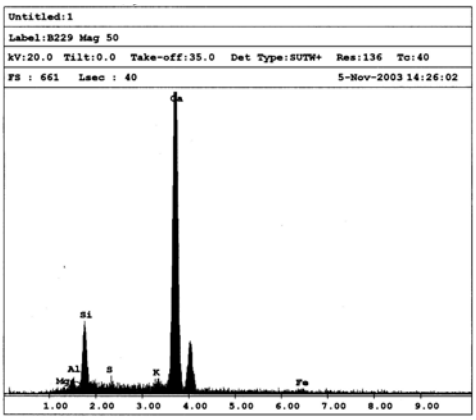

EDAX ZAF Quantification (Standardless)
Element Normalized
SEC Table : Default

Element	Wt %	At %	K-Ratio	Z	A	F
MgK	0.38	0.60	0.0017	1.0251	0.4324	1.0046
AlK	0.24	0.34	0.0014	0.9947	0.5745	1.0091
SiK	9.31	12.76	0.0677	1.0234	0.7030	1.0118
S K	0.97	1.16	0.0083	1.0201	0.8146	1.0360
K K	1.85	1.82	0.0200	0.9768	0.9534	1.1664
CaK	85.29	81.96	0.8243	0.9990	0.9668	1.0006
FeK	1.97	1.36	0.0163	0.9107	0.9111	1.0000
Total	100.00	100.00				

(a) Ettringite in Hole in Cement Paste

(b) Analysis of Cement Paste from Picture (a)

Figure 4.24: Old Court Rd over I-695 (0314200)

4.5.5 Bridge 1311000 (MD 32 EB over US 1)

Three cores were taken from the southeast wingwall; see Figure 4.25 for locations.

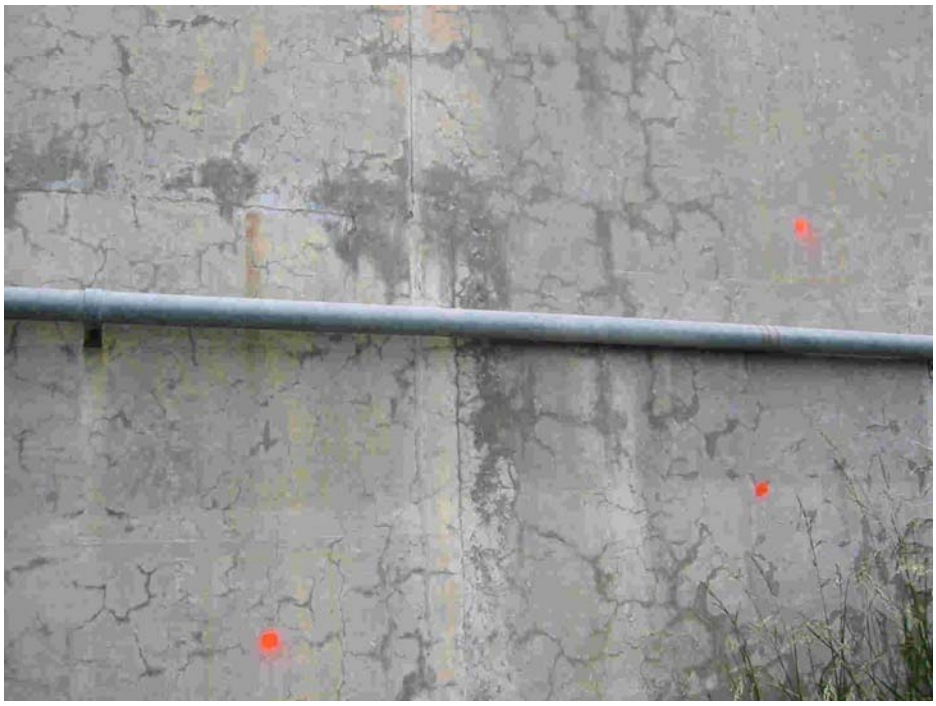

Figure 4.25: Coring Locations (1311000 – MD 32 EB over US 1)

All three cores exhibit ettringite formations throughout the samples, and three different types of ettringite formations were observed in these cores. First, in Figure 4.26 (a) and (b), the ettringite formations appear to be needle-like short crystals found on the fractured surface. Second, in Figures 4.26 (c), 4.26 (d), 4.27 (a), and 4.27 (b), the ettringite formations appear to be hexagonal prismatic in morphology. Third, in Figure 4.27 (c) and (d), tightly-packed ettringite is filling and lining voids. EDAX verifies the elemental composition of the crystal formations by showing the distinct aluminum, sulfur, and calcium pattern. The three cores do not vary considerably in

the type of ettringite formations or in the prevalence of ettringite formations in the samples.

The UV light ASR test confirms the presence of ASR gel in the wingwall. See Figures 4.28 (a) and (b) for ASR gel and analysis report. EDAX verifies the elemental composition of the gel by showing the distinct silicon and potassium pattern.

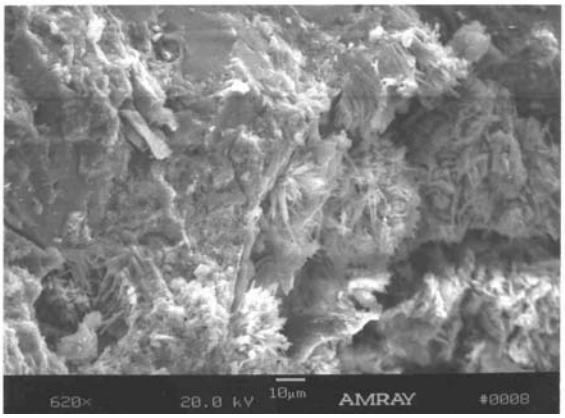

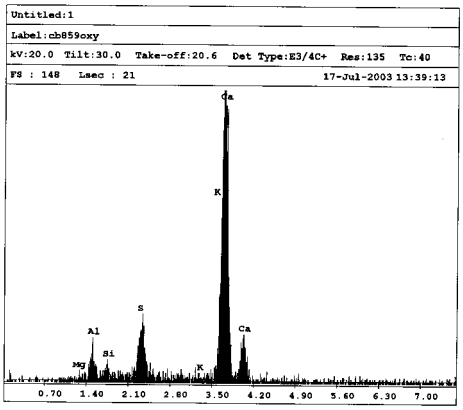

EDAX ZAF Quantification (Standardless)
Element Normalized
SEC Table : Default

Element	Wt %	At %	K-Ratio	Z	A	F
MgK	1.11	1.68	0.0044	1.0233	0.3875	1.0055
AlK	8.26	11.27	0.0430	0.9929	0.5206	1.0074
SiK	3.16	4.14	0.0188	1.0216	0.5754	1.0118
S K	11.37	13.05	0.0915	1.0171	0.7714	1.0259
K K	0.50	0.47	0.0048	0.9745	0.8829	1.1089
CaK	75.60	69.40	0.6942	0.9968	0.9212	1.0000
Total	100.00	100.00				

(a) Ettringite on the Surface **(b) Analysis of Whole Picture (a)**

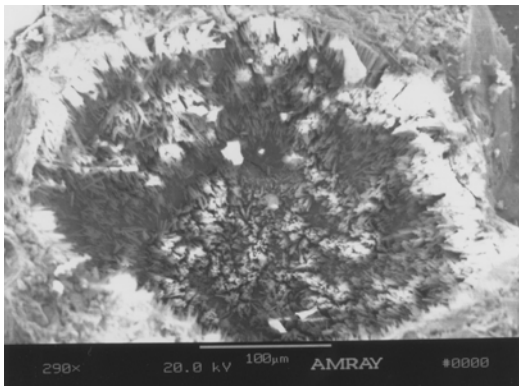

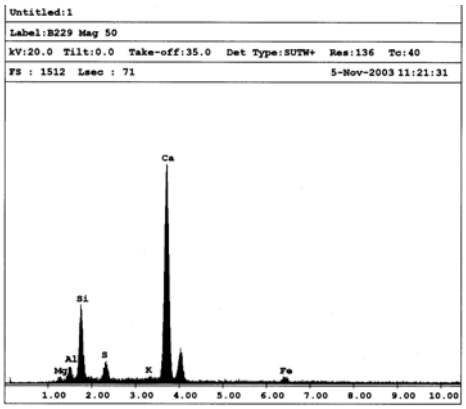

EDAX ZAF Quantification (Standardless)
Element Normalized
SEC Table : Default

Element	Wt %	At %	K-Ratio	Z	A	F
MgK	1.01	1.54	0.0048	1.0247	0.4556	1.0060
AlK	3.45	4.71	0.0205	0.9944	0.5924	1.0104
SiK	15.38	20.17	0.1095	1.0231	0.6890	1.0099
S K	4.55	5.22	0.0363	1.0187	0.7653	1.0252
K K	1.24	1.16	0.0123	0.9760	0.9138	1.1117
CaK	69.97	64.30	0.6570	0.9983	0.9393	1.0013
FeK	4.40	2.90	0.0370	0.9098	0.9225	1.0000
Total	100.00	100.00				

(c) Ettringite in Void **(d) Analysis of Whole Picture (c)**

Figure 4.26: MD 32 EB over US 1 (1311000)

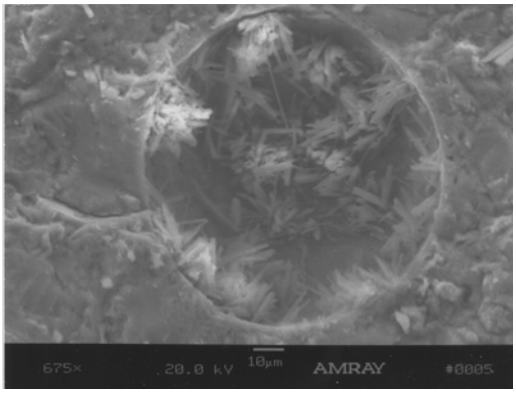

(a) Ettringite in Void

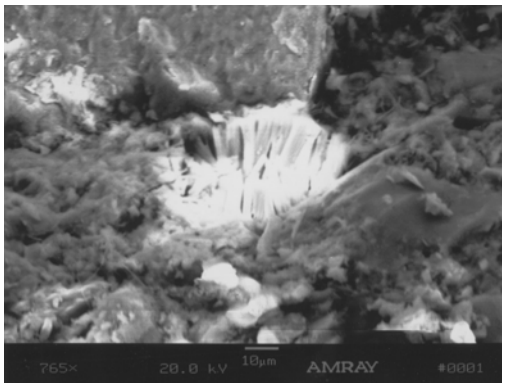

(b) Ettringite in Between Aggregate (Top) and Cement Paste (Bottom)

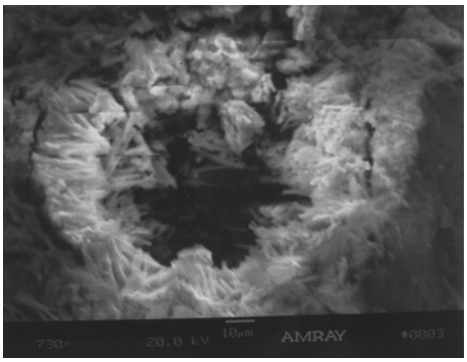

(c) Tightly-Packed Ettringite – 1

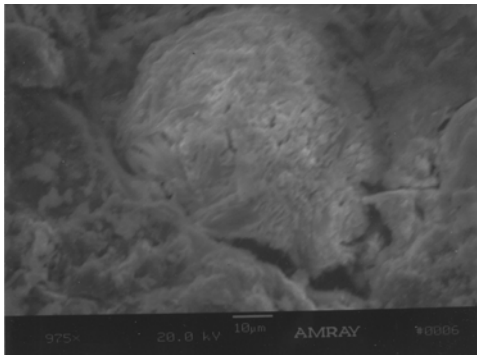

(d) Tightly-Packed Ettringite – 2

Figure 4.27: MD 32 EB over US 1 (1311000)

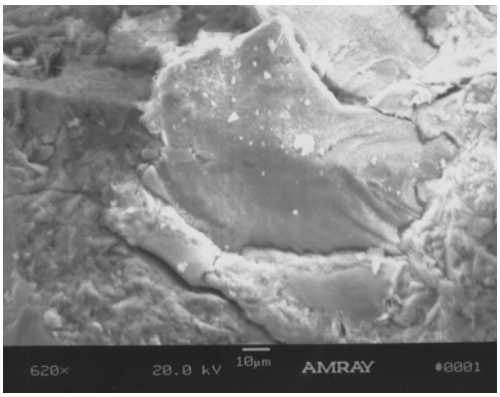

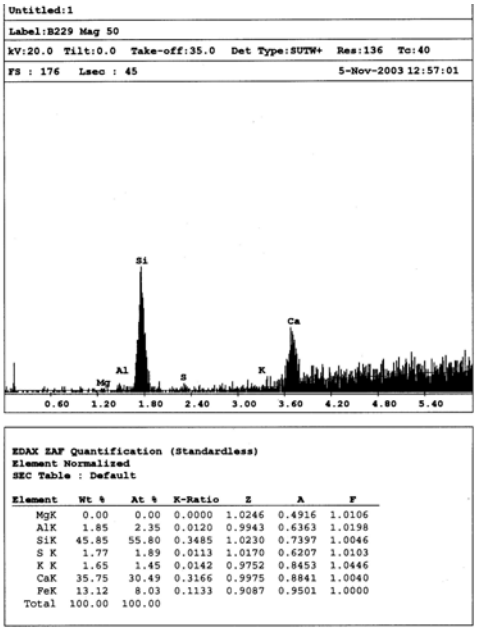

(a) Possible ASR Gel **(b) Analysis of Possible ASR Gel (a)**

Figure 4.28: MD 32 EB over US 1 (1311000)

4.5.6 Bridge 2203201 (US 13 NB over MD 346)

Two cores were taken from the center beam of the southernmost span; see Figure 4.29 for locations.

Figure 4.29: Coring Locations (2203201 – US 13 NB over MD 346)

The left core did not exhibit signs of either DEF or ASR gel, but the cement paste had extensive microcracking on the surface and in the voids, see Figure 4.30. The right core exhibited ettringite formations, which were unlike any form observed prior. Even at a high magnification, not shown here, a lamellar material appeared to cover the void surface, see Figure 4.31. EDAX verifies the elemental composition of the lamellar material as ettringite by showing the distinct aluminum, sulfur, and calcium pattern. No signs of ASR gel were observed in either core, using the SEM or the UV light test.

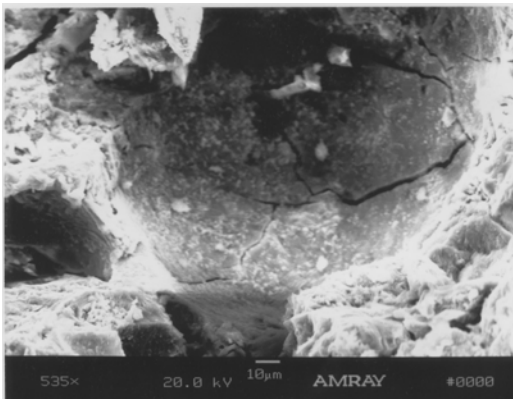

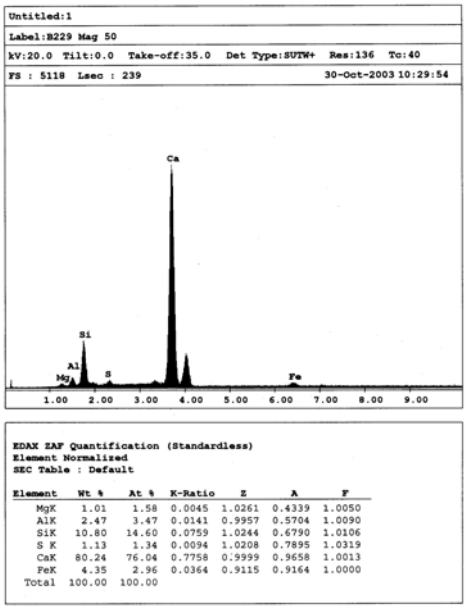

(a) Microcracking in the Void **(b) Analysis of Whole Picture (a)**

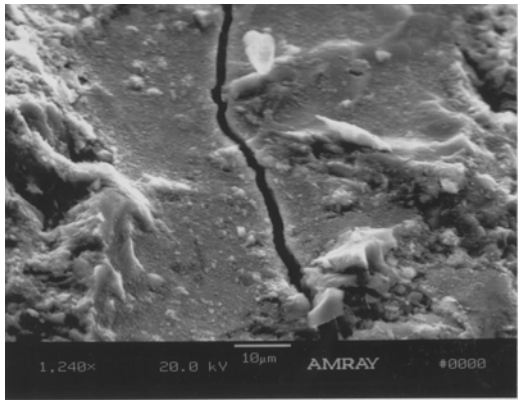

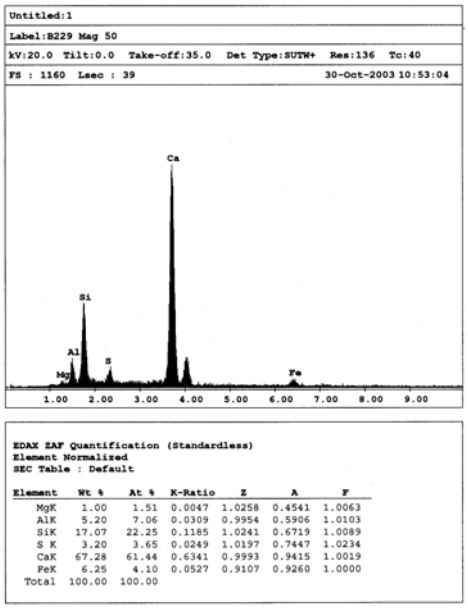

(c) Microcracking on the Surface **(d) Analysis of Whole Picture (c)**

Figure 4.30: US 13 NB over MD 346 (2203201)

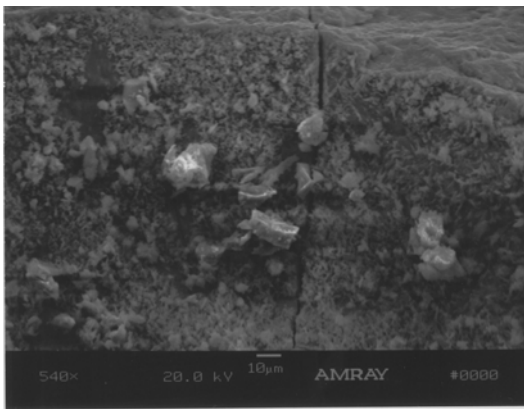

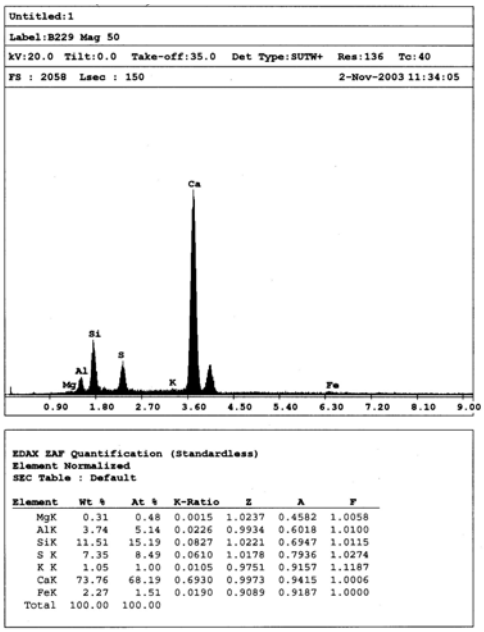

(a) Ettringite in a Void **(b) Analysis of the Whole Picture (a)**

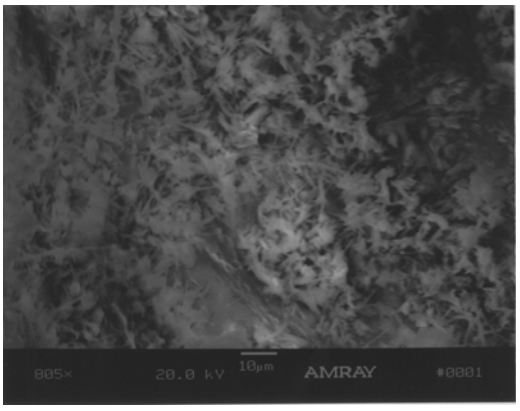

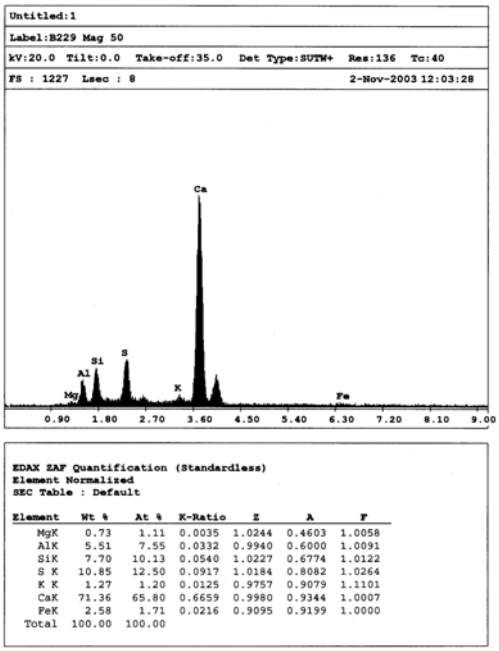

(c) Ettringite in a Void **(d) Analysis of the Whole Picture (c)**

Figure 4.31: US 13 NB over MD 346 (2203201)

4.5.7 Bridge 0800201 (MD 5 NB over Zekiah Swamp)

Three cores were taken from the inside face of the east parapet; see Figure 4.32 for locations.

Figure 4.32: Coring Locations (0800201 – MD 5 NB over Zekiah Swamp)

The leftmost core in the left image from Figure 4.32 exhibited no signs of DEF, see Figure 4.33 for typical images, but the right and center cores exhibited ettringite formations. In Figure 4.34, the ettringite formations appear to be hexagonal prismatic in morphology. EDAX verifies the elemental composition of the crystal formations by showing the distinct aluminum, sulfur, and calcium pattern.

The UV light ASR test confirms the presence of ASR gel in the wingwall. The right core contains possible locations of ASR gel as observed with the SEM, see Figure 4.35. EDAX verifies the elemental composition of the gel by showing the distinct silicon and potassium pattern for Figures 4.35 (a) and (b) with a potassium percentage by weight of 1.55, but the pattern is not as pronounced for Figures 4.35 (c) and (d) with a potassium percentage by weight of 0.91.

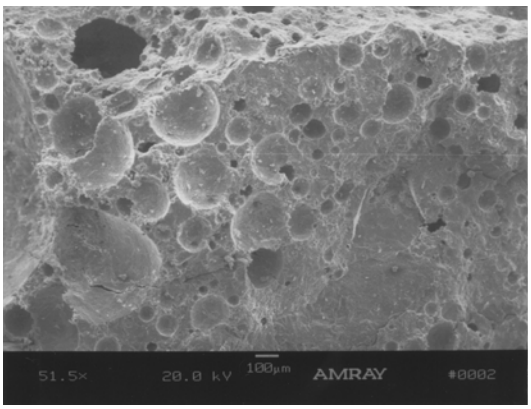

(a) Numerous Empty Voids

(b) Typical Void with Calcium Hydroxide

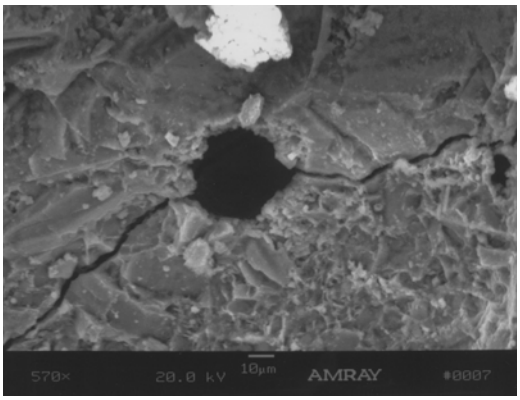

(c) Void with Crack

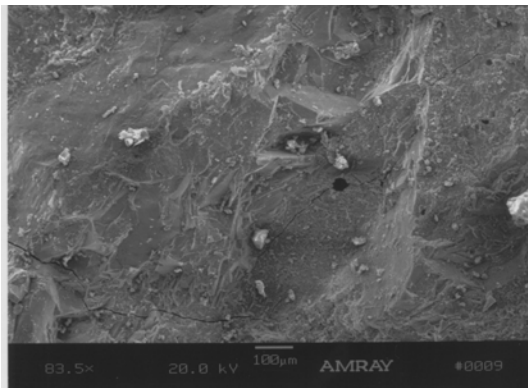

(d) Void with Crack

Figure 4.33: MD 5 NB over Zekiah Swamp (0800201)

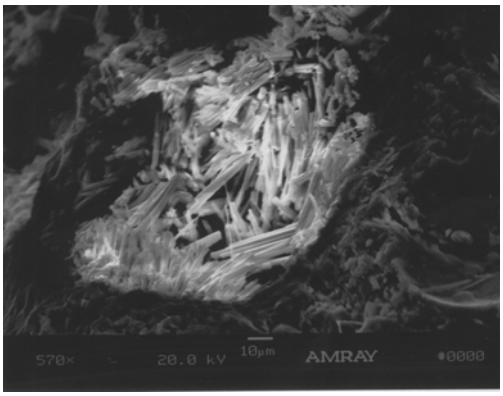

(a) Ettringite in Void

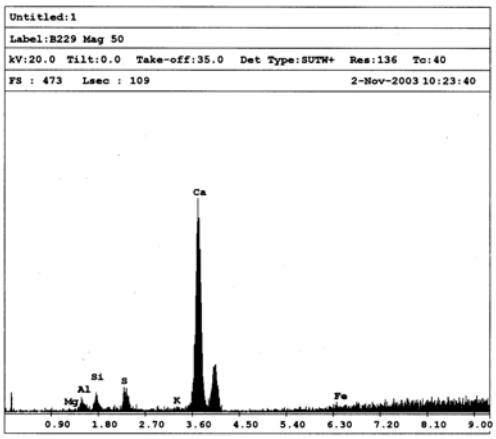

EDAX ZAF Quantification (Standardless)
Element Normalized
SEC Table : Default

Element	Wt %	At %	K-Ratio	Z	A	F
MgK	0.64	1.01	0.0028	1.0278	0.4260	1.0044
AlK	3.42	4.90	0.0195	0.9973	0.5653	1.0076
SiK	3.79	5.21	0.0262	1.0261	0.6665	1.0122
S K	5.69	6.85	0.0498	1.0229	0.8289	1.0335
K K	1.06	1.05	0.0112	0.9794	0.9396	1.1482
CaK	80.76	77.78	0.7776	1.0017	0.9599	1.0013
FeK	4.64	3.21	0.0388	0.9132	0.9146	1.0000
Total	100.00	100.00				

(b) Analysis of Ettringite in Void – Picture (a)

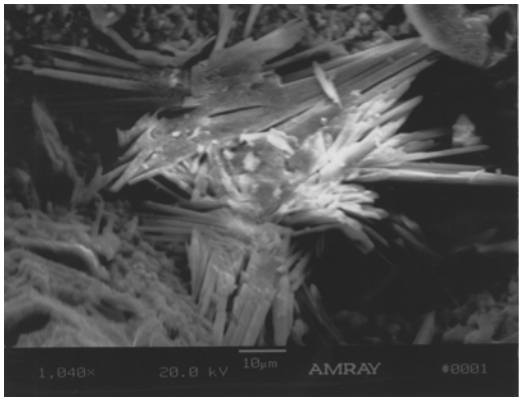

(c) Ettringite on the Surface

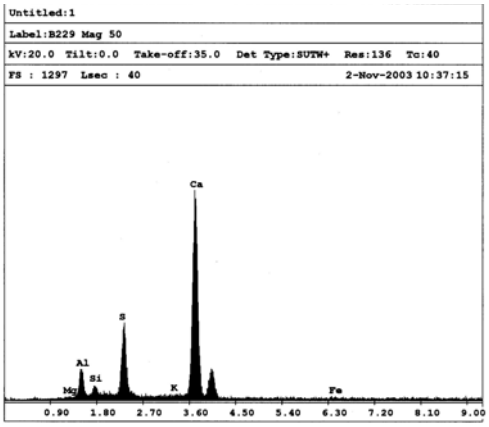

EDAX ZAF Quantification (Standardless)
Element Normalized
SEC Table : Default

Element	Wt %	At %	K-Ratio	Z	A	F
MgK	0.26	0.39	0.0012	1.0247	0.4606	1.0057
AlK	6.81	9.38	0.0413	0.9943	0.6049	1.0085
SiK	1.74	2.31	0.0121	1.0230	0.6702	1.0145
S K	16.98	19.67	0.1501	1.0188	0.8450	1.0267
K K	1.07	1.02	0.0104	0.9760	0.8987	1.1050
CaK	71.03	65.83	0.6584	0.9983	0.9280	1.0006
FeK	2.11	1.40	0.0176	0.9098	0.9189	1.0000
Total	100.00	100.00				

(d) Analysis of Ettringite – Picture (c)

Figure 4.34: MD 5 NB over Zekiah Swamp (0800201)

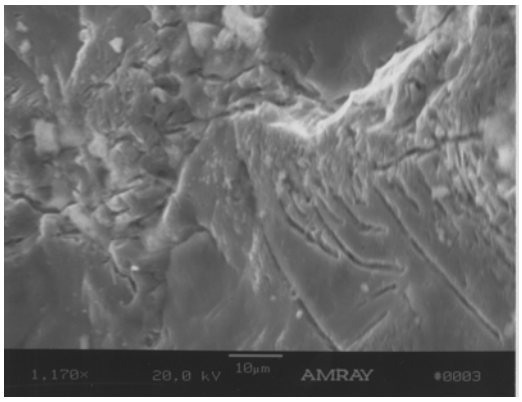

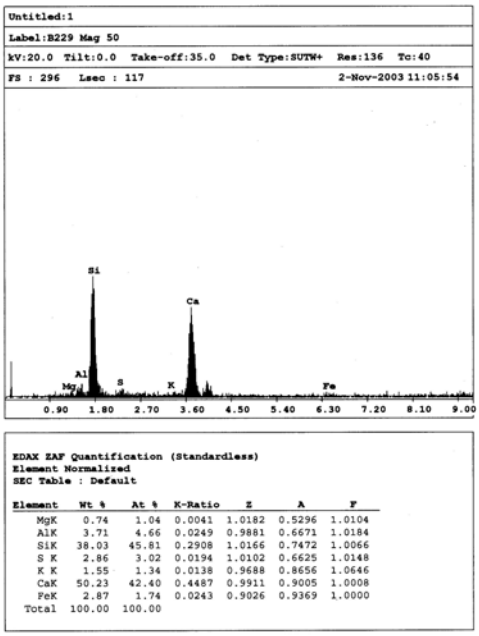

(a) Possible ASR Gel **(b) Analysis of Possible ASR Gel (a)**

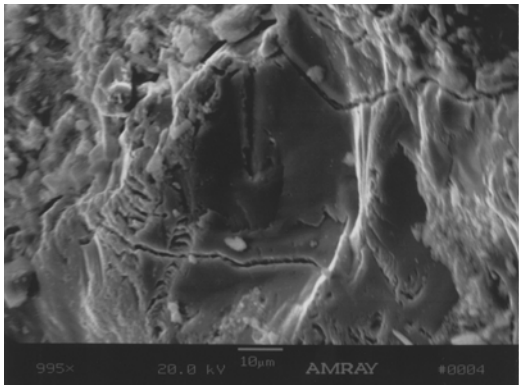

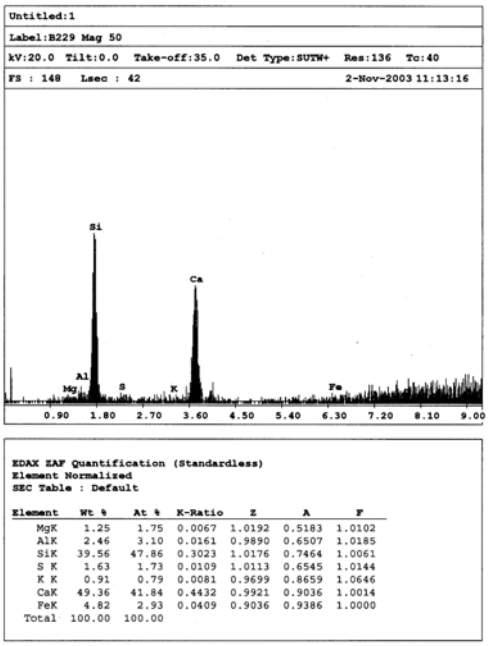

(c) Possible ASR Gel **(d) Analysis of Possible ASR Gel (c)**

Figure 4.35: MD 5 NB over Zekiah Swamp (0800201)

4.5.8 Bridge 1102100 (US 219 over Deep Creek Lake)

Three cores were taken from the northwest wingwall; see Figure 4.36 for locations.

Figure 4.36: Coring Locations (1102100 – US 219 over Deep Creek Lake)

All three cores exhibited ettringite formations throughout the samples, and two different types of ettringite formations were observed in these cores. In Figure 4.37 (a) and (b), the ettringite formations appear to be needle-like short crystals found on the fractured surface, and in Figures 4.37 (c) and (d), the ettringite formations appear to be hexagonal prismatic in morphology. EDAX verified the elemental composition of the crystal formations by showing the distinct aluminum, sulfur, and calcium pattern. The three cores do not vary considerably in the type of ettringite formations or in the prevalence of ettringite formations in the samples.

The UV light ASR test confirmed the presence of ASR gel in the wingwall. The left core contains possible locations of ASR gel as observed with the SEM, see Figure 4.38. EDAX verified the elemental composition of the gel by showing the distinct silicon and potassium pattern.

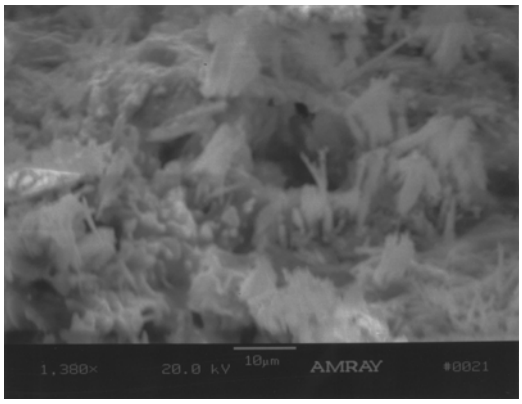

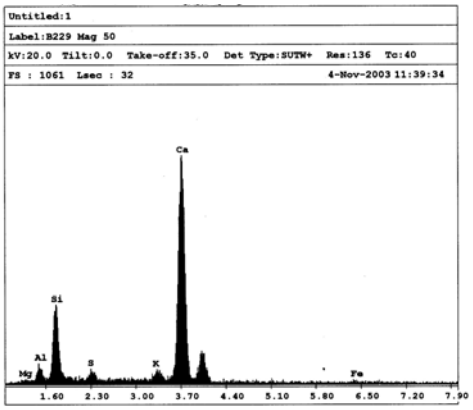

EDAX ZAF Quantification (Standardless)
Element Normalized
SEC Table : Default

Element	Wt %	At %	K-Ratio	Z	A	F
MgK	0.44	0.67	0.0021	1.0240	0.4604	1.0061
AlK	3.51	4.78	0.0212	0.9936	0.6028	1.0107
SiK	16.17	21.20	0.1164	1.0223	0.6976	1.0097
S K	2.36	2.72	0.0189	1.0179	0.7652	1.0265
K K	2.95	2.78	0.0297	0.9753	0.9229	1.1161
CaK	72.01	66.16	0.6746	0.9975	0.9385	1.0007
FeK	2.56	1.69	0.0214	0.9091	0.9200	1.0000
Total	100.00	100.00				

(a) Ettringite on the Surface **(b) Analysis of Whole Picture (a)**

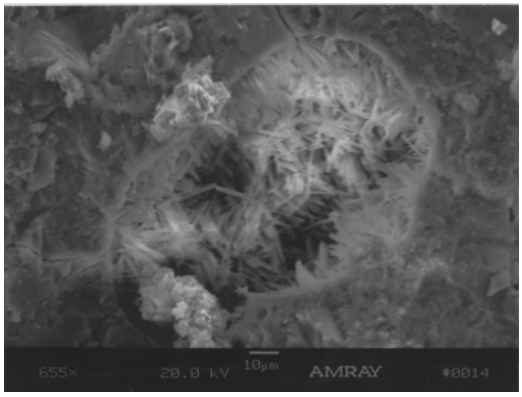

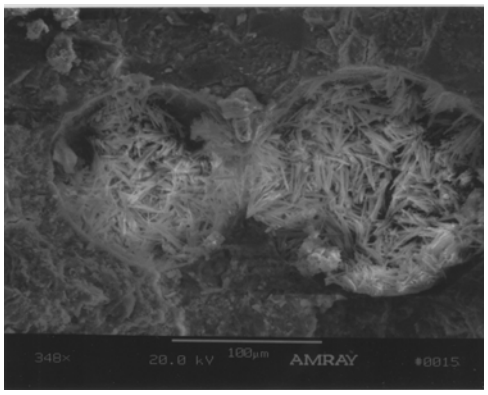

(c) Ettringite in Void **(d) Ettringite in Void**

Figure 4.37: US 219 over Deep Creek Lake (1102100)

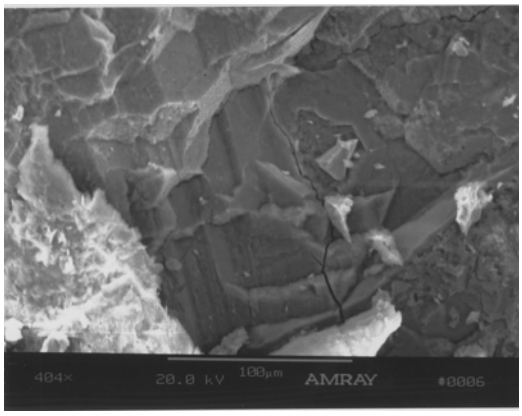

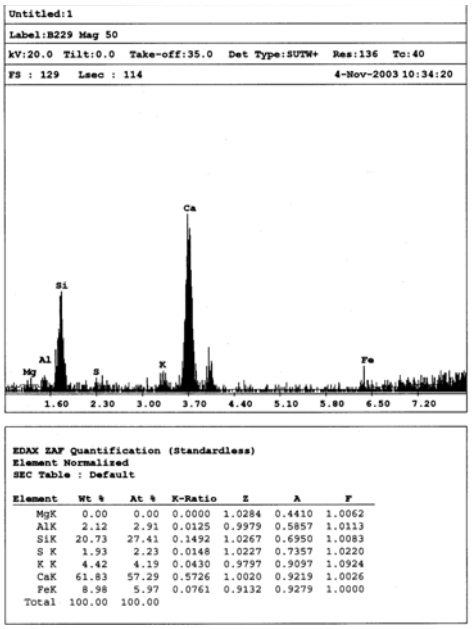

(a) Possible ASR Gel **(b) Analysis of Possible ASR Gel**

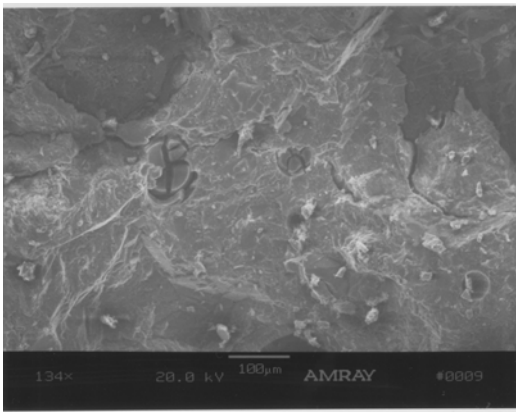

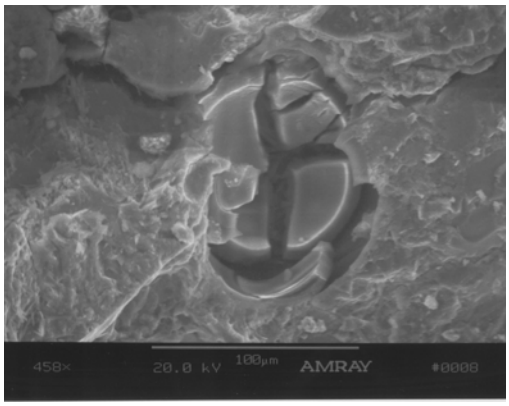

(c) Possible ASR Gel with Cracking

(d) Possible ASR Gel – Close-up of Picture (c)

Figure 4.38: US 219 over Deep Creek Lake (1102100)

4.5.9 Control Bridge 1301302 (US 29 over Middle Patuxent River)

Three cores were taken from the southwest wingwall; see Figure 4.39 for locations.

Figure 4.39: Coring Locations (US 29 over Middle Patuxent River)

All three cores exhibited ettringite formations throughout the samples, but the samples only contained hexagonal prismatic DEF in voids. The amount of DEF found in the voids was minimal compared to bridges with map cracking, see Figure 4.40.

The UV light ASR test does not show the presence of ASR gel in the wingwall. Also, no locations of ASR gel were identified with the SEM.

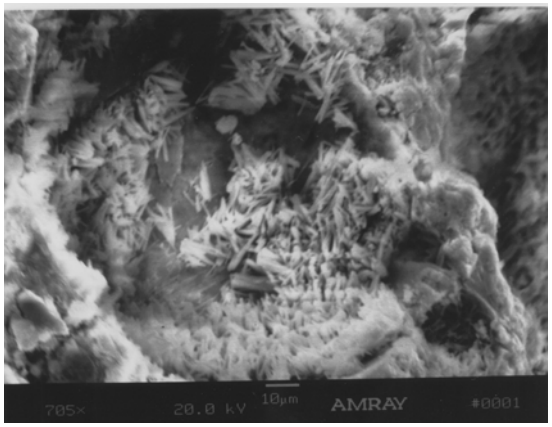

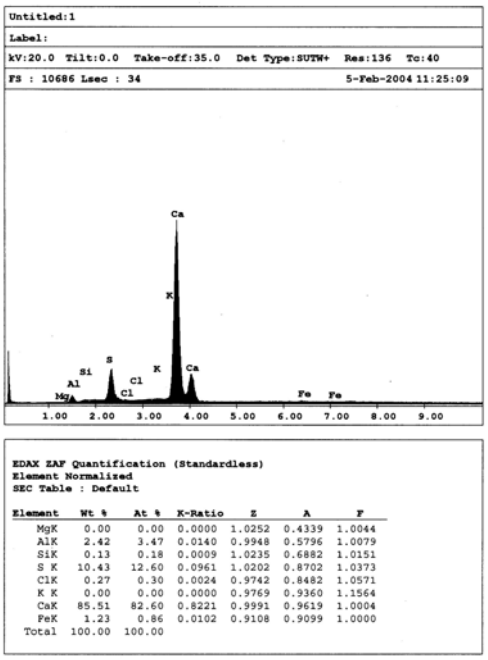

(a) Ettringite in Voids **(b) Analysis of (a)**

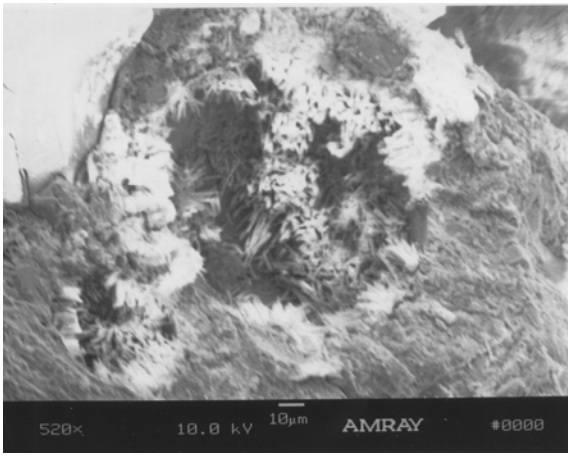

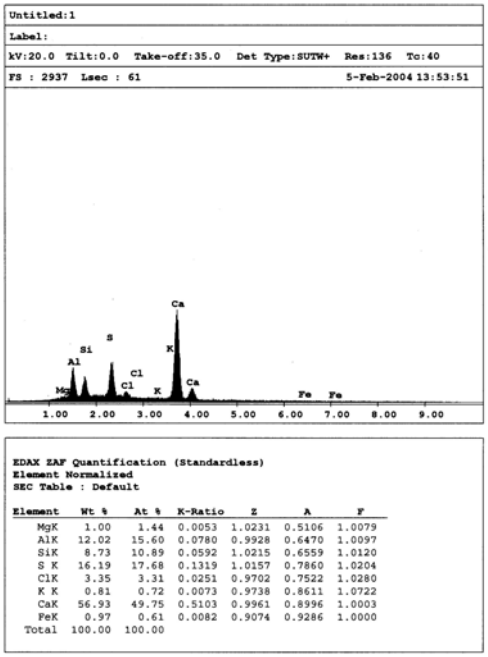

(c) Ettringite in Voids **(d) Analysis of (c)**

Figure 4.40: US 29 over Middle Patuxent River (1301302)

4.5.10 Control Bridge 0333702 (I-795 over Cockeys Mill Road)

Three cores were taken from the outside face of the west parapet above the northwest wingwall; see Figure 4.41 for locations.

Figure 4.41: Coring Locations (I-795 over Cockeys Mill Road)

All three cores exhibited ettringite formations throughout the samples, but the samples only contained hexagonal prismatic DEF in voids. The amount of DEF found in the voids was minimal compared to bridges with map cracking, and the DEF was found mixed in with calcium hydroxide crystals, see Figure 4.42.

The UV light ASR test did not show the presence of ASR gel in the parapet. One microscopic location of ASR gel was observed in the right core, but ASR does not appear to be of significant quantity to produce damage.

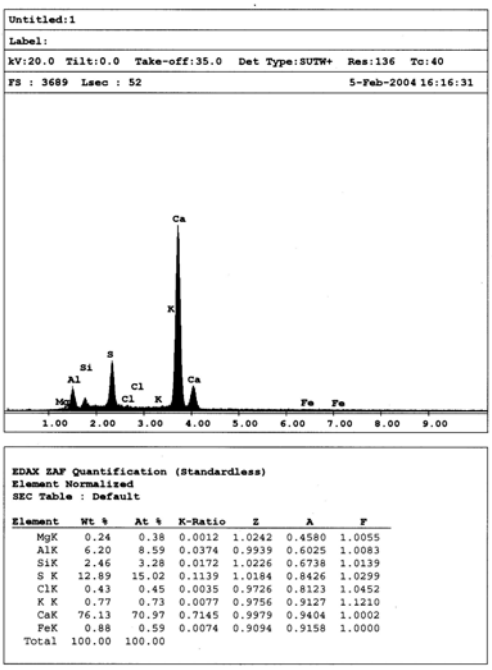

(a) Ettringite in Voids **(b) Analysis of (a)**

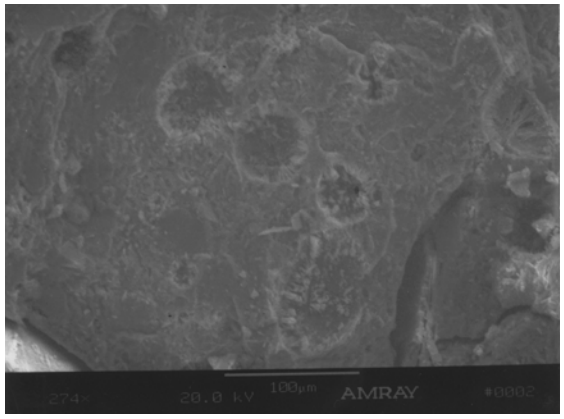

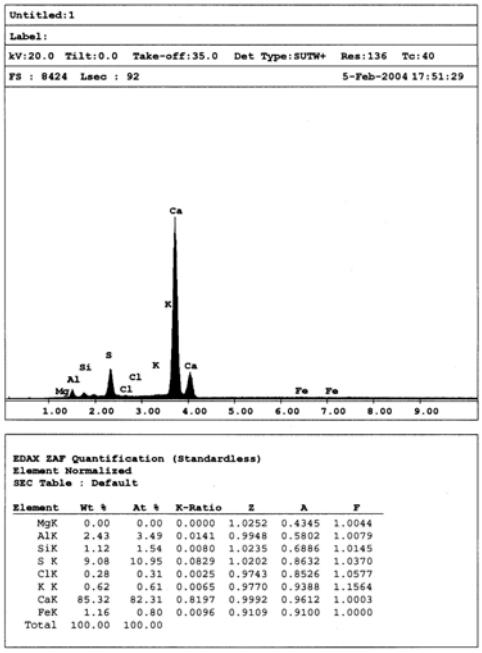

(c) Ettringite in Voids **(d) Analysis of (c)**

Figure 4.42: I-795 over Cockeys Mill Road (0333702)

4.6 Summary and Conclusion

Upon examining all 29 cores, 26 cores contained Delayed Ettringite Formation (DEF), and of the ten bridges, seven bridges contained Alkali-Silica Reaction (ASR) gel. In addition, four different types of ettringite formations were observed: needle-like crystals, hexagonal prismatic crystals, a tightly-packed, and a lamellar material.

The study confirms that MDSHA bridges exhibit DEF in the bridge population throughout the state. No statistical values can be derived from this study since the population was deliberately skewed toward bridges with suspect symptoms; more work is necessary in order to quantify the probability of DEF occurrence.

The study observed four different forms of DEF in samples from the field. The possibility of ettringite existing in different forms has been speculated by some researcher, but this topic is still highly debated. The results from this study should help shed some light on this topic.

Another debated topic is the role of DEF in the expansion process that leads to map cracking. The study compared the SEM results to the surface conditions, and several trends were observed including, the significance of DEF in concrete microcracks, and the quantity of tightly-packed DEF. Both are believed to be correlated with map cracking on the concrete surface. A hypothesis can be developed from this research suggesting a link between map cracking with associated moisture on the surface, extensive amounts of DEF in microcracks inside the concrete element, and ASR. Diamond suggests that ASR works to develop the initial microcracks and DEF propagates the cracks (1994). This explanation best describes the samples observed in this study. Because of the limited number of corings taken, a hypothesis

can be developed but future work will be needed to clarify and verify the hypothesis. A possible correlation between the surface map cracking and interior deficiencies would be very useful for bridge inspectors since no equipment would be needed to identify locations suffering from DEF / ASR deterioration. Once identified, the locations can be tested further or monitored as needed.

Future work should be preformed to test this hypothesis involving additional corings. A future coring regiment should focus on verifying the working hypothesis. Once the hypothesis is finalized, bridge inspectors can be trained to identify DEF / ASR deterioration throughout the State of Maryland. Further research should, also, be conducted into understanding the expansion process of DEF, which could lead to developing abatement processes and correcting the mix composition to prevent further incidences of DEF. Mitigation processes to prevent further damage for existing DEF cases would also be helpful.

Chapter 5

Phase 2 Field Survey – Scanning Electron Microscopy Analysis

5.1 Introduction

The scanning electron microscopy (SEM) was utilized for this project to examine samples of concrete taken from bridges throughout Maryland State Bridge Inventory. The SEM provides images of the cement paste for microcracking and alkali-silica reaction (ASR) gel, the voids for crystal formations contained inside, and aggregate pullouts for cracking along the aggregate / paste interface and crystal formations. The intent of the core sampling was to develop a better understanding of concrete deterioration that exhibits map cracking on the surface of a concrete element.

5.2 Scanning Electron Microscopy

Twelve additional bridges were cored during phase 2 in order to develop a better understanding of the significance of different types of DEF. Ettringite is identified visually using the scanning electron microscope (SEM) and elemental analysis of the crystals can be preformed using energy dispersive analysis x-ray

(EDAX). The SEM using a voltage of 20 kilovolt (kV) directs a stream of electrons at a concrete sample, which interacts with the surface of the sample. See Figure 5.1 (a) for an example micrograph; the micrograph gives the accelerated voltage (20.0 kV), the magnification power (595x), and a scale. Two significant signals are produced, secondary electrons (SE) and x-rays. The SE are used to "see" the sample, and the SEM interprets the signal to produce a visual image for the operator. X-rays are used to identify the elements present in the region of interest, because EDAX works on the principle of discrete energy level for the various elements, and each element can only emit x-rays (photons) with specific energy levels. EDAX detects the emitted x-rays and the associated energy, and from a database, it associates the various x-rays with the corresponding element that produced the x-ray, which allows positive identification of the presence of ettringite in the samples. See Figure 5.1 (b) for an example EDAX output. The EDAX output shows a chart with the number of counts per energy level, the relative number of count is shown in the peak heights and the x-ray energy level is shown on the x-axis. The elements are identified above their count peak, with calcium having two peaks the first large and the second much smaller in size. Below the chart is a table with elemental analysis, which shows the percentage of the counts (At %) from each element. From the ZAF database the program calculates the percentage by weight (Wt %) for each element. The value used for the calculation are provided in the table, (K-ratio, Z, A, and F). The SEM can produce images of objects less than 100 nm in size, and for this project, the objects of interest were in the order of 1μm to 100μm.

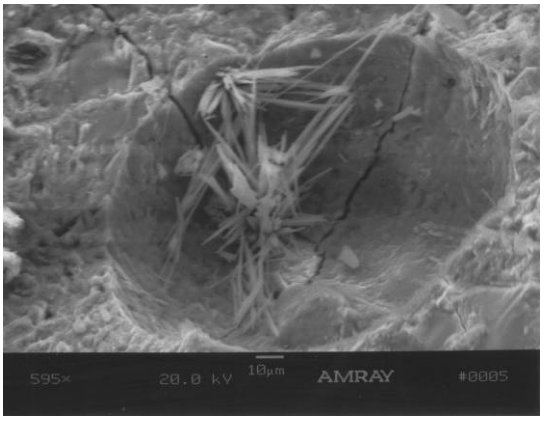

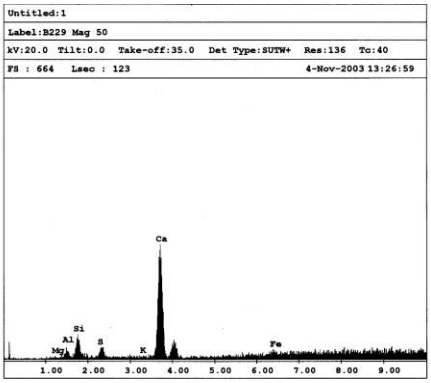

EDAX ZAF Quantification (Standardless)
Element Normalized
SEC Table : Default

Element	Wt %	At %	K-Ratio	Z	A	F
MgK	0.32	0.51	0.0014	1.0313	0.4161	1.0048
AlK	3.66	5.21	0.0205	1.0007	0.5566	1.0081
SiK	8.74	11.98	0.0597	1.0296	0.6563	1.0102
S K	5.16	6.19	0.0429	1.0264	0.7884	1.0269
K K	1.24	1.22	0.0126	0.9828	0.9228	1.1191
CaK	70.63	67.82	0.6738	1.0051	0.9463	1.0030
FeK	10.25	7.07	0.0867	0.9164	0.9231	1.0000
Total	100.00	100.00				

(a) Ettringite Crystals in Void – SEM

(b) Analysis of Ettringite Crystals in Void – EDAX

Figure 5.1: Sample Images from SEM and EDAX

5.3 Sample Preparation and Examination Methodology

A total of 60 cores, 2 inches in diameter and 2 to 3 inches deep, were taken from twelve bridges throughout the state, 36 cores of which or 3 cores per bridge were used to perform SEM and EDAX analysis, see Figure 5.2 for a typical core. In order to analyze the concrete, smaller samples of concrete are needed. Each core is broken into small pieces with a five pound sledge hammer, and a sample is selected which has a relatively flat side to allow mounting.

Once the sample is selected, the sample is dried. During the drying process, a cork and carbon stud is readied and the sample is logged. Carbon stud, adhesive, and coating are used since the X-ray energy level associated with carbon is not close to the elements of interest in concrete, ettringite, and ASR gel. After the sample is dried, the sample gets mounted onto the carbon stud with the carbon adhesive. The cork acts as a holder to keep the sample upright, as shown in Figure 5.3. The assembly is dried until the carbon adhesive is completely set. The final step is to coat the sample surface with carbon which provides a clear visual image of the surface and avoids electron charge buildup on the sample. The sample and stud are placed into a vacuum chamber, in which the pressure is lowered to 0.100 torr (1 torr = 1 millimeter of mercury or 133.32 pascal). At this pressure, the carbon coating is applied. After the coating, the sample is ready for the SEM. The sample assembly is placed into the SEM with the top surface at an approximately 30 degree angle to produce the maximum possible signal for the EDAX analysis process.

The sample is searched in an across-down-across-down pattern for possible locations of DEF and ASR gel, see Figure 5.4 (a) to (d). The intension of the search pattern is to document the prevalence of both forms of deterioration.

In order to quantify DEF or ASR in the sample, one additional step was added to the examination. Maps of the samples were developed with grids that provided a description of any substance found therein. See Figure 5.5 for an example map.

Since presence of ASR is possible in the cores, a separate test was preformed on a large sample taken from each core. AASHTO T299-93 defines the procedure for identifying ASR in the field (AASHTO Innovative Highway Technologies 1998). Since all of the tests were conducted in a lab, several simplifications were made, but the basic procedure was still followed. The procedure requires fresh concrete surface to test, and a large fragment was selected after the cores were fractured. The sample is then washed with clean water and a solution of dilute uranyl acetate is applied. After the sample has dried from at least 3 minutes, the sample can be placed under a short wave ultra-violet (UV) light (~250 nm). Once viewed under the UV light, ASR will appear yellow-green and tends to be found in cracks or around aggregates, see Figure 5.4 (e) and (f) for test procedure.

(a) Two Inches Diameter by Three Inches Deep Core

(b) Fractured Core

Figure 5.2: Sample Preparation - 1

(a) Samples Drying

(b) Corks and Carbon Stubs

(c) Samples Mounted with Carbon

(d) Carbon Coating Machine

Figure 5.3: Sample Preparation – 2

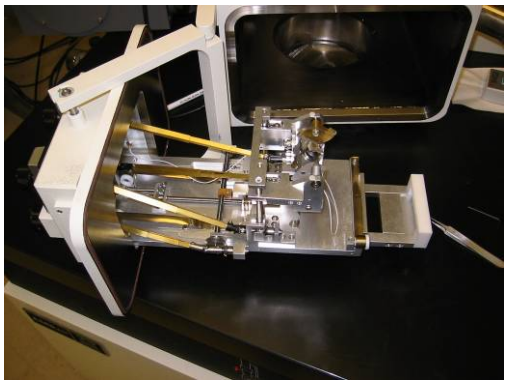

(a) Samples Mounted

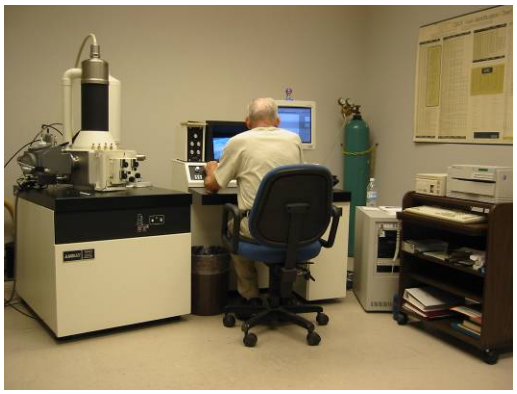

(b) Scanning Electron Microscope

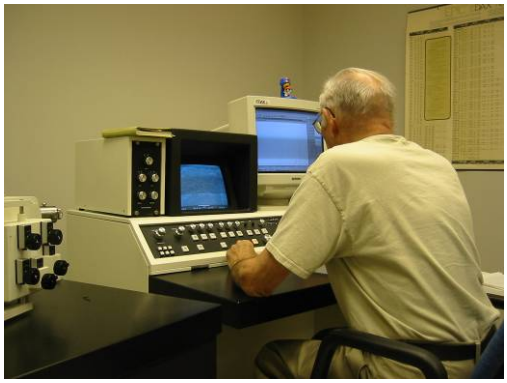

(c) Viewing an Image

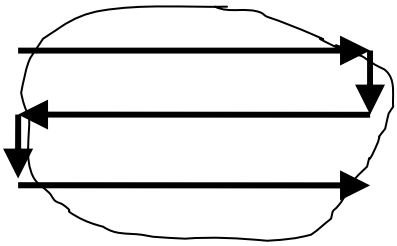

(d) Search Pattern

(e) Applying Uranyl Acetate

(f) Placing Sample Under UV Light

Figure 5.4: Sample Examination

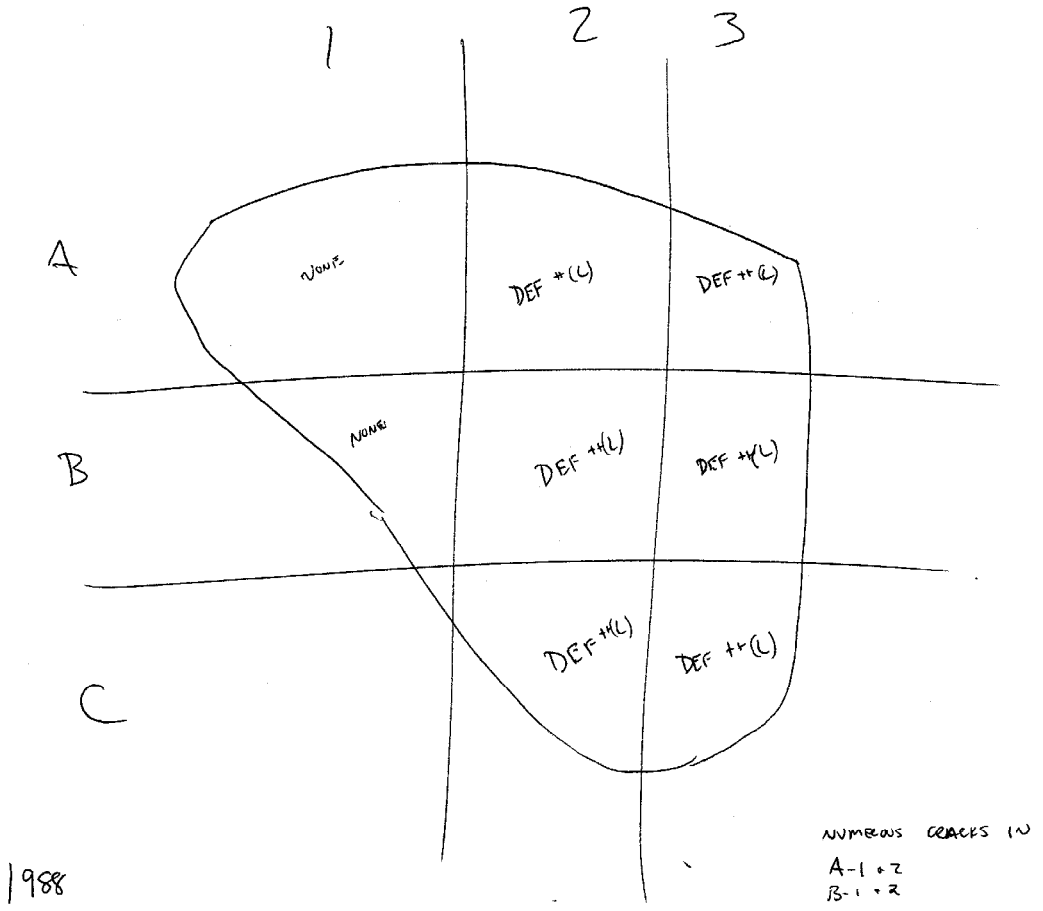

Figure 5.5: Example Map

5.4 Results

Results are presented in sub-subpopulation groups starting with clean bridges built before 1980. Following are clean bridges built after 1980, dirty bridges built before 1980, and dirty bridges built after 1980. Note that 5 cores where taken from all bridges, but only three were analyzed using SEM and EDAX. The other two are for additional testing that is not included in this dissertation. Results will include discussion about the presence, prevalence, and morphology of ettringite. Additional examinations will be preformed into the presence of ASR.

5.4.1 Clean Bridges Built Before 1980

5.4.1.1 Bridge 1005000 (MD 77 over Hunting Creek)

Five cores were taken from the southwest wingwall; see Figure 5.6 for locations.

Figure 5.6: Coring Locations (1005000 – MD 77 over Hunting Creek)

Two of the three cores examined contained no ettringite formations. The third core contained long ettringite crystals mixed in with calcium hydroxide $Ca(OH)_2$. The DEF fills much less than 5% of the voids. See Figure 5.7. Energy Dispersive Analysis X-ray (EDAX) verifies the elemental composition of the crystal formations by showing the distinct aluminum, sulfur, and calcium pattern with very high levels of calcium from the $Ca(OH)_2$. The bridge contained little to no ettringite in the cores sampled, see Figure 5.8 for typical core results.

In addition to the SEM and EDAX analysis, a large sample of the fractured cores was taken for ASR testing. The testing methodology is described in Section 4.3. The UV light ASR test indicates no presence of ASR gel in the wingwall.

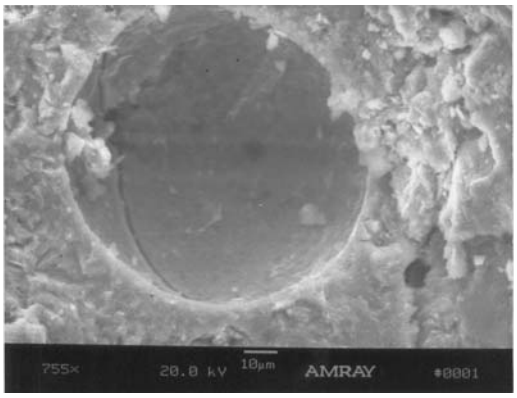

(a) Empty Void with Microcracking in the Background

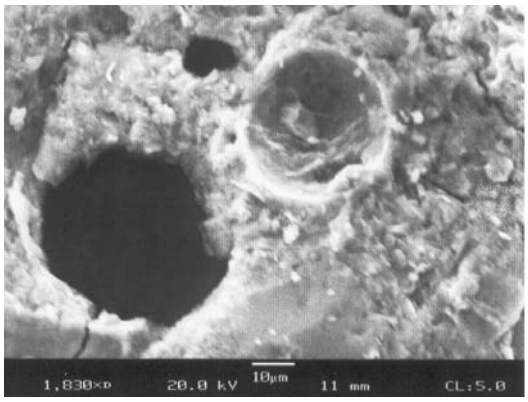

(b) Empty Voids

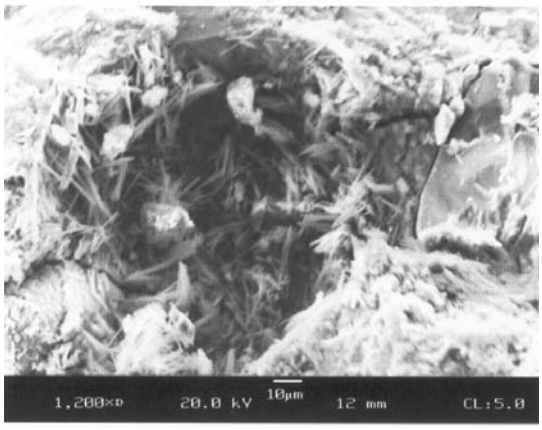

(c) Calcium Hydroxide and Ettringite in Void

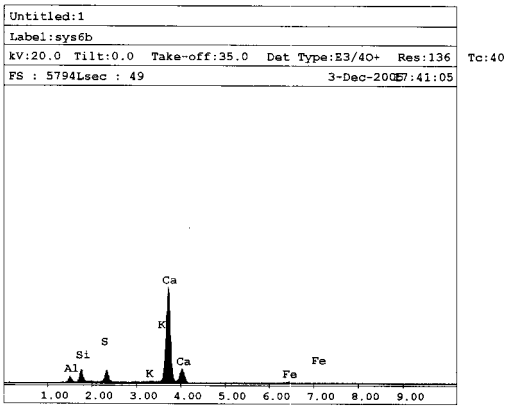

(d) Analysis of Crystals in (c)

Figure 5.7: MD 77 over Hunting Creek (1005000)

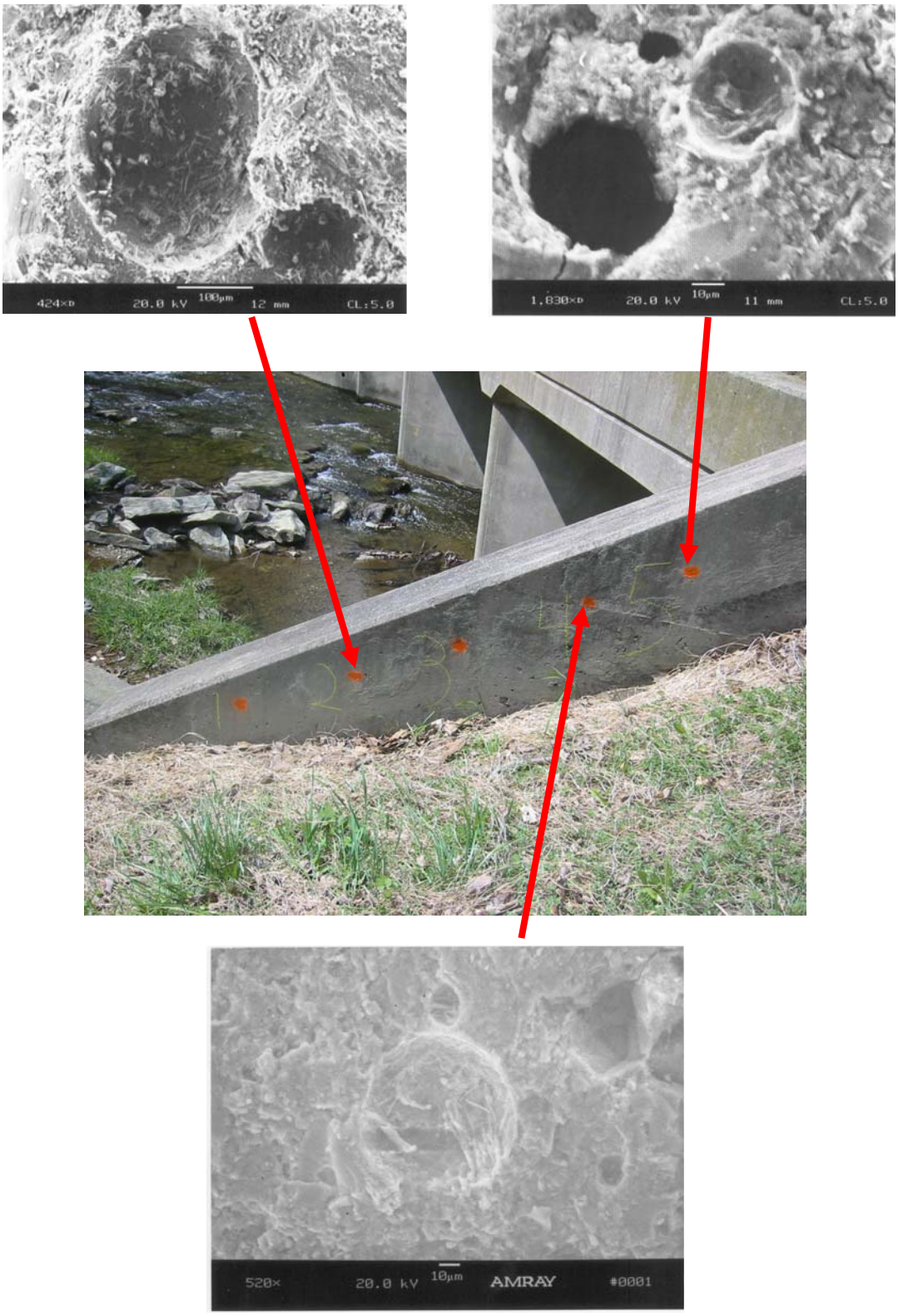

Figure 5.8: Ettringite Spatial Distribution

(1005000 – MD 77 over Hunting Creek)

5.4.1.2 Bridge 1011100 (US 15 SB over Fishing Creek)

Five cores were taken from the northwest wingwall; see Figure 5.9 for locations.

Figure 5.9: Coring Locations (1011100 – US 15 SB over Fishing Creek)

One of the three cores examined contained no ettringite formations. The other two cores contained long ettringite crystals mixed in with calcium hydroxide $Ca(OH)_2$ in some locations. The DEF fills much less than 5% of the voids. See Figures 5.10 and 5.11. Energy Dispersive Analysis X-ray (EDAX) verifies the elemental composition of the crystal formations by showing the distinct aluminum, sulfur, and calcium pattern in general. Figure 5.11 (b) has very high levels of calcium indicating the DEF is mixed with $Ca(OH)_2$. The bridge contained little to no ettringite in the cores sampled, see Figure 5.12 for typical core results.

In addition to the SEM and EDAX analysis, a large sample of the fractured cores was taken for ASR testing. The UV light ASR test indicates no presence of ASR gel in the wingwall.

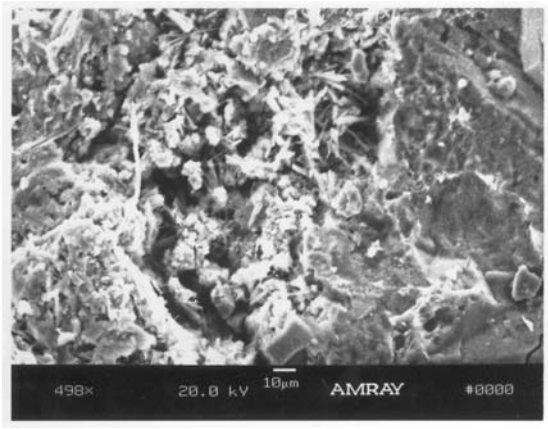

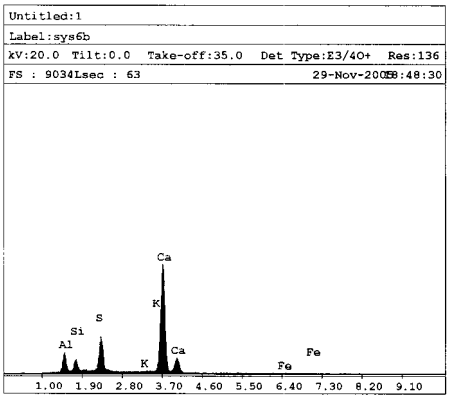

EDAX ZAF Quantification (Standardless)
Element Normalized
SEC Table : Default

Element	Wt %	At %	K-Ratio	Z	A	F
AlK	8.17	11.08	0.0508	0.9930	0.6210	1.0090
SiK	4.72	6.15	0.0328	1.0216	0.6710	1.0134
S K	15.14	17.27	0.1302	1.0170	0.8242	1.0257
K K	0.82	0.77	0.0079	0.9745	0.8971	1.1037
CaK	70.34	64.21	0.6508	0.9967	0.9280	1.0002
FeK	0.81	0.53	0.0067	0.9082	0.9196	1.0000
Total	100.00	100.00				

(a) Ettringite in Void **(b) Analysis of Ettringite in (a)**

Figure 5.10: US 15 SB over Fishing Creek (1011100) - 1

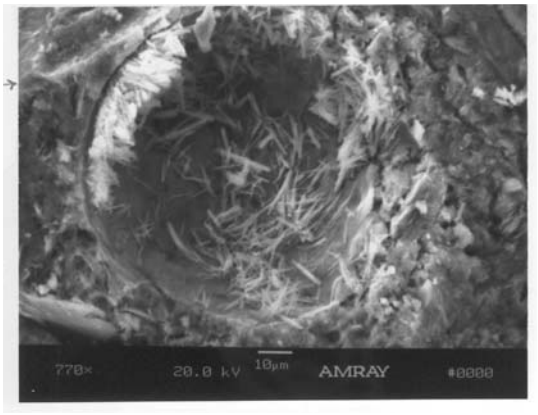

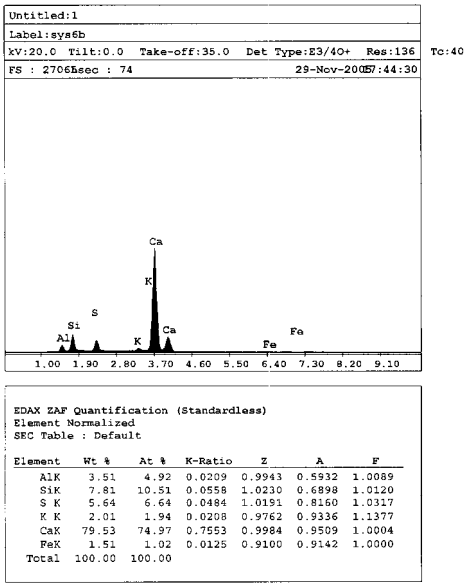

(a) Ettringite in Void **(b) Analysis of Crystals in (a)**

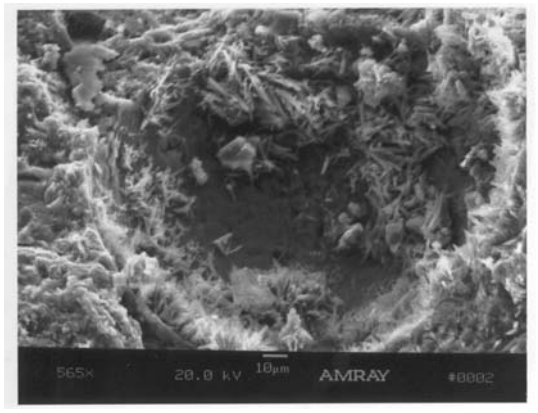

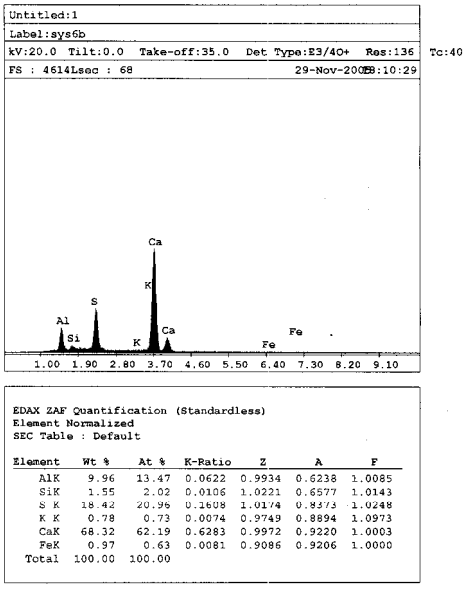

(c) Ettringite in Void **(d) Analysis of Crystals in (c)**

Figure 5.11: US 15 SB over Fishing Creek (1011100) - 2

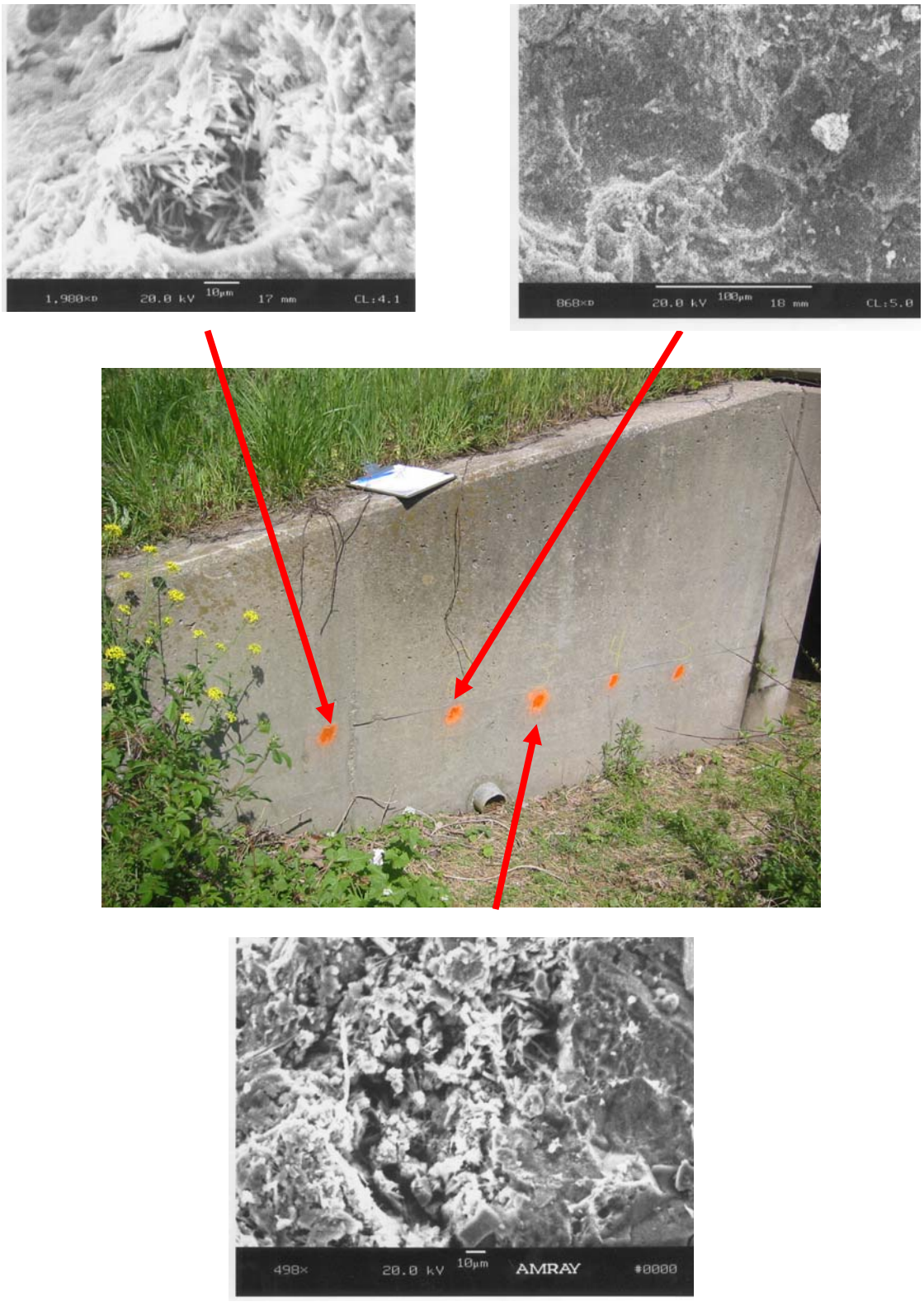

Figure 5.12: Ettringite Spatial Distribution

(1011100 – US 15 SB over Fishing Creek)

5.4.1.3 Bridge 1612300 (I-95 X SB over I-495 OL)

Five cores were taken from the inside face of the east parapet; see Figure 5.13 for location.

Figure 5.13: Coring Locations (1612300 – I-95 X SB over I-495 OL)

Two of the three cores examined contained no ettringite formations. The other core contained long ettringite crystals. The DEF fills greater than 50% of the small voids or lines the larger voids with long crystals than occupy approximately 5% of the void. See Figures 5.14 and 5.15. Energy Dispersive Analysis X-ray (EDAX) verifies the elemental composition of the crystal formations by showing the distinct aluminum, sulfur, and calcium pattern in general. The bridge contained long DEF crystal that fills greater than 50% of the voids to no ettringite in the cores sampled, see Figure 5.16 for typical core results.

In addition to the SEM and EDAX analysis, a large sample of the fractured cores was taken for ASR testing. The UV light ASR test indicates no presence of ASR gel in the parapet.

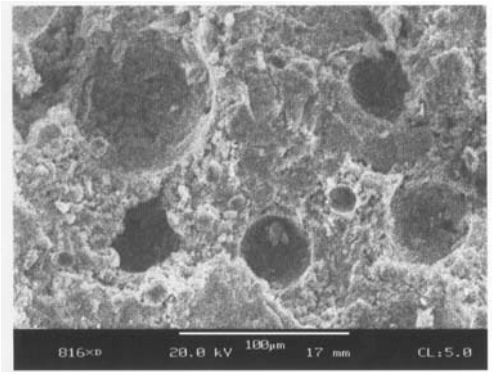

(a) Empty Voids

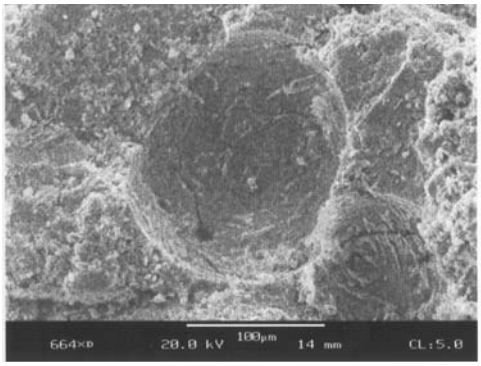

(b) Empty Voids

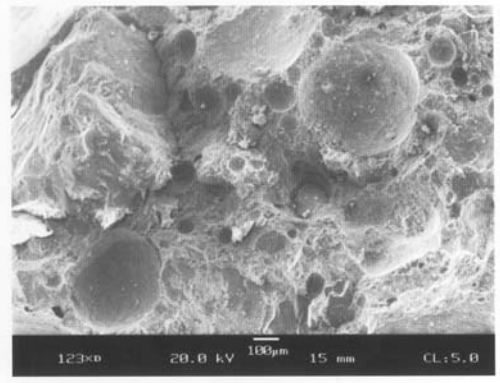

(c) Empty Voids

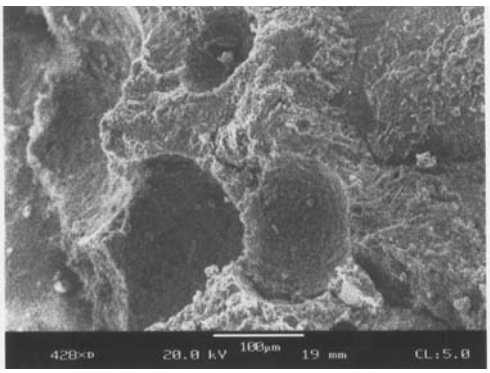

(d) Empty Voids

Figure 5.14: I-95 X SB over I-495 OL (1612300) - 1

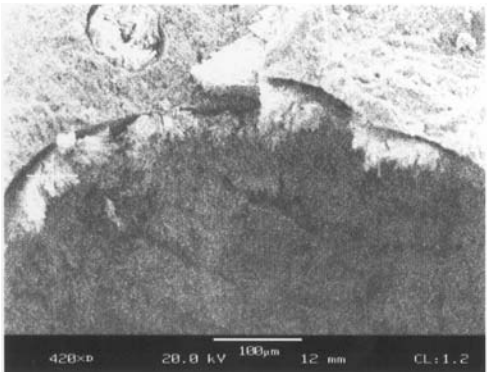

(a) Long Ettringite Crystals Lining Voids

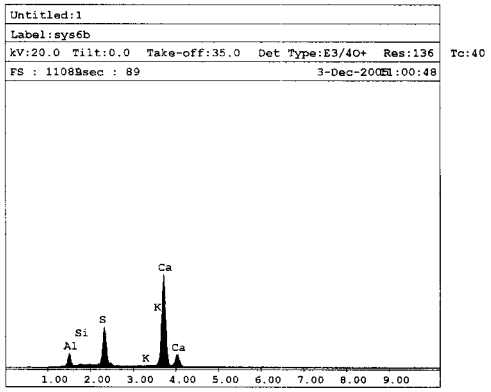

EDAX ZAF Quantification (Standardless)
Element Normalized
SEC Table : Default

Element	Wt %	At %	K-Ratio	Z	A	F
AlK	6.53	8.95	0.0404	0.9924	0.6179	1.0090
SiK	0.63	0.82	0.0044	1.0210	0.6832	1.0161
S K	19.97	23.02	0.1798	1.0166	0.8621	1.0274
K K	0.28	0.26	0.0027	0.9740	0.8934	1.1057
CaK	72.59	66.94	0.6707	0.9963	0.9274	1.0000
Total	100.00	100.00				

(b) Analysis of Ettringite in (a)

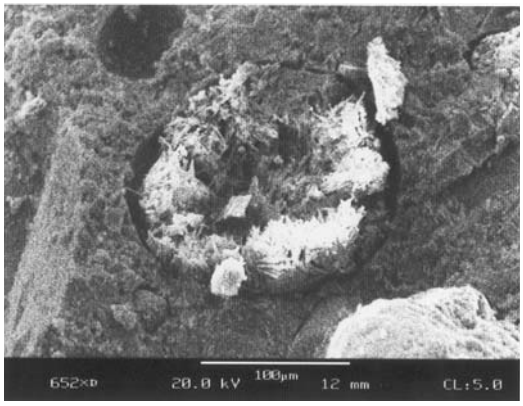

(c) Ettringite in Void

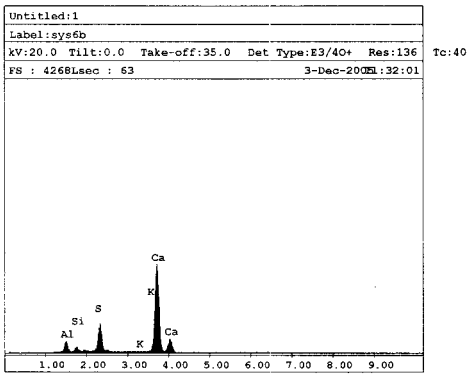

EDAX ZAF Quantification (Standardless)
Element Normalized
SEC Table : Default

Element	Wt %	At %	K-Ratio	Z	A	F
AlK	6.22	8.56	0.0382	0.9927	0.6129	1.0088
SiK	2.47	3.26	0.0174	1.0214	0.6820	1.0147
S K	15.51	17.96	0.1376	1.0170	0.8479	1.0288
K K	0.71	0.67	0.0070	0.9744	0.9059	1.1153
CaK	75.09	69.55	0.6999	0.9966	0.9353	1.0000
Total	100.00	100.00				

(d) Analysis of Ettringite in (c)

Figure 5.15: I-95 X SB over I-495 OL (1612300) - 2

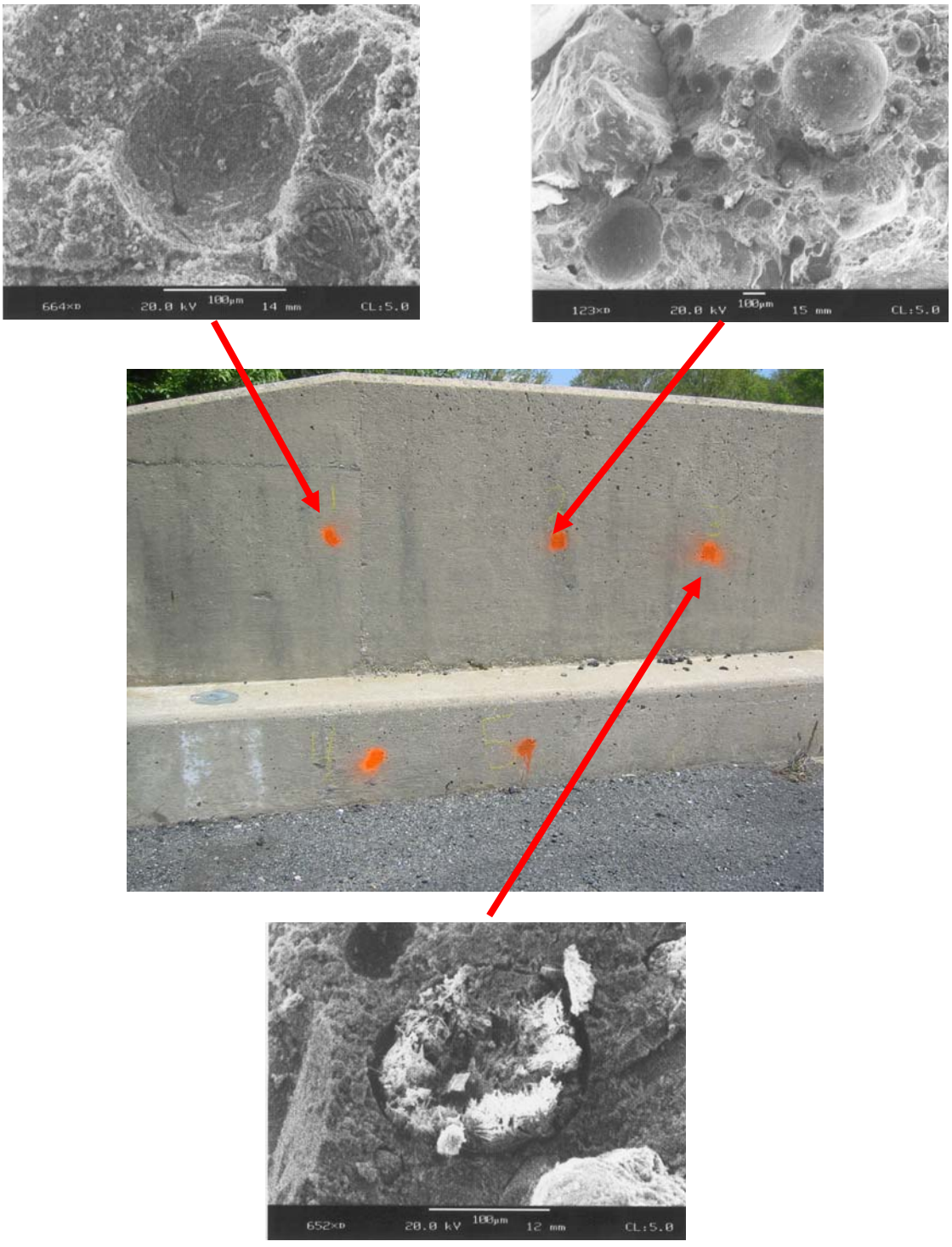

Figure 5.16: Ettringite Spatial Distribution

(1612300 – I-95 X SB over I-495 OL)

5.4.2 Clean Bridges Built After 1980

5.4.2.1 Bridge 0217202 (MD 10 SB Over MD 177)

Five cores were taken from the parapet near the southwest wingwall; see Figure 5.17 for locations.

Figure 5.17: Coring Locations (0217202 – MD 10 SB over MD 177)

One of the three cores examined contained no ettringite formations. The other two cores contained long ettringite crystals mixed in with calcium hydroxide $Ca(OH)_2$ in some locations. The DEF fills much less than 5% of the voids. See Figure 5.18. Energy Dispersive Analysis X-ray (EDAX) verifies the elemental composition of the crystal formations by showing the distinct aluminum, sulfur, and calcium pattern in general. The bridge contained little to no ettringite in the cores sampled, see Figure 5.19 for typical core results.

In addition to the SEM and EDAX analysis, a large sample of the fractured cores was taken for ASR testing. The UV light ASR test indicates no presence of ASR gel in the parapet.

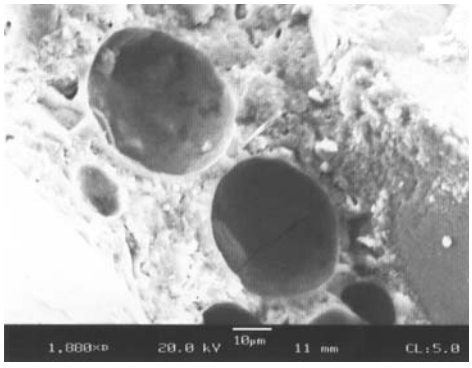

(a) Empty Voids

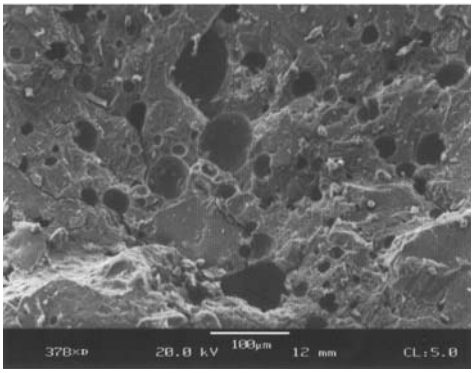

(b) Empty Voids

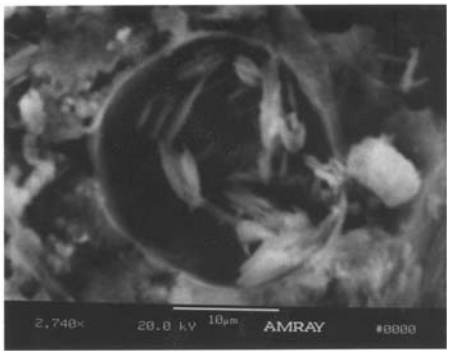

(c) Ettringite in Void

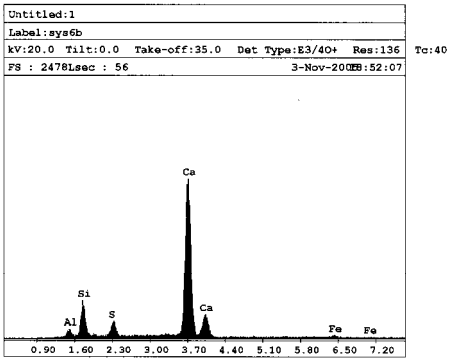

(d) Analysis of Ettringite in (c)

Figure 5.18: MD 10 SB over MD 177 (0217202)

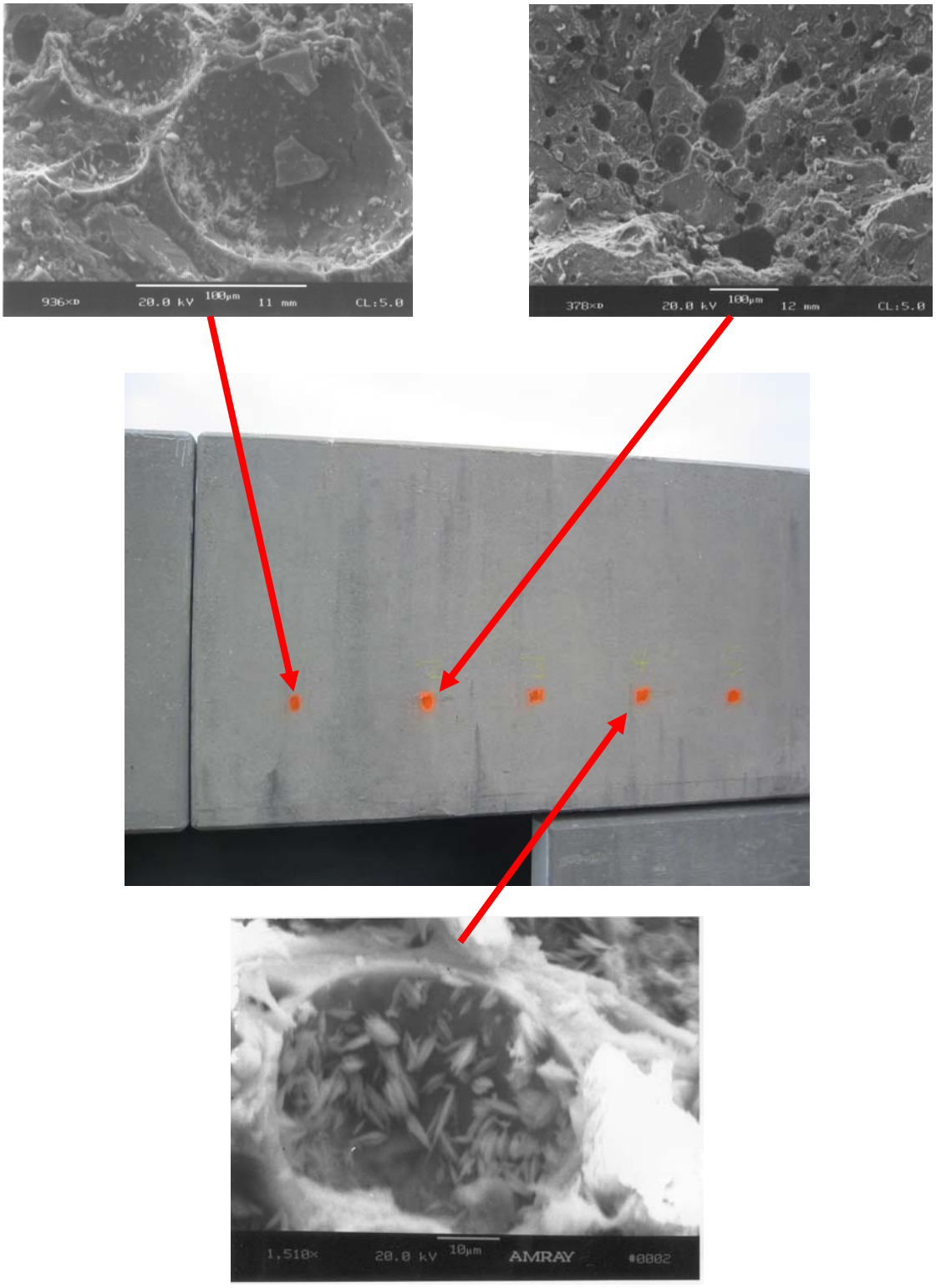

Figure 5.19: Ettringite Spatial Distribution

(0217202 – MD 10 SB over MD 177)

5.4.2.2 Bridge 0219000 (Queenstown Road over MD 100)

Five cores were taken from the northeast wingwall; see Figure 5.20 for locations.

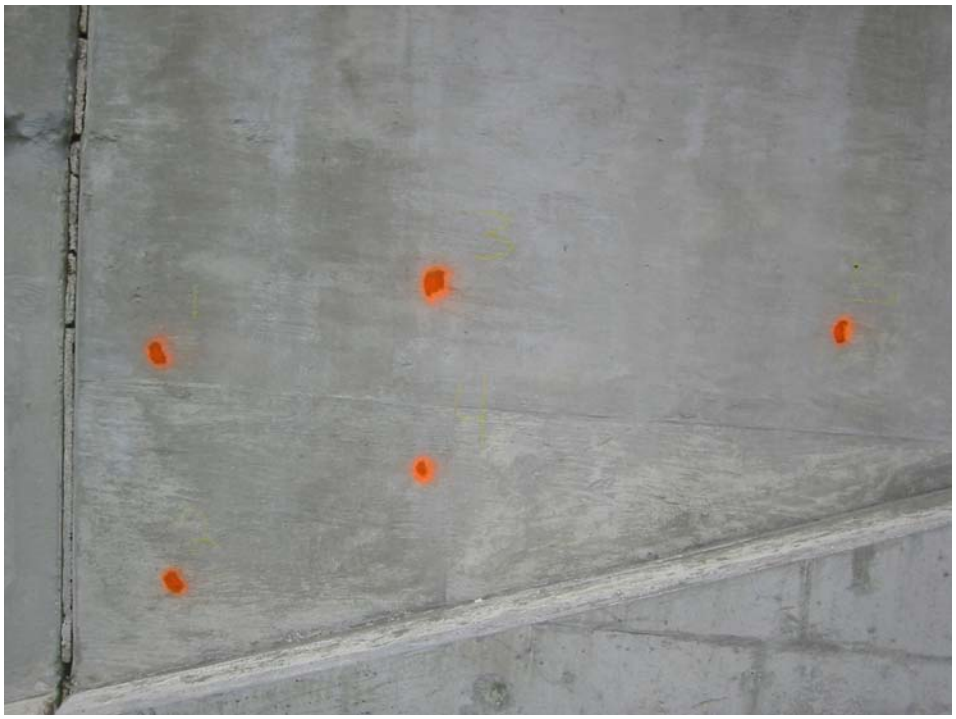

Figure 5.20: Coring Locations (0219000 – Queenstown Road over MD 100)

All three of the cores examined contained no ettringite formations. See Figure 5.21. The bridge contained no ettringite in the cores sampled, see Figure 5.22 for typical core results.

In addition to the SEM and EDAX analysis, a large sample of the fractured cores was taken for ASR testing. The UV light ASR test indicates no presence of ASR gel in the wingwall.

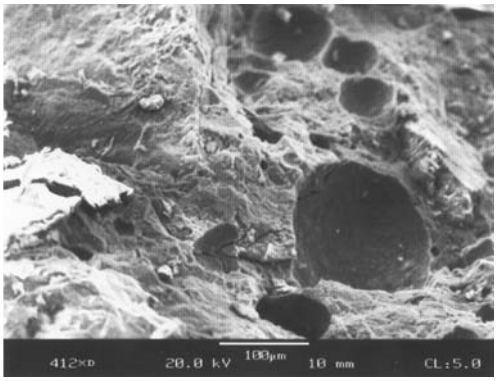

(a) Empty Voids

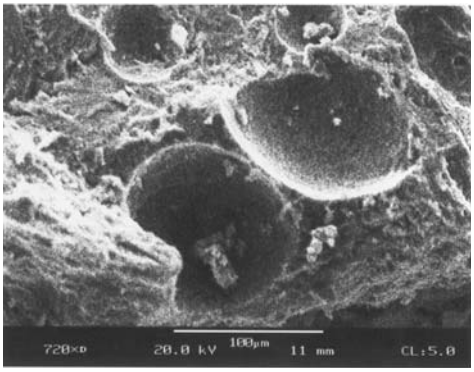

(b) Empty Voids

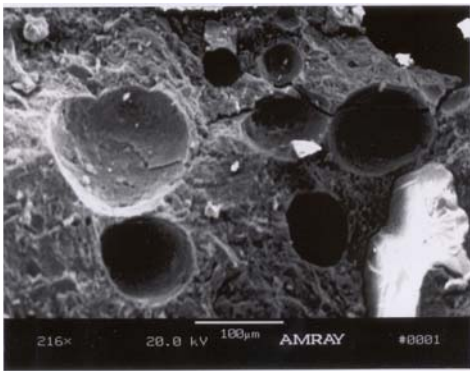

(c) Empty Voids

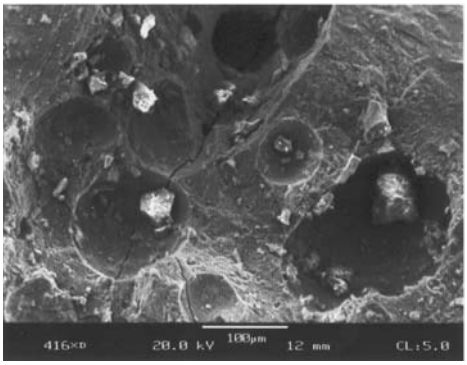

(d) Empty Voids

Figure 5.21: Queenstown Road over MD 100 (0219000)

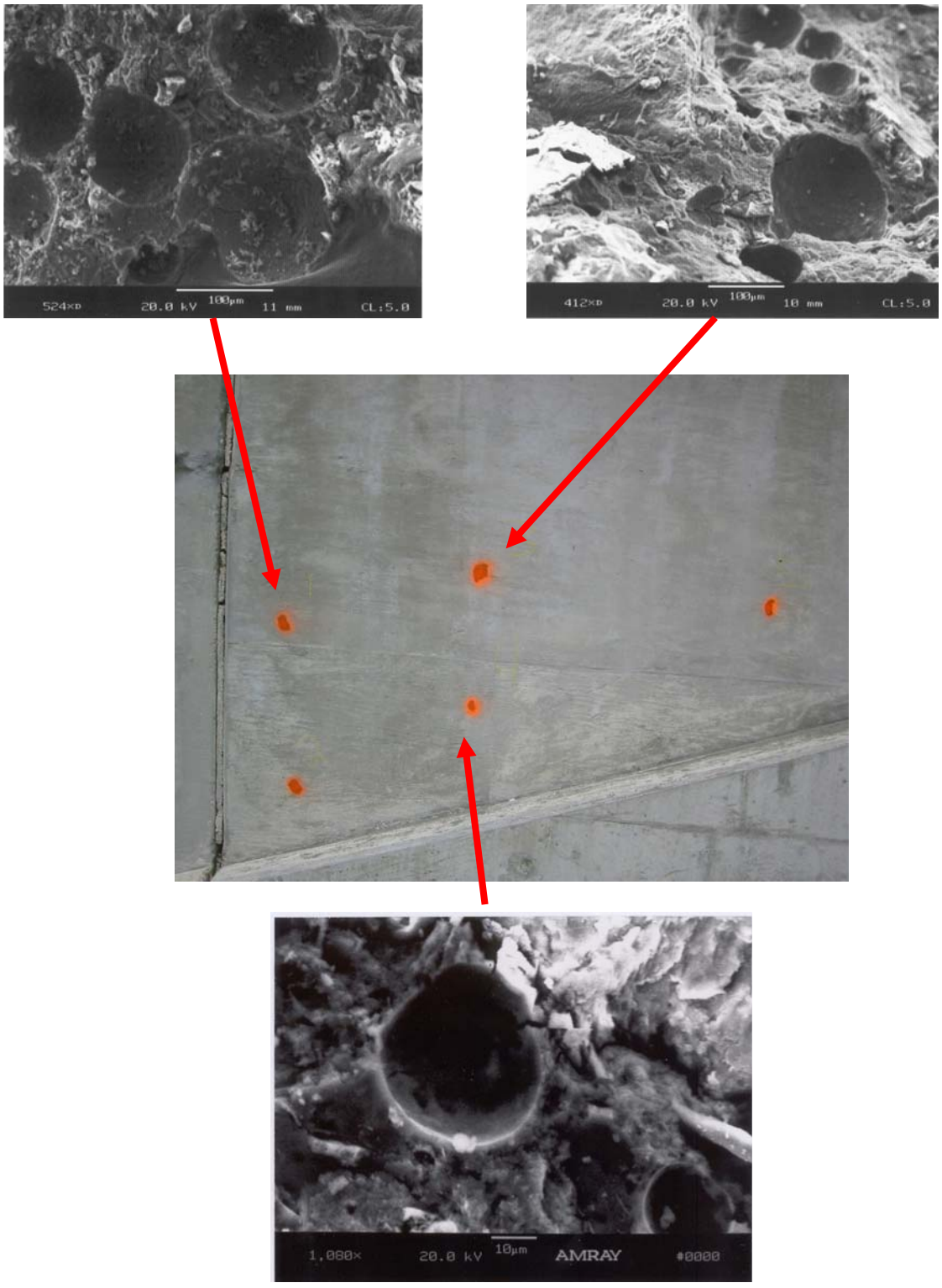

Figure 5.22: Ettringite Spatial Distribution

(0219000 – Queenstown Road over MD 100)

5.4.2.3 Bridge 1005600 (MD 77 over Double Pipe Creek)

Five cores were taken from the south parapet over the southeast wingwall; see Figure 5.23 for locations.

Figure 5.23: Coring Locations (1005600 – MD 77 over Double Pipe Creek)

All three of the cores examined contained ettringite formations. The cores contained long ettringite crystals that fills anywhere from much less than 5% to greater than 50% of the voids. See Figures 5.23 and 5.24. Energy Dispersive Analysis X-ray (EDAX) verifies the elemental composition of the crystal formations by showing the distinct aluminum, sulfur, and calcium pattern in general. The bridge contained long DEF crystal that fills anywhere from much less than 5% to greater than 50% of the voids in the cores sampled, see Figure 5.25 for typical core results.

In addition to the SEM and EDAX analysis, a large sample of the fractured cores was taken for ASR testing. The UV light ASR test indicates no presence of ASR gel in the wingwall.

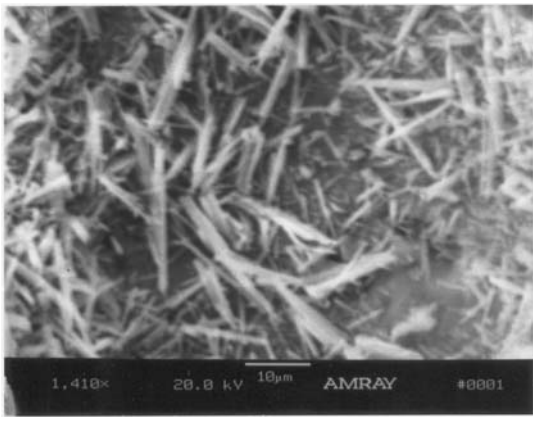

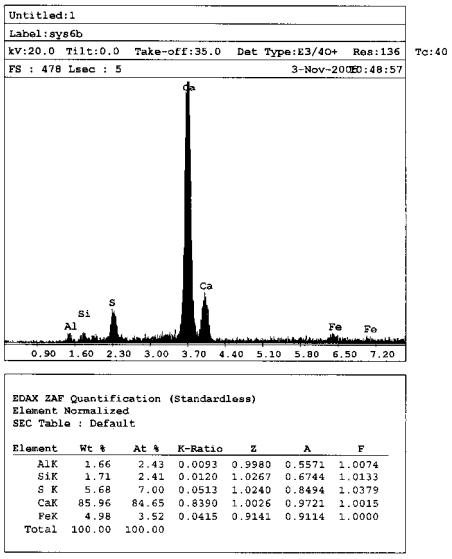

(a) Ettringite in Voids **(b) Analysis of Ettringite in (a)**

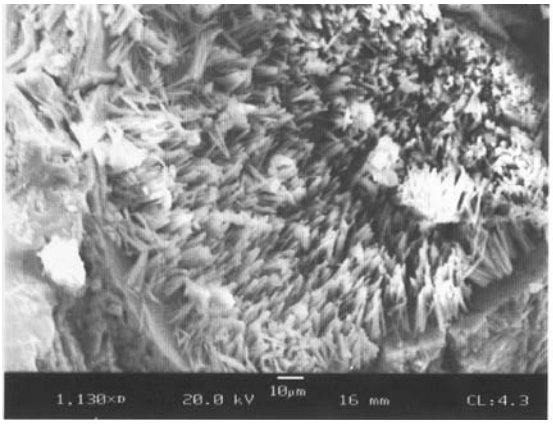

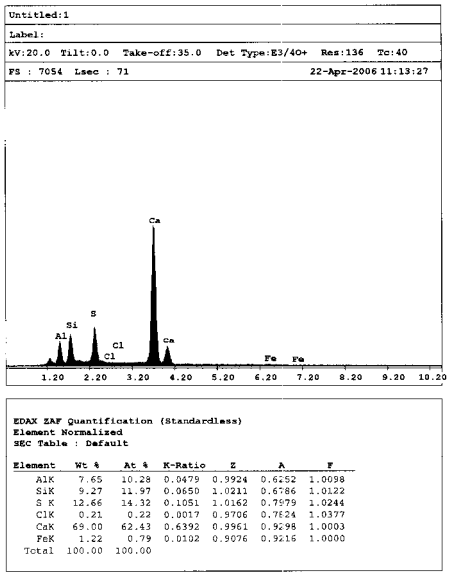

(c) Ettringite in Void **(d) Analysis of Ettringite in (c)**

Figure 5.24: MD 77 over Double Pipe Creek (1005600) - 1

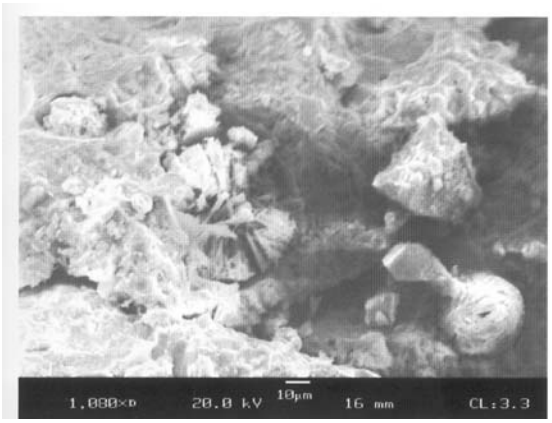

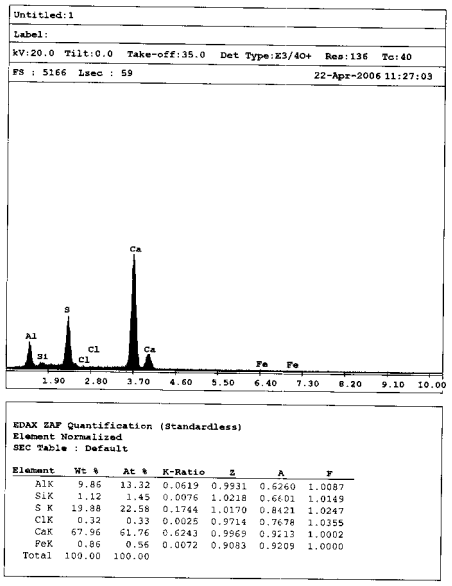

(a) Ettringite in Void **(b) Analysis of Ettringite in (a)**

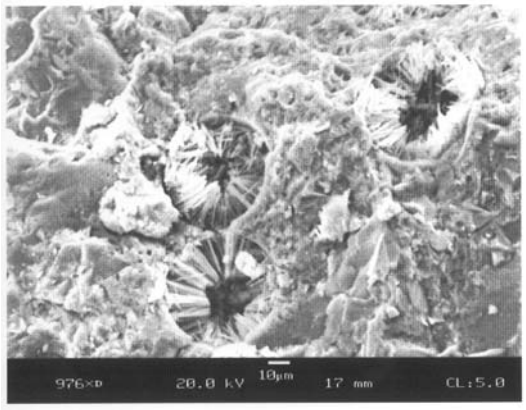

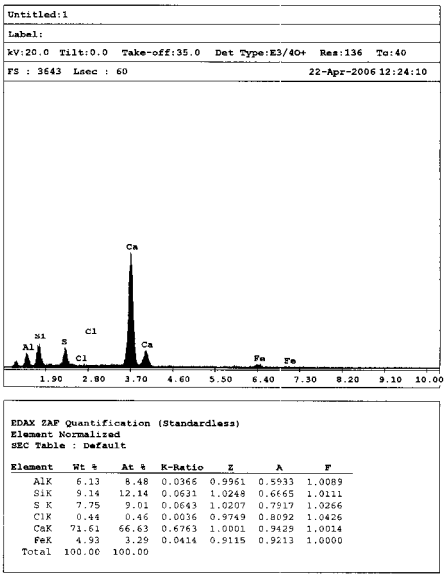

(c) Ettringite in Void **(d) Analysis of Ettringite in (c)**

Figure 5.25: MD 77 over Double Pipe Creek (1005600) - 2

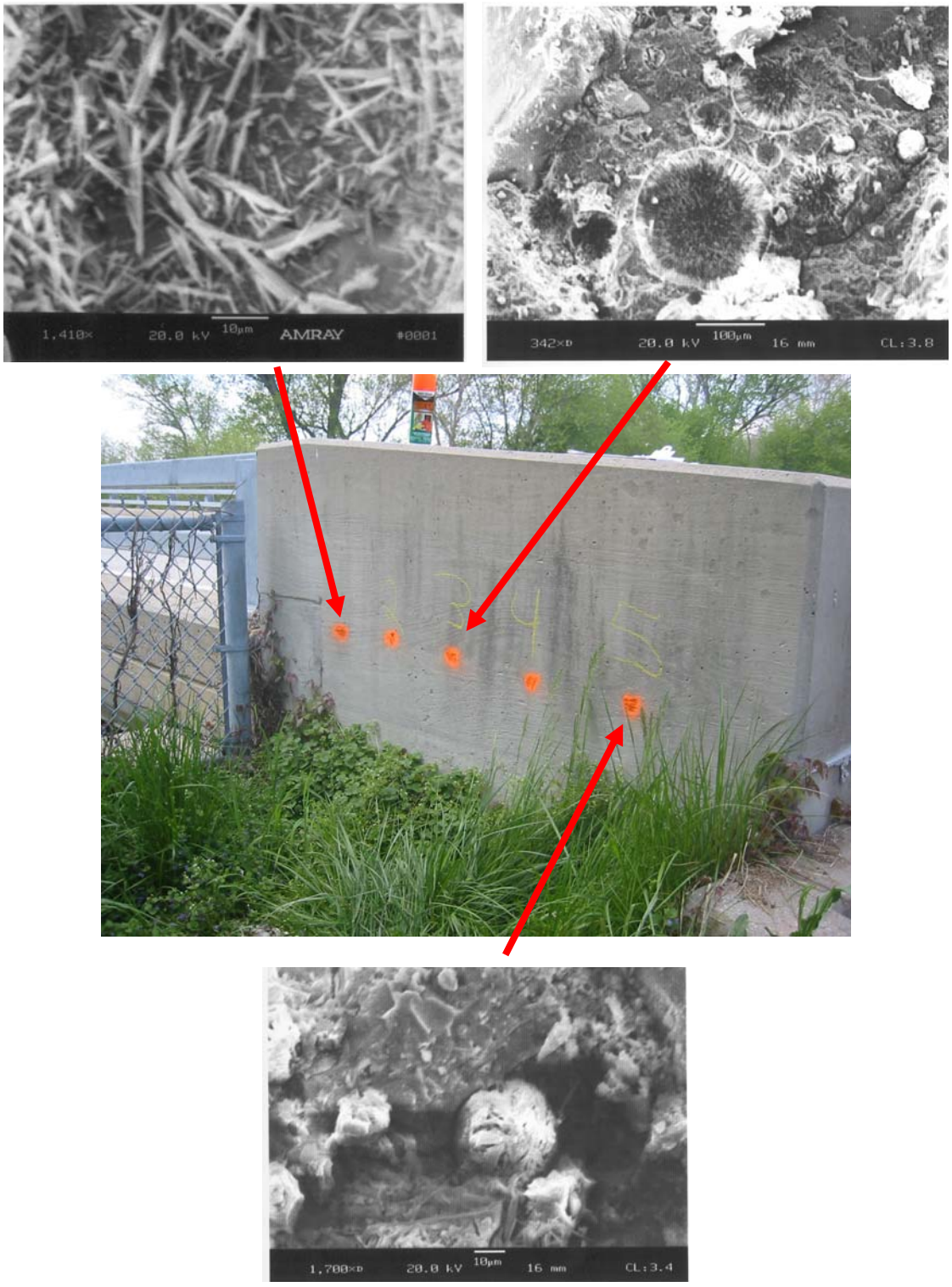

Figure 5.26: Ettringite Spatial Distribution

(1005600 – MD 77 over Double Pipe Creek)

5.4.3 Dirty Bridges Built Before 1980

5.4.3.1 Bridge 0208304 (MD 100 WB over MD 174)

Five cores were taken from the west abutment stem near the north end; see Figure 5.27 for locations.

Figure 5.27: Coring Locations (0208304 – MD 100 WB over MD 174)

Two of the three cores examined contained no ettringite formations. The other one cores contained long ettringite crystals, which filled the voids from much less than 5% to greater than 5% but less than 50% of the voids. See Figures 5.28 and 5.29. Energy Dispersive Analysis X-ray (EDAX) verifies the elemental composition of the crystal formations by showing the distinct aluminum, sulfur, and calcium pattern in general. The bridge contained long DEF crystal that fills less than 50% of the voids to no ettringite in the cores sampled; see Figure 5.30 for typical core results.

In addition to the SEM and EDAX analysis, a large sample of the fractured cores was taken for ASR testing. The UV light ASR test indicates no presence of ASR gel in the abutment.

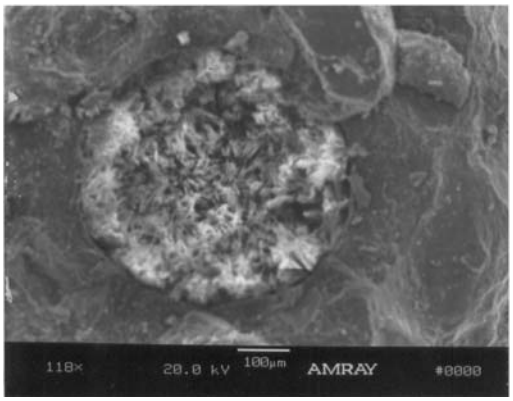

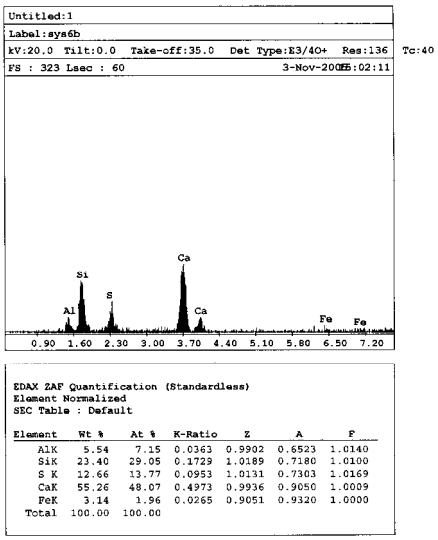

(a) Ettringite in Void **(b) Analysis of Ettringite in (a)**

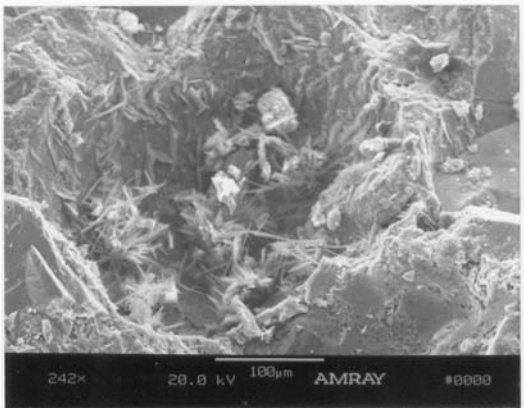

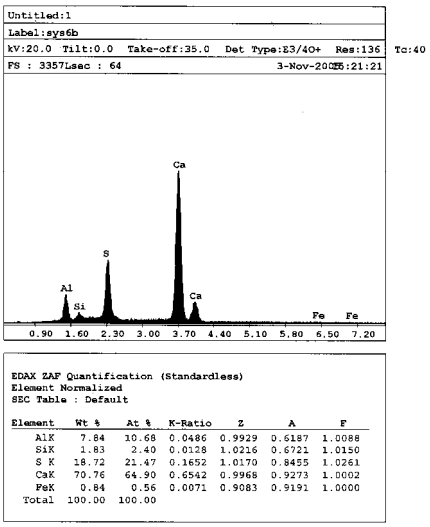

(c) Ettringite in Void **(d) Analysis of Ettringite in (c)**

Figure 5.28: MD 100 WB over MD 174 (0208304) - 1

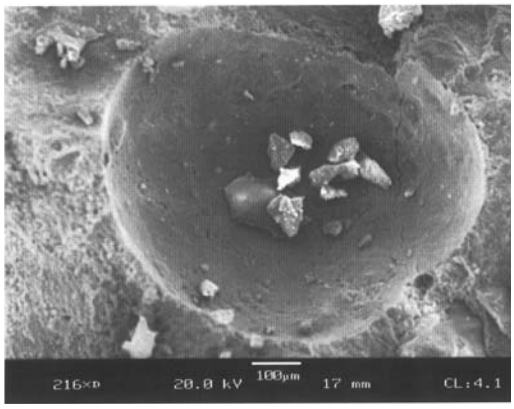

(a) Empty Void

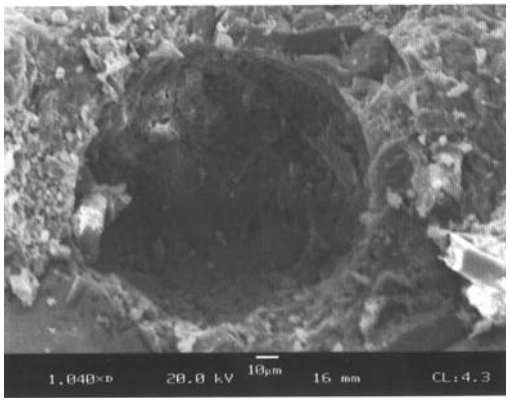

(b) Empty Void

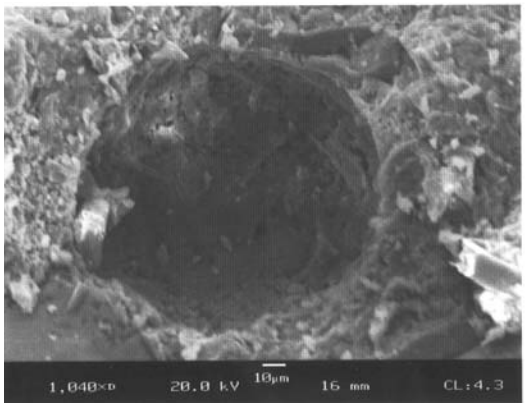

(c) Empty Void

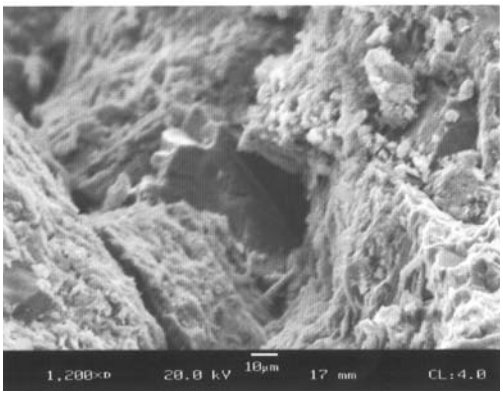

(d) Empty Void

Figure 5.29: MD 100 WB over MD 174 (0208304) - 2

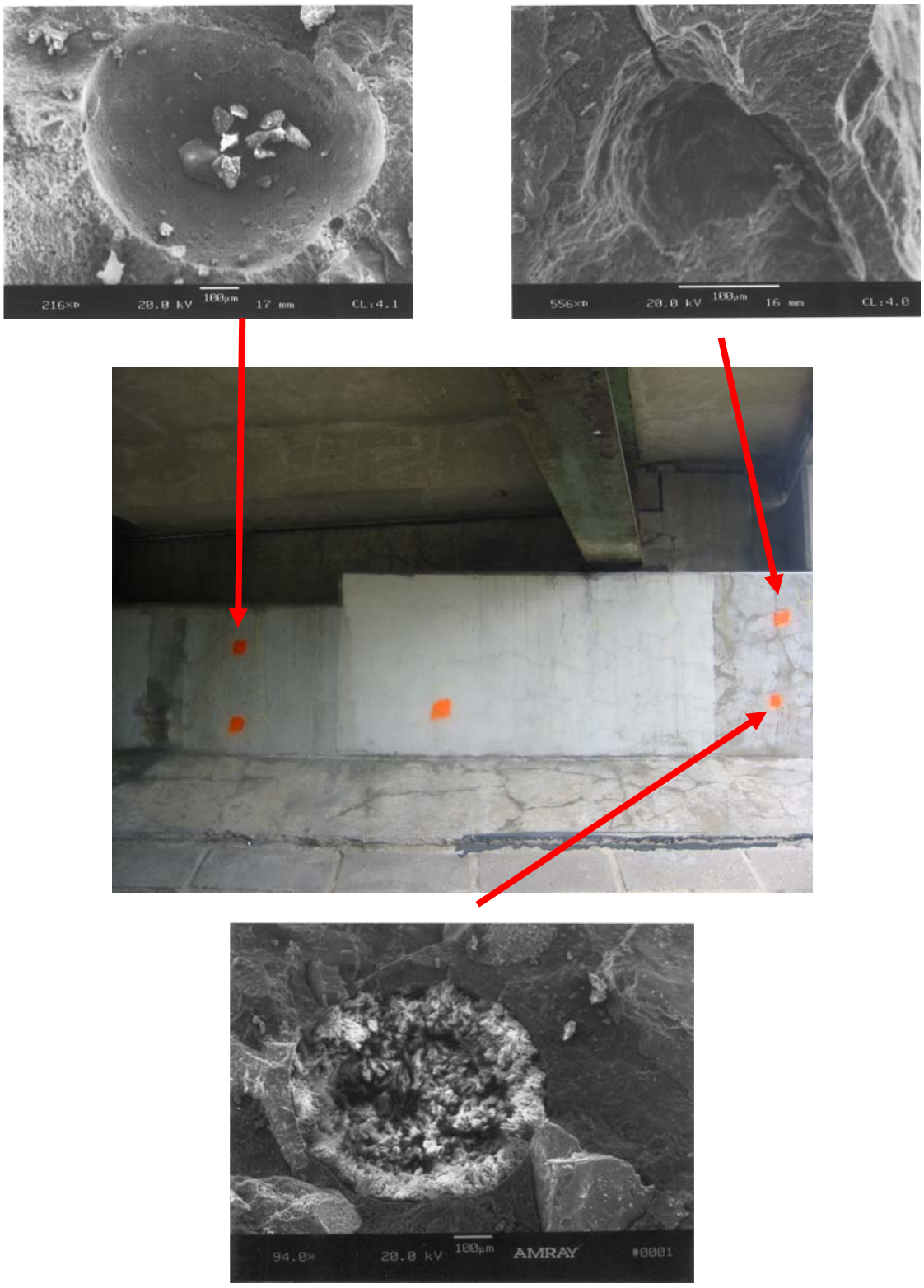

Figure 5.30: Ettringite Spatial Distribution

(0208304 – MD 100 WB over MD 174)

5.4.3.2 Bridge 0311100 (CSX Transportation over I-695)

Three cores were taken from the inside face of the northwest wingwall; see Figure 5.31 for locations.

Figure 5.31: Coring Locations (0311100 – CSX Transportation over I-695)

All three of the cores examined contained significant ettringite formations. The majority of the DEF observed was in laminar formations found on the sample surface. The ettringite of the surface would have been in a crack along which the concrete cracked in the sample preparation work. Occasionally voids were found with long ettringite crystals that filled anywhere from much less than 5% to greater than 50% of the voids. See Figures 5.32, 5.33, and 5.34. Energy Dispersive Analysis X-ray (EDAX) verifies the elemental composition of the crystal formations by showing the distinct aluminum, sulfur, and calcium pattern in general. The bridge contained significant quantities of laminar ettringite with occasional void containing long DEF

crystal that fills anywhere from much less than 5% to greater than 50% of the voids in the cores sampled, see Figure 5.35 for typical core results.

In addition to the SEM and EDAX analysis, a large sample of the fractured cores was taken for ASR testing. The UV light ASR test indicates no presence of ASR gel in the wingwall.

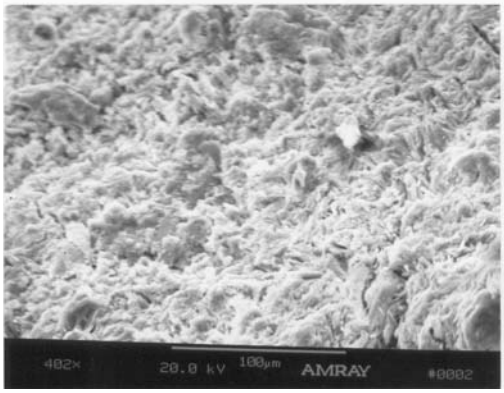

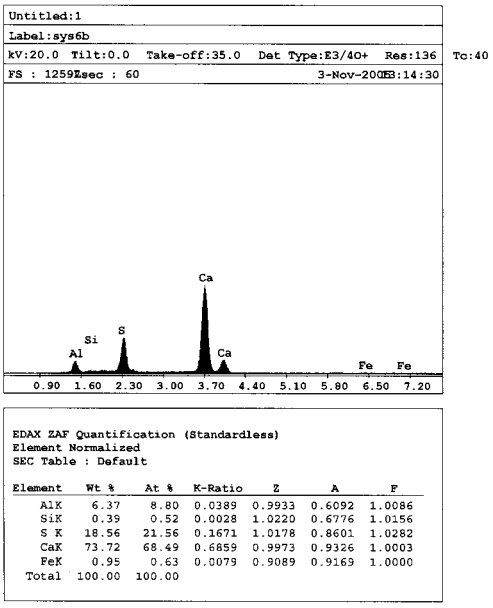

(a) Laminar Ettringite on Surface **(b) Analysis of Ettringite in (a)**

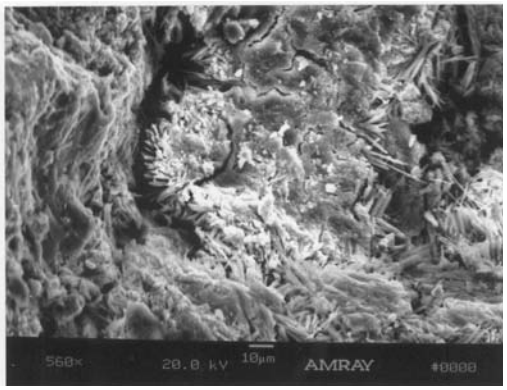

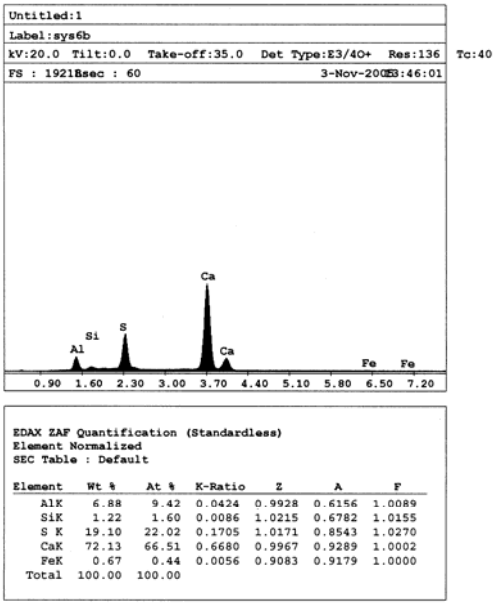

(c) Laminar Ettringite on Surface **(d) Analysis of Ettringite in (c)**

Figure 5.32: CSX Transportation over I-695 (0311100) - 1

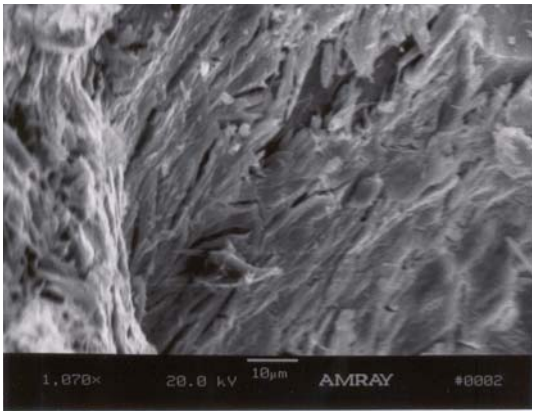

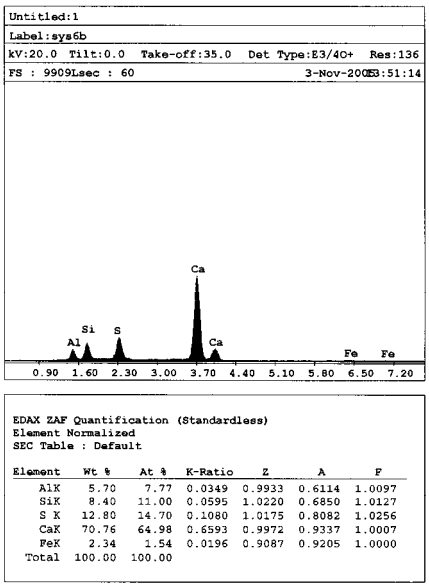

(a) Laminar Ettringite ofnSurface **(b) Analysis of Ettringite in (a)**

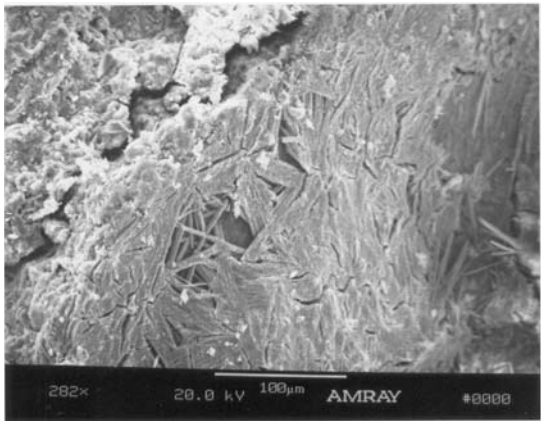

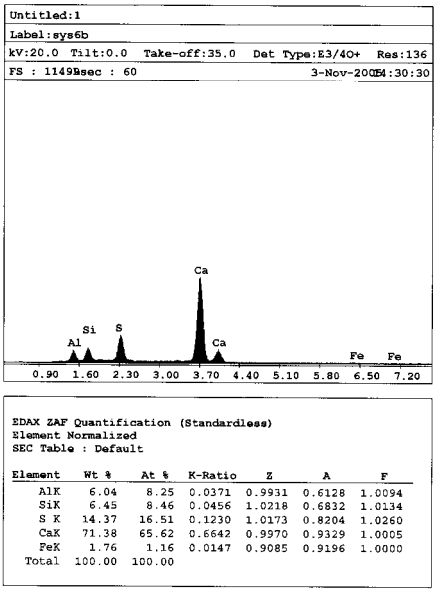

(c) Laminar Ettringite on Surface **(d) Analysis of Ettringite in (c)**

Figure 5.33: CSX Transportation over I-695 (0311100) - 2

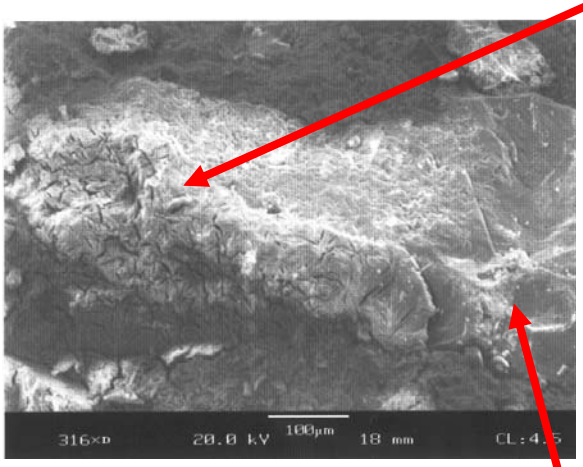

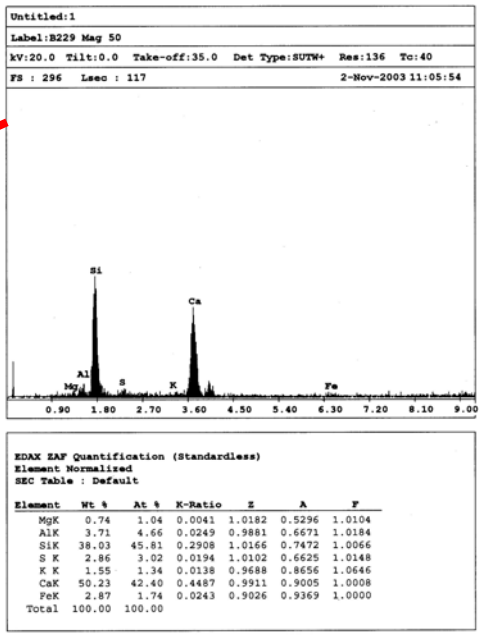

EDAX ZAF Quantification (Standardless)
Element Normalized
SEC Table : Default

Element	Wt %	At %	K-Ratio	Z	A	F
MgK	0.74	1.04	0.0041	1.0182	0.5296	1.0104
AlK	3.71	4.66	0.0249	0.9881	0.6671	1.0184
SiK	38.03	45.81	0.2908	1.0166	0.7472	1.0066
S K	2.86	3.02	0.0194	1.0102	0.6625	1.0148
K K	1.55	1.34	0.0138	0.9688	0.8656	1.0646
CaK	50.23	42.40	0.4487	0.9911	0.9005	1.0008
FeK	2.87	1.74	0.0243	0.9026	0.9369	1.0000
Total	100.00	100.00				

(a) Laminar Ettringite on Aggregate

(b) Analysis of Ettringite in (a)

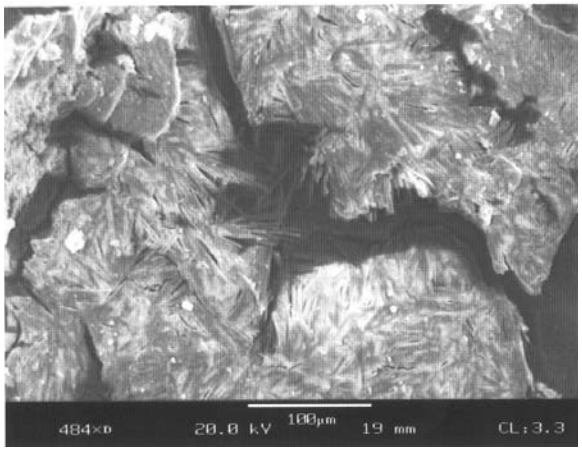

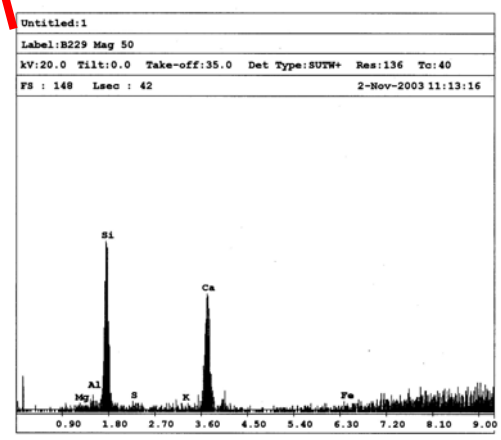

EDAX ZAF Quantification (Standardless)
Element Normalized
SEC Table : Default

Element	Wt %	At %	K-Ratio	Z	A	F
MgK	1.25	1.75	0.0067	1.0192	0.5183	1.0102
AlK	2.46	3.10	0.0161	0.9890	0.6507	1.0185
SiK	39.56	47.86	0.3023	1.0176	0.7464	1.0061
S K	1.63	1.73	0.0109	1.0113	0.6545	1.0144
K K	0.91	0.79	0.0081	0.9699	0.8659	1.0646
CaK	49.36	41.84	0.4432	0.9921	0.9036	1.0014
FeK	4.82	2.93	0.0409	0.9036	0.9386	1.0000
Total	100.00	100.00				

(c) Close-up of Laminar Ettringite on Surface

(d) Analysis of Aggregate in (a)

Figure 5.34: CSX Transportation over I-695 (0311100) - 3

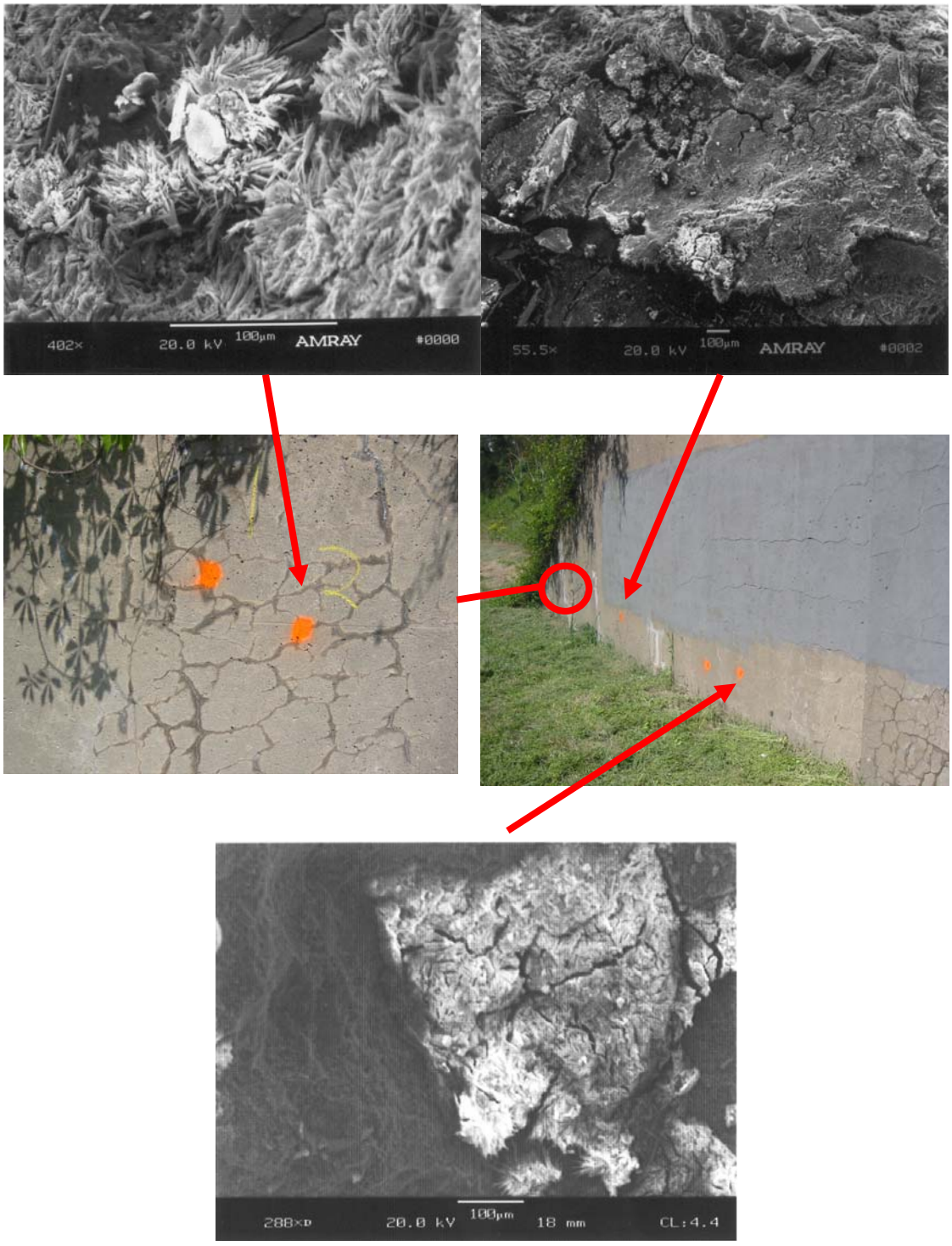

Figure 5.35: Ettringite Spatial Distribution

(0311100 – CSX Transportation over I-695)

5.4.3.3 Bridge 1308603 (MD 175 EB over US 29)

Three cores were taken from the outside face of the north parapet above the northeast wingwall; see Figure 5.36 for locations.

Figure 5.36: Coring Locations (1308603 – MD 175 EB over US 29)

One of the three cores examined contained no ettringite formations. The other two cores contained long ettringite crystals. The DEF fills much less than 5% to between 5% and 50% of the voids. See Figures 5.37 and 5.38. Energy Dispersive Analysis X-ray (EDAX) verifies the elemental composition of the crystal formations by showing the distinct aluminum, sulfur, and calcium pattern in general. The bridge contained little to no ettringite in the cores sampled, see Figure 5.39 for typical core results.

In addition to the SEM and EDAX analysis, a large sample of the fractured cores was taken for ASR testing. The UV light ASR test indicates no presence of ASR gel in the parapet.

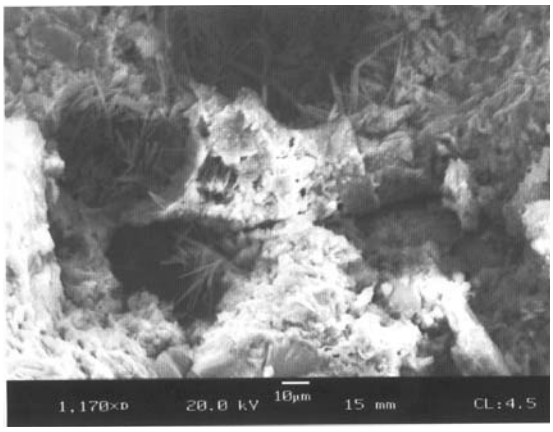

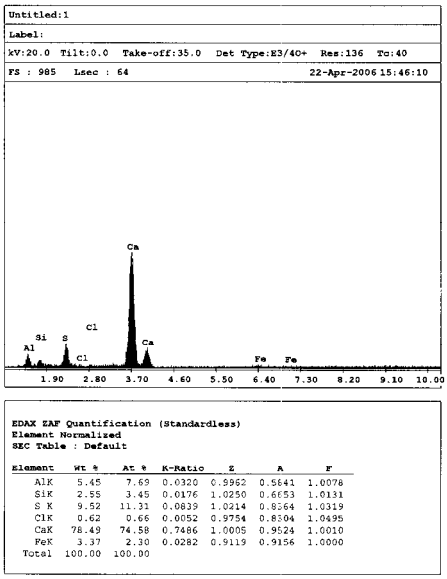

(a) Ettringite in Voids **(b) Analysis of Ettringite in (a)**

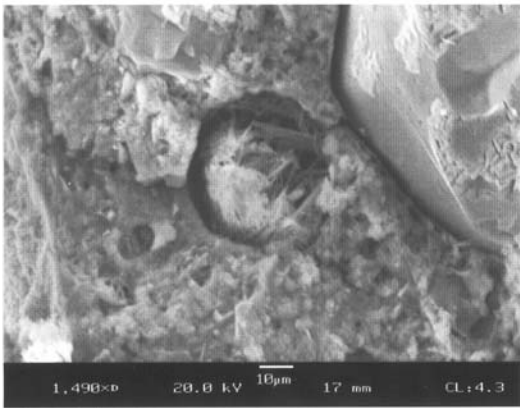

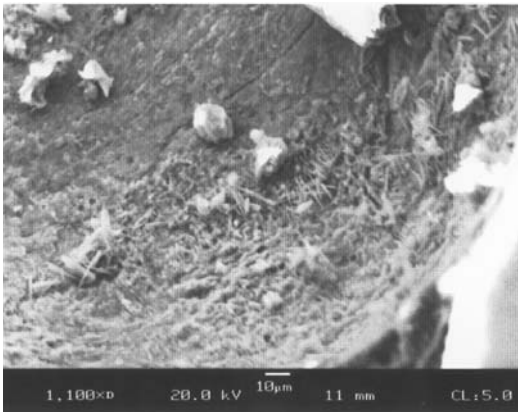

(c) Ettringite in Void **(d) Ettringite in Void**

Figure 5.37: MD 175 EB over US 29 (1308603) - 1

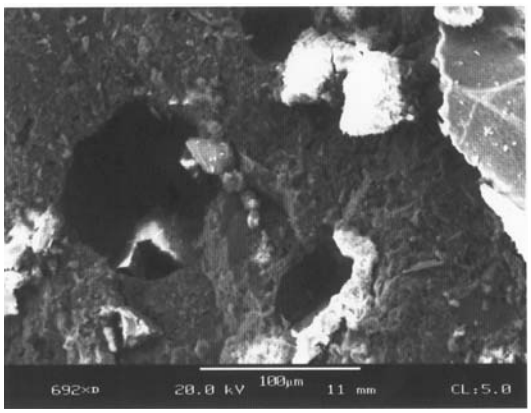

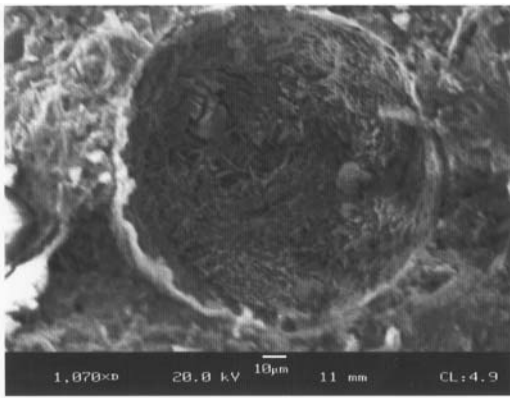

(a) Empty Voids **(b) Void with Calcium Hydroxide**

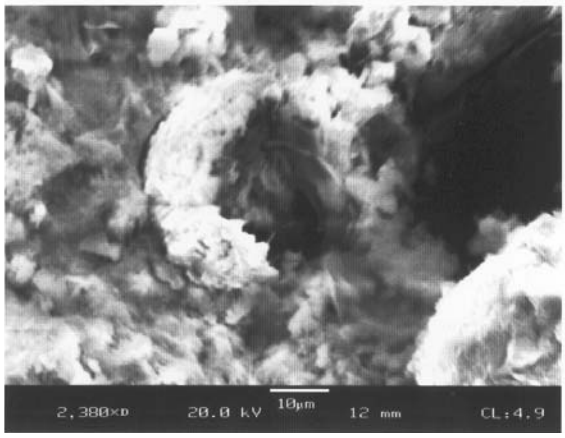

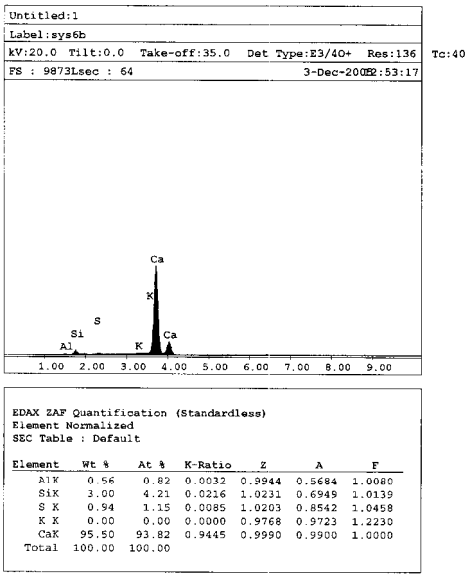

(c) Void with Calcium Hydroxide **(d) Analysis of Crystals in (c)**

Figure 5.38: MD 175 EB over US 29 (1308603) - 2

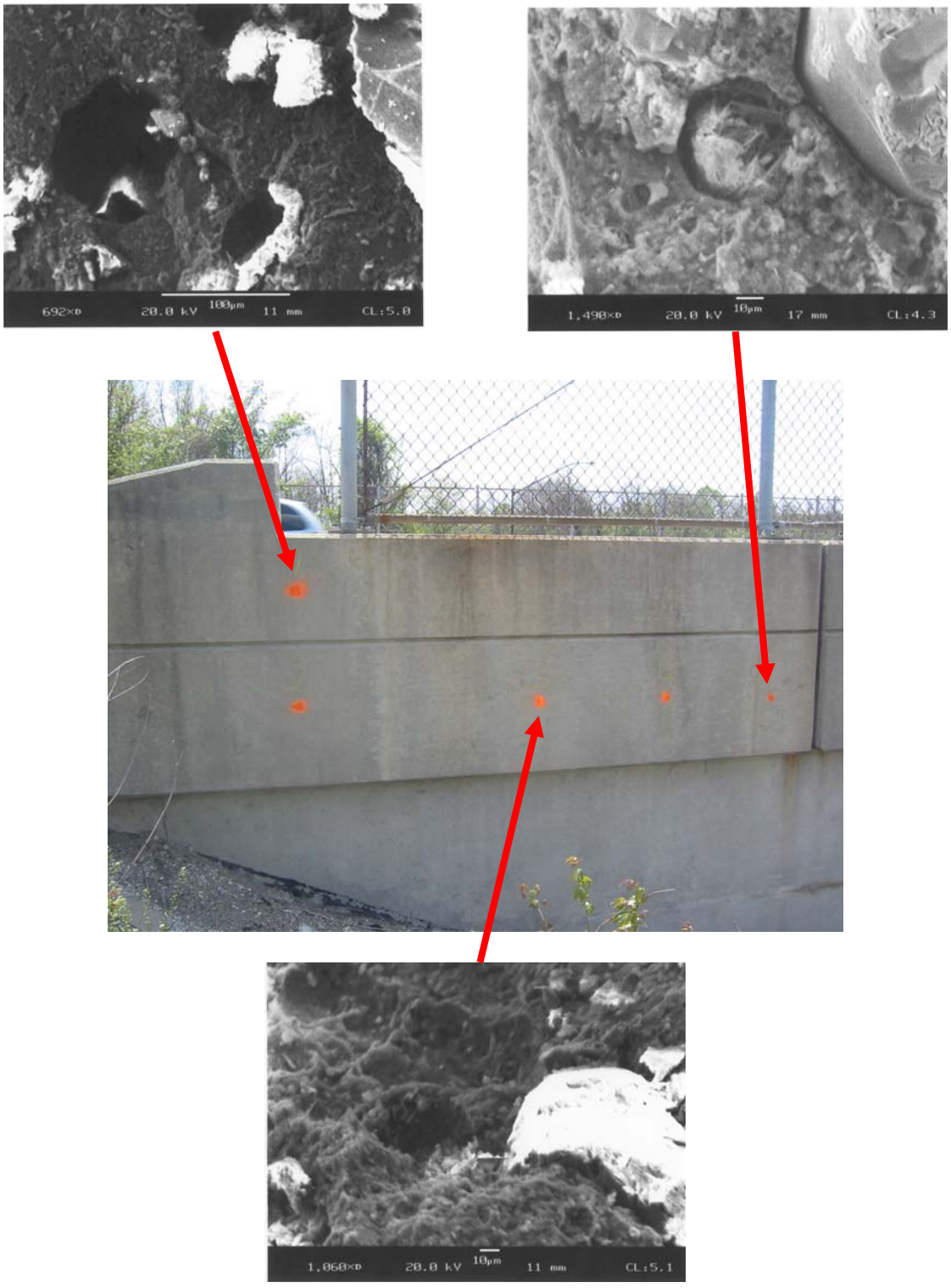

Figure 5.39: Ettringite Spatial Distribution

(1308603 – MD 175 EB over US 29)

5.4.4 Dirty Bridges Built After 1980

5.4.4.1 Bridge 0333900 (MD 140 SB over I-795 Ramp 'I' & 'G')

Three cores were taken from the northeast wingwall; see Figure 5.40 for locations.

Figure 5.40: Coring Locations (MD 140 SB over I-795 Ramp 'I' & 'G')

All three of the cores examined contained ettringite formations. The DEF exhibited long crystals morphology, which filled anywhere from much less than 5% to greater than 50% of the voids. See Figures 5.41 and 5.42. Energy Dispersive Analysis X-ray (EDAX) verifies the elemental composition of the crystal formations by showing the distinct aluminum, sulfur, and calcium pattern in general. The bridge contained little to no ettringite in the cores sampled, see Figure 5.43 for typical core results.

In addition to the SEM and EDAX analysis, a large sample of the fractured cores was taken for ASR testing. The UV light ASR test indicates no presence of ASR gel in the wingwall.

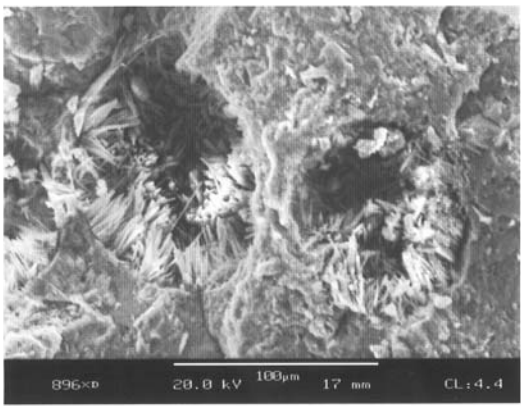

(a) Ettringite in Voids

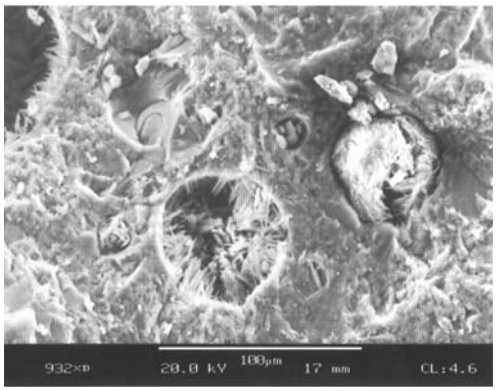

(b) Ettringite in Voids

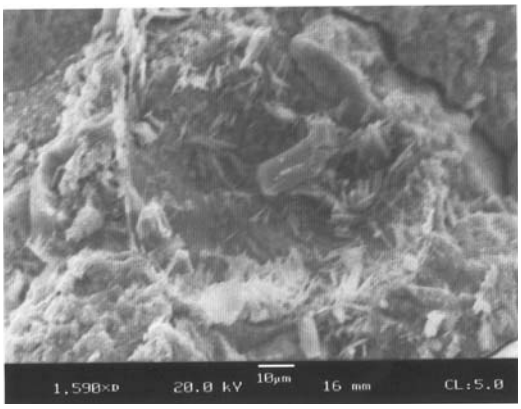

(c) Ettringite in Voids

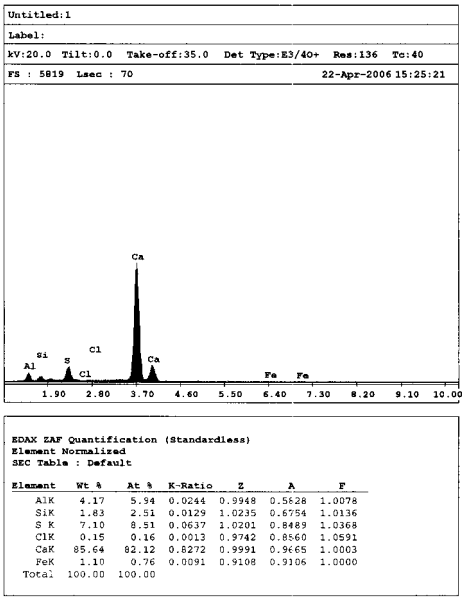

(d) Analysis of (c)

Figure 5.41: MD 140 SB over I-795 Ramp 'I' & 'G' (0333900) - 1

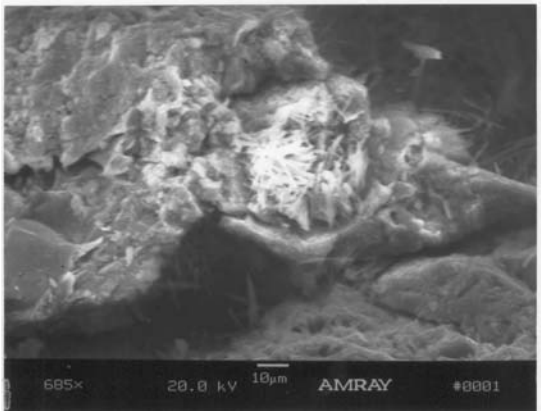

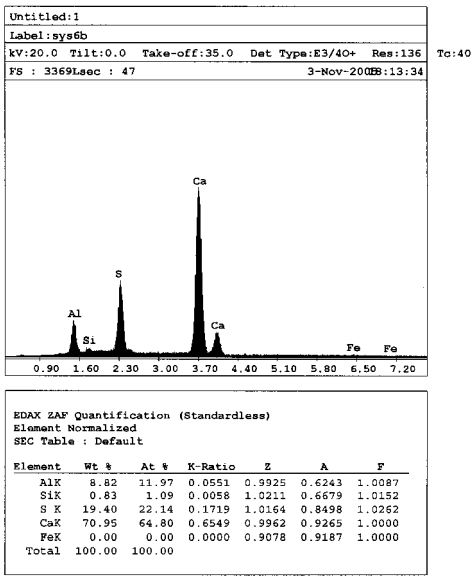

(a) Ettringite in Voids **(b) Analysis of Ettringite in (a)**

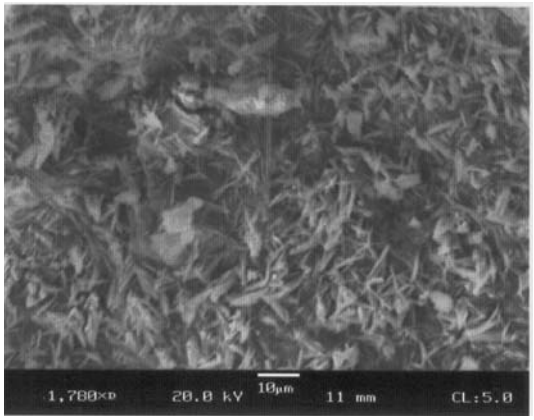

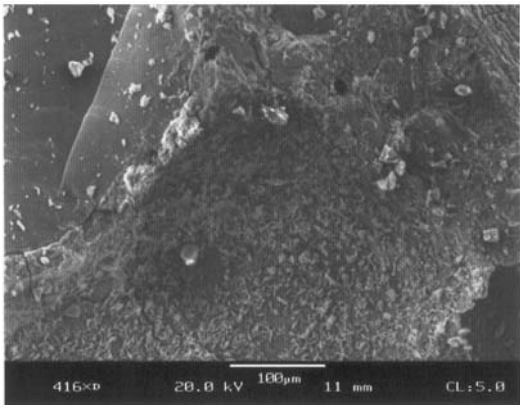

(c) Ettringite in Voids **(d) Ettringite in Voids**

Figure 5.42: MD 140 SB over I-795 Ramp 'I' & 'G' (0333900) - 2

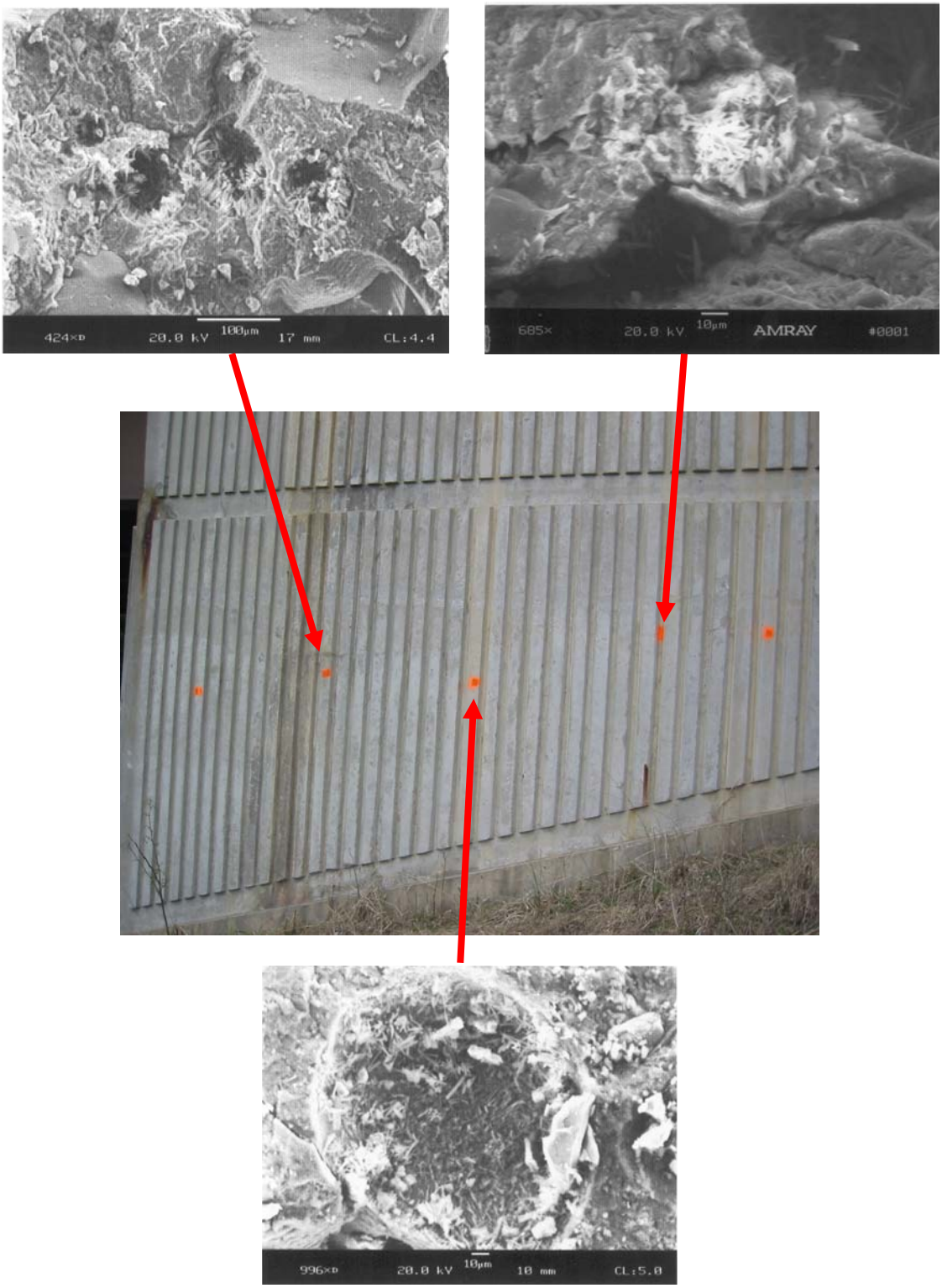

Figure 5.43: Ettringite Spatial Distribution

(MD 140 SB over I-795 Ramp 'I' & 'G')

5.4.4.2 Bridge 1315004 (MD 100 WB over Dorsey Station Road)

Three cores were taken from the outside face of the west parapet above the northwest wingwall; see Figure 5.44 for locations.

Figure 5.44: Coring Locations (MD 100 WB over Dorsey Station Road)

Two of the three cores examined contained no ettringite formations. The other one cores contained long ettringite crystals, which filled much less than 5% of the voids. See Figure 5.45. Energy Dispersive Analysis X-ray (EDAX) verifies the elemental composition of the crystal formations by showing the distinct aluminum, sulfur, and calcium pattern in general. The bridge contained long DEF crystal that fills much less than 5% of the voids to no ettringite in the cores sampled; see Figure 5.46 for typical core results.

In addition to the SEM and EDAX analysis, a large sample of the fractured cores was taken for ASR testing. The UV light ASR test indicates no presence of ASR gel in the wingwall.

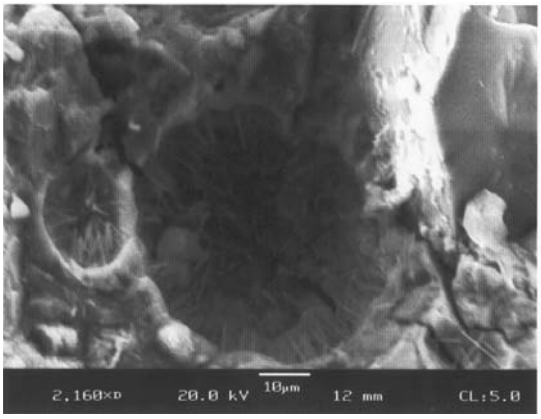

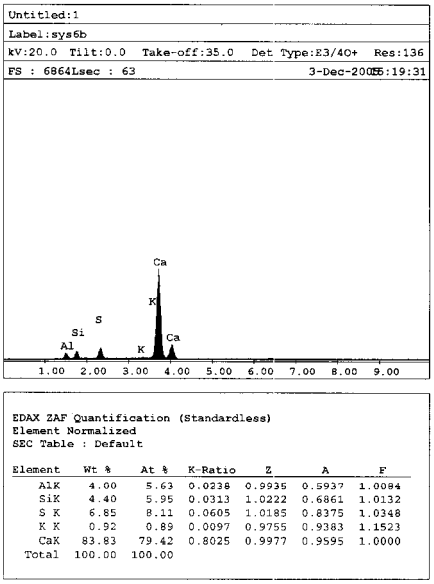

(a) Ettringite in Voids **(b) Analysis of (a)**

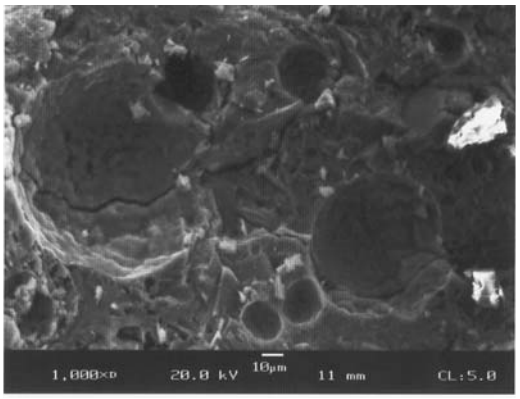

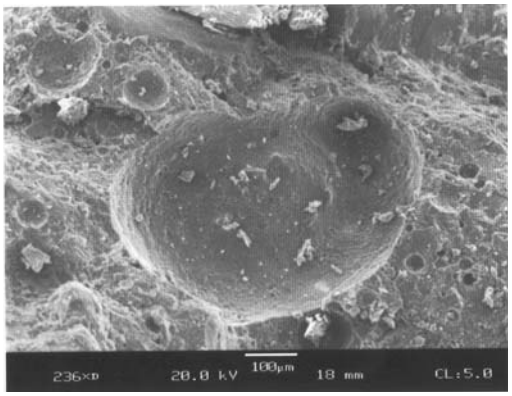

(c) Empty Voids **(d) Empty Void**

Figure 5.45: MD 100 WB over Dorsey Station Road (1315004)

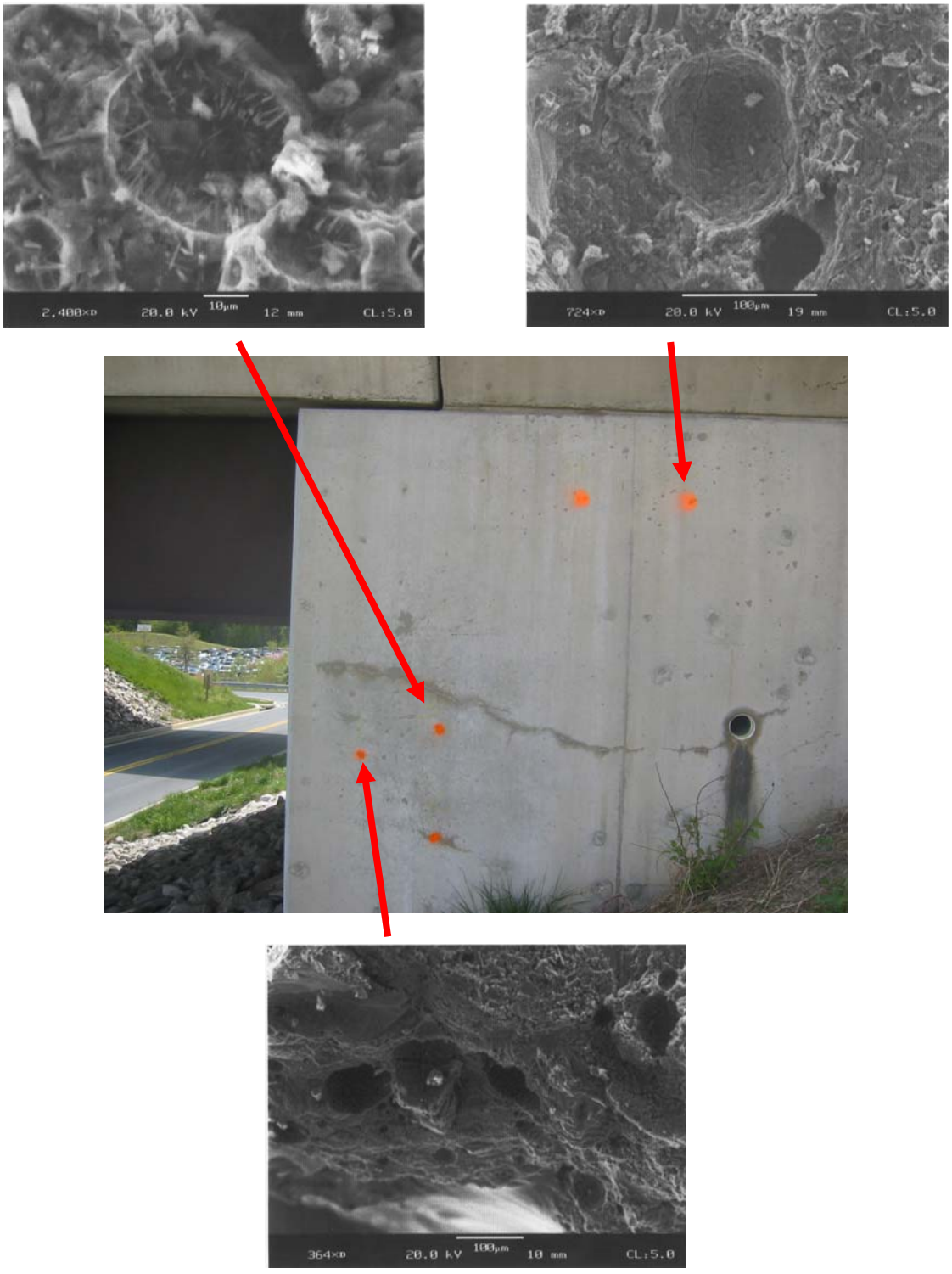

Figure 5.46: Ettringite Spatial Distribution

(MD 100 WB over Dorsey Station Road)

5.4.4.3 Bridge 1315700 (MD 32 over River Road & Patapsco River)

Three cores were taken from the outside face of the east parapet and northeast wingwall; see Figure 5.47 for locations.

Figure 5.47: Coring Locations (MD 32 over River Road & Patapsco River)

Two of the three cores examined contained no ettringite formations. The other one cores contained laminar ettringite formations on the sample surface and long ettringite crystals that filled much less than 5% of the voids. See Figures 5.48 and 5.49. Energy Dispersive Analysis X-ray (EDAX) verifies the elemental composition of the crystal formations by showing the distinct aluminum, sulfur, and calcium pattern in general. The bridge typically exhibited no ettringite, but the core from an area were moist mapping cracking is developing exhibited both long DEF crystal that fills less than 5% of the voids and laminar ettringite; see Figure 5.50 for typical core results.

In addition to the SEM and EDAX analysis, a large sample of the fractured cores was taken for ASR testing. The UV light ASR test indicates no presence of ASR gel in the parapet and wingwall.

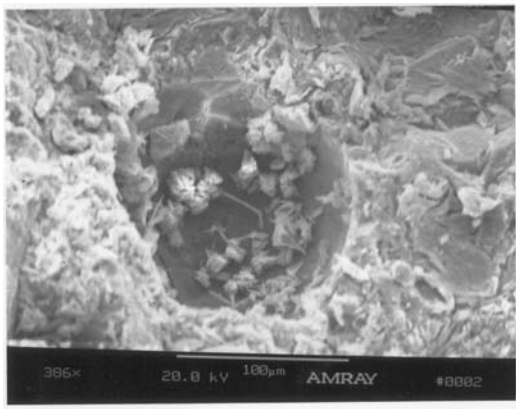

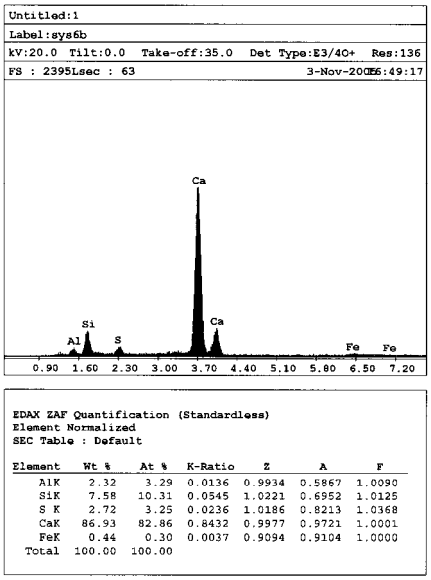

(a) Laminar Ettringite of Surface **(b) Analysis of (a)**

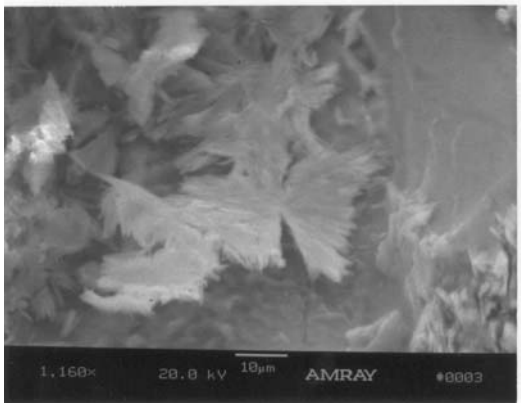

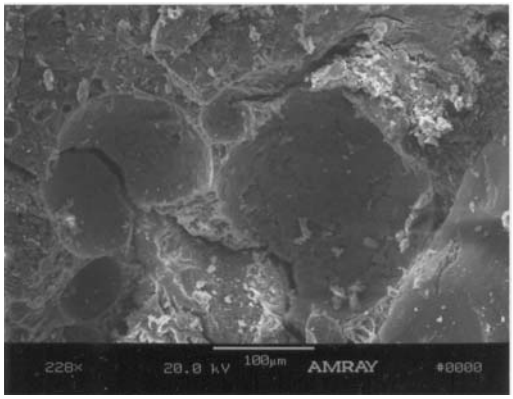

(c) Laminar Ettringite of Surface **(d) Empty Voids**

Figure 5.48: MD 32 over River Road & Patapsco River (1315700) - 1

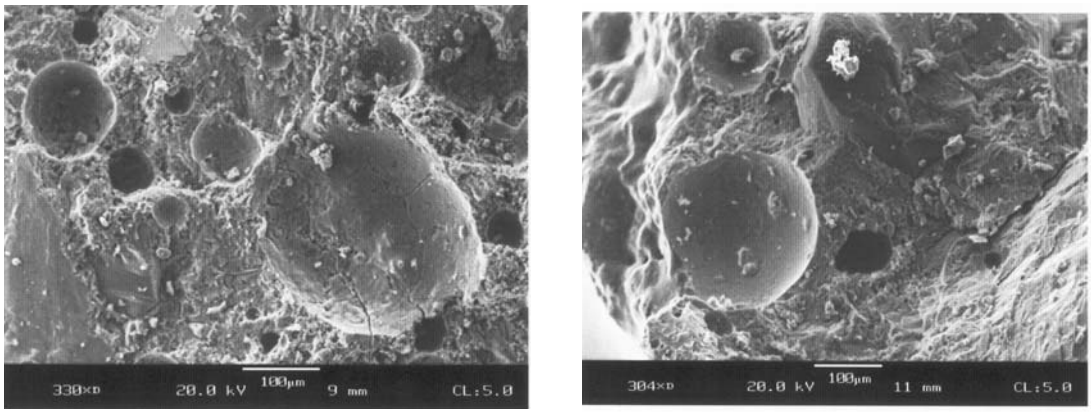

(a) Empty Voids **(b) Empty Voids**

Figure 5.49: MD 32 over River Road & Patapsco River (1315700) - 2

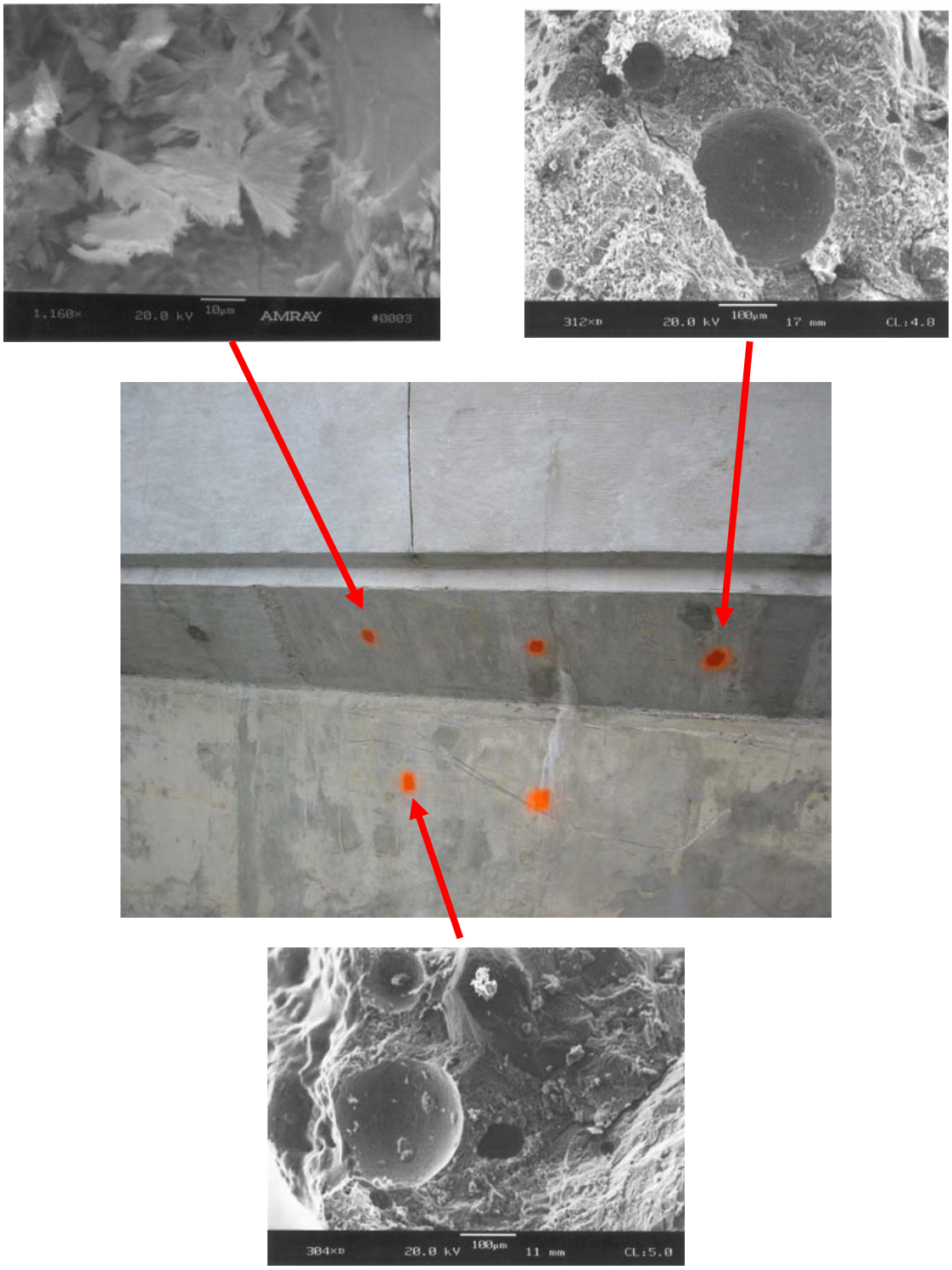

Figure 5.50: Ettringite Spatial Distribution

(1315700 - MD 32 over River Road & Patapsco River)

5.5 Summary and Conclusion

Upon examining 36 cores from 12 bridges, Delayed Ettringite Formation (DEF) was found in 11 of the 12 bridges, but 0 of the 12 bridges contained Alkali-Silica Reaction (ASR) gel. Phase 1 research results were similar with four different types of ettringite formations were observed: needle-like crystals, hexagonal prismatic crystals, a tightly-packed, and a lamellar material, see Chapter 4. Although DEF was found in the majority of the bridges, the clean bridges seemed to contain less DEF than the dirty bridges. This possibility will be investigated further in order to characterize the quantity of DEF in the samples. Chapter 6 discusses the method used to quantify DEF and the various correlations attempted to show the significant factors in identifying bridges with DEF-related damages.

Chapter 6
Discussion of Results

6.1 Summary of Field Studies

Upon completion of both phases of field investigation, several trends and observations were made. The goal of the research is to develop a better understanding of the occurrence and significant of Delayed Ettringite Formations (DEF) in Maryland cast-in-place bridge concrete.

Phase 1 research focused on documenting the presence of DEF in bridge concrete throughout the state. The bridges studied showed DEF was present in most of the bridges. This result was not a surprise since the selected population investigated bridges with moist map cracking. Amde and Livingston (2000) suggested a correlation between moist map cracking and DEF. DEF was identified using Scanning Electron Microscope (SEM) and Energy Dispersive Analysis X-ray (EDAX). The SEM provides visual identification of the ettringite crystals and shows the crystalline morphology. Once possible ettringite crystals are identified, the EDAX is used to confirm the elements present in the crystal. Ettringite has a very distinct output with three stair step peaks of Aluminum (Al), Sulfur (S), and Calcium (Ca). See Figure 6.1 for a typical EDAX output identifying ettringite crystals. Phase 1

showed DEF was present in bridge concrete throughout the State of Maryland, but the results raised questions as to the significance of ettringite crystals in the concrete.

Phase 2 research focused on trying to identify the significance of ettringite in DEF-related map cracking. This population focused on determining the difference between bridges with moist map cracking and without moist map cracking. The population also looked into possible links between bridges with air entrainment agents (AEA) and bridges without AEA. Phase 2 utilized the same analysis techniques as Phase 1.

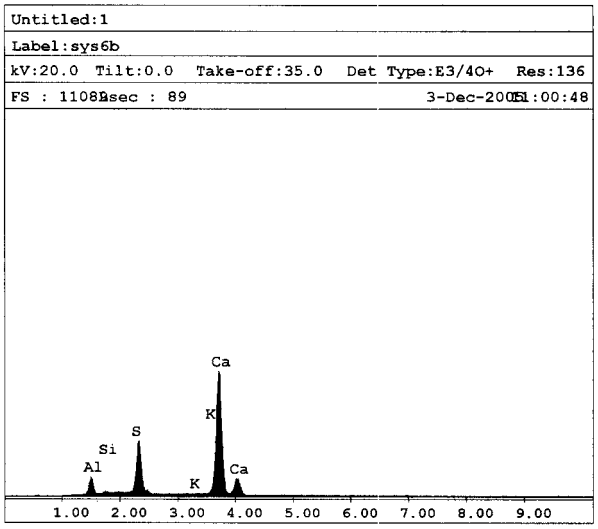

Figure 6.1: Typical EDAX Analysis of DEF

6.2 Observations for Phase 1 – Results of Coring Analysis

Phase 1 research investigated sixteen bridges as part of the overall project with Maryland State Highway Administration (MDSHA). Seven of the bridges were tested using the autoradiography method and all bridges with deterioration were tested with the impact-echo technique, and these bridges will not be discussed in this report.

Ten bridges, eight with deterioration and two control bridges, were cored for analysis by SEM, and EDAX which can positively verify the presence of DEF. Summary of bridge test data is given in Table 6.1. The results are presented herein including additional analysis preformed to document the quantity of DEF in the samples. Phase 1 bridges provide a means of testing hypothesis developed from the phase 2 results. This section presents the SEM analysis.

Table 6.1: Summary of Bridge Test Data

Bridge #	Number of Impulse Echo Waveforms	Number of Autoradiography Locations	Number of Cores
2203201	6	N/A	2
0500800 *	N/A	N/A	N/A
1511300	12	2	3
1600400	9	2	3
1620003	10	2	3
0311100	6	2	N/A
0314200	6	2	3
0333402	4	N/A	N/A
0208303	4	N/A	N/A
0800201	3	N/A	3
1102100	6	N/A	3
2115004	4	2	N/A
0605800	3	N/A	N/A
1311000	6	4	3
0333702	N/A	N/A	3
1301302	N/A	N/A	3

* - No Visible Damage

Twenty-six cores out of a total of twenty-nine exhibited signs of DEF. Also six bridges contained ASR gel as noted in the ultra-violet (UV) light alkali-silica reaction (ASR) test and SEM results. The overall results lead to two observations. First, several forms of ettringite morphology were observed in field concrete. Secondly, comparisons of the testing results with the level of observed deterioration lead the research team to observe several trends.

6.2.1 Ettringite Morphology

In the course of analyzing the core samples throughout the study, four different forms of DEF were observed in samples from the field, see Figure 6.2. The possibility of ettringite existing in different forms has been speculated by some researchers, but this topic is still highly debated. The four different types of ettringite formations observed are: needle-like crystals, hexagonal prismatic crystals, a tightly-packed ettringite formations, and a lamellar material.

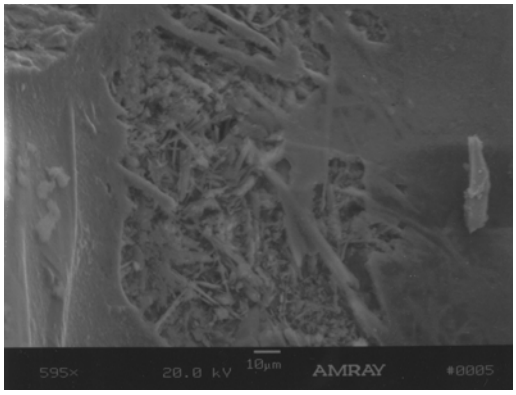

(a) Needle-like Ettringite Crystals

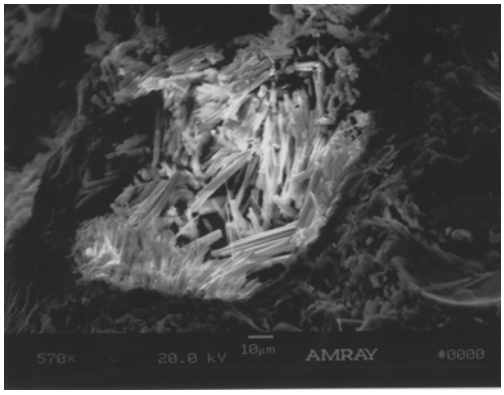

(b) Hexagonal Prismatic Ettringite Crystals

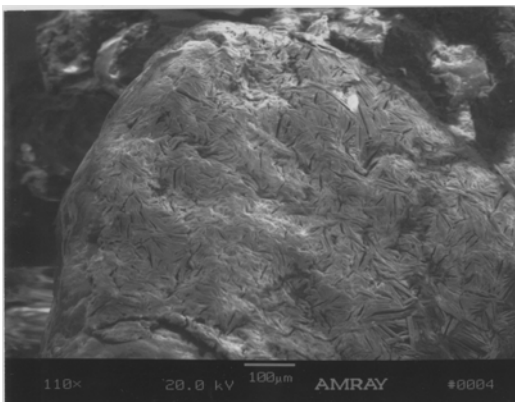

(c) Tightly-Packed Ettringite

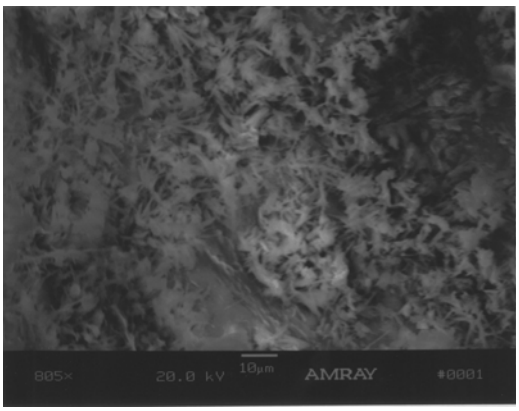

(d) Lamellar Ettringite

Figure 6.2: Ettringite Formations

6.2.2 DEF and ASR Observed Trends

Despite years of research, the roles of ASR and DEF remain uncertain and the mechanism of deterioration is still unclear. ASR gel is formed from reactive aggregates and alkalis, which are either present in the Portland cement or infiltrate from external sources such as deicing salts or the local environment (Mehta 1986,

Taylor 1990). The ASR gel formation *per se* is not deleterious, but once the relative humidity in the concrete reaches eighty percent (80%), the ASR gel expands and is believed to exceed the tensile strength of the concrete causing cracks to form and propagate (Stark 1994). DEF forms from available sulfates and aluminates in the Portland cement (Day 1992). The ettringite crystals hydrate in the hardened concrete and are believed to cause expansion in existing cracks (Diamond, Zhang, and Olek 2002). Researchers believe both ASR and DEF cause microcracking that result in visible cracking on the surface of the concrete element.

The bridges investigated in this study exhibited several trends including

- No map cracking with DEF
- Localized map cracking with DEF
- Localized map cracking with both ASR and DEF
- Widespread map cracking with both ASR and DEF

The research team defined bridges based on visual inspection of the concrete element. Map cracking is commonly defined as cracking which occurs in a distributed pattern. For this study, the research team defined localized map cracking as a small area of map cracking, which is significantly less than the surface area of the concrete element. Therefore, widespread map cracking is defined as significant areas of map cracking on a concrete element. The research team observed coexistence of ASR and DEF, which has also been observed in numerous studies (Mielenz et al. 1995 and Diamond, Ong, and Bonen 1994). Still, little is understood about the significance of both forms of possible deterioration, DEF and ASR, coexisting.

6.2.2.1 No Map Cracking with DEF

Control Bridge 1301302, US 29 SB over Middle Patuxent River, did not exhibit map cracking on the southwest wingwall where the cores were taken, see Figure 6.3. The SEM results show ettringite crystal growth in the voids, see Figure 6.4. The crystals were hexagonal prismatic which grew in unrestrained spaces, and are not necessarily considered evidence of deleterious expansion since the crystals were free to expand.

Control Bridge 0333702, I-795 SB over Cockeys Mill Road, did not exhibit map cracking on the northwest wingwall where the cores were taken, see Figure 6.5. The SEM results show ettringite crystal growth and a location of ASR gel in the voids, see Figure 6.6. The crystals were hexagonal prismatic which grow in unrestrained spaces, and are not necessarily considered evidence of deleterious expansion since the crystals are free to expand. The ettringite is mixed heavily with calcium hydroxide ($CaOH_2$), which makes distinguishing between the calcium hydroxide and the ettringite formations difficult. In Figure 6.6 (a), both formations are readily visible. ASR gel was observed in a void, and though ASR gel was observed with the SEM, the ultraviolet ASR test indicated that ASR gel was not present in large quantities. The ASR gel quantity is insignificant, probably because of very limited supply of reactive aggregate.

Figure 6.3: Sampled Area (1301302 – US 29 SB over Middle Patuxent River)

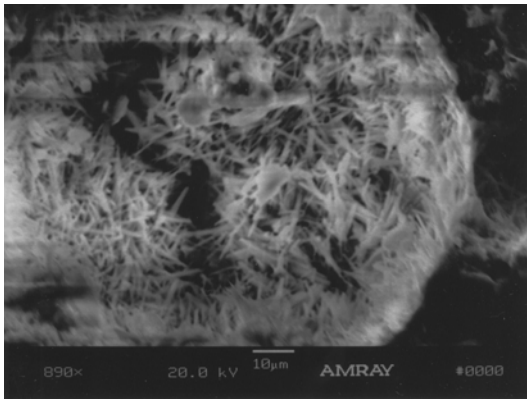

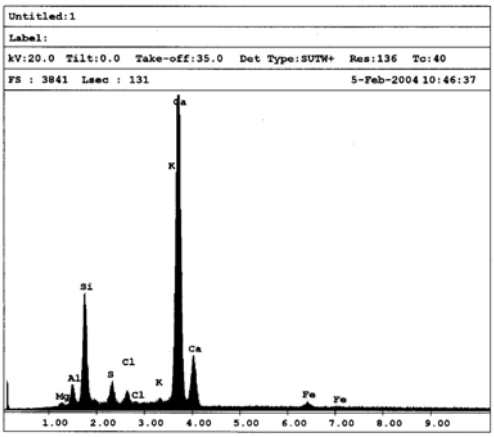

EDAX ZAF Quantification (Standardless)
Element Normalized
SEC Table : Default

Element	Wt %	At %	K-Ratio	Z	A	F
MgK	0.62	0.94	0.0029	1.0246	0.4584	1.0060
AlK	3.12	4.27	0.0188	0.9942	0.5991	1.0105
SiK	15.06	19.80	0.1086	1.0229	0.6979	1.0103
S K	3.30	3.80	0.0267	1.0186	0.7724	1.0273
ClK	1.92	2.00	0.0160	0.9728	0.8234	1.0437
K K	1.07	1.01	0.0106	0.9759	0.9137	1.1147
CaK	71.84	66.16	0.6745	0.9981	0.9399	1.0009
FeK	3.08	2.03	0.0258	0.9096	0.9205	1.0000
Total	100.00	100.00				

(a) Ettringite in Void **(b) Analysis of Whole Picture (a)**

Figure 6.4: Typical Voids (1301302 – US 29 SB over Middle Patuxent River)

Figure 6.5: Sampled Area (0333702 – I-795 SB over Cockeys Mill Road)

(a) Ettringite in Void

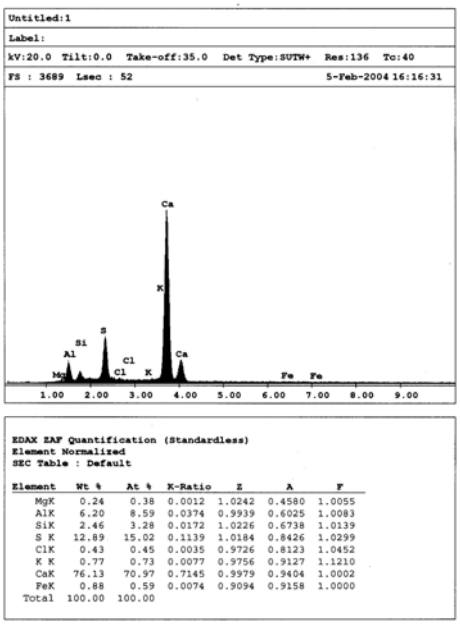

(b) Analysis of DEF Crystals in(a)

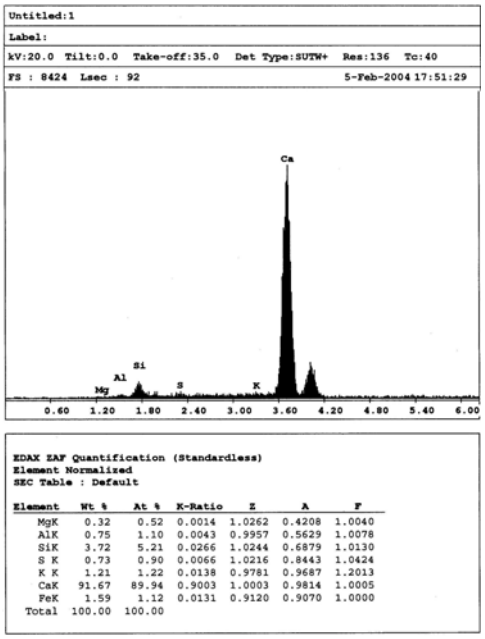

(c) Analysis of Calcium Hydroxide Crystals in(a)

Figure 6.6: Typical Voids (0333702 – I-795 SB over Cockeys Mill Road)

6.2.2.2 Localized Map Cracking with DEF

Bridge 0314200 (Old Court Rd over I-695) exhibited map cracking in localized areas, see Figure 6.7. The SEM results show ettringite crystal growth in the voids and on the surface of crack fractures, see Figure 6.8. The ettringite crystals were long hexagonal prismatic and short thin needles.

Bridge 2203201 (US 13 NB over MD 346) exhibited map cracking in localized areas, see Figure 6.9. The SEM results show ettringite crystal growth in the voids, see Figure 6.10. DEF in the voids was lamellar.

Diamond, Zhang, and Olek suggest that, if microcracks are present prior to the development of ettringite, ettringite crystals can develop at the crack tip, and due to the high stress modification factor associated with crack tips, ettringite can then propagate the crack (2002). They indicate that several factors can cause microcracks, and they tested concretes and found that strains as low as 0.02% can develop microcracking. Their research with modern concrete indicates that some concretes during the drying process exceed this strain limit, and therefore, microcracks are available for the ettringite to form in and then to propagate cracks.

Figure 6.7: Localized Map Cracking (0341200 - Old Court Road over I-695)

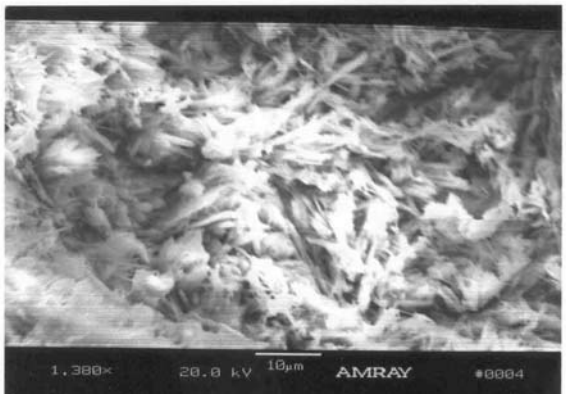

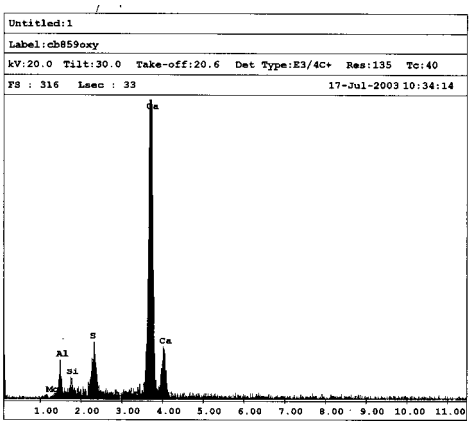

EDAX ZAF Quantification (Standardless)
Element Normalized
SEC Table : Default

Element	Wt %	At %	K-Ratio	Z	A	F
MgK	0.48	0.74	0.0018	1.0239	0.3729	1.0049
AlK	6.40	8.92	0.0327	0.9935	0.5103	1.0072
SiK	2.19	2.93	0.0132	1.0222	0.5848	1.0121
S K	8.96	10.50	0.0740	1.0182	0.7879	1.0298
CaK	81.98	76.91	0.7699	0.9976	0.9414	1.0000
Total	100.00	100.00				

(a) Ettringite on the Surface **(b) Analysis of Whole Picture (a)**

Figure 6.8: Typical Ettringite Formations (0341200 - Old Court Road over I-695)

Figure 6.9: Localized Map Cracking (2203201 - US 13 NB over MD 346)

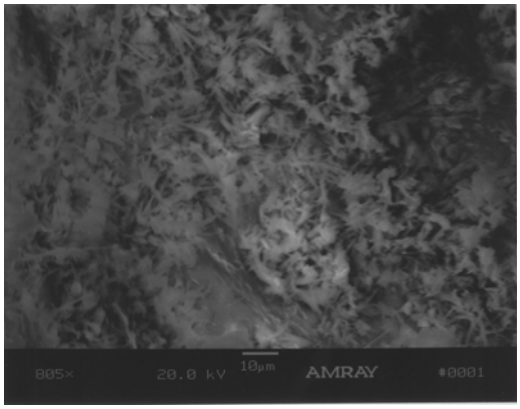

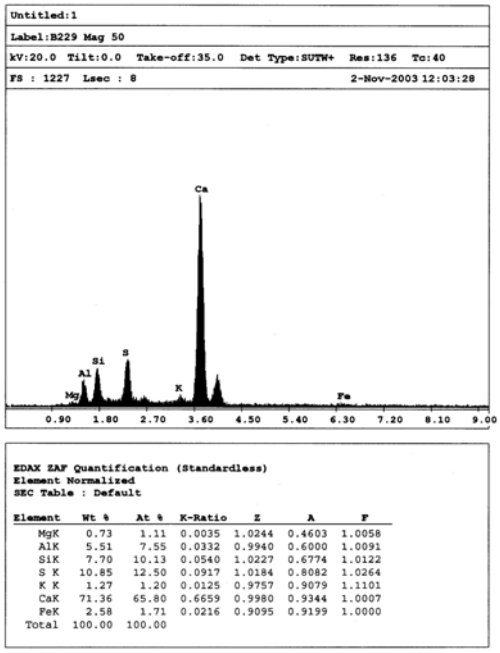

(a) Ettringite in Void **(b) Analysis of (a)**

Figure 6.10: Typical Voids (2203201 - US 13 NB over MD 346)

6.2.2.3 Localized Map Cracking with Both ASR and DEF

Bridge 0800201 (MD 5 NB over Zekiah Swamp), Bridge 1600400 (US 1 over Paint Branch), and Bridge 1620003 (MD198 over I-95) exhibit localized areas of map cracking. The areas typically have numerous cracks with uncracked concrete in adjacent areas, see Figures 6.11 to 6.13. ASR gel was located with the scanning electron microscope (SEM) and identified using an energy dispersive x-ray analysis (EDAX). An ultraviolet light test was also used to determine if ASR gel was prevalent in the core. All bridges contained ASR gel as determined by the SEM and ultraviolet light test, see Figure 6.14 for typical ASR gel location. In addition to ASR gel, DEF was found in each bridge, and the various forms of morphology included hexagonal prismatic and tightly packed formations, see Figures 6.15 and 6.16.

Bridges 1600400 and 1620003 contained DEF and ASR in all cores, but Bridge 0800201 only contained DEF and ASR in one (1) core, with the other two (2) cores being free of DEF and ASR.

Figure 6.11: Localized Map Cracking (0800201 - MD 5 NB over Zekiah Swamp)

Figure 6.12: Localized Map Cracking (1600400 - US 1 over Paint Branch)

Figure 6.13: Localized Map Cracking (1620003 - MD198 over I-95)

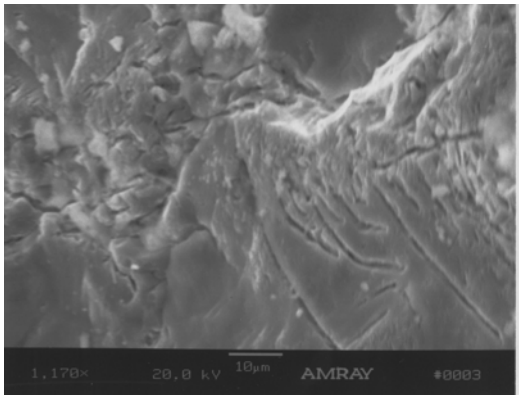

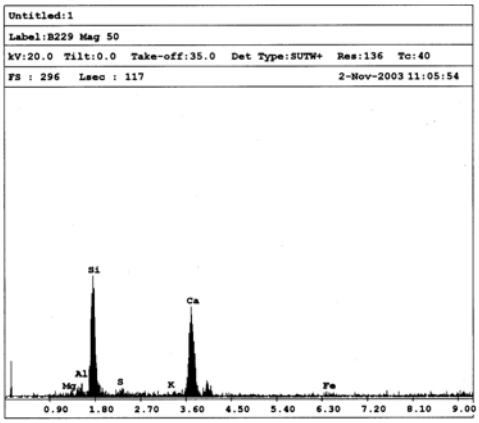

EDAX ZAF Quantification (Standardless)
Element Normalized
SEC Table : Default

Element	Wt %	At %	K-Ratio	Z	A	F
MgK	0.74	1.04	0.0041	1.0182	0.5296	1.0104
AlK	3.71	4.66	0.0249	0.9881	0.6671	1.0184
SiK	38.03	45.81	0.2908	1.0166	0.7472	1.0066
S K	2.86	3.02	0.0194	1.0102	0.6625	1.0148
K K	1.55	1.34	0.0138	0.9688	0.8656	1.0646
CaK	50.23	42.40	0.4487	0.9911	0.9005	1.0008
FeK	2.87	1.74	0.0243	0.9026	0.9369	1.0000
Total	100.00	100.00				

(a) ASR Gel **(b) Analysis of ASR Gel (a)**

Figure 6.14: Typical ASR Gel (0800201 - MD 5 NB over Zekiah Swamp)

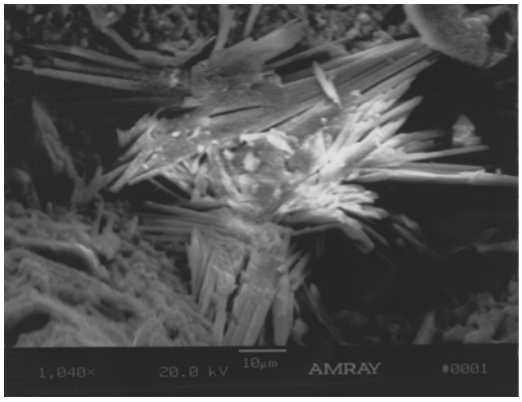

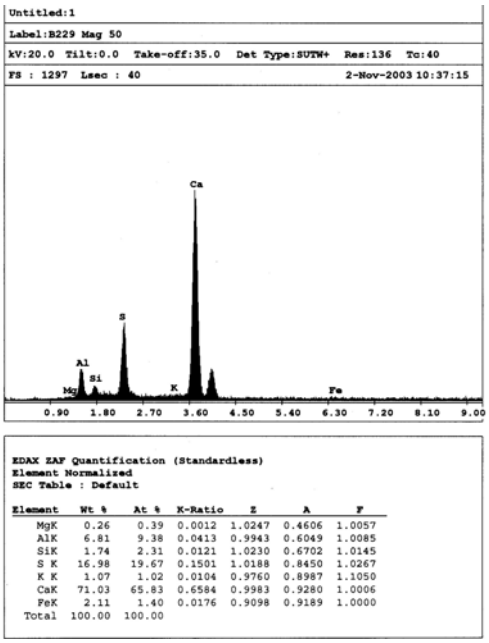

(a) Ettringite on the Surface **(b) Analysis of Ettringite in (a)**

Figure 6.15: Ettringite (0800201 - MD 5 NB over Zekiah Swamp)

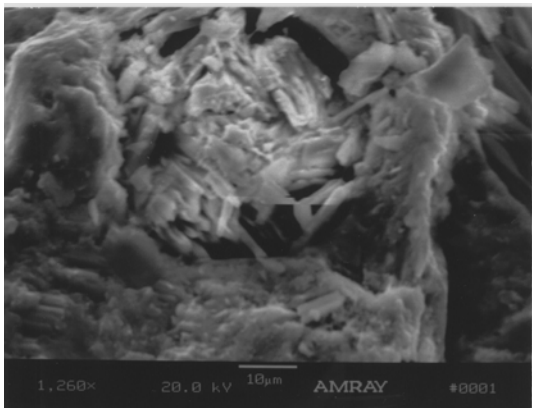

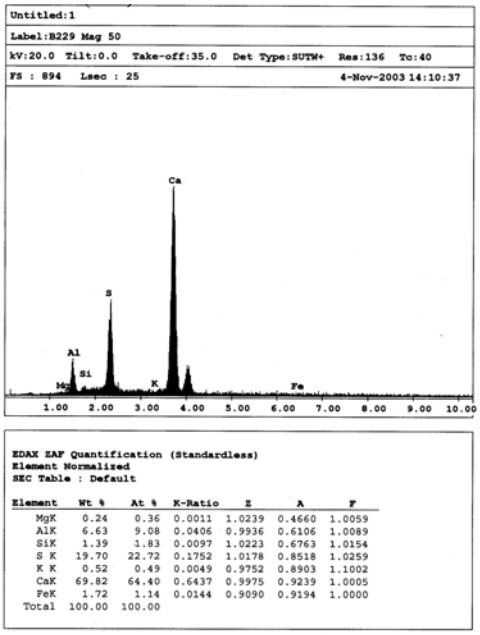

(a) Ettringite Filling Void

(b) Analysis of Ettringite Filling Void (a)

Figure 6.16: Ettringite (1620003 - MD198 over I-95)

6.2.2.4 Widespread Map Cracking With Both ASR and DEF

Bridge 1102100 (US 219 over Deep Creek Lake), Bridge 1311000 (MD 32 EB CD over US 1), and Bridge 1511300 (Greentree Road over I-495) exhibited map cracking covering the entire surface of the affected concrete element, see Figures 6.17 to 6.19. Using the scanning electron microscope (SEM) and energy dispersive x-ray analysis (EDAX), ASR gel was observed in all bridges. Furthermore, an ultraviolet light test was used to determine if ASR gel was prevalent in large quantities in the core, see Figure 6.20 for typical ASR gel location. In addition to ASR gel, DEF were found in each bridge, and the various forms of morphology included hexagonal prismatic and tightly packed formations, see Figures 6.21 to 6.23.

Diamond, Ong, and Bonen in a study of steam cured railroad ties found the coexistence of ASR and DEF highly likely (1994). This study finds that the coexistence of ASR and DEF is also highly likely for cast-in-place concrete.

Figure 6.17: Map Cracking (1102100 - US 219 over Deep Creek Lake)

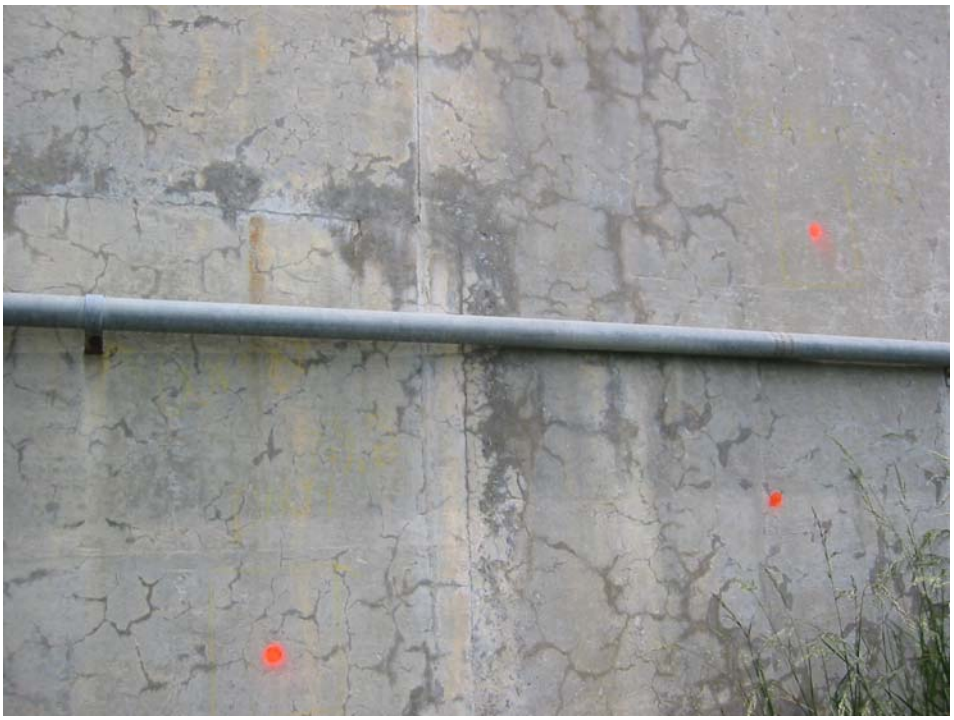

Figure 6.18: Map Cracking (1311000 - MD 32 EB CD over US 1)

Figure 6.19: Map Cracking (1511300 - Greentree Rd over I-495)

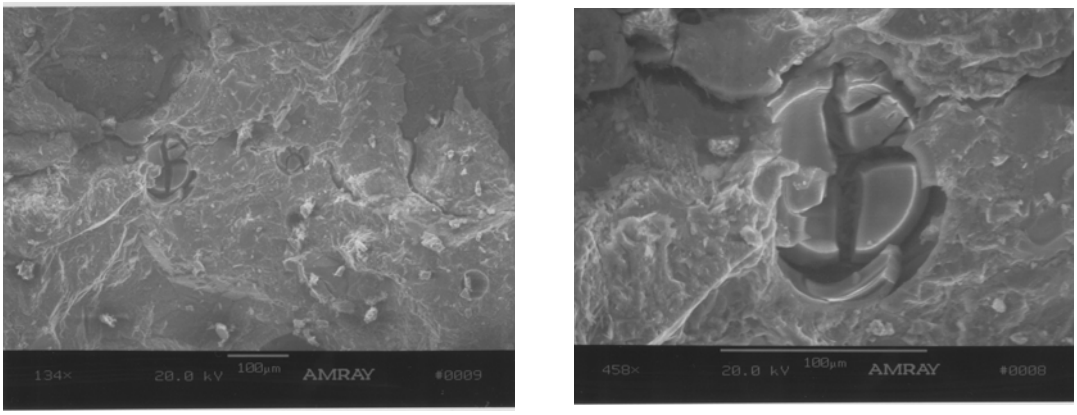

(a) ASR Gel with Cracking **(b) ASR Gel – Close-up of (a)**

Figure 6.20: ASR Gel (1102100 - US 219 over Deep Creek Lake)

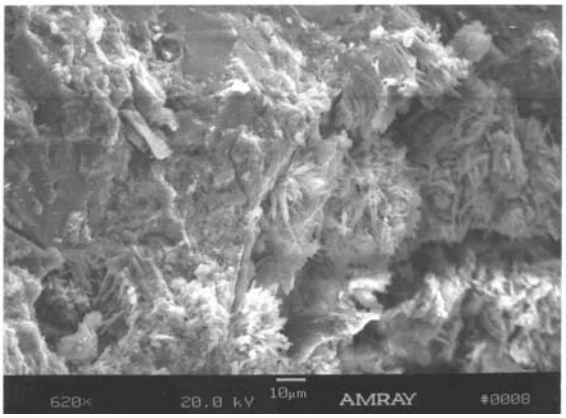

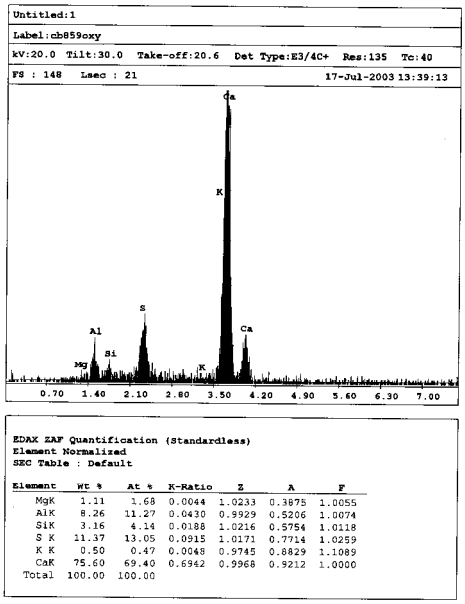

(a) Ettringite on the Surface **(b) Analysis of Whole Picture (a)**

Figure 6.21: Hexagonal Prismatic Ettringite (1311000 - MD 32 EB CD over US 1)

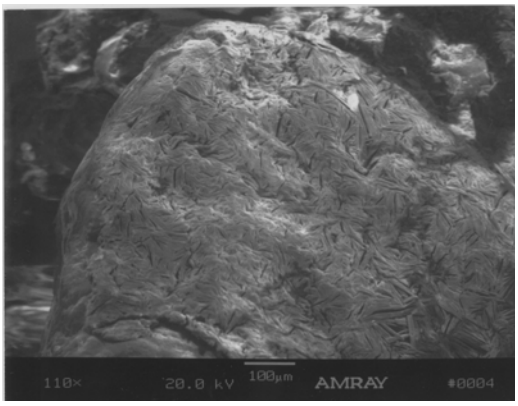

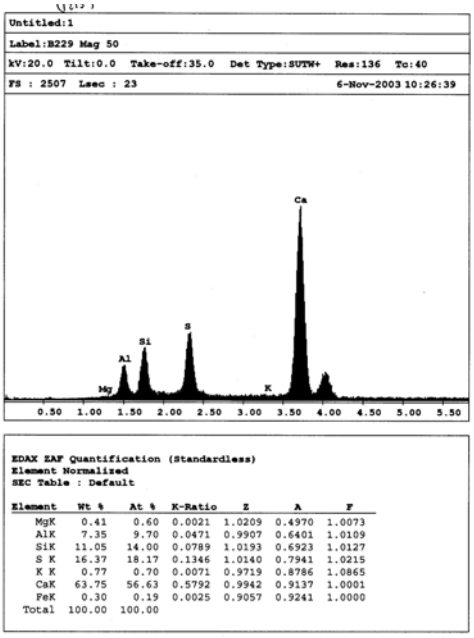

(a) Ettringite Mass on Surface of the Aggregate **(b) Analysis of Whole Picture (a)**

Figure 6.22: Tightly Packed Ettringite (1511300 - Greentree Rd over I-495)

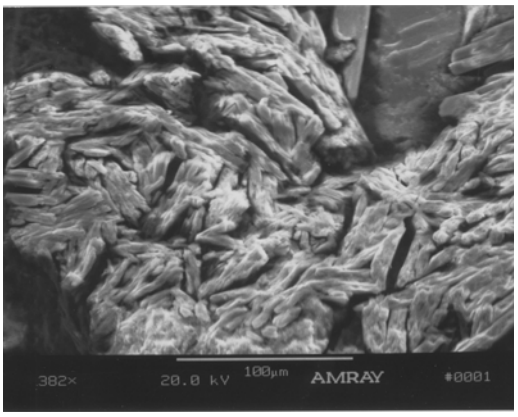

(a) Ettringite Mass on Surface of the Sample

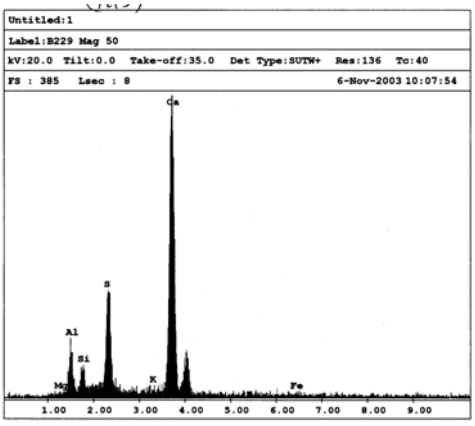

EDAX EAF Quantification (Standardless)
Element Normalized
SEC Table : Default

Element	Wt %	At %	K-Ratio	Z	A	F
MgK	0.46	0.70	0.0022	1.0237	0.4703	1.0061
AlK	7.21	9.81	0.0443	0.9934	0.6128	1.0089
SiK	3.50	4.57	0.0244	1.0221	0.6729	1.0142
S K	17.62	20.16	0.1533	1.0175	0.8341	1.0250
K K	0.79	0.74	0.0075	0.9749	0.8913	1.0987
CaK	68.71	62.90	0.6331	0.9972	0.9235	1.0005
FeK	1.71	1.12	0.0143	0.9087	0.9205	1.0000
Total	100.00	100.00				

(b) Ettringite Mass in (a)

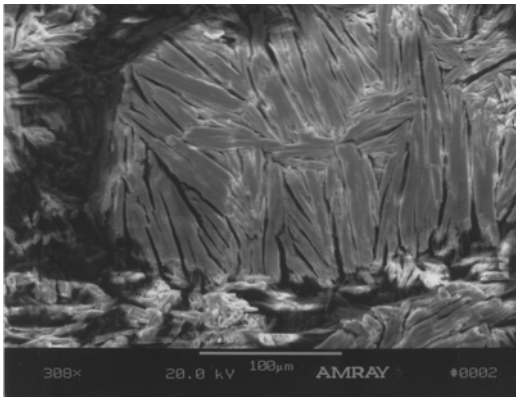

(c) Ettringite Filling Void

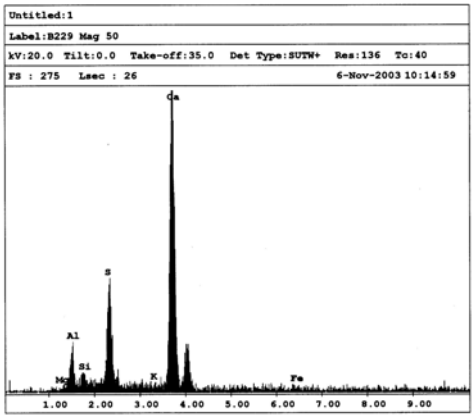

EDAX EAF Quantification (Standardless)
Element Normalized
SEC Table : Default

Element	Wt %	At %	K-Ratio	Z	A	F
MgK	0.00	0.00	0.0000	1.0251	0.4571	1.0057
AlK	6.64	9.16	0.0402	0.9947	0.6036	1.0085
SiK	2.33	3.09	0.0162	1.0235	0.6707	1.0142
S K	16.40	19.05	0.1443	1.0193	0.8412	1.0267
K K	0.91	0.87	0.0089	0.9765	0.8995	1.1058
CaK	71.04	66.03	0.6598	0.9987	0.9293	1.0007
FeK	2.68	1.79	0.0224	0.9102	0.9191	1.0000
Total	100.00	100.00				

(d) Analysis of Ettringite in (c)

Figure 6.23: Tightly Packed Ettringite (1511300 - Greentree Rd over I-495)

6.2.3 Conclusions of Phase 1 Research

The goal of this research was to help the Maryland State Highway Administration (MDSHA) better understand DEF and the possible effects DEF may have on reducing the life span of concrete elements used for bridge structures. In order to study DEF, a statistical sample of bridges was selected from the MDSHA Bridge Management Information System (MDSHA BMIS) with the presence of map cracking used as the selection criterion. Map cracking is recorded in the MDSHA BMIS for 37 percent of the inventory. All the bridges in this sample, that were cored, were found to have some form of ettringite. However, two bridges that were not recorded as having map cracking also had ettringite. Thus map cracking by itself is not a definitive indicator of DEF. On the other hand, map cracking has often been assumed to be a sign of ASR. This study has shown that DEF can occur with map cracking in the absence of ASR. Therefore, map cracking is not a definitive indicator of ASR either. Nevertheless, the presence of map cracking indicates that some type of damage is taking place, and it calls for more intensive analyses.

This study has shown that DEF definitely exists in bridges in Maryland. Hence it is not a problem that is localized to a few geographical sites such as Texas. Given the similarity of construction methods and materials, it is likely that DEF will also be found in neighboring states. Therefore, it would be very desirable to extend this survey to those states.

In the bridges that were studied, DEF was found in cast in place bridge elements. This therefore refutes the theory that DEF happens only as a result of high-temperature curing.

Four distinct forms of ettringite morphology were observed including: short thin needle-like crystals, long hexagonal prismatic crystals, tightly packed formation, and a lamellar formation. These may indicate progressive stages in the DEF damage process, but because of the limited number of data, additional samples will be needed to confirm this hypothesis.

In addition to differences in morphology, differences were noticed in the distribution of moist map cracking on the concrete surface. Three distinct patterns were observed which include no moist map cracking, localized moist map cracking, and widespread moist map cracking, see Figures 6.24 to 6.26. Further testing should investigate the significance of widespread versus localized moist map cracking.

Figure 6.24: No Moist Map Cracking

Figure 6.25: Localized Moist Map Cracking

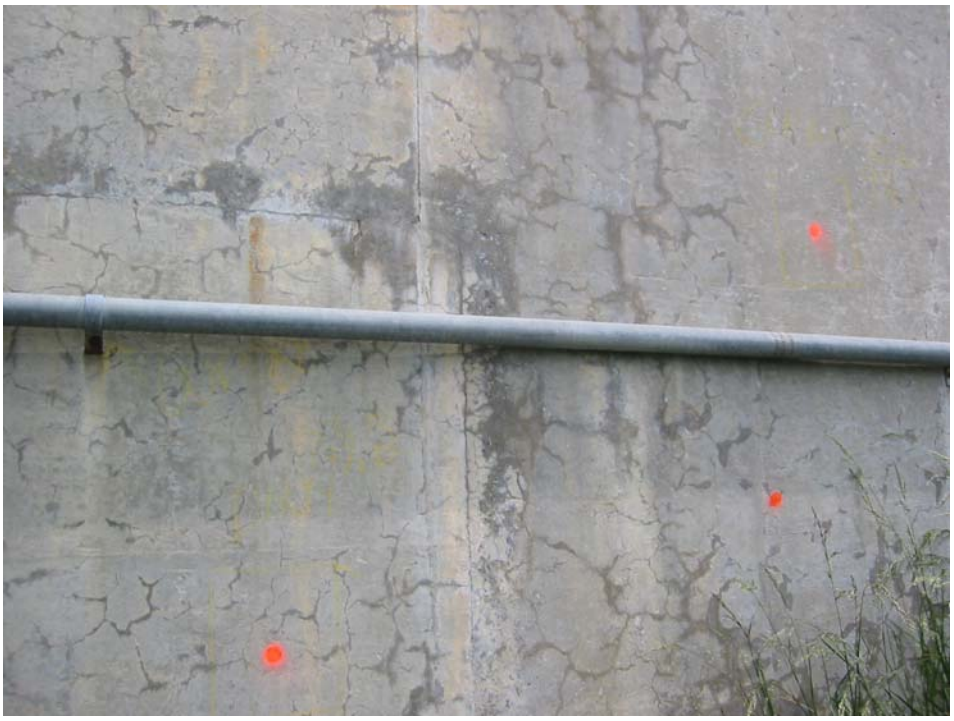

Figure 6.26: Widespread Moist Map Cracking

6.3 Observations for Phase 2

Phase 1 of the research identified differences in the ettringite morphologies and in the extent of the moist map cracking on the concrete surface (Amde et al. 2004). Phase 2 research was developed to further develop a better understanding of the significance of these observed differences. In order to accomplish meaningful correlations, wider selection criteria were used versus the Phase 1 population. Half the population was selected with moist map cracking and the other half without moist map cracking. The bridges with moist map cracking also had more variation in degree of moist map cracking than Phase 1 population in order to understand variations in DEF relative to extent of surface damage.

In addition, the population will consider the role of air entrainment agent (AEA) on the prevalence of DEF in bridges that used AEA versus bridges constructed before AEA was required. Additional literature research indicated that ettringite grows well in AEA (Cody et al 2001). According to the Office of Materials and Technology for the Maryland State Highway Administration, AEA was introduced into the concrete mix in 1980 or 1981 depending on the letting of the construction contract. In order to insure that AEA was used or not used the concrete tested, no bridges were selected from 1980 or 1981. Half the population was selected with construction dates before 1980 and the other half with construction dates after 1981.

The two population selection criteria are independent; therefore one large population can be developed with both selection criteria in mind. The resulting population will have four subsets including:

1. Bridges without moist map cracking built before 1980.
2. Bridges without moist map cracking built after 1981.
3. Bridges with moist map cracking built before 1980.
4. Bridges with moist map cracking built after 1981.

The minimum subset size is 3 bridges, which will result in a total population of 12 bridges. Bridges were selected from Maryland Bridge Inventory data that includes physical data like type, size, location, and date of construction and defect data like map cracking. Candidate bridges were selected on a random basis from the Greater Baltimore-Washington area (excluding Eastern Shore, Western Maryland, and Southern Maryland to limit driving distances). From this list, target bridges were selected based on ease of access. The target bridges were than visited to verify if the bridge inventory data was accurate. Several bridges were rejected because moist map cracking was identified on the concrete surface that had not been indicated in the bridge inventory database. If the bridge was rejected due to the sub-subpopulation being filled, near by bridges were investigated which meet needed criteria.

Once the population was developed, cores were taken from all bridges for Scanning Electron Microscope (SEM) Analysis. Several samples were analyzed from each core and three cores were analyzed from each bridge, totaling 36 cores and 72 samples. In order to evaluate the differences between sample, SEM sample mapping techniques were utilized, see Figure 6.27 for sample SEM mapping. The mapping

then can be analyzed to produce semi-quantitative comparisons. This method is used commonly when performing SEM investigations.

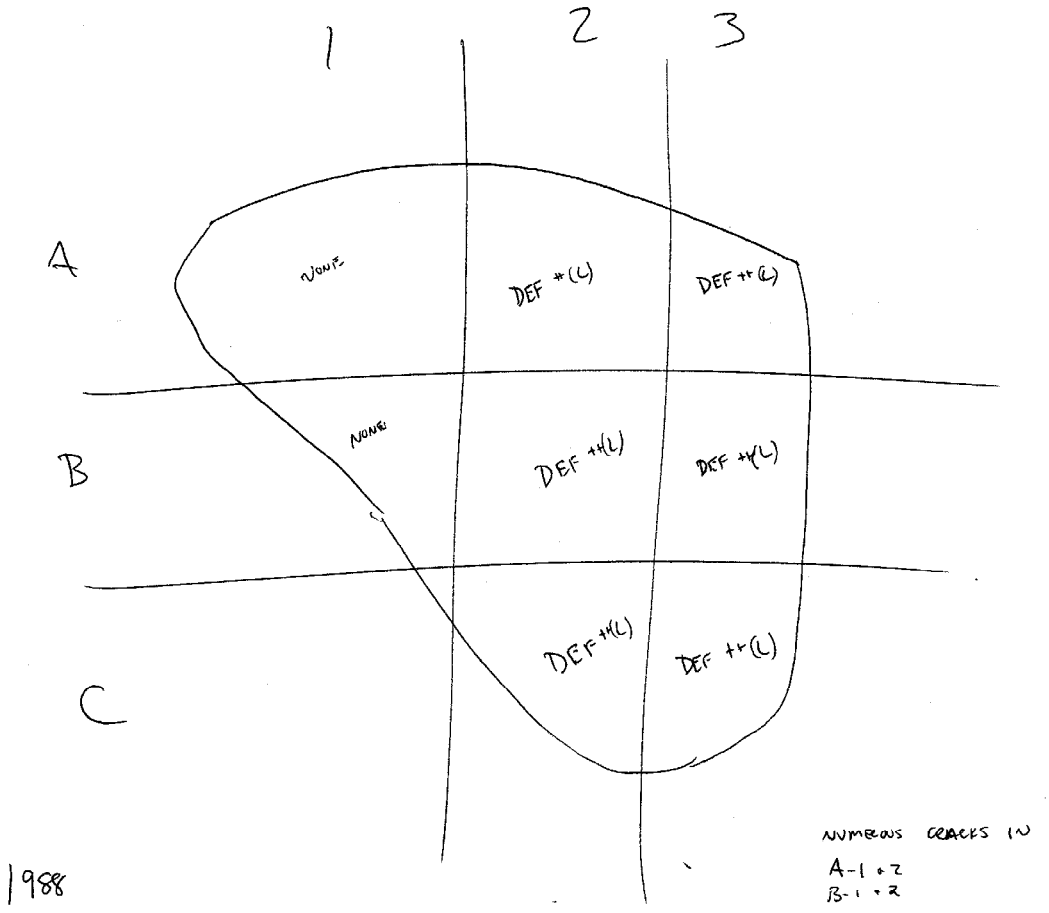

Figure 6.27: Sample SEM Mapping

6.3.1 Ettringite Morphology

In the course of analyzing the core samples from the phase 2 bridges, similar ettringite morphologies were observed, see Figure 6.28. Field studies conducted in the US, Canada, France, and Germany has documented similar ettringite morphologies as identified in phase 1 bridges (Gress 1997, Stark and Bollman 1997, Lawrence et al. 1999, Cody et al. 2001, Amde et al. 2004, and Divet, Pavoine, and Clement 2006). Of

particular interest is the French study which showed tightly packed or lamellar formations in cast-in-place bridge concrete (Divet, Pavoine, and Clement 2006).

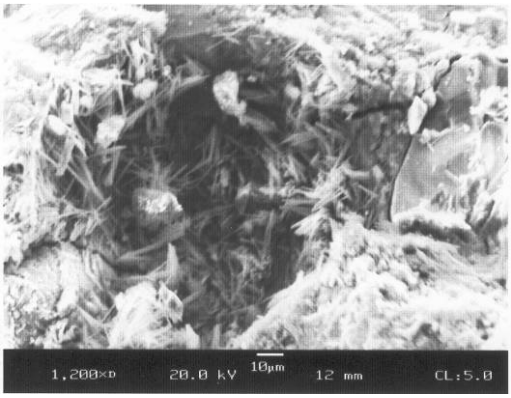

(a) Sparse Hexagonal Prismatic Ettringite Crystals

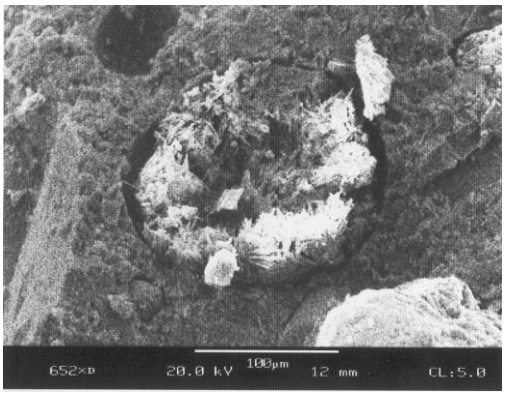

(b) Hexagonal Prismatic Ettringite Crystals

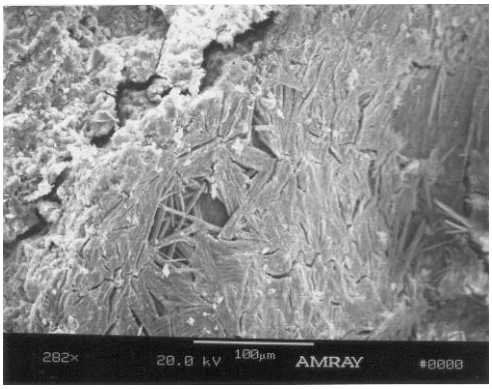

(c) Tightly-Packed Ettringite

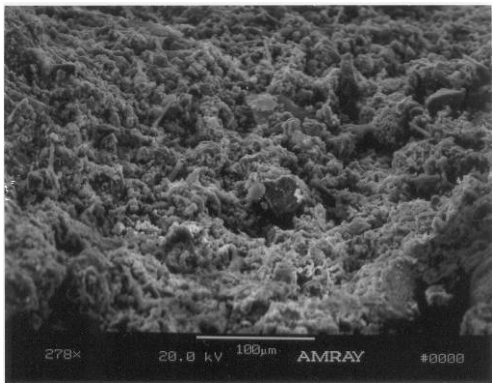

(d) Lamellar Ettringite

Figure 6.28: Ettringite Formations

6.3.2 DEF and ASR Observed Trends

Phase 1 results showed locations of ASR gel in some of the samples analyzed. In order to better study DEF, the phase 2 population was biased toward Central Maryland that results in higher probability of crushed limestone aggregate. The crushed limestone has a low MDSHA ASR reactivity rating.

The population had no cases of ASR identified, whereas DEF was readily identified in most bridges. DEF was found in at least one (1) of the six (6) samples in eleven (11) of the twelve (12) bridges. These results were expected, but a more advanced method of analysis is required. Two possible patterns were identified in phase 1 work. The first suggested that the tightly-packed or lamellar ettringite morphologies were connected to DEF-related damage. To test this hypothesis, the ettringite morphologies will be compared with the visual surface defects. The other pattern suggested that the quantity of DEF in the sample is proportionate to the amount of visual surface defects. SEM mapping was used in order to quantify DEF.

6.3.2.1 Classifying DEF Morphologies – Moist Map Cracking

Classifying ettringite morphologies involves developing correlations between morphologies and DEF related damages. The DEF related damage of interest is moist map cracking of the surface of the concrete. For this damage to be visible on the surface, DEF has developed and / or propagate the cracking to the exterior surface on the concrete. This type cracking results in deterioration of the concrete.

In order to track the DEF morphologies, the samples were viewed using a SEM and the results are shown the Tables 6.2 to 6.4 and in Figure 6.29. The morphologies were divided into seven (7) categories including:

1. No DEF
2. Long Needles in Voids (<< 5% of Void Filled)
3. Bundles / Balls in Voids or on the Surface
4. Long Needles in Voids (> 5% but < 50% of Void Filled)
5. Long Needles in Voids (> 50% of Void Filled)
6. Lamellar Formations Filling Voids
7. Lamellar Formations on the Surface

See Figure 6.30 and 6.31 for samples of the morphology types. The results show that most samples had no DEF (37 of 72) or occasional long needle ettringite crystals in voids (20 of 72), which totals 57 of the 72 samples analyzed. This suggest the normal condition of concrete, and show that occasional long needle ettringite crystals in voids is not indicative of ettringite that leads to DEF related damage. Furthermore, two (2) morphologies observed in laboratory or other field studies were not observed in this survey. This could suggest possible transition phases observed during early ettringite development. The bundles / balls are readily observed in laboratory testing at early stages in the development of DEF. The bundles / balls may progress into a different morphology. If this is the case, it would explain the absence of bundles / balls in the field samples that are between 3 and 50 years old. The other morphology that was not observed was lamellar ettringite in voids. This morphology was observed in phase 1

field study. The fact that the morphology was not observed could indicate a special condition and not a normal condition.

From Table 6.2, two trends can be identified. First, most the samples (90%) had either no DEF or long needle crystals in voids with varying degrees of percent of void filled. This result is independent of visual moist map cracking on the surface; both "clean" without and "dirty" with moist map cracking. The resulting trend either suggests that there is no correlation between DEF morphology and visual moist map cracking or that the moist map cracking should be categorized differently. The second trend shows lamellar ettringite or tightly-packed ettringite morphology is only found in bridges with moist map cracking. Based on this observation, lamellar ettringite could be indicative of DEF related damage. The question remains, though, why is lamellar ettringite not found in every bridge with visual moist map cracking? Since morphology did not provide a clear correlation, the research focused on quantifying DEF in the samples.

Table 6.2: Summary of DEF Morphology Code per Sample

Bridge #	Status	# of Code 1	# of Code 2	# of Code 3	# of Code 4	# of Code 5	# of Code 6	# of Code 7
0208304	dirty	4	1	0	1	0	0	0
0217200	clean	3	3	0	0	0	0	0
0219000	clean	6	0	0	0	0	0	0
0311100	dirty	0	0	0	0	0	0	6
0333900	dirty	0	4	0	2	0	0	0
1005000	clean	5	1	0	0	0	0	0
1005600	clean	0	4	0	0	2	0	0
1011100	clean	2	4	0	0	0	0	0
1308603	dirty	3	2	0	1	0	0	0
1315004	dirty	5	1	0	0	0	0	0
1315700	dirty	5	0	0	0	0	0	1
1612300	clean	4	0	0	1	1	0	0
Total		**37**	**20**	**0**	**5**	**3**	**0**	**7**
% of Total		**51%**	**28%**	**0%**	**7%**	**4%**	**0%**	**10%**

Table 6.3: DEF Morphology of Bridges without Moist Map Cracking

Clean Bridges					
		Code 2	Code 4	Code 5	Code 7
Bridge Number	Core Number	Long Needles			Lamellar
		<<5%	5%-50%	>50%	Formations
0217200	1	X	-	-	-
	2	-	-	-	-
	4	X	-	-	-
0219000	1	-	-	-	-
	2	-	-	-	-
	4	-	-	-	-
1005000	2	X	-	-	-
	4	-	-	-	-
	5	-	-	-	-
1005600	1	X	-	-	-
	3	X	X	X	-
	5	X	X	X	-
1011100	1	X	-	-	-
	2	-	-	-	-
	3	X	-	-	-
1612300	1	-	-	-	-
	2	-	-	-	-
	3	X	X	X	-

Table 6.4: DEF Morphology of Bridges with Moist Map Cracking

Dirty Bridges					
		Code 2	Code 4	Code 5	Code 7
Bridge Number	Core Number	Long Needles			Lamellar
		<<5%	5%-50%	>50%	Formations
0208304	1	-	-	-	-
	4	-	-	-	-
	5	X	X	-	-
0311100	2	-	-	-	X
	3	X	-	X	X
	5	-	-	-	X
0333900	2	X	X	-	-
	3	X	-	-	-
	4	X	X	X	-
1308603	1	-	-	-	-
	3	X	-	-	-
	5	X	X	-	-
1315004	1	-	-	-	-
	2	X	-	-	-
	5	-	-	-	-
1315700	1	X	-	-	X
	2	-	-	-	-
	5	-	-	-	-

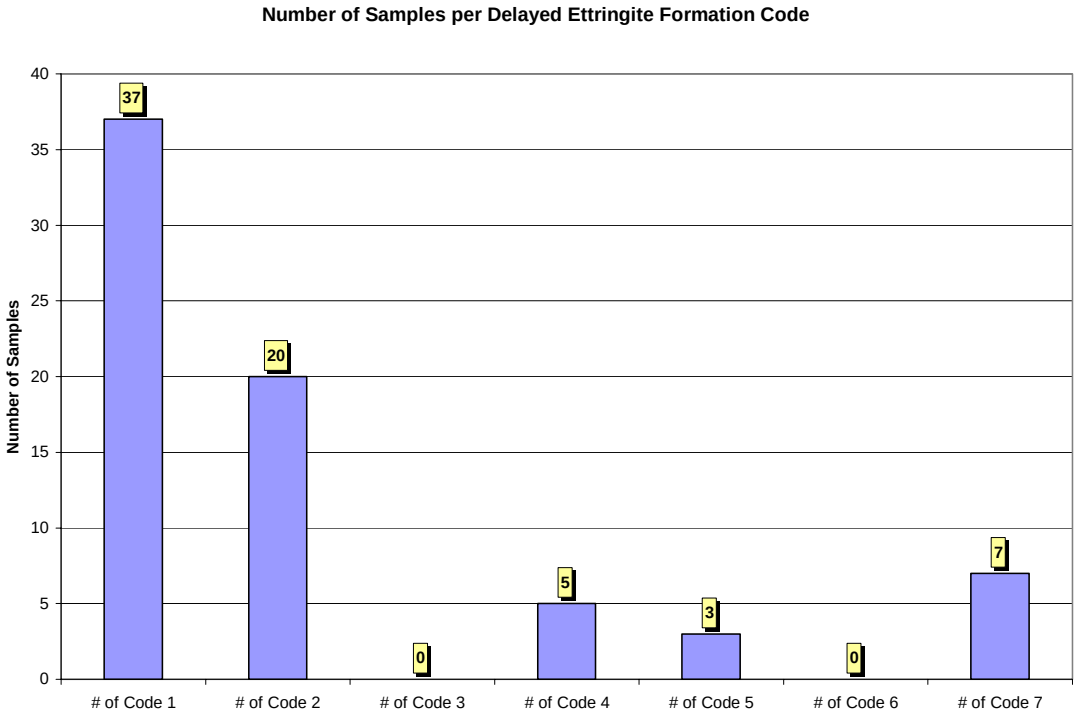

Figure 6.29: Number of Samples per DEF Morphology Code

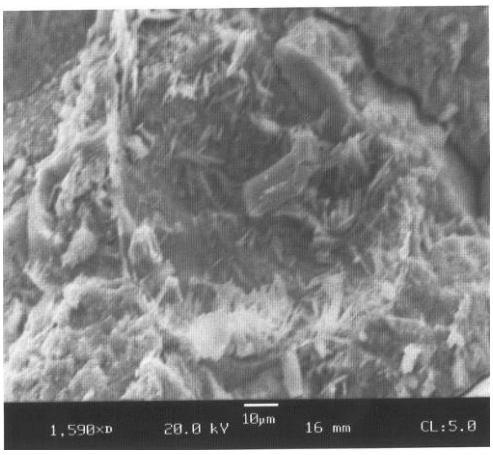

(a) Long Needles in Voids (<<5%)

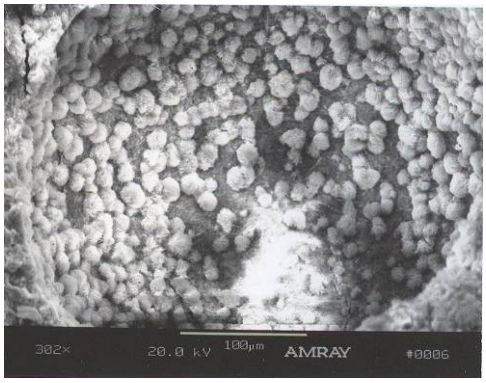

(b) Bundles / Balls in Voids

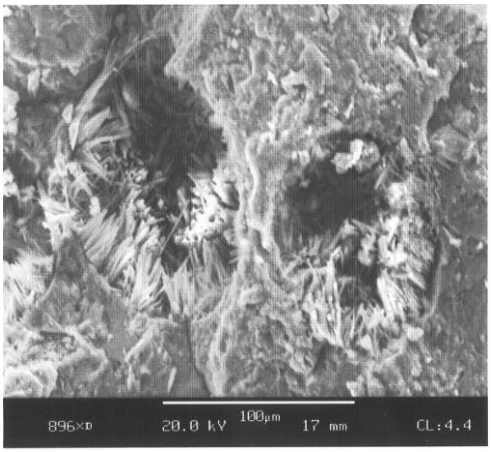

(c) Long Needles in Voids (5%-50%)

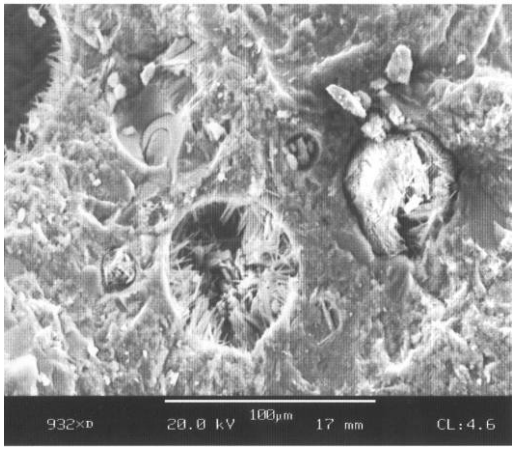

(d) Long Needles in Voids (>50%)

Figure 6.30: Ettringite Formations - 1

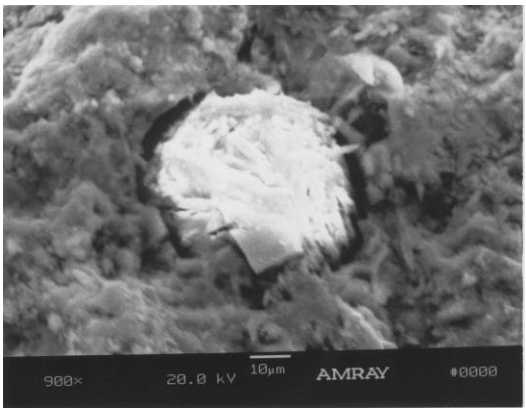

(a) Lamellar Formations in Voids

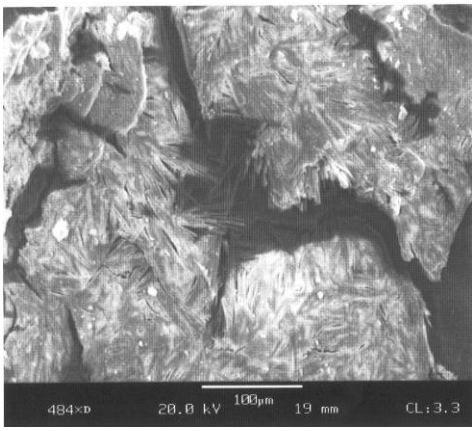

(b) Lamellar Formations on the Sample's Fractured Surface

Figure 6.31: Ettringite Formations – 2

6.3.2.2 Quantifying DEF – Moist Map Cracking

Quantifying DEF involves developing correlations between the prevalence of DEF and moist map cracking of the surface of the concrete. This type cracking results in deterioration of the concrete.

In order to quantify DEF, the samples were viewed using a SEM, and the relative quantity was recorded in a gird system on a sample map, see Figure 6.27 for typical mapping. The relative quantity was divided into five (5) categories including, see Figures 6.32 and 6.33 for representative micrographs:

1. No DEF
2. Minor (noted as DEF-)
3. Moderate (noted as DEF)
4. Heavy (noted as DEF+)
5. Severe (noted as DEF++)

Every sample is placed into one (1) of these five (5) categories, and the bridge rating will be the average of all six (6) samples. The results are show in Table 6.5 and 6.6, but the do not provide a clear correlation.

Looking back at the population selected, the dirty population had a large difference in the degree or extent of the moist map cracking. Some bridges had localized areas and other had damage throughout the concrete element, see Figures 6.34 and 6.35. Additionally, phase 1 research suggested that noticeable differences were observed in the extent of the visual moist map cracking on the surface. In order to establish a correlation between moist map cracking and quantities of ettringite, several correlations were attempted. Ultimately, three categories were required to characterize the extent of the moist map cracking which include;

- No moist map cracking,
- Localized moist map cracking, and
- Widespread moist map cracking.

Localized moist map cracking is defined as small isolated area(s) of moist map cracking that are less than 25% of the total element surface area; see Figure 6.34 which shows the cracking only on the right side of the abutment. Widespread moist map cracking is any element that has more than 25% of the surface area(s) of moist map cracking; see Figure 6.35.

All three definitions are based of visual inspection of the affected concrete element (i.e. beam, abutment, pier, wingwall, parapet etc.) as long as the element was constructed using the same cement mix including aggregate and cement source. This stipulation is typical of most concrete constructed in normal bridges.

Once the bridges are grouped based on these three cases, that characterized the exterior face of the concrete being tested, patterns can be seen in the SEM work preformed. Since the samples from phase 1 were available for quantitative mapping, those samples were added to increase the level of confidence in the final correlation, see Tables 6.7 and 6.8 for the results. Factoring in phase 1 samples and using the visual moist map cracking breakdown, the results show a clear distinction between widespread moist map cracking and the other two; see Table 6.9 and Figure 6.36 for the results.

The widespread moist map cracking exhibited significantly higher levels of ettringite, with an average of 3.8 and a standard deviation of 0.7. The other two cases; bridges without moist map cracking and bridges with localized map cracking had averages of 1.8 with a standard deviation of 0.6 and 1.7 with a standard deviation of 0.5, respectively. These two cases show no overall significant differences. Clearly, the results suggest that large amounts of DEF in concrete can have deleterious effects on cast-in-place concrete, which is evident by the widespread moist map cracking on the surface of the concrete. Whereas, in the case of localized moist map cracking versus no moist map cracking no overall differences were noticed, but locally in the concrete, areas with moist map cracking have more ettringite than areas without the cracking. This suggests uneven distribution of reactants in the cement used mixing the concrete. To show this correlation, the cores must be compared within the bridges with localized map cracking. Since the core locations were selected in these bridges from an area without moist map cracking and an area with moist map cracking, comparisons are possible. The core taken from the areas without moist amp cracking

had a DEF quantity rating average of 1.2 with a standard deviation of 0.4. Whereas the cores from the areas with localized moist map cracking (dirty) had a DEF quantity rating average of 2.3 with a standard deviation of 0.8. Comparison of these two cores shows more ettringite in the core taken from within the localized moist map cracking; see Table 6.10 and Figure 6.37.

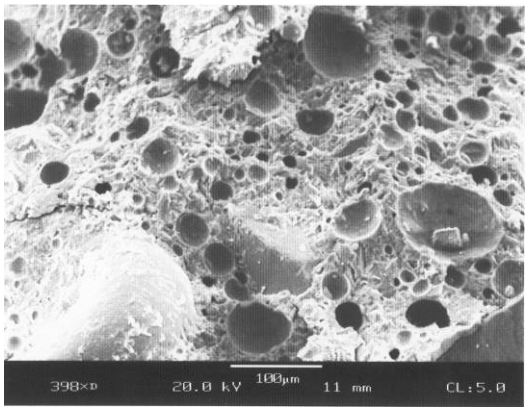

(a) No DEF

Empty Voids

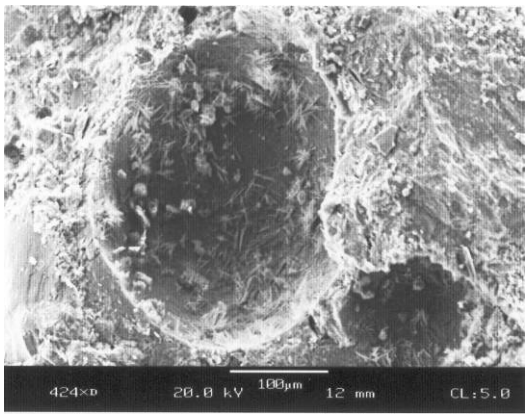

(b) Minor (Noted as DEF-)

Typical Voids

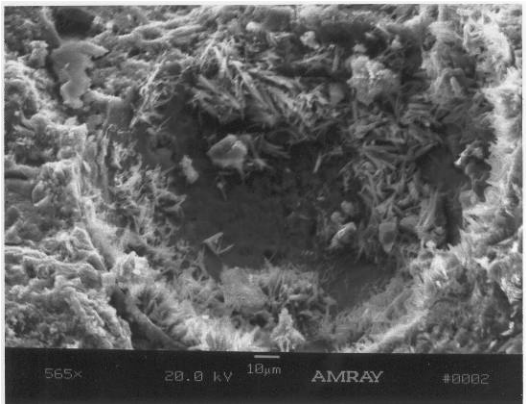

(c) Moderate (Noted as DEF)

Typical Void

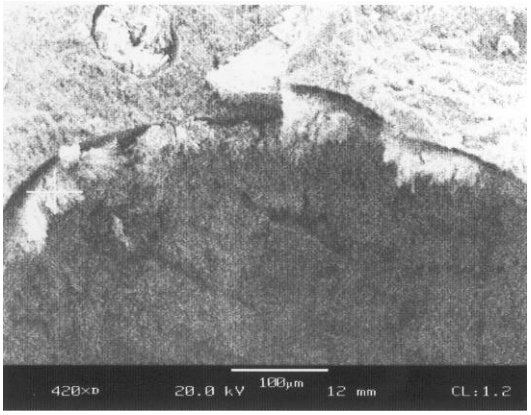

(d) Heavy (Noted as DEF+)

Typically Lining Large Voids or

Partially Filling Small Voids

Figure 6.32: Quantification Classification - 1

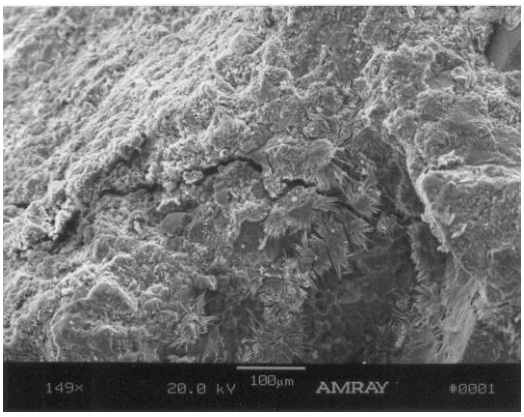

(a) Severe (Noted as DEF++)
Typical Lamellar on Sample's
Fractured Surface

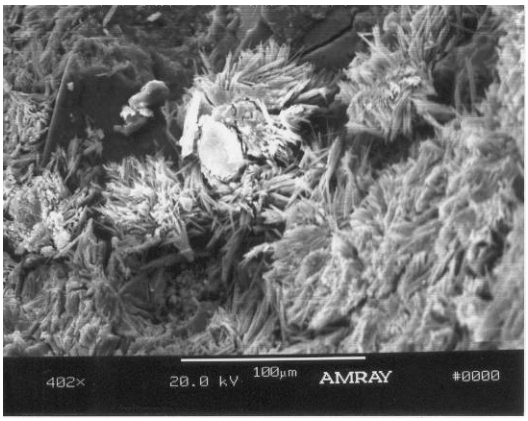

(b) Severe (Noted as DEF++)
Close-up View

Figure 6.33: Quantification Classification - 2

Figure 6.34: Typical Localized Moist Map Cracking
(Cracking is on the Right Side of the Abutment)

Figure 6.35: Typical Widespread Moist Map Cracking

Table 6.5: Summary of DEF Quantity Rating per Sample – Clean Bridges

Clean Bridges

Bridge Number	Core Number	Sample Number	Quantity Code	Bridge Median
0217200	1	2059	2	
		2060	1	
	2	2061	1	
		2062	1	
	4	2007	3	
		2008	3	1.00
0219000	1	2045	1	
		2046	1	
	2	2047	1	
		2048	1	
	4	2005	1	
		2006	1	1.00
1005000	2	2067	1	
		2068	2	
	4	2069	1	
		2070	1	
	5	1995	1	
		1996	1	1.00
1005600	1	1985	2	
		1986	2	
	3	2113	2	
		2114	4	
	5	2111	4	
		2112	2	2.00
1011100	1	2033	3	
		2034	3	
	2	2035	1	
		2036	1	
	3	2037	2	
		2038	2	2.00
1612300	1	2039	1	
		2040	1	
	2	2041	1	
		2042	1	
	3	2043	4	
		2044	4	1.00

Table 6.6: Summary of DEF Quantity Rating per Sample – Dirty Bridges

Dirty Bridges

Bridge Number	Core Number	Sample Number	Quantity Code	Bridge Median
0208304	1	2115	1	
		2116	1	
	4	2117	1	
		2118	1	
	5	1991	4	
		1992	3	1.00
0311100	2	1987	5	
		1988	5	
	3	1989	5	
		1990	5	
	5	2127	5	
		2118	5	5.00
0333900	2	2123	4	
		2124	2	
	3	2063	2	
		2064	2	
	4	2003	2	
		2004	4	2.00
1308603	1	2049	2	
		2050	1	
	3	2051	2	
		2052	1	
	5	2125	3	
		2126	1	2.00
1315004	1	2053	1	
		2054	1	
	2	2055	1	
		2056	2	
	5	2119	1	
		2120	1	1.00
1315700	1	1993	1	
		1994	4	
	2	2065	1	
		2066	1	
	5	2121	1	
		2122	1	1.00

Table 6.7: Summary of Phase 1 DEF Quantity Rating per Sample – 1

Phase 1 Bridges

Bridge Number	Sample Number	Quantity Code	Bridge Median
0314200	1213	1	
	1214	1	
	1245	1	
	1246	1	
	1282	4	1.00
0800201	1201	1	
	1202	1	
	1203	3	
	1263	4	
	1264	1	1.00
1102100	1205	2	
	1206	2	
	1207	2	
	1254	2	
	1255	2	
	1256	5	
	1257	2	
	1258	5	
	1259	5	2.00

Table 6.8: Summary of Phase 1 DEF Quantity Rating per Sample – 2

Phase 1 Bridges

Bridge Number	Sample Number	Quantity Code	Bridge Median
1311000	1211	4	
	1212	3	
	1248	5	
	1249	5	
	1250	5	
	1251	5	
	1281	3	5.00
1511300	1215	5	
	1216	3	
	1222	3	
	1240	3	
	1241	4	
	1242	3	
	1243	5	
	1244	5	4.00
1600400	1223	3	
	1224	3	
	1225	3	
	1275	3	
	1276	4	
	1277	3	
	1278	4	
	1279	3	
	1280	4	3.00
1620003	1208	3	
	1209	3	
	1210	3	
	1269	4	
	1270	4	
	1271	4	
	1272	3	
	1273	4	
	1274	3	3.00
2203201	1200	1	
	1204	2	
	1266	2	
	1267	1	
	1268	1	1.00

Table 6.9: Summary of DEF Quantity Rating by Visual Moist Map Cracking Breakdown

All Bridges

Bridges without Moist Map Cracking

Bridge Number	Bridge Median
0217200	1.00
0219000	1.00
1005000	1.00
1005600	2.00
1011100	2.00
1612300	1.00
Median	**1.000**

Bridges with Local Moist Map Cracking

Bridge Number	Bridge Median
0208304	1.00
0314200	1.00
0333900	2.00
0800201	1.00
1308603	2.00
1315004	1.00
1315700	1.00
2203201	1.00
Median	**1.000**

Bridges with Moist Map Cracking Throughout

Bridge Number	Bridge Median
0311100	5.00
1102100	2.00
1311000	5.00
1511300	4.00
1600400	3.00
1620003	3.00
Median	**4.000**

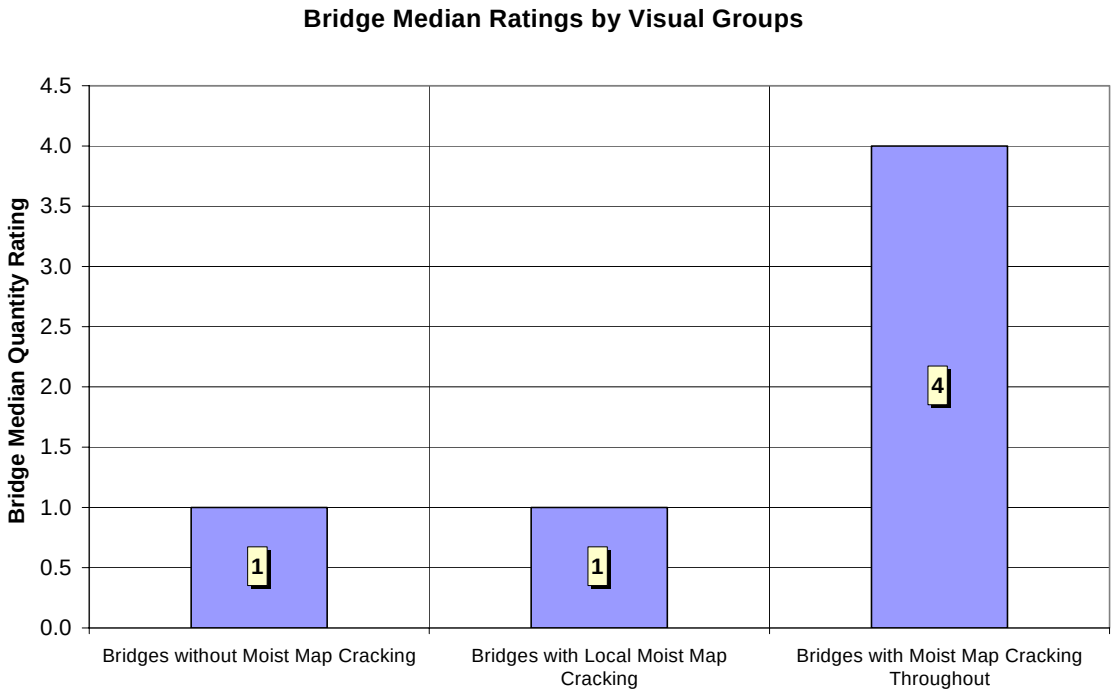

Figure 6.36: Bridge Median Rating by DEF Quantity Ratings

Table 6.10: DEF Quantity Rating Comparing Clean Versus Dirty Cores in Bridges with Localized Moist Map Cracking

Comparison of Bridge with Localized Moist Map Cracking

Bridge Number	Core Desc.	Sample Number	Quantity Code	Core Median
0208304	Clean	2115	1	
		2116	1	1
	Dirty	1991	4	
		1992	3	3
0314200	Clean	1213	1	
		1214	1	1
	Dirty	1246	1	
		1282	4	2
0333900	Clean	2063	2	
		2064	2	2
	Dirty	2003	2	
		2004	4	3
0800201	Clean	1201	1	
		1202	1	1
	Dirty	1263	4	
		1264	1	2
1308603	Clean	2049	2	
		2050	1	1
	Dirty	2125	3	
		2126	1	2
1315004	Clean	2119	1	
		2120	1	1
	Dirty	2053	1	
		2054	1	1
1315700	Clean	2065	1	
		2066	1	1
	Dirty	1993	1	
		1994	4	2
2203201	Clean	1267	1	
		1268	1	1
	Dirty	1200	1	
		1204	2	1

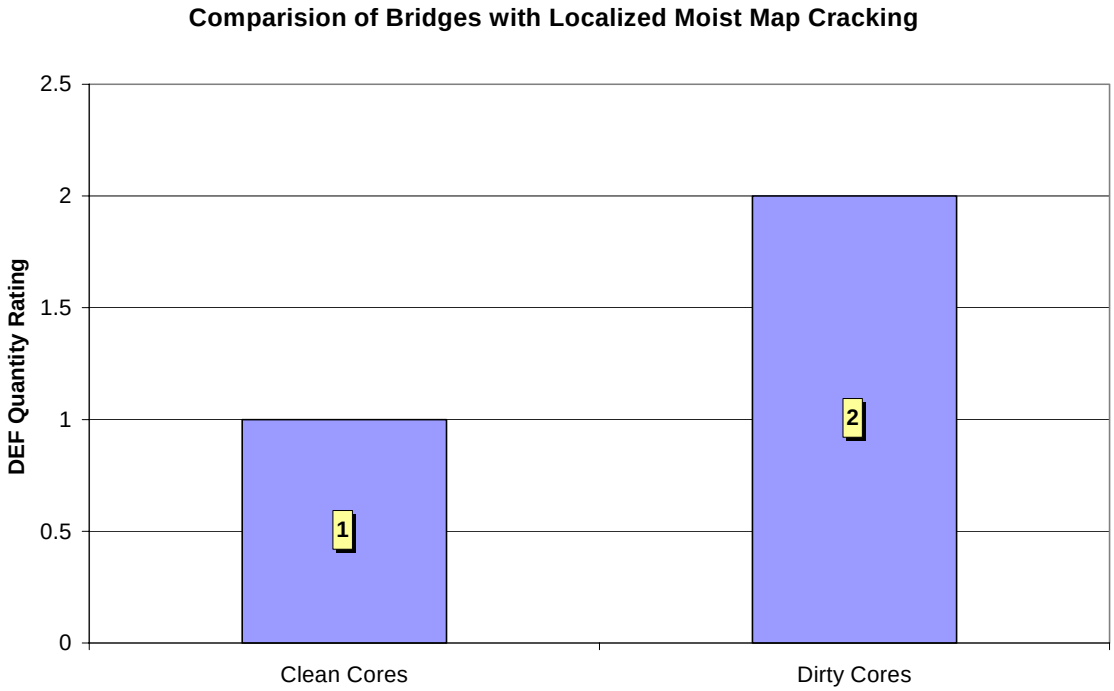

Figure 6.37: DEF Quantity Ratings for Clean Versus Dirty Cores in Bridges with Localized Moist Map Cracking

6.3.2.3 Classifying DEF - Air Entrainment Agent

In addition to attempting to develop correlations between visible moist map cracking, the research tried to confirm if adding air entrainment agent (AEA) to the concrete mix had delirious effects. Similar to developing correlations between moist map cracking and DEF, both qualitative and quantitative methods were evaluated.

Using the case method as described in section 6.3.2.1, bridges were divided into two groups based on age. Maryland State Highway Administration started using AEA in approximately 1980, but depending on the status of the construction contract fully implementation took a couple of years. In order to avoid any confusion, bridges constructed between 1980 and 1982 were excluded from the original population development. Bridges built before 1980 do not have AEA in the concrete mix, and bridges built after 1982 have AEA in the concrete mix. See Table 6.11 and 6.12 for DEF morphologies. No clear pattern was identified from the qualitative analysis, with all morphologies being observed in both populations.

Table 6.11: Summary of DEF Morphologies of Bridges without AEA

Bridges without Air Entrainment Agent(s)

Bridge Number	Core Number	Long Needles			Lamellar Formations
		<<5%	5%-50%	>50%	
0208304	1	-	-	-	-
	4	-	-	-	-
	5	X	X	-	-
0311100	2	-	-	-	X
	3	X	-	X	X
	5	-	-	-	X
1005000	2	X	-	-	-
	4	-	-	-	-
	5	-	-	-	-
1011100	1	X	-	-	-
	2	-	-	-	-
	3	X	-	-	-
1308603	1	-	-	-	-
	3	X	-	-	-
	5	X	X	-	-
1612300	1	-	-	-	-
	2	-	-	-	-
	3	X	X	X	X

Table 6.12: Summary of DEF Morphologies of Bridges with AEA

Bridges with Air Entrainment Agent(s)

Bridge Number	Core Number	Long Needles			Lamellar Formations
		<<5%	5%-50%	>50%	
0217200	1	X	-	-	-
	2	-	-	-	-
	4	X	-	-	-
0219000	1	-	-	-	-
	2	-	-	-	-
	4	-	-	-	-
0333900	2	X	X	-	-
	3	X	-	-	-
	4	X	X	X	-
1005600	1	X	-	-	-
	3	X	X	X	-
	5	X	X	X	-
1315004	1	-	-	-	-
	2	X	-	-	-
	5	-	-	-	-
1315700	1	X	-	-	X
	2	-	-	-	-
	5	-	-	-	-

6.3.2.4 Quantifying DEF - Air Entrainment Agent

Since the qualitative analysis showed no difference between bridges with and without AEA, the research focused on developing a quantitative correlation between bridge with AEA and DEF. The results are given in Tables 6.13 to 6.16. Bridges without AEA had an average DEF quantity rating of 2.7 with a standard deviation of 1.3, and bridges with AEA had an average DEF quantity rating of 2.2 with a standard deviation of 1.3. See Figure 6.38. The results show no detrimental effect of AEA in the concrete mixture, in fact the results show a slight reduction of DEF quantity in the bridges constructed since 1982. There is no reason to believe that the addition of AEA has lead to the slight reduction in DEF quantities in the newer bridges. Better reasons could be concrete mix design, aggregate selection, addition of fly ash, limits on reactants in the cement.

Table 6.13: Summary of DEF Morphologies of Bridges without AEA – 1

Bridge Number	Sample Number	Quantity Code	Bridge Median
0208304	2115	1	
	2116	1	
	2117	1	
	2118	1	
	1991	4	
	1992	3	1.00
0311100	1987	5	
	1988	5	
	1989	5	
	1990	5	
	2127	5	
	2118	5	5.00
1005000	2067	1	
	2068	2	
	2069	1	
	2070	1	
	1995	1	
	1996	1	1.00
1011100	2033	3	
	2034	3	
	2035	1	
	2036	1	
	2037	2	
	2038	2	2.00
1308603	2049	2	
	2050	1	
	2051	2	
	2052	1	
	2125	3	
	2126	1	2.00
1612300	2039	1	
	2040	1	
	2041	1	
	2042	1	
	2043	4	
	2044	4	1.00

Table 6.14: Summary of DEF Morphologies of Bridges without AEA – 2

Bridge Number	Sample Number	Quantity Code	Bridge Median
1311000	1211	4	
	1212	3	
	1248	5	
	1249	5	
	1250	5	
	1251	5	
	1281	3	5.00
1511300	1215	5	
	1216	3	
	1222	3	
	1240	3	
	1241	4	
	1242	3	
	1243	5	
	1244	5	3.00
1620003	1208	3	
	1209	3	
	1210	3	
	1269	4	
	1270	4	
	1271	4	
	1272	3	
	1273	4	
	1274	3	3.00
2203201	1200	1	
	1204	2	
	1266	2	
	1267	1	
	1268	1	1.00
0800201	1201	1	
	1202	1	
	1203	3	
	1263	4	
	1264	1	1.00

Table 6.15: Summary of DEF Morphologies of Bridges with AEA – 1

Bridge Number	Sample Number	Quantity Code	Bridge Median
0217200	2059	2	
	2060	1	
	2061	1	
	2062	1	
	2007	3	
	2008	3	2.00
0219000	2045	1	
	2046	1	
	2047	1	
	2048	1	
	2005	1	
	2006	1	1.00
0333900	2123	4	
	2124	2	
	2063	2	
	2064	2	
	2003	2	
	2004	4	2.00
1005600	1985	2	
	1986	2	
	2113	2	
	2114	4	
	2111	4	
	2112	2	2.00
1315004	2053	1	
	2054	1	
	2055	1	
	2056	2	
	2119	1	
	2120	1	1.00

Table 6.16: Summary of DEF Morphologies of Bridges with AEA – 2

Bridge Number	Sample Number	Quantity Code	Bridge Median
1315700	1993	1	
	1994	1	
	2065	1	
	2066	1	
	2121	4	
	2122	4	1.00
0314200	1213	1	
	1214	1	
	1245	1	
	1246	1	
	1282	4	1.00
1102100	1205	2	
	1206	2	
	1207	2	
	1254	2	
	1255	2	
	1256	5	
	1257	2	
	1258	5	
	1259	5	2.00

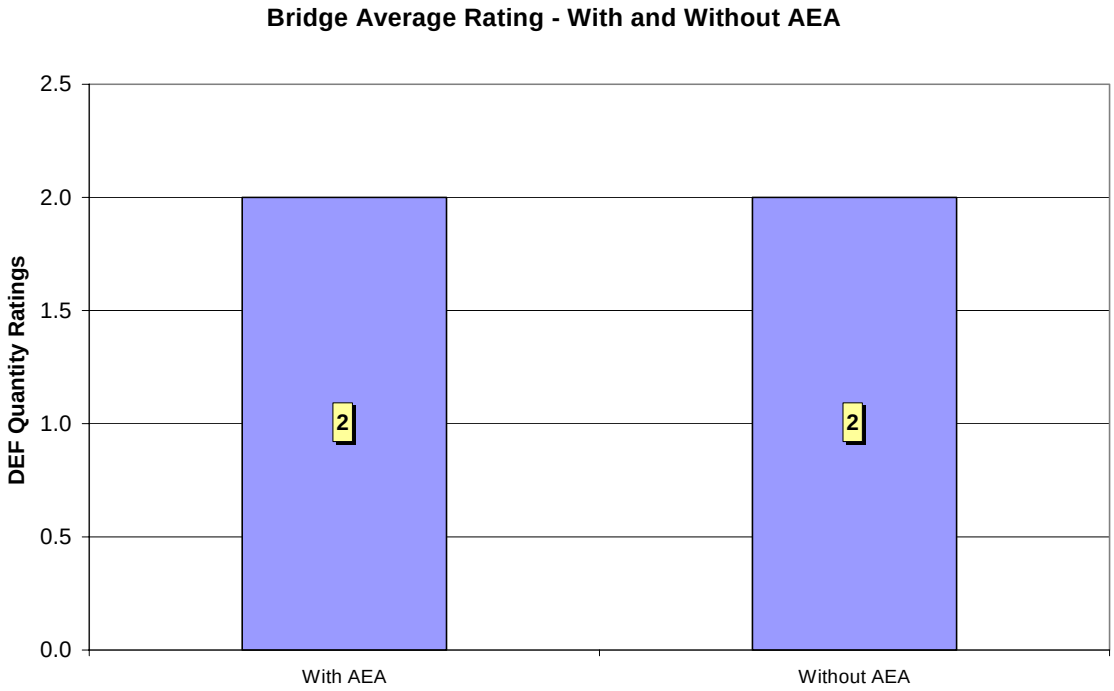

Figure 6.38: Bridge Averages by DEF Quantity Ratings – AEA

Chapter 7
Mitigation Testing Techniques for Existing Concrete

7.1 Purpose for Testing

Since the phase 1 field testing showed DEF present in Maryland bridge concrete, part of the phase 2 research included testing the effectiveness of various mitigation treatments in the laboratory. The testing focuses on practical treatments for concrete showing signs of DEF related damages. The products must ultimately be applied in the field without extensive loss of use of the facility. The research involved reviewing current literature to identify possible treatments, developing / modifying laboratory test to simulate affected concrete, performing the test, and discussing the results. Mr. Shaikh took the general testing program outlined in this chapter and preformed the laboratory work as part of the research requirements for his master's thesis. After reviewing Mr. Shaikh's results, several modifications were made to the initial testing program to better model existing field conditions. Mr. Hung, a master student, preformed the modified test laboratory testing and proved the data for analysis. The results and conclusion are presented herein.

7.2 Mitigation of DEF in the Literature

Not much research had been performed when this testing program was being developed, but two states in particular, Texas and Iowa, were currently trying to identify products to mitigate DEF in existing concrete. Due to differences in treatment locations and type of concrete, the approach was very different, but the research show different avenues for possible treatment techniques and products.

7.2.1 Iowa Department of Transportation – Mitigation Treatments

Iowa State University has conducted research into mitigating DEF in existing concrete pavement, and the research tested numerous products which cans be used for treating concrete with DEF (Cody et al. 2001). Cody et al. conducted laboratory test on new and existing concrete blocks in solution of crystal inhibitors, and the results suggest that Dequest 2060S and Good-rite K752 inhibit the formation of DEF (2001). In determining the best candidates for future real world trails, Cody et al. looked at numerous products which varied greatly from sugar to phosphates.

The test investigated if a product can be applied to existing concrete which will retard the growth of Delayed Ettringite Formation (DEF) in the affected concrete. In 1997, Cody et al. presented findings showing the growth of ettringite in various solutions, and concluded that four products showed promise for future testing.

The products include, see Figure 7.1 for chemical structure:

A. Dequest 2010 (1-Hydroxyethylidene1, 1-Diphosphonic Acid)

B. Dequest 2060S (Diethylenetriaminopenta or Methylenephosphonic acid)

C. Noveon Good-Rite K752 (Polyacrylate)

D. Wayhib S (Phosphate Ester Nitrilo Tri(ethyl acid Phosphate)

The test involved immersing cubes of existing concrete and newly cast specimen into solution of sodium sulfate (Na_2SO_4) with varying concentrations of one (1) of the four (4) mitigation products. The specimens were subjected to either wetting and drying cycle, freezing and thawing cycles, or continuous immersion. The results show retardation of growth of ettringite in the concrete and reduced cracking as event on the surface of the concrete specimen.

From this study, two products were considered for evaluation in the UMD mitigation testing. Dequest 2060S, a phosphonic acid, and Noveon Good-Rite K752, a polyelectrolyte (polyarcylic acid), appeared to show promise and warrant further testing.

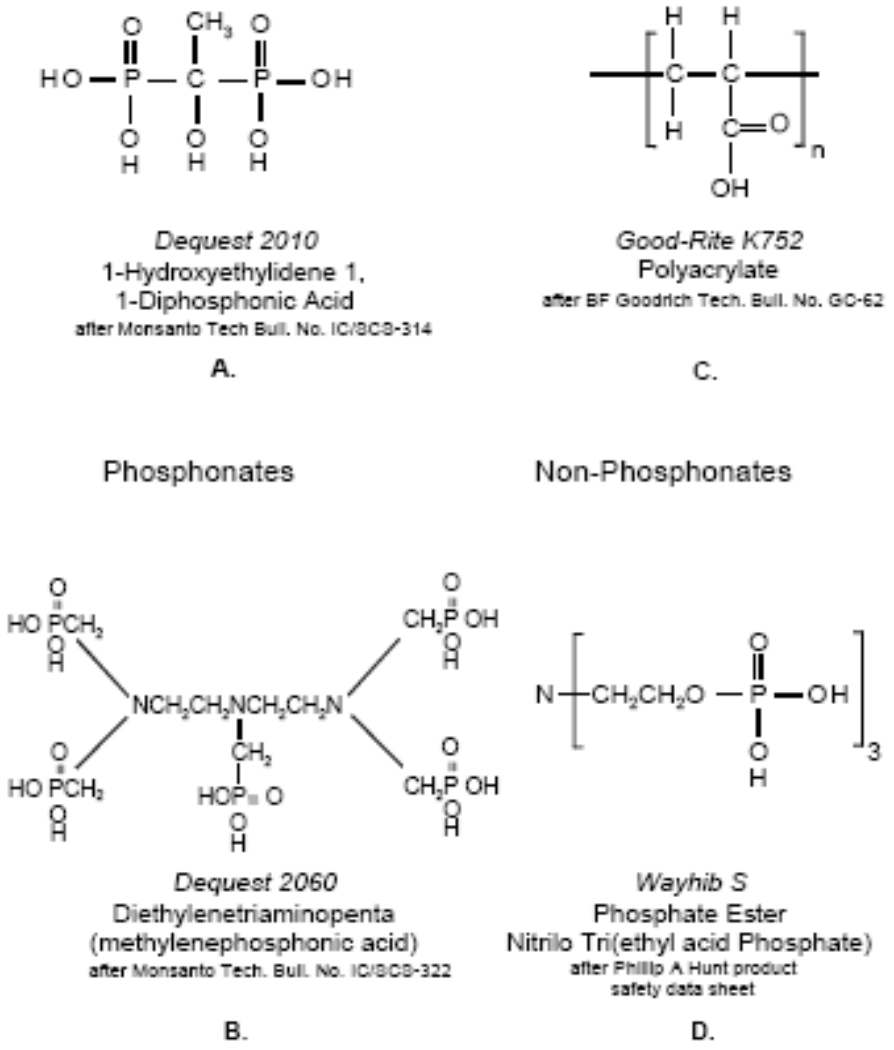

Figure 7.1: Chemical Structure of Products Used in IOWA Study

(Cody et al. 2001)

7.2.2 Texas Department of Transportation – Mitigation Treatments

In 1995, Texas DOT found damage to pre-stressed beams, abutments, columns, and bents requiring remedial repair or removal from service only after a few years (Lawrence 1999). The damage was revealed in the form of map cracking produced by alkali-silica reaction (ASR), delayed ettringite formation (DEF) or both.

The 1995 investigation was prompted when fifty-six of sixty-nine box girders fabricated in San Marcos, Texas were damaged by ASR, DEF, or both. Sixteen other structures were found to have similar damage. Petrographic analysis on the damaged structures confirmed DEF in the cement paste and cracks of the pre-cast box girders. The field investigation found four high mast illumination pole foundations along U.S. 59 with DEF related cracking. Additionally, thirty percent of the pre-stressed Type IV beams on IH 45 were found to be deteriorated after only six years of service. DEF related cracking was also found on two adjacent cast-in-place bent caps and columns on IH 37 (Klinger and Fowler 2001a, 2001b, 2002a, 2002b, 2004a, 2004b, and 2004c).

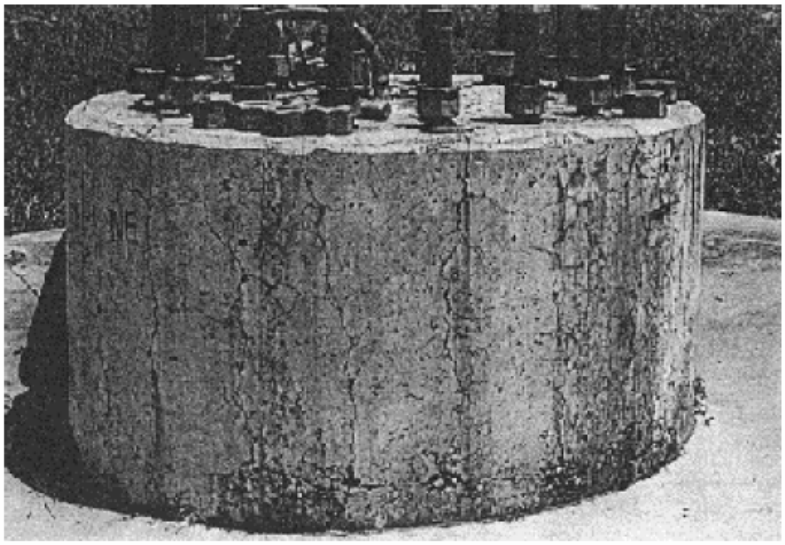

Figure 7.2 - High Mast Pole Foundations with DEF Related Map Cracking (Lawrence 1999)

7.3 Mitigation Test Development

The purpose of the testing is to apply mitigation treatments to existing concrete with DEF. In order to simulate existing concrete with DEF in the laboratory, this test utilized a similar testing program as previous DEF testing at the University of

Maryland. The test program involves casting Type III concrete with limestone coarse aggregate and reactive sand and stream curing. The testing is accelerated and ettringite is developed during the UMD-FHWA modified Duggan Cycle heating regiment. Previous testing at UMD has shown storage in water also accelerates ettringite growth and will also be used in this testing. Once ettringite is developed in the specimen, mitigation treatments are applied to simulate treatment of aged concrete afflicted with DEF.

The goal of the testing involves slowing or stunning the growth of ettringite in the concrete specimen. Because the testing program allows ettringite to develop prior to application of the treatment, the presence of DEF in the concrete will not show the treatment ineffective. A future test can be preformed to test the effectiveness of the treatment by applying the treatment before the Duggan cycle.

7.3.1 Concrete Mix Requirements

Previous research conducted by the University of Maryland showed high sulfate cement, sands with high alkali-silica reaction susceptibility, and high potassium were prone to developing DEF (Ramadan 1999, Amal 2003, Williams 2003, and Ceesay 2006). The goal of the testing is to emulate cast-in-place concrete that exhibits DEF-related damage so that mitigation treatments can be applied and evaluated. The concrete mix was selected in order to produce specimen affected with DEF and the treatment was applied after the beginning of the active expansion phases.

Table 7.1: Concrete Mix

Material	Type	Reason
Cement	Type III	High Sulfate Content
Coarse Aggregate	Limestone	Non-reactive
Fine Aggregate	Natural Sand	MD ASR rating >0.20
Potassium	Potassium Carbonate	Increase Potassium Content

7.3.2 Curing / UMD-FHWA Modified Duggan Cycle / Storage Condition

Following previous research, the concrete will be stream cured at 85 ºC for 4 hours and allowed to cooling before water curing for the next eight days. In order to accelerate the development of DEF, the UMD-FHWA modified Duggan cycle was utilized. After the UMD-FHWA modified Duggan cycle, the specimens were stored in water baths for the duration of the experiment.

Both the UMD-FHWA modified Duggan cycle and the storage condition were selected to accelerate the development of ettringite in the concrete. Ettringite requires an ample supply of water to form and hydrate, and as a result research shows moist or submerged storage condition encourages ettringite to form rapidly (Ramadan 1999, Amal 2003, Williams 2003, and Ceesay 2006). The specimen will be submerged in a lime water bath. The lime water is used to prevent leeching of the calcium from the concrete during storage.

7.3.3 Suggested Testing and Analysis

For the duration of the testing program, measurements will be taken to track expansion, weight, and strength. The expansion, weight, and strength measurements will be used to evaluate the effectiveness of the mitigation product. Scanning Electron

Microscope (SEM) analysis should be preformed at the same time as the strength compression test. SEM analysis will show DEF presence and document the changes with treatment and time.

7.3.4 Specimen

For the expansion and weight test, five (5) concrete prisms will be cast. The prisms measure 3" x 3" x 11.25". Three (3) additional prisms will be cast for SEM analysis. Four sets of three (3) for a total of twelve (12) - 4" diameter cylinders will be cast for strength compression testing at approximately 30, 60, 120, and 360 days.

7.4 Results

7.4.1 Testing Overview

Preliminary testing was preformed testing four products including:

- ChimneySaver
- Radcon Formula #7
- Dequest 2060S
- Noveon Good-Rite K-752

Research conducted for Texas Department of Transportation focused on waterproofing the affected concrete as a method of treatment (Merrill 2004). After preforming a review of literature, the research team with Maryland State Highway Administration assistance selected ChimneySaver and Radcon Formula #7. In contrast, Iowa Department of Transportation focused on stunning the development of ettringite before the molecules can crystalizes (Cody et. al. 2001). Again, after a

review of literature, the research team with Maryland State Highway Administration assistance selected Dequest 2060S and Good-Rite K-752.

Since the two treatment theories were independent, cross combinations were tested in addition to the individual treatments, for example a waterproofing product was applied after a crystal inhibitors product was applied.

7.4.1.1 ChimneySaver

ChimneySaver® is a siloxane based water repellent which reacts with the concrete and ultraviolet light to form a hydrophobic zone 1/16" to ¼" below the surface. This hydrophobic zone prevents water molecules from penetrating the concrete resulting in the slower growth of ettringite. See Figure 7.3 for the technical data. ChimneySaver is used for waterproofing concrete or masonry chimneys.

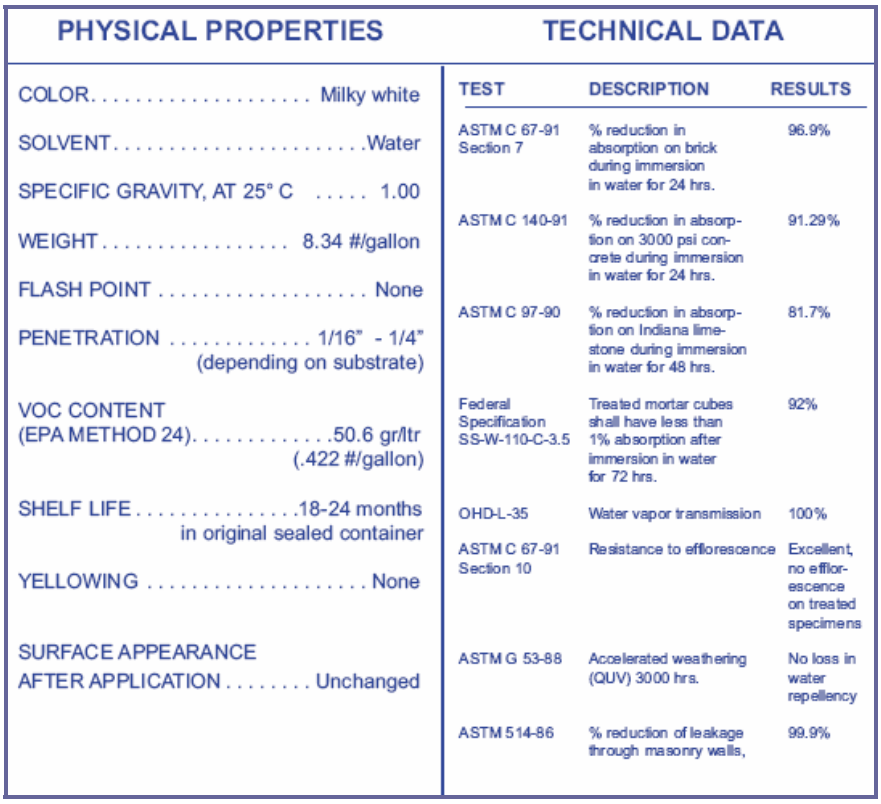

PHYSICAL PROPERTIES

COLOR . . . . . Milky white

SOLVENT . . . . . .Water

SPECIFIC GRAVITY, AT 25° C 1.00

WEIGHT . . . . . 8.34 #/gallon

FLASH POINT . . . . . None

PENETRATION . . . . . 1/16" - 1/4" (depending on substrate)

VOC CONTENT (EPA METHOD 24). . . . . .50.6 gr/ltr (.422 #/gallon)

SHELF LIFE . . . . . .18-24 months in original sealed container

YELLOWING . . . . . None

SURFACE APPEARANCE AFTER APPLICATION . . . . . Unchanged

TECHNICAL DATA

TEST	DESCRIPTION	RESULTS
ASTM C 67-91 Section 7	% reduction in absorption on brick during immersion in water for 24 hrs.	96.9%
ASTM C 140-91	% reduction in absorption on 3000 psi concrete during immersion in water for 24 hrs.	91.29%
ASTM C 97-90	% reduction in absorption on Indiana limestone during immersion in water for 48 hrs.	81.7%
Federal Specification SS-W-110-C-3.5	Treated mortar cubes shall have less than 1% absorption after immersion in water for 72 hrs.	92%
OHD-L-35	Water vapor transmission	100%
ASTM C 67-91 Section 10	Resistance to efflorescence	Excellent, no efflorescence on treated specimens
ASTM G 53-88	Accelerated weathering (QUV) 3000 hrs.	No loss in water repellency
ASTM 514-86	% reduction of leakage through masonry walls,	99.9%

Figure 7.1 - ChimneySaver Physical Properties and Technical Data (SaverSystems 2005)

7.4.1.2 Radcon Formula #7

Radcon® Formula #7 is a sodium silicate solution that reacts with calcium and water in the concrete to form a gel like substance in pores and cracks, see Table 7.2. This gel creates a sub-surface hydrophobic zone which prevents water molecules and chloride ions from entering the concrete. Radcon® Formula #7 is used in waterproofing of rooftops, decks, parking garages, runways, and other concrete structure.

Table 7.2 - Radcon Formula #7 Physical Properties and Performance Characteristics (Radcrete Pacific Pty. Ltd. 2005)

Radcon Formula #7 – Physical Properties	
Color	Clear to slightly opaque
Specific Gravity at 25^{o} C	1.225
Flash Point	None
Viscosity	14.3 cps or 0.1172 Stokes
pH	11.7
Radcon Formula #7 – Performance Characteristics	
Reduction of chloride diffusion coefficient by 89%	
Water permeability reduced by 70%	
Reduces scaling in freeze-thaw environments by 89%	
Allows 84.1% moisture permeability	

7.4.1.3 Dequest 2060S

Dequest 2060S is a phosphonic acid based solution with exceptional scale inhibition ($CaCO_3$) capability. Dequest 2060S is a highly viscous solution with a honey like quality and a pH < 2, see Table 7.3. Dequest 2060S is used in cooling water treatment, peroxide bleach stabilization and scale control in oil fields (Solutia Inc. 2005).

Table 7.3 - Dequest 2060S Physical Properties and Performance Characteristics (Solutia Inc. 2005)

Dequest 2060S – Physical Properties	
Color	Amber
Specific Gravity at 20^{o} C	1.42
Odor	Pungent
Viscosity	~1000 cP
pH	<2.0
Dequest 2060S – Composition	
Methylene Phosphonic Acid	48% - 52%
Hydrogen Chloride	15% - 17%
Phosphonic Acid	3%
Formaldehyde: <100 PPM	< 100 PPM

7.4.1.4 Noveon Good-Rite® K-752

Noveon Good-Rite® K-752 is a water soluble acrylic acid polymer, see Table 7.4. It is composed 47% by polyacrylic acid and has a pH between 2.2 and 3.0. Good-Rite® K-752 has a clear color and viscosity of 950 centa-poise at 25^{o}C. Noveon Good-Rite® K-752 is used in scale control agents in water treatment applications and soil removal and antiredeposition aids in detergents and cleaners (Noveon Inc. 2005).

Table 7.4 - Good-Rite K-752 Physical Properties and Performance Characteristics (Noveon Inc. 2005)

Good-Rite® K-752 – Physical Properties	
Color	Clear/Amber
Specific Gravity at 25^{o} C	1.2
Odor	Slightly Acidic
Viscosity 25^{o} C	950 cP
pH	2.2 – 3.3
Good-Rite® K-752 – Composition	
Polyacrylic Acid	47%
Water	37%
Sodium Polyacrylate	16%

7.4.2 Preliminary Testing

Preliminary testing was conducted on various mitigation products or combination of products. The goal of the testing was to identify products for further testing and to evaluate the benefit of treating affected concrete in existing bridges.

The testing consisted of four products: ChimneySaver, Radcon Formula #7, Dequest 2060S, and Noveon Good-Rite K752. ChimneySaver and Radcon Formula #7 are water repellents, and Dequest 2060S and Noveon Good-Rite K752 are crystal growth inhibitors. Because the two types of products are fundamentally different, cross combinations of a crystal growth inhibitor and water repellents were also tested.

The final expansion results for specimens in the preliminary testing were above 1% gain in total length. The follow-up testing will test the products identified as promising in the preliminary tests but the test will be conducted in such a way that the total expansion will be less than what was observed in the preliminary test.

7.4.2.1 Expansion Results

The expansion results are obtained from measurements of five 3" x 3" x 11.25" concrete prisms per set taken periodically. Each point on the graphs represents the average of the five expansion measurements. See Figure 7.4 for expansion graph and Table 7.5 for final expansion values. The error bars in Figures 7.5 to 7.7 represent the standard deviation of the five measurements.

The results show that five (5) sets had expansion results lower than the control and three (3) sets had expansion results higher than the control after 300 days of measurements. The cross combinations were insignificant or detrimental to the expansion when compared to the single treatments. For instance, both Set #2 (ChimneySaver) and Set # 8 (Noveon Good-Rite K752 / ChimneySaver) had a total expansion of 1.68%, and Set #4 (Dequest 2060S) had less expansion than Sets #5 and #6 which are the cross combinations with the waterproofing treatments.

From these results, single treatment of ChimneySaver, Dequest 2060S, and Noveon Good-Rite K752 should be considered for further testing with 1.68%, 1.82%, 1.86% total expansion. The results show a decrease from the Control set that had 2.18% total expansion. See Figure 7.8 for the comparison of the treatment set versus the Control set.

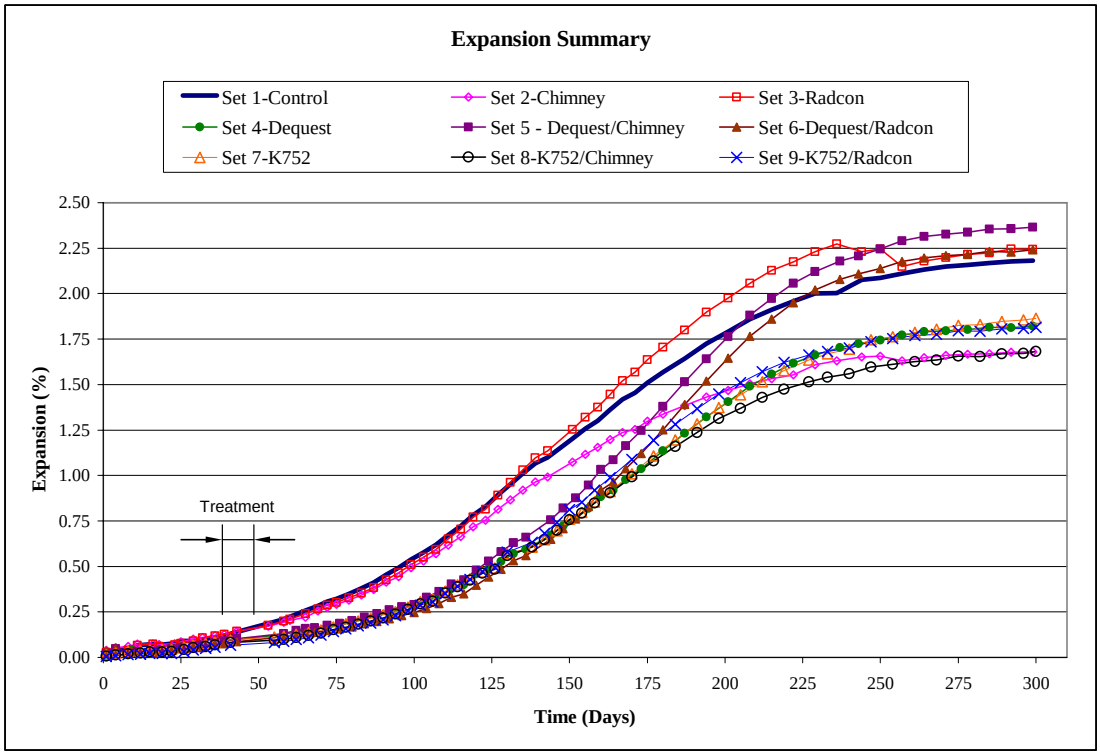

Figure 7.4 - Summary of Expansion vs. Time (Nine Sets)

Table 7.5 - Summary of Expansion Values and Rankings

Set	Maximum Expansion (%)
1	2.18
2	1.68
3	2.27
4	1.82
5	2.36
6	2.24
7	1.86
8	1.68
9	1.81

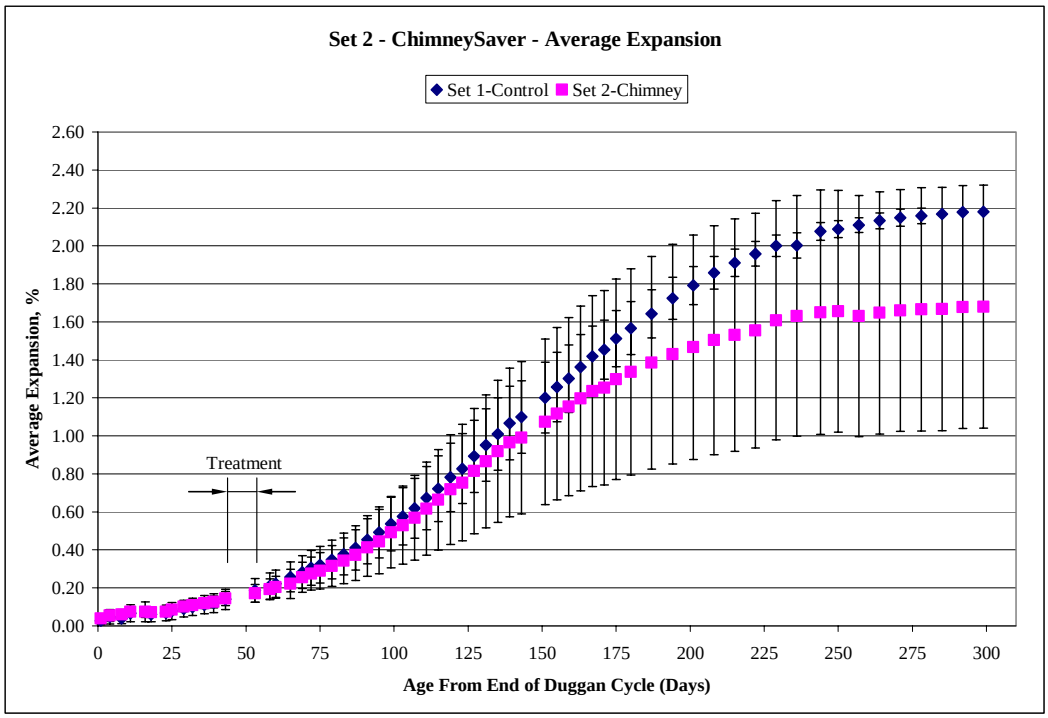

Figure 7.5 - SET 2 Expansions versus Time with Error Bars

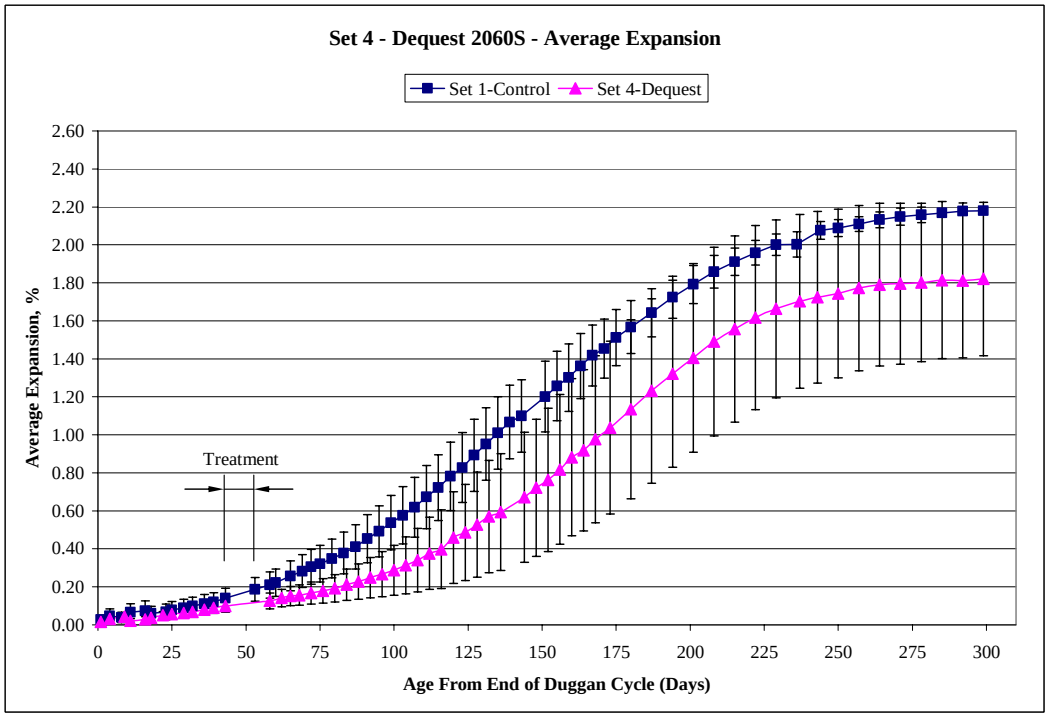

Figure 7.6 - SET 4 Expansions versus Time with Error Bars

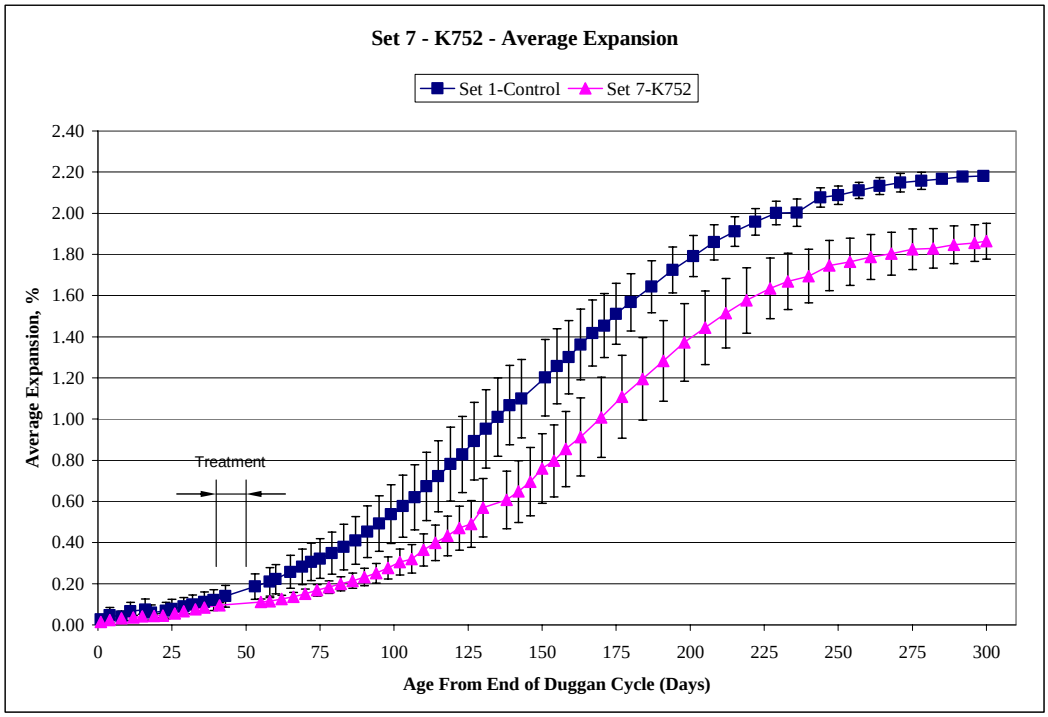

Figure 7.7 - SET 7 Expansions versus Time with Error Bars

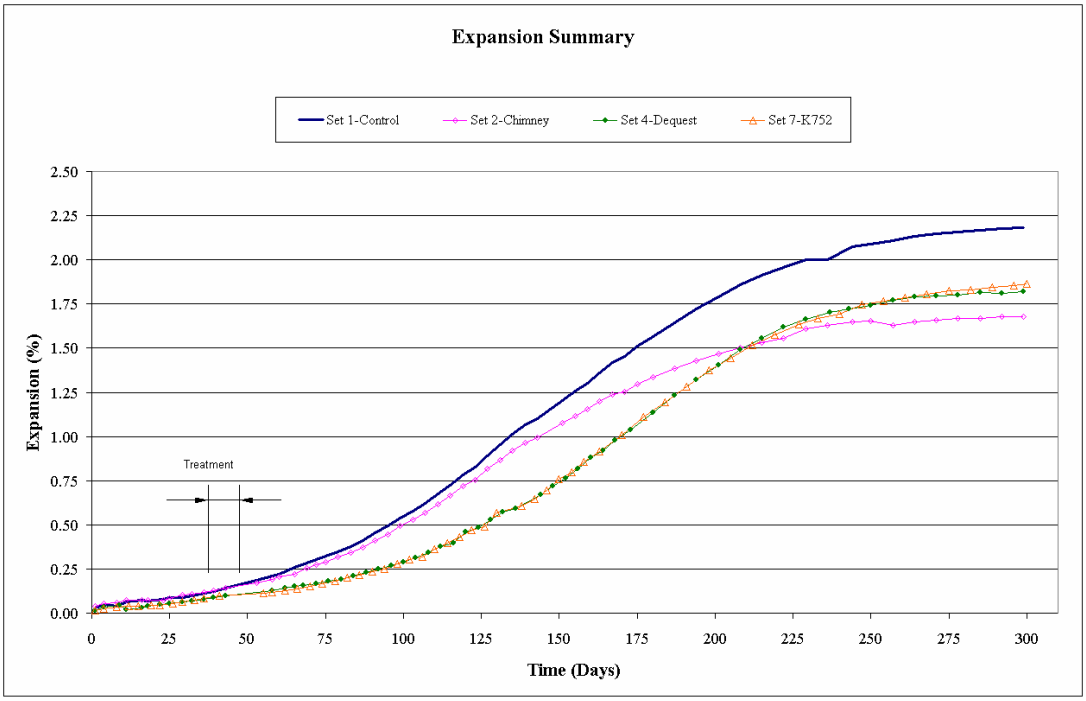

Figure 7.8 - Summary of Expansion vs. Time (Sets #1, #2, #4, and #7)

7.4.2.2 Suggested Modifications for Further Testing

Using the crystal inhibitors was difficult due to the visocity of both products. In order to improve the workability of Dequest 2060S and Noveon Good-Rite K752, the treatments will be diluted to 1% by volume. The dilution will allow the products to be applied, similar to ChimneySaver, with a low pressure hand sprayer. This will also minimize any discoloration of the concrete due to treatment.

The follow-up test will store the specimen in a moist room instead of underwater to better model field conditions. The moist room is still needed to accelerate the test.

7.4.3 Follow-up Testing

Based on the DEF mitigation products and techniques applied earlier, a follow-up research was conducted. The steam curing was revised for better simulation of field conditions while still accelerating the testing time frame. Four (4) sets of concrete samples were prepared during this testing phase. A control set and three (3) of the best mitigation products identified in the preliminary testing, namely the ChimmeySaver, Noveon Good-Rite K752 and Dequest 2060S, were used. In setting up the testing, alternate methods of application for the crystal growth inhibitor was researched. Spry et al. (2001) had tested several levels of dilution to mitigate DEF in roadway concrete. The research team chose one application of one percent (1%) by volume for this testing. These products were diluted with distilled water, and the resulting solution resulted in easy application on the concrete. The ChimneySaver was not modified, and was used per manufacture's recommendation. Similar to the

preliminary testing, the mitigation products were applied on the concrete specimens after 45 days of storage. After the application of the mitigation products, the specimens were kept in the moisture room for the rest of the test duration.

7.4.3.1 Steam Curing

A less severe steam curing program such as in Figure 7.9 was used to minimize or reduce damage attributed to excessive thermal heating of the fresh concrete. In addition, exposed parts of the specimens were covered with aluminum foil throughout the heat treatment program to prevent over drying and shrinkage. The concrete specimens were subjected to the Duggan heat cycle after the steam curing and subsequently stored in limewater for six (6) days.

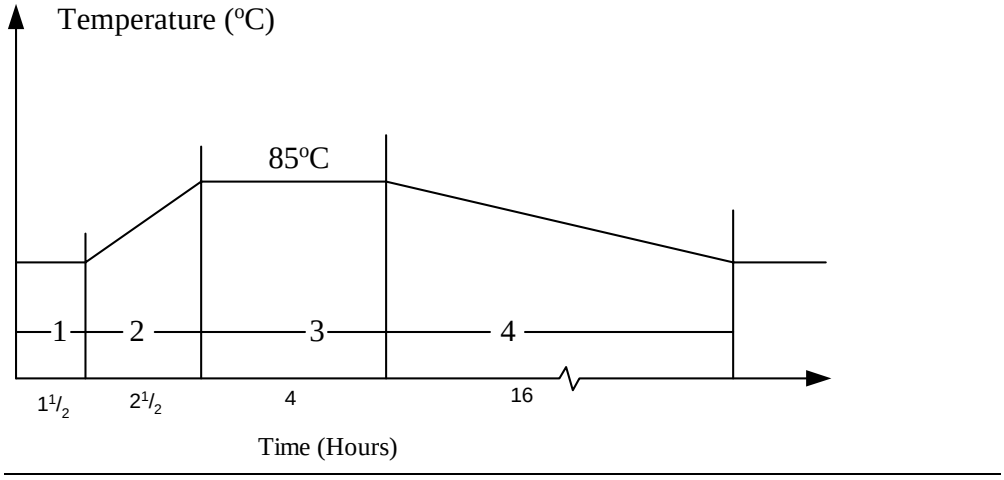

1 – The Presetting time

2 – Heating

3 – Heat (Steam) Curing at 85°C

4 – Cooling, overnight

Figure 7.9 – Heat Treatment Program (Adapted from Azzam, 2002)

7.4.3.2 Expansion Results

The average expansion of three (3) concrete prisms per set taken periodically was used. The expansion value of the concrete prisms in each set exceeds 0.05% after 45 days of storage in the moisture room. DEF mitigation products that retard the growth of ettringite in the microstructure of the concrete specimen were applied. The expansion values of the concrete prisms decreases immediately after the application of the different mitigation products. After 100 days of storage, the expansion values were 0.659%, 0.393%, 0.368% and 0.462% for the control (MS1), Chimmey Saver (MS2), Noveon Good-Rite K752 (MS3) and Dequest 2060S (MS4) respectively. The control concrete specimens exhibited the highest expansion values throughout the test

period. After 200 days of storage, the expansion values were 1.44%, 1.10%, 1.18% and 1.12% for the control (MS1), Chimmey Saver (MS2), Noveon Good-Rite K752 (MS3) and Dequest 2060S (MS4) respectively. All the DEF mitigation products used in this follow-up study showed reduced expansion values for the treated concrete prisms similar to the preliminary testing. Figure 7.10 shows the average expansion against time for the steam cured concrete prisms treated with different DEF mitigation products.

After 200 days of storage, the total expansion was higher than 1.00% therefore the testing regiment will need future modifications to produce better strength results. The three (3) products still show promise in reducing the total expansion by about 75% similar to the results obtained in the preliminary testing.

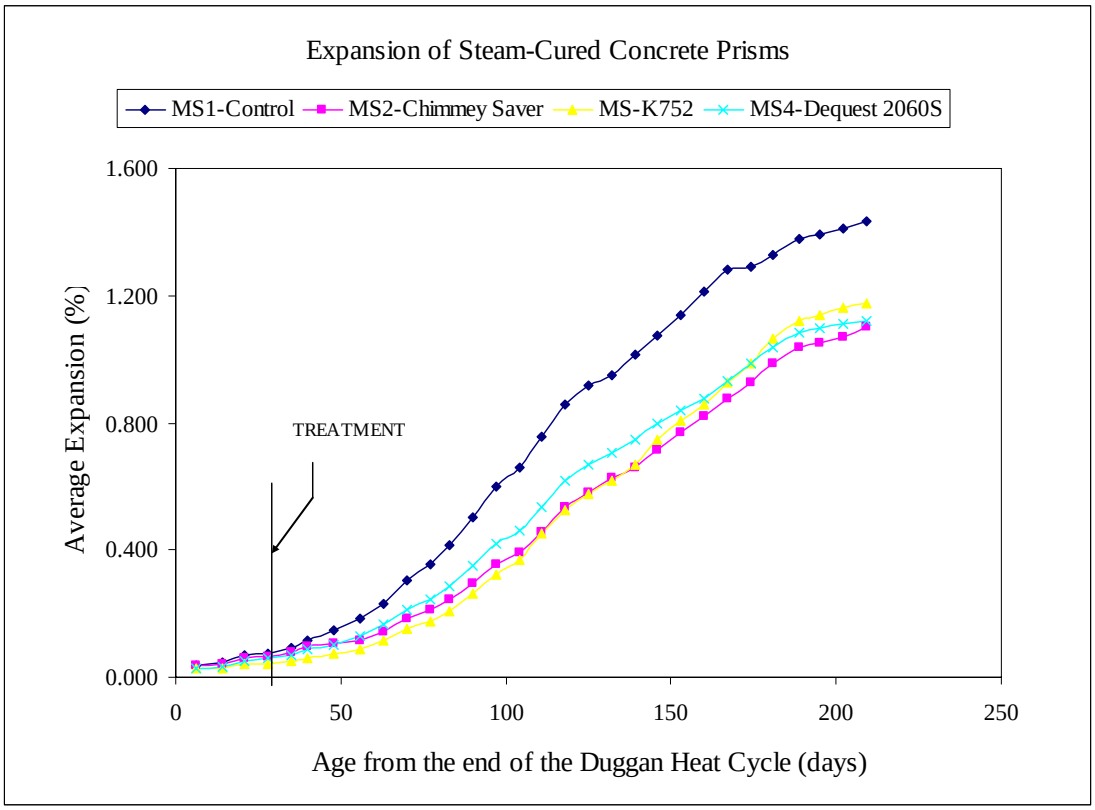

Figure 7.10 - Expansion vs. Time of Concrete Prism Subjected to DEF Mitigation Products

7.4.3.3 SEM and EDAX Analysis Results

SEM analysis with EDAX was employed before treatment at 45 days and at 90, 120 and 240 days after the completion of the Duggan Cycle. The SEM and EDAX analyses were used to determine the chemical composition of the mineral deposits, within the microstructure of the concrete specimens, which were treated with different mitigation products. The occurrence of ettringite in the treated concrete specimens appears to be slightly reduced and hence less deleterious expansion values are observed. Ettringite was observed in the control specimens throughout the research. All ages typically produced ettringite with similar morphologies including spheres, laths, and needles. Ettringite spheres, lamellar and needle were observed throughout the control concrete specimens. Ettringite was found in cavities, on the surface and in the cement matrix. Figure 7.11 shows ettringite lamellar filling a cavity just before treatment. Less ettringite spheres or lamellar were observed in the treated concrete specimens at age 90 days as shown in Figures 7.12 and 7.13.

Future testing should apply the mitigation products prior to the 45 days used in this study. The SEM work at 45 days found lamellar ettringite, which the field portion of this research showed as significant in the deterioration of the concrete matrix. Deterioration of the concrete matrix will results in significant loss of concrete strength.

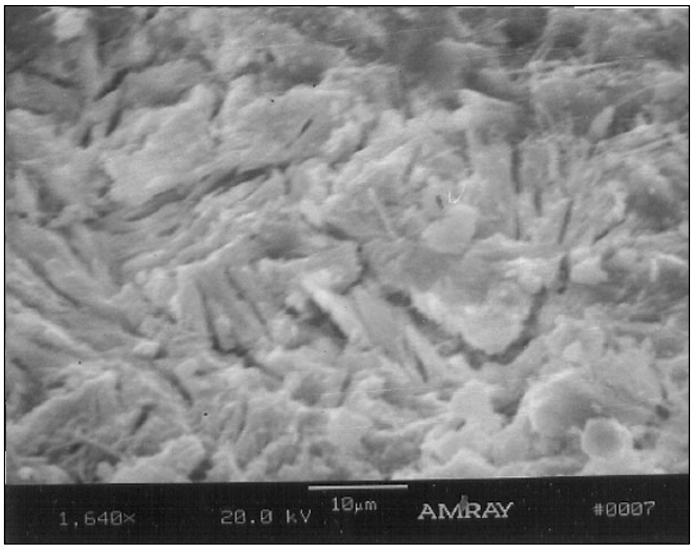

Figure 7.11 – Lamellar Ettringite in Control Prism (Set No. 1) at Day 45.
SEM Sample of Exterior Region of Prism
Ca-S-Al Ratio (Wt %) = 79.03 – 10.57 – 4.79

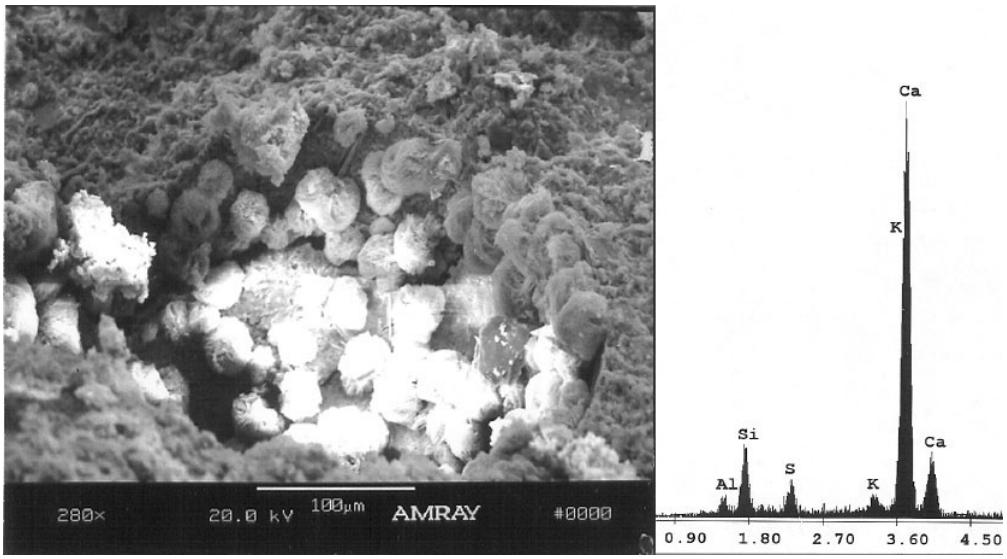

Figure 7.12 – Spherical Ettringite Balls in ChimneySaver (Set No. 2) at Day 90.
SEM Sample of Exterior Region of Prism
Ca-S-Al Ratio (Wt %) = 77.46 – 3.73 – 1.79

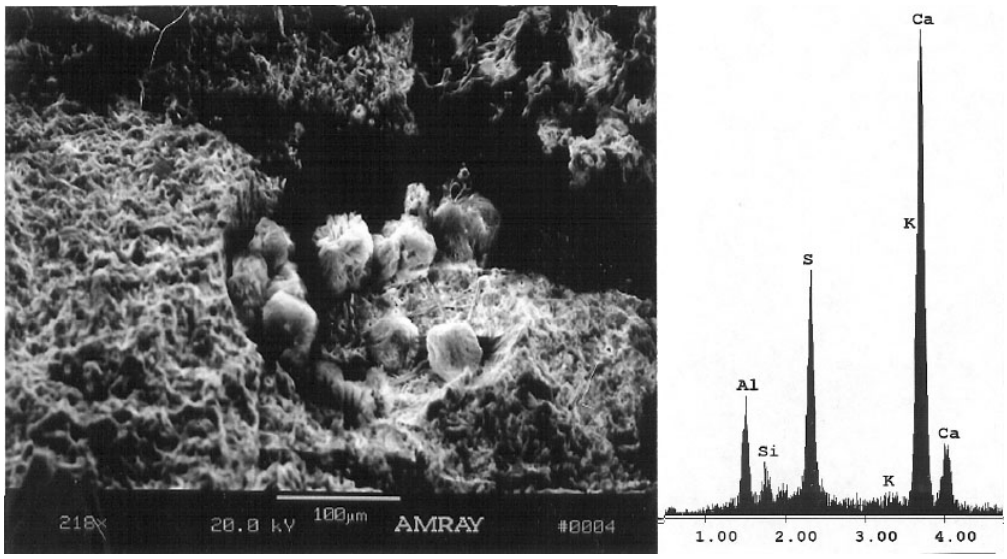

Figure 7.13 – Spherical Ettringite Balls in Noveon Good-Rite K572 (Set No. 3) at Day 90. SEM sample of Exterior Region of Prism.
Ca-S-Al Ratio (Wt %) = 69.09 – 21.76 – 10.72

Chapter 8
Conclusion and Future Research

8.1 Conclusions

8.1.1 Field Studies

Two field studies proved useful and the results show trends in DEF formation in cast-in-place concrete. The first study showed that DEF is present throughout the Maryland Bridge Inventory. Whereas, the second study showed trends indicating significance in the amount of DEF observed in the concrete sample.

The design of the sample selection procedure based on the presence or absence of map cracking was effective since it yielded significant differences between the two categories. The method of classifying the ettringite crystal morphology also produced significant results as did the method of quantifying the amount of ettringite into discrete levels. However, the small number of data points and the fact that the variables were discrete rather than continuous indicates that conventional statistical analyses that depend on the Law of Large Numbers are not appropriate. Instead the use of nonparametric statistical methods is necessary.

Results from the field revealed that it is important to collect data on the macroscopic distribution of the map cracking areas across the surface of the structure. The mapped crack areas did not have a uniform probability distribution in the sense

that there was not a continuum from the most damaged to the least damaged. Instead the damage was either present over the entire structure or occurred only in sparse patches. This may reflect differences in the concrete batches or in the local microclimate around the bridge. These results were based on the judgments of the operators. There is a need for more quantitative approaches such as automated image analysis of digital photographs of the structure.

The observed differences in ettringite morphology may be indicative of the conditions under which it was formed. It is proposed here that the acicular form is associated with primary ettringite. This normally disappears a few hours after formation, but in situations where it is isolated from the pore solution, such as in air voids, it can persist. In contrast, the lamellar morphology develops only after prolonged environmental exposure and thus appears to be delayed ettringite. This term is used only to indicate the time of occurrence. It is not possible to determine from the SEM images whether the lamellar ettringite is the cause of the damage or simply a secondary phase that grows in the cracks after they propagate.

This distinction between the different morphologies may help to resolve the controversy over the occurrence of ettringite in concrete. One school of thought maintains that ettringite can always be found in concrete, and therefore, its occurrence provides no useful information. The results of this study show that when the differences in morphology and sites are taken into account, the ettringite found in undamaged concrete may simply be left over primary ettringite, while the lamellar ettringite in damaged concrete is the result of delayed formation. It should also be noted that previous studies tended to be biased toward damaged concrete because they

were usually undertaken for forensic reasons. In this study, apparently undamaged concrete bridges were also sampled, and in some cases no ettringite was found.

Thus widespread moist map cracking appears to be a good indicator of significant DEF present in the affected concrete. On the other hand, no ASR gel was observed in any of the bridges. This confirms the results of the Phase I field survey, that map cracking is not a reliable predictor of ASR occurrence.

There appears to be no significant differences in the occurrence of ettringite based on time of construction pre or post 1980. This implies that the use of air entrainment agents does not play a role in delayed ettringite formation. However, in this case the time of construction was used as a surrogate for the presence or absence of AEA. This reflects the prevailing lack of records on actual mix designs, which makes it difficult to relate DEF with the original constituents of the concrete mix.

8.1.2 Mitigation Laboratory Studies

Testing conducted during Phase 2 research evaluated various mitigation products that can be applied to concrete in existing bridges. The goal of the mitigation is to reduce or limit the future development of DEF in the affected concrete.

Preliminary studies tested four (4) mitigation products and four (4) cross combination of those products. The testing consisted of four products: ChimneySaver, Radcon Formula #7, Dequest 2060S, and Noveon Good-Rite K752. ChimneySaver and Radcon Formula #7 are water repellents, and Dequest 2060S and Noveon Good-Rite K752 are crystal growth inhibitors. Because the two types of

products are fundamentally different, cross combinations of crystal growth inhibitors and water repellents were also tested.

The results of the preliminary work showed that ChimneySaver, Dequest 2060S, and Novean Good-Rite K-752 limited the total expansion experienced by the laboratory specimens. The results showed promise, but the total expansion was higher than desired. A follow-up study was conducted to better represent field conditions. The products that showed promise in the preliminary study were included in the follow-up study. In order to increase the usability of Dequest 2060S and Noveon Good-Rite K752, both products were diluted to enable spray applications.

The results of the follow-up study verified that the products continue to limit the total expansion compared to the control specimens. Again, the results showed promise, but the total expansion was slightly higher than desired based on strength testing.

Mitigation products tested during Phase 2 research, provided reduction in the overall expansion. Preliminary and follow-up testing demonstrated that ChimneySaver, Dequest 2060S, and Novean Good-Rite K-752 limited the total expansion experienced by the specimen. All three (3) products can be applied with low pressure sprayers and can easily and safely be handled by state workers or a contractor. The products are also environmentally safe. During the follow-up testing, the researchers did not notice any discoloration of the concrete specimen. Additional testing should be preformed to verify these findings.

8.2 Future Research

8.2.1 Field Studies

Although this survey did produce some significant results, they are still based on a very limited number of bridges. It would be very desirable to increase the database both in geographical coverage and in the number of bridges in a given state to see if these conclusions hold true.

Given the absence of construction records, the concrete cores need to be examined in more detail petrographically to determine such things as aggregate type and air void distribution. This applied to both the cores from the existing study and to future field surveys.

The extent of macroscopic damage should be quantified using automated image analysis of close range photogrammetry. Data on local microclimate such as exposure to rain or runoff, contact with soil moisture and solar exposure should also be collected. It should be noted that some researchers in France have gone as far as modeling the temperature distributions in the concrete during curing. The degree of damage to the concrete should also be quantified. Methods based on ultrasonics have shown some promise.

8.2.2 Mitigation Laboratory Studies

Additional testing should be conducted to determine the effectiveness of the treatments with respect to age after the UMD / FHWA Modified Duggan Cycle. During the follow-up testing, the specimen at 45 days of storage contained lamellar ettringite, which the field study showed as significant in the development or propagation of map cracking.

REFERENCES

AASHTO Innovative Highway Technologies (1998). "Alkali-Silica Reaction" SHRP C-315. http://leadstates.tamu.edu/asr/library/C315/c315d.stm (24 February 2004).

Amde, A.M., Azzam, A., Sabnis, G. and Livingston, R. A., (2006) "The Effects of Mix Water Conditioner on Internal Sulfate Attack in Concrete," Seventh International Congress on Advances in Civil Engineering (ACE 2006), Istanbul, Turkey, October 11-13, 2006.

Amde, A.M., Ceary, M. and Livingston, R. A., (2005a) "Investigation of Maryland Bridges for DEF And ASR," ICACS 2005 Int. Conf., Chennai, India, January 2005, 809-816, (***Keynote Paper***).

Amde, A.M., Williams, K. and Livingston, R.A., (2005b) "Influence of Fine Aggregate Lithology on DEF In High Early Strength Concrete," *Indo US workshop (sponsored by NSF) on High Performance Cement- based Concrete Composites**,** American Ceramic Society**,*** Chennai, India, January 2005, 199-209.

Amde, A.M., Ceary, M. and Livingston, R.A., (2005c) "Investigation of Maryland Bridges for DEF and ASR," J of Structural Engineering, Vol. 32, No. 1, Apr.-May 2005, 33-36.

Amde, A.M., Azzam, A. and Livingston, R.L., (2005d) "Mitigation of DEF using Class F Fly Ash or Mix Water Conditioner," OWICS 05-Engaging the Future, Singapore, August 2005, 191-198, (**Bauchemie Award 2005 for Best Paper**).

Amde, A.M., Ceary, M. and Livingston, R., (2005e) "Correlation Between Map Cracking and DEF in Field Specimens," *The 11th Int. Conf. on Fracture*, (2005f) Turin, Italy, Sec.15, #4526, Mar. 2005.

Amde, A.M. and Livingston, R.A., (2004a) "UMD/FHWA Studies on Delayed Ettringite Formation," *International Conference on Advances in Concrete and Construction* (ICACC2004), Hyderabad, India, December 2004, 425-434 (***Keynote Paper***).

Amde, A. M., Ceary, M., Livingston, R. A., and McMorris, N. (2004b), Pilot Field Survey of Maryland Bridges for Delayed Ettringite Formation Damage, Maryland State Highway Administration, Vol. 1, MD-04-SP107B4U.

Amde, A. M., Williams, K., and Livingston, R. A. (2004c), Influence of Fine Aggregate Lithology on Delayed Ettringite Formation in High Early Strength Concrete, Maryland State Highway Administration, Vol. 2, MD-04-SP107B4U.

Amde, A. M., Livingston, R. L. and Azzam, A., (2003a) "Influence of Alkali Content and Development of Accelerated Test Method for Delayed Ettringite Formation," *Proceedings of the International Innovative world of Concrete Conference*, Pune, India, 2003.

Amde, A.M., Ceary, M. and Livingston, R., (2003b) "Measurement of Expansion Associated with DEF," *106th Annual meeting & Exposition of the American Ceramic Society*, Indianapolis, 2003.

American Association of State Highway and Transportation Officials (2000). "Manual for Condition Evaluation of Bridges," 2nd ed. Washington, DC.

Azzam, A., (2002), "Delayed Ettringite Formation, the influence of aggregate types, curing conditions, exposure conditions, alkali content, fly ash and mix water conditioner (MWC)," Ph.D Dissertation, University of Maryland, College Park, USA.

Ceary, M., (2003), "Pilot NDT Field Survey of Maryland Bridges For Delayed Ettringite Formation Damage," M.S. Thesis, University of Maryland, College Park, USA.

Ceesay, J., (2006), "Title," Ph.D Dissertation, University of Maryland, College Park, USA.

Cody, R., Cody, A., Spry, P., Hyomin, L. (2001), "Reduction of Concrete Deterioration by Ettringite Using Crystal Growth Inhibition Techniques," Iowa Department of Transportation, TR-431.

Collepardi, M., Baladini, G., Pauir, M., Corradi, M. (1978), "Tricalcium Aluminate Hydration in the Presence of Lime, Gypsum or Sodium Sulfate," Cement Concrete Research.

Day, R. L.(1992), "The Effect of Secondary Ettringite Formation on the Durability of Concrete: A Literature Analysis," Portland Cement Association.

Diamond, S., Ong, S., and Bonen, D., (1994), "Characteristics of Secondary Ettringite Deposited in Steam Cured Concretes Undergoing ASR." Proceedings of the Sixteenth International Conference on Cement Microscopy, Richmond, VA.

Diamond, S., Zhang, Z., and Olek, J., (2002), "Strain Capacity, Expansion, DEF, and All That!" Proceedings of the Twenty-Fourth International Conference on Cement Microscopy, San Diego, CA.

Divot, L., Pavoine, A., and Clement, J.L., (2006), "Les Methods de Diagnostic et de Prognostic Appliques a la Formation Differee de L'Ettringite." 7th CANMET / ACI Inter. Conf. on Durability of Concrete, SP 234.

El-Sayed, H. A., El-Wahed, M. G. Abd, Ali, A. H., (1987), "Some Aspects of the Corrosion of Reinforcing Steel in Concrete Marine Atmospheres," Durability of Building Materials, Vol.5, N1, pp. 13-25.

Gress, D. (1997), Early Distress in Concrete Pavements. FHWA-SA-97-045, Federal Highway Administration, Washington, DC.

Heinz, D., and Ludwig, U. (1987), "Mechanism of Secondary Ettringite Formation in Mortars and Concretes Subjected to Heat Treatment," Concrete Durability, SP-100, Vol. 2, American Concrete Institute, Detroit, MI. 2059-2071.

Kennerly, R. A., (1965), “Ettringite Formation in Dam Gallery,” ACI Journal, pp. 559-576.

Klingner, R.E., Fowler, T.J., et al. (2001a), “Bridges with Premature Concrete Deterioration: Fatigue Testing of Full-Scale, Prestressed Box Girders Failing in Shear,” University of Texas, Center for Transportation Research, CTR 1857-3.

Klingner, R.E., Fowler, T.J. (2001b), “Bridges with Premature Concrete Deterioration: Field Observations and Large Scale Testing,” University of Texas, Center for Transportation Research, CTR 1857-1.

Klingner, R.E., Fowler, T.J., et al. (2002a), “Bridges with Premature Concrete Deterioration: Damage Indices, Strand-Pullout Tests, and Field Observations” University of Texas, Center for Transportation Research, CTR 1857-4.

Klingner, R.E., Fowler, T.J., et al. (2002b), “Nondestructive Testing of Prestressed Bridge Girders with Distributed Damage,” University of Texas, Center for Transportation Research, CTR 1857-2.

Klingner, R.E., Fowler, T.J., et al. (2004a), “Mitigation Techniques for In-Service Structures with Premature Concrete Deterioration: A Literature Review,” University of Texas, Center for Transportation Research, CTR 4069-1.

Klingner, R.E., Fowler, T.J., et al. (2004b), “Mitigation Techniques for In-Service Structures with Premature Concrete Deterioration: Development and Verification of New Test Methods,” University of Texas, Center for Transportation Research, CTR 4069-2.

Klingner, R.E., Fowler, T.J., et al. (2004c), “Mitigation Techniques for In-Service Structures with Premature Concrete Deterioration: Synthesis Report,” University of Texas, Center for Transportation Research, CTR 4069-3.

Johanson, V., Thaulow, N., Skalny, J. (1993), "Simultaneous Presence of Alkali-Silica Gel and Ettringite in Concrete," Advances in Cement Research, 23-29.

Larive, C. and Louran, N. (1992), "Diagnosis of Alkali Aggregate Reaction and Sulfate Reaction in French Structures," Proceedings of the 9th International Conference on Alkali Aggregate Reactions, Concrete Society, London, England, 587-598.

Lawrence B. L., Moody, E. D. Guillemette, R. N. Carrasquillo, R. L. (1999), "Evaluation and Mitigating Measures for Premature Concrete Distress in Texas Department of Transportation Concrete Elements," Cement, Concrete, Aggregates, 73-81.

Lawrence, C. D., Dalziel, J. A., Hobbs, D. W. (1990), "Sulfate Attack Arising from Delayed Ettringite Formation," Interm Technical Note, 12, British Cement Association, Wexham Springs, Slough, UK.

Lawrence, C. D. (1994), "Delayed Ettringite Formation: An Issue?," Materials Science of Concrete IV, American Ceramic Society, Westerville.

Livingston, R. A., C. Ormsby, A. M. Amde, M. Ceary, N. McMorris and P. Finnerty (2006). "Field Survey of Delayed Ettringite Formation Related Damage in Concrete Bridges in the State of Maryland." *CANMET Conference on Durability of Concrete*, Montreal, CANADA: in press.

Livingston, R. A., M. Ceary and A. M. Amde (2002). "Statistical Sampling Design for a Field Survey of Delayed-Ettringite-Formation Damage in Bridges." *Structural Materials Technology V : An NDT Conference*, Cincinnati, OH, ASNT: 411-420.

Livingston, R.A., Amde, A.M. and Ramadan, E. (2001a). "Characterization of Damage in Portland Cement Concrete Associated with DEF." *Proc. of the 6th Int. Conf. CONCREEP 6 @ MIT* (eds. Ulm, Bazant, and Wittmann), Elsevier, Cambridge: 463 – 468.

Livingston, R. A., H. H. Saleh, E. O. Ramadan and A. M. Amde (2001b). Characterization of Damage in Portland Cement Concrete Associated with Delayed Ettringite Formation. *Creep, Shrinkage and Durabiity Mechanics of Concrete and Other Quasi-Brittle Materials*, Amsterdam, Elseveier: 463-468.

Livingston, R. A. and Amde, A. M. (2000). "Nondestructive Test Field Survey for Assessing the Extent of Ettringite-Related Damage in Concrete Bridges" in 10th Int. Symposium on Nondestructive Characterization of Materials," Elsevier Science, Ltd., Karaizawa, Japan.

Maryland State Highway Administration. "District Offices, Shops & Labs," Baltimore,: MD.

Maryland State Highway Administration Office of Bridge Development (1993), "Guide for Completing Structure Inventory and Appraisal Input Forms.," Baltimore, MD.

Maryland State Highway Administration Office of Bridge Development (1996), PONTIS Element Data Collection Manual. Baltimore, MD.

Mehta, P. (1986), "Concrete Structures Properties and Materials," Prentice Hall Inc., Engle Cliffs, NJ.

Merrill, B. D. (2004) "Durability of Concrete in Highway Facilities," Internet. http//:gem1.cive.uh.edu/content/conf_exhib/00_present/9.htm Accessed 09/23/04.

Mielenz, R., Marusin, S., Hime, W., and Jugovic, Z. (1995) “Investigation of Prestressed Concrete Railway Tie Distress,” Concrete International, Vol. 17, No. 12, 62-68.

Noveon, Inc. (2005), “Good-rite K-752 Polyacrylate,” Internet. http://www.noveoncoatings.com/products/americas/documents/goodrite/GRK-752tds.pdf, Accessed 05/28/05.

Ozol, M, A., Strand, Walter III, June 2002, “Delayed Ettringite Formation at Brewer Stadium, Boone, North Carolina,” Cement, Concrete Aggregates, CCAGDP, Vol. 22, No. 1, pp. 24-34.

Pettifer, K., and Nixon, P. J., 1980, “Alkali Metal Sulfate-A factor Common to Both Alkali Aggregate Reaction and Sulfate Attack on Concrete,” Cement and Concrete Research, Vol. 10, pp. 173-181.

Radcrete Pacific Pty. Ltd. (2005), “Radcon® Formula #7,” Internet. http://www.radcrete.com.au/Downloads/02-Radcon%20Brochure.pdf, Accessed 05/28/05.

Ramadan, E. O., Amde, A. M., Livingston, R. A. (2000), "The Effect of Potassium and Initial Curing Concrete Expansion Associated with Delayed Ettringite Formation," ACI Materials Journal (under review).

Ramadan, E., (1999), “Experimental and Theoretical Study of Delayed Ettringite Damage in Concrete,” Ph.D. Dissertation, University of Maryland, College Park, USA.

SaverSystems (2005), “ChimneySaver® Product Data,” Internet. http://www.chimneysaver.com/ProductData/waterbase.pdf, Accessed 05/28/05.

Schlorholtz, S. (2000) "Determine Initial Cause for Current Premature Portland Cement Concrete Pavement Deterioration," CTRE, Ames, IA.

Scrivener, K., and Taylor, H. F. W. (1993), "Delayed Ettringite Formation a Microstructural and Microanalytical Study," Advances in Cement Research, 139-145.

Shaikh, H., (2007), “Mitigation of Delayed Ettringite Formation in Laboratory Specimens,” M.S. Thesis, University of Maryland, College Park, USA.

Shimada, Y., Johansen, V.C., Miller, F.M., and Mason, T., (2005) "Chemical Path of Ettringite Formation in Heat-Cured Mortar and Its Relationship to Expansion: A Literature Review." Portland Cement Association, RD136.

Solutia Inc. (2005), “Dequest 2060S Product Information,” Internet. http://www.dequest.com/pages/products/product.asp?re=ap&id=134, Accessed 05/28/05.

Spry, P.G., and Cody, R.D. (2004), " Reduction of Concrete Deterioration by Ettringite Using Crystal Growth Inhibition Techniques: Part II Field Evaluation of Inhibitor Effectiveness." Iowa Department of Transportation, TR-469.

Stark D., (1994), “Alkali-Silica Reaction in Concrete,” Significance of Tests, and Properties of Concrete-Making Materials: STP169C. P. Kleiger and J. F. Lamount, Eds., American Society for Testing and Materials, West Conshohocken, PA, 365-371

Stark, J. and Bollmann, K. 1999, Ettringite: “The Sometimes Host of Destruction,” SP-177, B. Erlin, (ed.), American Concrete Institute, Farmington Hills, MI, pp. 183-198.

Taylor, H. F. W. (1990), Cement Chemistry, Academic Press, London, England

Taylor, H. F. W. (1993), "Delayed Ettringite Formation," Advances In Cement and Concrete," Proc. Eng. Foundation Conf. Durham, NH, 122-131.

Tepponen. P., and Eriksson, B.E. (1987), "Damages in Concrete Railway Sleepers in Finland," Concrete Research, 199-209.

Thomas, M., Delayed Ettringite Formation in Concrete: Recent Developments and Future Directions, in Materials Science of Concrete VI, S. Mindess and J. Skalny, Editors. 2001, The American Ceramic Society: Westerville, OH, 435-481.

Tuhin Basu & Associates (2002), "2001 Biannual Inspection, Cecil County Bridge CE-003 (Dr Jack Road over Octorio Creek,". Baltimore, MD.

Volkwein, A. and Springenschmid, R., Sept. 5, 1981, “Corrosion of Reinforcement in Concrete Bridges at Different Ages due to Carbonation and Chloride Penetration, 2nd Intnl. conf. on durability of Building Materials and Components,” 14 – 16, Publ. By NBS, Washington D.C., pp. 119-209.

Williams, Kenneth L, Jr., "Influence of Fine Aggregate Lithology on Delayed Ettringite Formation in High Early Strength Concrete," MS Thesis, University of Maryland, College Park, Maryland (2003).

Yang, R., Lawrence, C. D., Lynsdale, C. J., Sharp, J. H. (1999), "Delayed Ettringite Formation in Heat-cured Portland Cement Mortars," Cement and Concrete Research, 17-25.